Quarterly Publication

ISSN 3572 - 2383

Global Journal of Environmental Science and Management

Volume 8, Number 3, Summer 2022

Global Journal of Environmental Science and Management (GJESM)

(QUARTERLY PUBLICATION)

OPEN ACCESS

Editorial Contact Information
No. 2, Unit 213, Kouhestan Deadend,
Janpour Street, Darabad Square,
Tehran, Iran
Phone: +9821-26105110-11
Email: *gjesm.publication@gmail.com*
editor@gjesm.net

Website: https://www.gjesm.net/

Publication Center
GJESM Publisher
publisher@gjesm.net

Publication authorization is certified by the Ministry of Culture and Islamic Guidance; No. 93/3629; 14 May 2014
Scientific-Research grade is accredited by the Ministry of Science, Research and Technology; No. 3/18/59975; 20 June 2015

Circulation: 500

***p*ISSN 2383 - 3572** ***e*ISSN 2383 - 3866**

Aims and Scope

Global Journal of Environmental Science and Management (GJESM) is an international scholarly refereed research journal which aims to promote the theory and practice of environmental science and management. A broad outline of the journal's scope includes; peer reviewed original research articles, case and technical reports, reviews and analyses papers, short communications and notes to the editor, in interdisciplinary information on the practice and status of research in environmental science and management, both natural and man-made. The main aspects of research areas include, but are not exclusive to; environmental chemistry and biology, environments pollution control and monitoring, transport and fate of pollutants in the environment, concentrations and dispersion and trace of wastes in air, water, and soil, point and non-point sources pollution, heavy metals and organic compounds in the environment, atmospheric pollutants and trace gases, solid and hazardous waste management; soil biodegradation and bioremediation of contaminated sites; environmental impact assessment, industrial ecology, ecological and human risk assessment; improved energy management and auditing efficiency and environmental standards and criteria.

Vision and Mission

Global Journal of Environmental Science and Management (GJESM) publishes original. Peer-reviewed and technical environmental articles serve those environmental science and management through the on time quarterly publication with reliable information. GJESM is an integral partner with the scientific and technical communities, delivering superior information products and services that foster communication, build insights and enables individual and collective advancement in environmental research. Providing environmental science and management information to the general public with descriptions of contemporary advances in environmental issues to be used in improving environmental protection and management.

Abstracting and Indexing

Web of Science (ESCI); Scopus; Scimago Journal Rank (SJR); ProQuest (Agricultural and Environmental Science + Natural Science Collection + Ulrichsweb); Chemical Abstract (CAS); CABI Abstract; Global Health Abstract; Agricola; Committee on Publication Ethics (COPE); PubMed-NCBI; DOAJ; Open J-Gate; Google Scholar; Academia.edu; Geomar; WorldCat; Academic Resource Index; Environmental XPRT; Information Matrix for the Analysis of Journals (MIAR); Bibliothek Humburg; ScienceMedia; JournalTOCs; MSRT; ISC; RICeST; SID; Civilica; Magiran.

Global
Journal of Environmental Science and Management (GJESM)

Editor-in-Chief
Professor J. Nouri

pISSN 2383 - 3572
eISSN 2383 - 3866

QUARTERLY FULL OPEN ACCESS PEER REVIEWED PUBLICATION

Journal Abbreviation: Global J. Environ. Sci. Manage.

CALL FOR PAPERS

Publication benefits in
Global Journal of Environmental
Science and Management

- *Quarterly Publication journal*
- *Online submission and reviewing*
- *Online status inquiry*
- *Double blind peer reviewing*
- *Rapid evaluation and publication*
- *Immediate publication on the net*
- *Open access to all PDF full text of published articles*
- *No pay charge for publication*
- *Indexed and cited in well-known databases;*
  particularly Web of Science and Scopus

www.gjesm.net
www.gjesm.org

editor@gjesm.net
global.jesm@gmail.com
gjesm.publication@gmail.com

Tel.: +9821 2610 5110
Fax: +9821 2610 5111

CONTENTS

Volume 8, Number 3, Summer 2022

COVERING LETTER

Subject: **Submission of manuscript**

Dear Editor,

I would like to submit the following manuscript for possible evaluation

Manuscript Title:

Running Title (Short title):

Main Subjects:

Name and address of corresponding author:

Telephone #

Fax #

Email:

I affirm that the manuscript has been prepared in accordance with Global Journal of Environmental Science and Management guide for authors.

I have read the manuscript and I hereby affirm that the content of this manuscript or a major portion thereof has not been published in a refereed journal, and it is not being submitted fully or partially for publication elsewhere. The manuscript has been read and approved by all listed authors.

The source(s) of financial support of study (if any):

Type of Manuscript (check one):

- ☐ Original research paper
- ☐ Case report
- ☐ Research note
- ☐ Short communication
- ☐ Review paper

Name:

Corresponding Author Signature:

Date:

Global J. Environ. Sci. Manage. 8(3): 297-314, Summer 2022, Serial #31

Global Journal of Environmental Science and Management
(GJESM)

Homepage: https://www.gjesm.net/

ORIGINAL RESEARCH ARTICLE

Soil classification in a seismically active environment based on join analysis of seismic parameters

Y. Asnawi[1,2,3], A. V.H. Simanjuntak[3,4], U. Muksin [3,*], M. Okubo[5], S.I. Putri[3], S. Rizal[1], M. Syukri[1]

[1] *Graduate School of Mathematics and Applied Sciences, Universitas Syiah Kuala, Banda Aceh 23111, Indonesia*

[2] *Universitas Islam Negeri Ar-Raniry, Banda Aceh 23111, Indonesia*

[3] *Tsunami and Disaster Mitigation Research Center, Universitas Syiah Kuala, Jl. Prof. Dr. Ibrahim Hasan, Gampong Pie, Indonesia*

[4] *Meteorological, Climatological, and Geophysical Agency, BMKG, Banda Aceh 23234, Indonesia*

[5] *Natural Science Cluster, Science and Technology Unit, Kochi University, Akebono-cho Kochi, Japan*

ARTICLE INFO

Article History:
Received 16 September 2021
Revised 25 October 2021
Accepted 02 December 2021

Keywords:
Earthquake
Seismic amplification
Seismic wave velocity
Spatial autocorrelation
Spectral ratio

ABSTRACT

BACKGROUND AND OBJECTIVES: Soil or rock properties where buildings are situated play an important role in the ground shaking caused by an earthquake. The highly populated Banda Aceh city in the northernmost Sumatra is flanked by two active faults, the Seulimeum and the Aceh segment. Therefore, it is crucial to investigate the subsurface characteristics of the region to reduce the earthquake risk as there was no regional study has been conducted so far.
METHODS: Characteristics of the soil or rock of the subsurface were derived from various seismic parameters. The seismic microtremors were recorded at 36 sites covering the highly populated city and the two active faults. The spatial autocorrelation method was used to obtain a dispersion curve based on the relationship between seismic frequencies and phase velocity from triangular geophones array to determine the shear wave velocity of the subsurface layer. The seismic amplification, dominant frequency and vulnerability value at each measurement point were measured using the horizontal-to-vertical spectral ratio method. The maps of velocity structure and HVSR parameters were generated from the interpolation of those seismic parameters.
FINDINGS: Based on the variation of the four geophysical parameters: shear wave velocity, seismic amplification, dominant frequency, and seismic vulnerability, the study area can be clustered into five different groups: I) Banda Aceh, II) Jantho, III) Krueng Raya, IV) Lhoknga-Lhoong, and V) Seulawah, which classify the different types of rocks. The classification of soil properties from the combination of shear wave and horizontal-to-vertical spectral ratio data correlates with the geology of the study area.
CONCLUSION: The Banda Aceh city, flanked by the two active faults, is characterized by low shear wave velocity and high amplification because the city stands on the sedimentary basin; thus, it requires a detailed investigation prior to constructing infrastructures. The other clusters are located on the relatively less vulnerable areas, indicated by moderate shear wave velocity and moderate to low seismic vulnerability indexes. The joint analysis shows that the combination of physical properties, including the shear wave velocity, seismic amplification, and dominant frequency, can be used to investigate lithology and seismic vulnerability into a specific cluster. The research results are essential for hazard mitigation and can be used for disaster risk management by the local government. A detailed investigation with denser measurement points needs to be conducted to comprehensively describe the types of rocks in Banda Aceh and its surrounding.

DOI: 10.22034/gjesm.2022.03.01

NUMBER OF REFERENCES	NUMBER OF FIGURES	NUMBER OF TABLES
51	8	1

*Corresponding Author:
Email: *muksin.umar@unsyiah.ac.id*
ORCID: 0000-0001-7297-8065

Note: Discussion period for this manuscript open until October 1, 2022 on GJESM website at the “Show Article”.

INTRODUCTION

Seismic amplification and soil properties based on seismic shear wave velocity parameters are crucial to investigate, particularly seismically active and highly populated regions. Banda Aceh and its surrounding areas in the northernmost Sumatra are among the most earthquake-prone zones because they are surrounded by earthquakes sources (Fig. 1). Large offshore earthquakes (e.g. the Mw 9.3 Sumatra–Andaman earthquake and the Mw 8.5 Nias earthquake) mainly occur along active subduction zones. Meanwhile, onshore earthquakes tend to occur along the northern segment of the Sumatra Fault System, including the Aceh fault, Seulimeum fault (Sieh and Natawidjaja, 2000), Pidie Jaya fault (Muzli *et al.*, 2018; Idris *et al.*, 2019) and Central Aceh fault (Muksin *et al.*, 2019). The Seulimeum fault generated an earthquake with a magnitude of M 7.0 in 1936, and such an event caused building collapse and severe property damage, along with several reported fatalities (Untung *et al.*, 1985). Although no major event has been recorded in the last 170 years along the Aceh segment, the occurrence of a large earthquake remains possible (Ito *et al.*, 2012). Therefore, mitigation plans for earthquake events in Banda Aceh should be prioritized. The city is one of Sumatra's most economically developed areas and is becoming a highly populated region. Bilham (2009) suggested that rapid development has put developed cities at relatively high risk for a significant increase in fatalities and economic losses caused by damages to buildings or other infrastructure in the coming years. Earthquake intensity and construction quality play an important role in building damages. Several geophysical parameters can extend infrastructure damages, including seismic amplification, ground acceleration, rock or soil properties of sites, and geology of regions (Goda *et al.*, 2015). Seismic amplification, which represents the possible extent of ground shaking of sites during earthquakes, can be defined by the maximum value of the horizontal-to-vertical spectral ratio (HVSR) at a certain dominant frequency (Nakamura, 1997). Areas with high damage ratios during earthquake events have high values of HVSR and low dominant frequencies (Nakamura, 1997).

Several studies have shown that the types of soils or rocks can be classified based on the velocity of shear waves (Vs) passing through the subsurface. Very dense soil has Vs values between 360 and 760 m/s, whereas soft soil has Vs values of less than 180 m/s. Several methods can be used to determine Vs values, including multichannel surface wave analysis (Park *et al.*, 2007) and the less invasive method, called spatial autocorrelation (SPAC) (Cho *et al.*, 2004; Cho, 2019). For regional studies, shallow structures can be derived by ambient noise tomography (Ryberg *et al.*, 2016), while the seismic refraction of very localized areas can be used to determine the velocity of pressure (Vp) and shear waves (Vs). Among the methods, SPAC is one of the least expensive ones, but it remains reliable when applied to inaccessible areas, such as the Banda Aceh region in the northernmost Sumatra. Some successful SPAC research around the world includes those conducted in Nevada (Scott *et al.*, 2006), Italy (Forte *et al.*, 2019), and Japan (Matsuoka *et al.*, 2006). The objective of the research is to investigate the geophysical properties of the shallow and vulnerability of the northernmost Sumatra. The Vs values are used to derive the types of soil based on the classification of the National Earthquake Hazards Reduction Program (NEHRP). The combination of various HVSR data, including seismic amplification and dominant frequency and Vs values, can be used to derive more detailed soil clusters in the northernmost Sumatra. The results can be used to investigate the probabilistic seismic hazards of Banda Aceh and update the loss assessment map of Banda Aceh developed by Rusydy *et al.* (2020) for different earthquake model scenarios.

Geology of study area

A complex tectonic process makes Banda Aceh and its surrounding areas prone to moderate–large earthquakes that potentially generate massive ground shaking on the surface. Such shaking is attributed to the Banda Aceh basin, formed since the Quaternary and pre-Quaternary and recognized as alluvium deposited. The Banda Aceh basin is mostly influenced by recent alluvium and marine sediment products consisting of gravel, sand, silt, and clay (Rusydy *et al.*, 2020). The upper layer of the southeastern part of the Banda Aceh basin is covered by pre-Quaternary rocks from Pliocene to Pleistocene (Fig. 1) up to 500 m; these rocks consist of calcareous and tuffaceous sandstones (Siemon and Steuer, 2010). As a result of oblique subduction, the Banda Aceh basin is flanked by the Aceh fault in the southwest and the Seulimeum

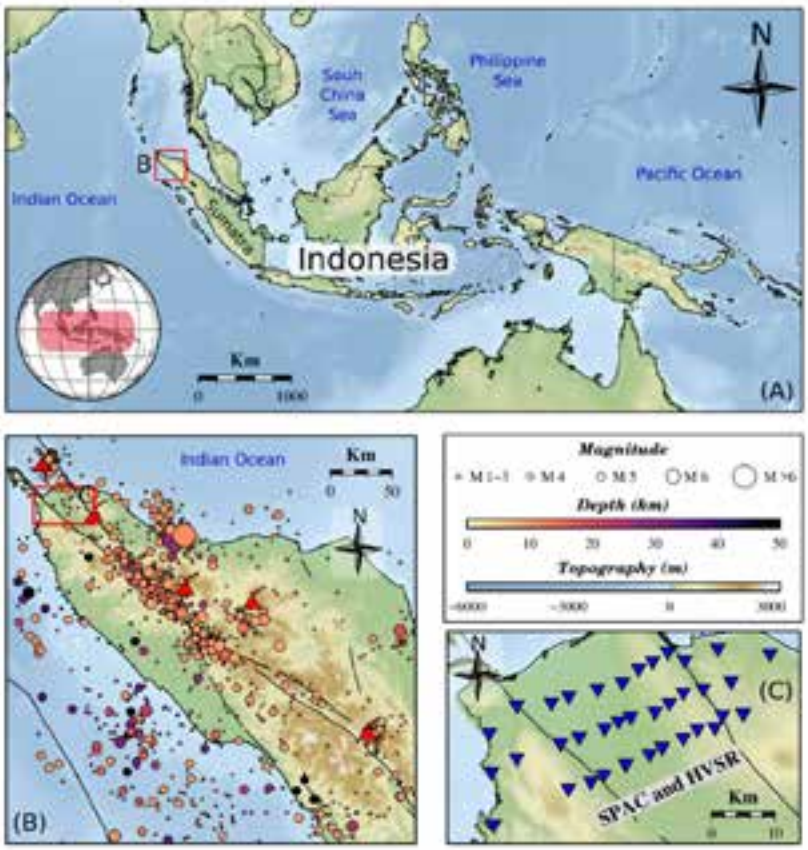

Fig. 1: (a) Geographical map of Indonesia and the study area in the Aceh Province. (b) Seismic activities map of Aceh Province showing earthquake distribution that mostly occurred along active faults and subduction zones. The red square marks the study area for this study in the Banda Aceh city and its surrounding. (c) The Study area in the Banda Aceh city and its surrounding and the observation points (blue triangle) while Aceh fault in the left part and Seulimeum fault in the right part (black line).

fault in the northeast (Muksin *et al.*, 2019). The Aceh fault marks the boundary between the Banda Aceh basin and the limestone formed from Jurassic to Cretaceous as an oceanic accretion rock that is part of the Woyla group (Barber *et al.*, 2005). In addition, the Seulimeum fault was formed within the volcanic Quaternary in the northwest of the Krueng Aceh basin (Siemon and Steuer, 2010). Therefore, Culshaw *et al.*, (1979) categorized this basin as a graben-type structure.

A previous study conducted by Asrillah *et al.*, (2019) indicated that the soil properties beneath the Banda Aceh basin have a Vs structure that generally dips down from SE to NW and gradually declines from SW to NE. This result may be affected by the soil type around the Seulimeum fault being denser than that around the Aceh fault, as also related to geology. As shown in Fig. 2, the geological structure in the Banda Aceh basin is dominantly formed by young alluvium sediments that can amplify ground shaking on the surface. With sandbar formations and material structures with a low density, Banda Aceh and Aceh Besar are likely to be earthquake- and liquefaction-prone zones. The current study aims to investigate the physical properties of the subsurface of the northernmost Sumatra. This study was carried out in Aceh Besar and Banda Aceh region in 2020.

MATERIALS AND METHODS

Data Acquisition

The experiment was conducted at 36 measurement points in the northernmost Sumatra

Fig. 2: Geological map of Banda Aceh and Aceh Besar regency (modified Barber et al., 1998). Most materials around the study area are composed of young alluvium (Qh), volcanic rocks (QTvt) and limestone (Murl) from the Cenozoic until the Tertiary. Measurement points are at 36 locations around Banda Aceh and Aceh Besar cross the Sumatran and Seulimeum faults, with the distance between each site being 5–10 km

covering the Banda Aceh city, the sedimentary basin and the Seulimeum and the Sumatran faults (Fig. 2). The measurement of microtremors using center-less triangle seismic arrays was performed using three high sensitivity geophones (80 V/m) with a natural frequency of 5 Hz and operating temperature range of −40 °C–80 °C. The instrument has a harmonic distortion of less than 0.1% and can thus reduce the problems caused by the overheating and overloading of power system equipment. The distance between sites was 5–10 km, and the data recording time for each site was 30–45 min. The geophones were set with a distance of 3 m as the center-less curricular array (Cho *et al.*, 2006); therefore, the array radius was 2.6 m. The sampling rate in the DSS Cube as the data logger was set to 100 sps (samples per second), and the effective resolution was set to 22 bits; at this condition, the recording of interval stability and time accuracy lasted 0.01 ms. Recordings were made by placing three one-component geophones at azimuths of 0°, 120°, and 240° into three-component (north–south, east–west, and vertical) channels of DSS Cube as the data logger. To derive the classification of rocks and soils, the data from the recordings were used to determine the shear velocity (Vs) beneath the measurement points based on the SPAC method. At the same locations, microtremors were also used by a Nanometrics trillium compact broadband seismometer with a sensitivity of 750 V/m ± 0.5%. The seismic waveforms were stored in DSS Cube. The recording was performed for 40 min for each site at a sampling rate of 100 sps. The data were used to determine the amplification and dominant frequency of the sites, as well as the value of seismic vulnerability, based on the HVSR method. These parameters represent the vulnerability of buildings or areas to be affected by earthquakes.

Vs modeling using SPAC

The SPAC method is used to obtain a dispersion curve (curve of frequency vs. phase velocity) and model the shear wave velocity structure (Vs) in the

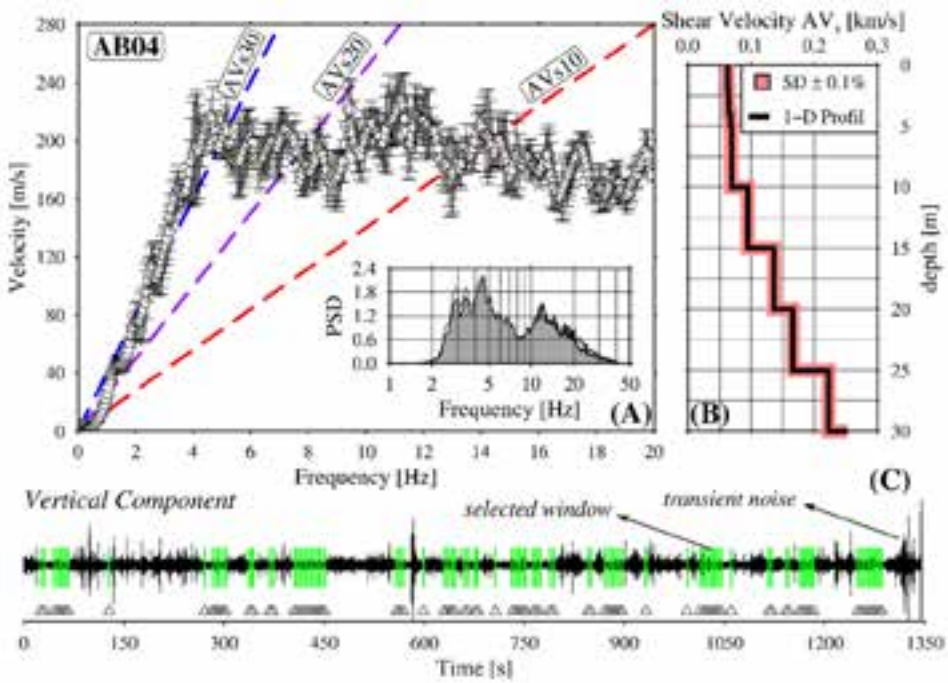

Fig. 3: (a) Dispersion curve of microtremors recorded at site AB09 describing the relationship between frequency and velocity following the linear trend (AVs_{1-10} (blue), AVs_{11-20} (purple), and AVs_{21-30} (red)). The AVs trend at a specific depth (10, 20, and 30 m) was set based on the average value in the thick layer at a shallow depth. (b) AVs was converted with Eq. 3 to obtain Vs as the representative value for a specific depth. The graph shows a three-layer graph formed by Vs over depths of 10, 20, and 30 m. (c) Example of waveform recording in the vertical component at AB09 and the segmentation window (green triangle)

subsurface layer based on microtremors (Thein *et al.*, 2015). A microtremor is assumed to be complex mixed waves consisting of Rayleigh waves that arrive from multiple directions to the field (Okada, 2006). Therefore, the accuracy of microtremor analysis is highly dependent on the shape and size of arrays. Such dependence is avoided by conducting microtremor array surveys using circular seismic arrays with a certain distance. In the SPAC method, observation records are transformed into the Fourier domain, and the autocorrelation function of each geophone is calculated. Autocorrelations calculated from a triangular array configuration are referred to as SPAC functions, useful in estimating dispersion curves, which help obtain subsurface structures under realistic conditions. In the current work, BIDO2.0 tool (Cho, 2019) was used to estimate the dispersion curve of the recorded microtremor data (Fig. 3a). The recorded data were filtered, with a range of 0.1–10 Hz. For the spectral analysis of microtremors, the recorded data were divided into 10.24 s segments (Fig. 3b) to avoid transient noise from civilian and machine activities near the measurement points. The segments containing significant data variations were removed from the calculation based on the short-term average–long-term average (STA/LTA) ratios (Fig. 3c). Selected quiet segments were used to calculate the power spectra and then smoothed by fitting the parzen windows with a bandwidth of 0.3 Hz. The SPAC coefficient was calculated by averaging all azimuths. A root-solving method combining the bisection and secant methods was applied to average the spectra ratio by fitting the Bessel function to search for the radius times the wavenumber rk and the parameter of the Bessel functions in the range [0, rk_{max}]. The value of rk_{max} corresponded to the first maximum or minimum function value. The obtained rk was used to calculate the phase velocity (c) using Eq. 1.

$$c = 2\pi \frac{f}{k} \quad (1)$$

Where, f is the frequency and k is the wavenumber. Given these parameters, the SPAC coefficient, averaged spectra ratio, and dispersion curve were calculated using the BIDO2.0 tool. In general, dispersion forms when waves propagate in the layers of soil and subsurface rocks with different velocity values. The crossing point between a dispersion curve and a surface wavelength proportional to the array radius and frequency represents the phase velocity of the corresponding wavelength (Fig. 3a). Thus, the averaged phase velocity (AVs) of the layered subsurface was obtained in this work. For example, AVs_{30} is the AVs between 0 m (surface) and 30 m. The average shear wave velocities for depths of 0–10 m, 11–20 m, and 21–30 m, labeled respectively as AVs_{10}, AVs_{20}, and AVs_{30}, are obtained when Rayleigh wave velocities correspond to the wavelengths of 13 m, 25 m, and 40 m (Cho *et al.*, 2008). The method has limited accuracy but effectively visualizes the relative spatial variations in shear wave velocities. In this research, three averaged velocity values were estimated: AVs_{10}, AVs_{20}, and AVs_{30}, for each site. With these values, Vs structure of the three-layer subsurface interval velocities can be determined using Eqs. 2, 3 and 4.

$$Vs_{(0-10\,m)} = AVs_{10} \tag{2}$$

$$Vs_{(11-20\,m)} = \frac{(AVs_{11} \cdot AVs_{20})}{(2 \cdot AVs_{11} - 2.AVs_{20}} \tag{3}$$

$$Vs_{(21-30\,m)} = \frac{(AVs_{21} \cdot AVs_{30})}{(3 \cdot AVs_{21} - 2 \cdot AVs_{30})} \tag{4}$$

The Vs values of the layers can be then compared with data from Tohari *et al.* (2015) who assessed the Vs values below stratum using the Cone Penetration Test.

Horizontal to Vertical Spectral Ratio

The HVSR has routinely been considered a quick tool to assess possible amplification effects in seismic hazard studies. The microtremor records in the time domain of the horizontal and vertical components were transformed into the frequency domain to obtain the horizontal and vertical spectra. The current work used the method by Nakamura (1989) involving the HVSR of the single station microtremor records. Generally, the amplitude of a vertical component does not change significantly, whereas that of a horizontal component is affected by soil properties. Vertical components cannot be amplified around frequency ranges, in which horizontal components receive large amplification (Nakamura, 2000). Nakamura (2000) assumed that the horizontal-to-vertical (H/V) spectrum as a frequency function is closely related to the site transfer function of shear waves and that the HVSR represents one of the amplification factors. The different H/V values for the three locations indicate the variations of the site conditions representing the rock properties of the area. In Nakamura's method (Nakamura, 1989, 2000), the local effect arising from surface geology is calculated by the spectral ratio of the horizontal and vertical components (i.e., HVSR) using Eq. 5.

$$\frac{H}{V} = \frac{\sqrt{NS^2 + EW^2}}{V} \tag{5}$$

Where, NS is the spectrum amplitude of the north–south component, EW is the east–west component, and V is the vertical component. The amplitude of the horizontal component (NS and EW) was averaged using the root mean square equation and subsequently divided by the amplitude of the vertical component to obtain the average H/V spectrum. From the H/V spectrum, the dominant frequency and period (f and T) were obtained, as well as the H/V peak, associated with the amplification (A) at each measurement location. The dominant frequency is closely related to the lithological conditions and thickness of the subsurface. Low dominant frequency values are associated with thick layers of soft sedimentary sub surfaces, whereas high dominant frequencies are related to thin subsurface layers (Gallipoli *et al.*, 2004; El-Hady *et al.*, 2012). The high value for a dominant period (low dominant frequency) is due to the thick layer of sediments in the subsurface that trap Rayleigh waves for long periods (Stanko et al., 2017). The H/V spectrum is mostly influenced by wave speed and rock density. If the wave speed is low, the H/V value is high. Furthermore, the amplification value is large for areas composed of low-density rocks or soil. Seismic surface waves propagate slowly in soft sediments, and ground shaking can be amplified and thereby cause severe damage. The seismic vulnerability index (K_g) can be calculated by dividing the square of the

amplification by the dominant frequency value using Eq. 6 (Nakamura, 1989).

$$K_g = \frac{A^2}{F} \quad (6)$$

The Kg value is used to identify soft soil regions and qualitatively estimate possible damage areas (Gosar, 2007; Beroya-Eitner *et al.*, 2009; Asten *et al.*, 2014; Pamuk *et al.*, 2018). Many researchers have used the HVSR method to characterize soil resonance frequency and calculate the vulnerability parameters used for earthquake mitigation plans (Tün *et al.*, 2016; Maresca *et al.*, 2018; Alamri *et al.*, 2020).

RESULTS AND DISCUSSION

Shear wave velocity

An example of the recorded data and the 1D velocity modelling for site AB09 is shown in Fig. 3. The microtremor data were bandpass filtered, with a frequency of 0.1–10 Hz and segmented into several 10 s windows. All segments were converted into the frequency domain using fast Fourier transform to obtain the dispersion curve (Fig. 3a) for the measurement point of AB09. Phase velocity is inversely proportional to frequency, increasing over depth. The dispersion curve for site AB09 shown in Fig. 3 reflects the average shear velocity (AVs) controlled by the frequency range depending on the physical properties of rocks at a depth of 30 m. The relationship between AVs and frequency suggests the vertical heterogeneity of the structure beneath the site. The difference values of the shear wave velocity at all points indicate the lateral heterogeneity of the rocks in the subsurface at a depth of 30 m.

The AVs value at a depth of 20–30 m was 180 m/s (5.9 Hz), while that at 10–20 m is 160 m/s (7.7 Hz). The increasing value of AVs over certain depths suggests increasingly compact rocks or soil in deep layers. Given the average velocity AVs, the shear wave velocity Vs at a certain depth can be determined using Eq. 3. The values of Vs of 100, 160, and 200 m/s at depths of 10, 20, and 30 m, were obtained respectively. The example of Vs beneath site AB09 is shown in Fig. 3b. The graph of Vs is more representative than that of AVs as it shows the increase of Vs at certain depths. The Vs values were interpolated in the vertical and horizontal directions to observe the structure beneath the study area for further analysis. The thickness of the sedimentary layer and the identification of the geological structure can be investigated from the vertical cross section shown in Fig. 4. Three vertical slices showing the structure of the subsurface are provided. Parallel lines crossing the Sumatran and Seulimeum faults were chosen to differentiate the lithologies along the lines. The type of soil along the A-B profile at a depth of 1–10 m with a Vs range of 80–100 m/s is considered as class E soil (Table 1). At greater depths, the soil is classified as class D soil. The Banda Aceh basin can also be seen beneath profiles C–D and E–F in Fig. 4.

The thickness of the sedimentary layer and the identification of the geological structure can be investigated from the vertical cross section in Fig. 4. Three vertical slices showing the structure of the subsurface were presented. Parallel lines crossing the Sumatran and Seulimeum faults differentiate the lithologies along the lines. The type of soil along the A-B profile at a depth of 1–10 m with a Vs range of 80–100 m/s is considered class E soil while at the greater depths, the soil is classified as class D soil (Table 1). The sediment formation of the Banda Aceh basin can also be seen beneath profiles C–D and E–F in Fig. 4 with a similar range. The Vs_{30} figure that is vital for earthquake hazard analysis was presented. The Vs_{30} are different in each station due to the subsurface condition. In Fig. 5, the 1-D velocity model ranges higher to the active fault while lower to the central part.

Fig. 5 shows the lateral variation of the Vs_{30} values between 200 and 240 m/s. The high value of Vs_{30} (between 215 and 220 m/s) is located along the high elevation in the Sumatran fault. The lowest value of Vs_{30} is located in the Banda Aceh basin at 210 m/s (Fig. 4).

Seismic vulnerability

The seismic records were used with minimal transient effect by applying the anti-triggering STA/LTA, with a minimum threshold of 0.1–0.5 s and a maximum threshold of 1.5–2.0 s. After reducing the transient effect in the evaluation stages, a bandpass filter, with a range of 0.005–20 Hz with a 5% cosine taper, was used. The time domain microtremors were converted to frequency domain ones and then windowed using the Konno–Ohmaci method (1998) with b = 40 bandwidth. The spectral ratio graphics

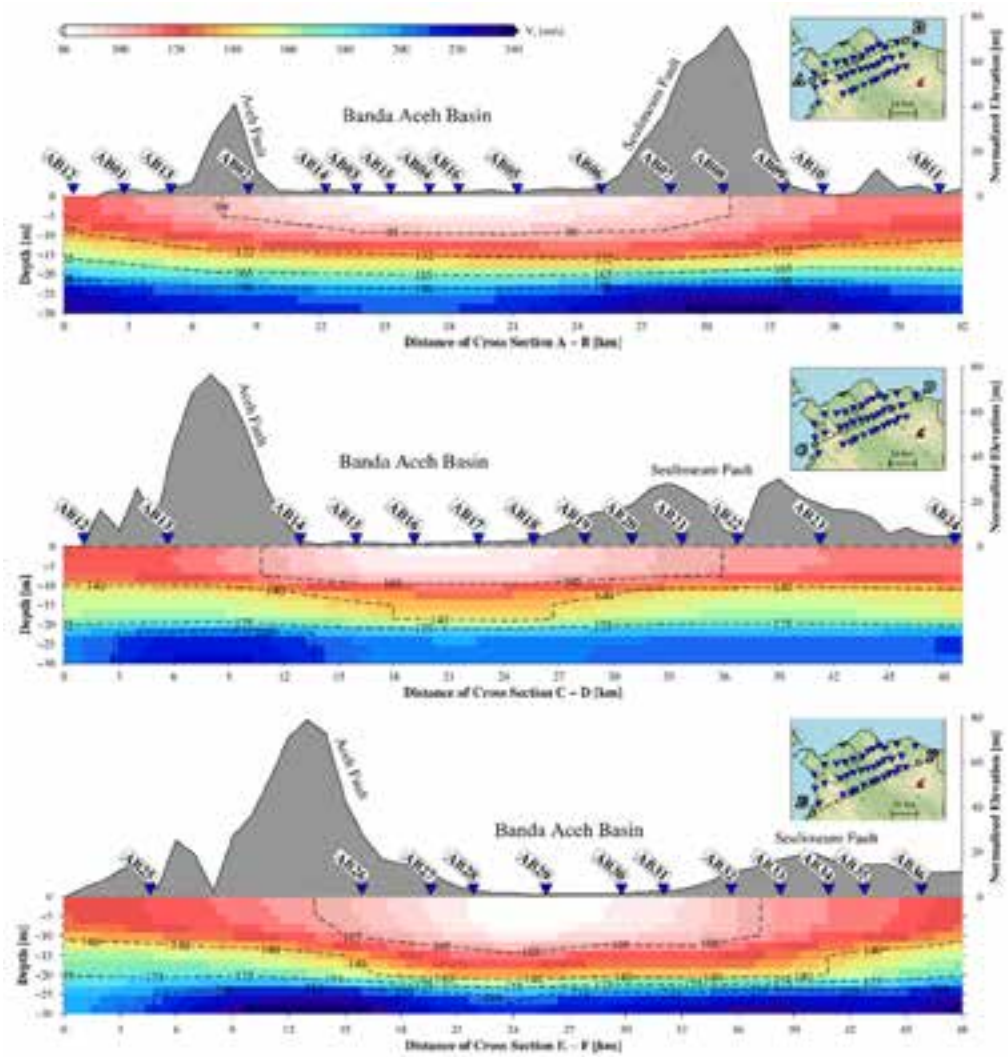

Fig. 4: Three slices are set up to figure the vertical profile of Vs over depth along lines (a) A–B, (b) C-D, and (c) E-F, respectively. The vertical profiles clearly show the existence of the Banda Aceh basin that stand on alluvial sediment in the central part, while the Aceh and Seulimeum fault stand on limestone and volcanic structure in the left and right part

Table 1**:** Five clusters classified from different geophysical parameters (the geological map is considered to define the possible types of rocks)

Cluster	Amplification (A)	Frequency (f)	Vs30	Soil class	Possible types of rocks
I	Low–Moderate	Moderate–High	High	E–D	Young Alluvium
II	Moderate	Low–Moderate	Low	D	Alluvial Sediment
III	High	Low–Moderate	Low	E	Young Alluvial Sediment
IV	Moderate	Moderate	Moderate	D	Limestone
V	Low	High	High	C	Volcanic Rock

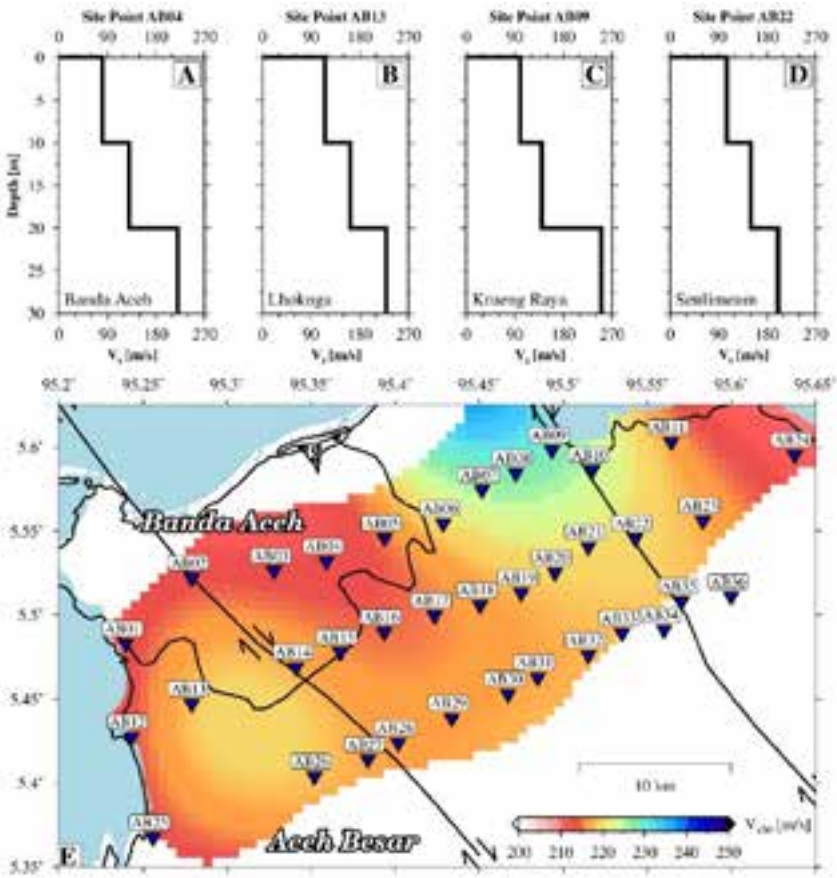

Fig. 5: (a) Examples of 1D velocity model derived from microtremor data obtained by SPAC beneath four sites AB04, AB13, AB09, and AB22; and (b) horizontal profile view of Vs30 as a result of the interpolation of Vs values at all locations

were then obtained by calculating the ratio of the horizontal components to the vertical components as the H/V amplitude. Three examples of microtremor recorded at different locations (along the Sumatran fault, Seulimeum fault, and Banda Aceh basin) and the results of the HVSR analysis are shown in Fig. 6. The different H/V values for the three locations indicate the variations of the site conditions depending on the rock properties of the area.

After analyzing the data from all sites, the values were compiled and the dominant period (T) and vulnerability index (K_g) were calculated. The maps of the dominant frequency and period, the H/V values, and the vulnerability index are provided in Fig. 7. High dominant frequencies were recorded along the Sumatran and Seulimeum faults, while low frequency microtremors were recorded in the Banda Aceh basin of the study area (Fig. 7). In contrast to dominant frequencies, low dominant periods were observed along the faults (Fig. 7b). The authors also calculated the amplification value (A) (Fig. 7c) from the vertical axis of the peak of the H/V curve. Low H/V values were found along the two main faults because hard rocks constituted the areas. Meanwhile, the Banda Aceh basin was characterized by high values of amplification; thus, the seismic vulnerability K_g was also high. As shown in Fig. 7, the highest value of K_g is located in the basin area, while the values of K_g along the two active faults are relatively low.

Statistically, all geophysical properties from HVSR and SPAC analysis can be analyzed to measure the correlation between those parameters, as shown in Fig. 8. Each square provides the correlation values between the variables on each axis, ranging from -1 to +1. The small correlation coefficient (closer to zero) means no linear trend between the two variables,

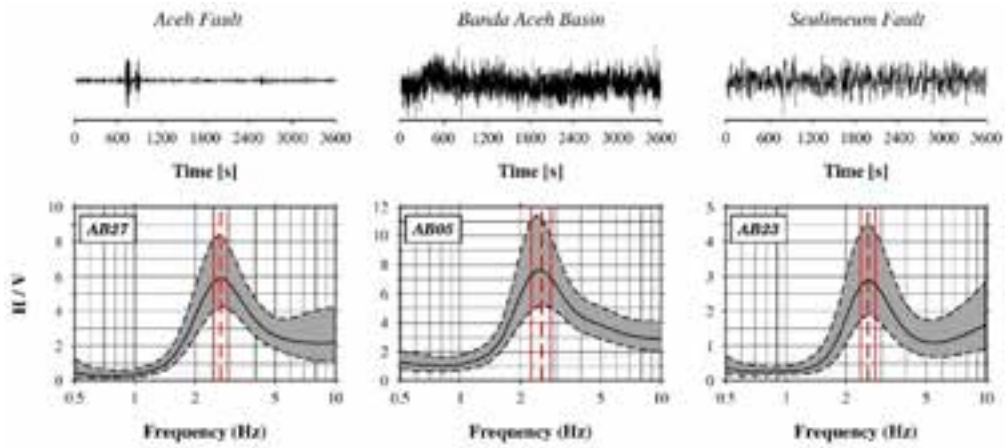

Fig. 6: Three recording examples in AB27, AB05, and AB23 show different waveforms depending on site properties. The spectrum analysis of AB27, AB05, and AB23 generated a normal curve graph of amplitude (A) and frequency (f)

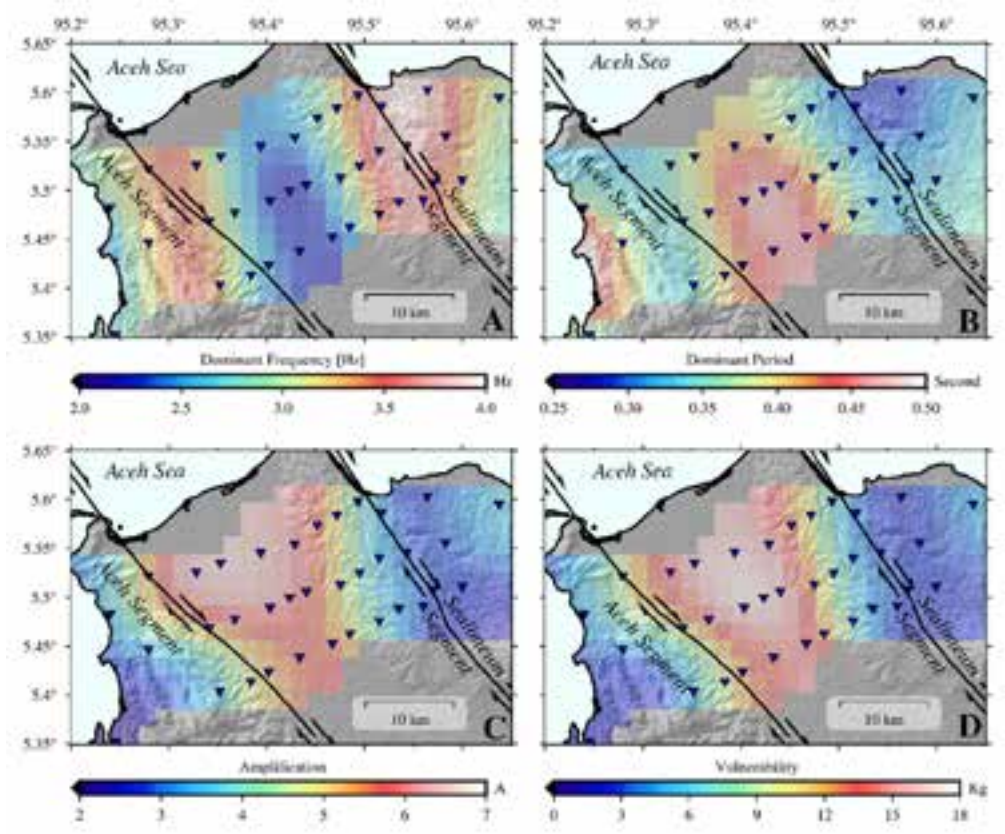

Fig. 7: Maps of (a) dominant frequency, (b) dominant period, (c) amplification, and (d) vulnerability index resulting from HVSR analysis

while the closer to 1 correlation value indicates a positive correlation between the two parameters. The values closer to -1 also indicate a good correlation between parameters. The frequency parameter strongly correlates to shear wave velocity at a depth of 20 m but almost independent seismic amplification.

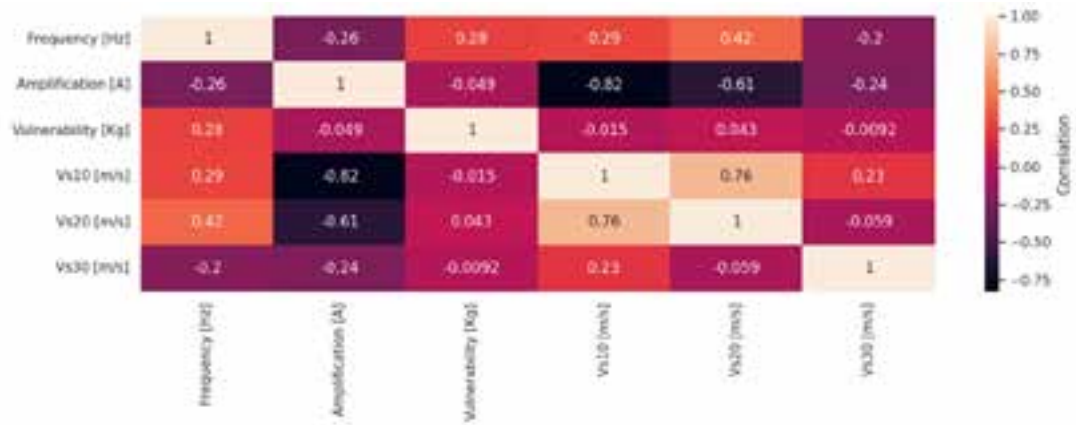

Fig. 8: Correlation index of seismic parameters: frequency, amplification, vulnerability, and shear wave velocities

The amplification has a weak relationship with shear wave velocity at a depth of 10 m. The vulnerability positively correlates to frequency and shows no correlation to shear wave velocity (Vs).

General interpretation of physical properties

The soil or rock characteristics were derived from the geophysical parameters of dominant frequency, amplification, and shear velocity. The authors connected Vs_{30} with the H/V parameters to classify the soil properties into different categories, following the recommendation from the 1997 NEHRP; (Boore, 2004). The clustering results showed different soil classes: soft soil (E), rigid soil (D), and soft rock (C), as specified in Table 1. In most sites, nearly uniform Vs values of over 200 m/s in the third layer (21–30 m) were found, regarded as a more compact and steadier structure than the upper layer.

The soil or rocks at certain depths were considered stiff, given high values of Vs (Fig. 4). Such structures are classified as the class D. The Vs value of the third layer at a depth of 30 m, i.e., Vs_{30}, is important because it is often used in geotechnical investigations. It highlights the characteristics of rocks at a depth of 30 m. The results of the SPAC and H/V analyses indicate a reciprocal relationship between the different geophysical parameters. The area was clustered based on different geophysical properties, Vs_{30}, amplification, and dominant frequency (Fig. 9). The area with physical properties of low Vs_{30}, high amplification, and relatively high dominant frequency was called Cluster I, and the rock type was classified as class E. Clusters II and III had Vs_{30} values between 210 and 228 m/s with a relatively low amplification of 2.5–6. The area with amplification between 2–3, Vs_{30} between 230–244, and dominant frequency of 3–4 Hz was called Cluster IV. Cluster V had the highest values of Vs_{30} between 250–265 and, thus, the highest density; it also had the lowest amplification values and was considered the least seismically prone area. The maps of the clusters in Fig. 7 are shown in Fig. 9 to discuss the seismic soil properties of each area.

Cluster I (Banda Aceh)

Cluster I, where Banda Aceh is located (Fig. 9), is the most important area in this study because it is a densely populated region and is the center of economic and governmental activities. Banda Aceh, standing above the basin, is predominantly composed of alluvium (Fig. 2). This soil type correlates with low Vs, high amplification, and low dominant frequency (Fig. 8). The interpolation of Vs from the first slice A–B shown in Fig. 4 indicates the existence of the Banda Aceh basin and two active faults in the northern part of the study area. Asrillah *et al.* (2019) also profiled the top layer of the Banda Aceh basin as less dense with soft soil and slightly flat layered sediments. The less-dense soil at the top surface is associated with the young alluvium (Qh) suggested by Barber (1998) in the geological map (Fig. 2). From the Cone Penetration Test data, Tohari *et al.* (2015) suggested that the topsoil layers in Banda Aceh mainly consists of clay and sand, coinciding with low shear wave velocity found by this study. During the 2004 Sumatra–Andaman tsunami, many reports raised a possible liquefaction phenomenon in Banda Aceh.

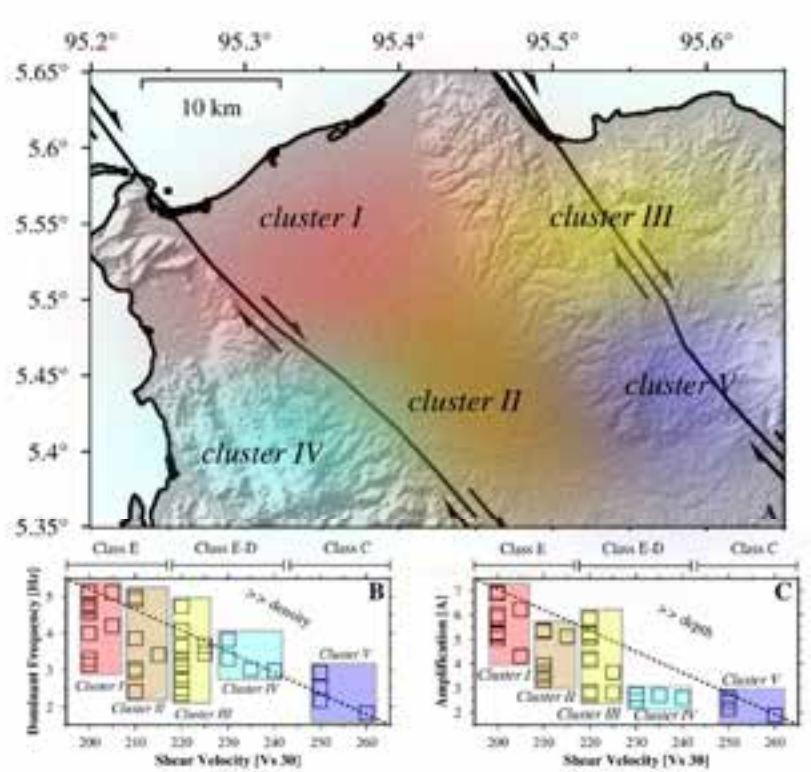

Fig. 9: Clusters of zonation derived from the combination of Vs_{30}, dominant frequency and amplification (A). There is five clusters specifically located by different parameters, Cluster I in the Banda Aceh Basin, called the Banda Aceh cluster, Cluster II in the southern part of Basin Aceh, called the Jantho cluster, cluster III in the northern part of Seulimeum fault, called the Krueng Raya cluster, cluster IV along Aceh fault, called the Lhoknga-Lhoong cluster, and cluster V along Seulimeum fault and Mount Volcano of Seulawah Agam, called the Seulawah cluster

Meanwhile, seismic activities from the two closest active faults, namely, Aceh and Seulimeum, can cause shock effects. Large earthquakes along the two faults with high intensity can potentially cause liquefaction in Banda Aceh (Jalil *et al.*, 2020). Rusydy, *et al.* (2020) analyzed whether an earthquake with Mw 7.0 can cause massive structural damage throughout Banda Aceh; if such an earthquake occurs during the day, their estimates showed a fatality rate of 3.5%–20% of the total population in buildings in general and economic losses reaching thousand million USD.

Cluster II (Jantho)

Jantho Cluster (Cluster II) is characterized by low Vs_{30} and high seismic amplification. The soil and rocks in this area consist of a variety of sedimentary and rock structures, such as the Idi Formation (Idi), Lam Teuba Volcano Formation (QTvt), Seulimeum Formation (QTps), Jantho Complex Formation (Tuic), Meucampi Formation (Tim), and Alluvium Formation. These various formations are due to the cluster location in the complex of the meeting point of the Aceh and Seulimeum faults. This cluster's soil material has been formed since the Late Jurassic to the Holocene because it is incorporated in the Seulawah and Lhoknga–Raba structures. The amplification value is moderate, while the frequency is in the low–moderate range. Vs_{30} is low because the material predominantly contains alluvial sediments but is denser than the same material in the Banda Aceh cluster. This cluster is also located in the same basin as Banda Aceh, and the soil is categorized class D (Tabel 1). The measurement results in this cluster prove the existence of the Banda Aceh basin in the southern part up to the meeting point of the Aceh and Seulimeum faults.

Cluster III (Krueng Raya)

The Krueng Raya cluster is located at the northernmost part of the Seulimeum fault, close to the coastline. The area's rock formation has been formed since the Pleistocene–Holocene with three different formations: Young Alluvium (Qh), Lam Teuba Volcanic (QTvt), and Seulimeum Formation (QTps). The volcanic rock material in this cluster mainly influences the surface profile and other eruption products, such as lahar and pyroclastic flows. The parameter results indicate that the soil group in this cluster is class D, given the moderate amplification value, dominant frequency, and Vs_{30}. In 1936, the northern part of the Seulimeum fault generated an earthquake with a magnitude of M 7.0, causing the collapse and damage of several buildings and leading to several fatalities in the Lam Teuba district. Thus, the vulnerability index is moderate, meaning that a building must match the dominant period (~0.3 s). Furthermore, the cluster has the exact topographical contours as the Lhoknga-Lhoong cluster with a dense rock structure.

Cluster IV (Lhoknga-Lhoong area)

Cluster IV (Lhoknga-Lhoong area) is located in the western part of the Aceh fault, and the subsurface sediments in this area contain alluvium and limestone. The geological formations, such as the Raba Limestone (Murl), Lhoknga Formation (Mul), and Peunasu Formation (Tlp), were formed from the Late Jurassic to the Early Cretaceous. The values of Vs_{30} suggest that the soil in the Lhoknga-Lhoong cluster is categorized class E–D, with low–moderate amplification value, moderate–high dominant frequency, and low Vs_{30}. The moderate–high value range is mainly influenced by the density of the rock structures scattered along the Aceh fault. The vulnerability index in the Lhoknga-Lhoong cluster is relatively low because of the linear relationship between amplification and frequency. Moreover, an active fault passes through this cluster, and thus, mitigation measures must be implemented to reduce destructive effects in the future. No major event has been recorded in the last 170 years in the Aceh segment, but major earthquakes remain possible (Ito *et al.*, 2012).

Cluster V (Seulawah)

The Seulawah cluster is located in the central part of Seulimeum is and close to the Seulawah Agam stratovolcano zone. Most of the rock structures in Lam Teuba Volcanism (QTvt) contain volcanic rocks, formed since the Holocene. The dominant parameter shows high frequency recordings because the rock material is dense and provides low amplification. This soil is class C and is allowed for high construction though other parameters, such as the peak ground acceleration, or possible earthquake intensity. The Vs_{30} is also high, indicating that the subsurface soil properties may support basic construction. This cluster stands on the active Seulimeum fault that moves at a ~2 cm/year slip rate and can produce earthquakes with magnitudes of up to M 7.0. The Seulimeum earthquake in 1930 inflicted significant damages and resulted in many fatalities. This cluster can also be associated with the Seulawah stratovolcano, reported being active in 1839, 1975, and 2010. Volcanic tremors can also be triggered by microseismicity in the central part of the Seulimeum fault.

CONCLUSION

The combination of shear wave velocity, determined by the Spatial Autocorrelation method and parameters of dominant frequency and seismic amplification derived from Horizontal-to-Vertical Ratio, was used to classify the soil properties beneath the northernmost Sumatra, one of the most seismically active regions. The clusters classified from the variation of geophysical data coincide well with geological properties from previous research and studies. Five different clusters representing various types of rocks were classified based on three different seismic properties recorded from the microtremor study at 36 points, covering the sedimentary basin, the active faults, and the Banda Aceh city and its surroundings. The highly populated Banda Aceh city (Cluster I) is among the most vulnerable areas because it stands on a thick sedimentary basin characterized by high amplification and low shear wave velocity. The low-velocity values in Banda Aceh indicate the soft soil types of rock, as observed by the previous study using the Cone Penetration Tests. Therefore, a detailed investigation is required before constructing large and high-altitude infrastructure in Banda Aceh. Cluster II (Jantho) and III (Krueng Raya) are the second most vulnerable areas because the regions are characterized by moderate shear wave

velocity and seismic amplification and are located along the Sumatran and the Seulimeum faults, respectively. The limestone is exposed in Cluster IV, correlating well to the moderate value of Vs and low amplification. Although the Seulawah volcanic region (Cluster V) is categorized by high shear wave velocity, low frequency and low seismic amplification, it is also considered a vulnerable area since it is located along the Seulimeum active fault. The sedimentary layer between the two active faults is imaged by low shear wave velocity along the three vertical profiles. The lateral variation of each geophysical property was mapped by interpolating the wide distance data points at the unsampled locations so that the anomalies between the data points could be missed. However, the research results provide a good picture of the regional structure. A comprehensive study with denser measurement points for Vs and HVSR needs to be conducted to better describe the properties of rocks. The detailed survey and analysis will support the currently available and less-resolution geological map of the study area.

AUTHOR CONTRIBUTIONS

Y. Asnawi contributed in conducting field experiment, HVSR data analysis and drafting the manuscript. A. Simanjuntak performed SPAC data analysis, produced maps and figures as well as interpreted the results. U. Muksin is the corresponding author and the leader of the project who provided funding for the project. S. Putri involved in data acquisition and SPAC data analysis. M. Okubo performed SPAC data analysis and wrote Method part of the manuscript and provided funding supported JSPS KAKENHI. S. Rizal supervised the field experiment and data analysis as well as provided critical revision of the manuscript. M. Syukri supervised the data acquisition in the field and data analysis.

ACKNOWLEDGEMENT

This scientific collaboration between Indonesian and Japanese scientists was supported by JSPS KAKENHI under grant number [17H04577] and Doctoral Dissertation Research Program under grant number [66/UN11.2.1/PT.01.03/DPRM/2021].

CONFLICT OF INTEREST

The authors declare no potential conflict of interest regarding the publication of this work. In addition, the ethical issues including plagiarism, informed consent, misconduct, data fabrication and, or falsification, double publication and, or submission, and redundancy have been completely witnessed by the authors.

ABBREVIATIONS

%	Percentage value
°C	Degree in Celsius
0–10 m	Depth between 0 – 10 m
0°	Azimuth angle in 0 degree
10–20 m	Depth between 11 – 20 m
1D	1-Dimension profile
20–30 m	Depth between 21 – 30 m
A	Amplification
A	Amplitude
A-B	Line of cross section from A to B
A^2	Square of the amplification
AB04	04th observation Point
AB05	05th observation Point
AB09	09th observation Point

AB13	13th observation Point
AB22	22th observation Point
AB23	23th observation Point
AB27	27th observation Point
AVs	Average shear velocity
AVs_{10}	Average shear velocity at 0 – 10 m
AVs_{20}	Average shear velocity at 11 – 20 m
AVs_{30}	Average shear velocity at 21 – 30 m
B	Bandwidth coefficient
BIDO2	SPAC analysis program
Bits	Bit per sample
c	Phase velocity
C	Soil class for sediment – Rock
C-D	Line of cross section from C to D
Cm	Centimetre
cm/year	Centimetre over year
D	Soil class for sediment
DSS	Decision Support System
E	Soil class for soft sediment
E-D	Soil class between soft sediment and hard soil
E-F	Line of cross section from E to F
e.g.	Latin phrase example gratia (for example)
Eq	Equation
EW	Spectrum amplitude in the horizontal east-west component
EW	East-west
F	Frequency
f	Dominant frequency
Fig.	Figure
H/V	The horizontal-to-vertical spectrum
H/V peak	Maximum peak of horizontal-to-vertical spectrum
HVSR	Horizontal to vertical spectral ratio
Hz	Hertz
i.e.	Latin phrase Id est (this is)
Idi	Idi Formation
K	Wavenumber
K_g	Seismic vulnerability index
Km	Kilometre
M	Meter
M	Magnitude
m/s	Meter per second
min.	Minute
Ms	Millisecond
Mul	Lhoknga formation
Murl	Lhoknga limestone rock
NEHRP	National Earthquake Hazards Reduction Program
NS	Spectrum amplitude in the horizontal north–south component
NS	North-South
NW	North-West
Qh	Alluvial sediment structure
QTps	Seulimeum formation
Qtvt	Lam Teuba Volcanic
Rk	Radius between geophone
rk_{max}	Maximum radius between geophone
S	Second
SPAC	Spatial autocorrelation
sps	Sampling per second
STA/LTA	Ratio between the amplitude
SW	South-West
T	Period
Tim	Meucampi formation
Tlp	Peunasu formation
Tuic	Jantho complex formation
USD	United State Dollar
V	Spectrum amplitude in the vertical component of seismic waveform
V/m	Seismometer sensitivity (volt/meter)
Vp	Velocity of pressure
Vs	Share velocity

$Vs_{(0\text{-}10\ m)}$	Shear wave velocities for depths of 0–10 m
$Vs_{(11\text{-}20\ m)}$	Shear wave velocities for depths of 11–20 m
$Vs_{(21\text{-}30\ m)}$	Shear wave velocities for depths of 21–30 m
Vs_{10}	Shear wave velocities for depths of 0–10 m
Vs_{20}	Shear wave velocities for depths of 11–20 m
Vs_{30}	Shear wave velocities for depths of 21–30 m
Z	Vertical Component
π	Pi is a mathematical constant (3,14159)

REFERENCES

Alamri, A.M.; Bankher, A.; Abdelrahman, K.; El-Hadidy, M.; Zahran, H., (2020). Soil site characterization of Rabigh City, western Saudi Arabia coastal plain, using HVSR and HVSR inversion techniques. Arab. J. Geosci., 13(2): 1- 16 (**16 pages**).

Arai, H.; Tokimatsu, K., (2005). S-wave velocity profiling by joint inversion of microtremor dispersion curve and horizontal-to-vertical (H/V) spectrum. Bull. Seismol. Soc. Am., 95(5): 1766–1778 (**13 pages**).

Asrillah, A.; Marwan, M.; Muksin, O.; Ibnu, R.; Takao, S.; Yoshinori, F.; Yuichiro, M.; Hikime, C., (2019). Estimation of vs structure of Krueng Aceh and its suburb basin of Aceh Province, Indonesia. Derived from microtremor measurements. Geosciences. 1–12 (**12 pages**).

Asten, M.W.; Askan A.; Ekincioglu E.E.; Sisman F.N.; Ugurhan B., (2014). Site characterisation in north-western turkey based on SPAC and HVSR analysis of microtremor noise. Explor. Geophys., 45(2): 74–85 (**12 pages**).

Barber, A.J.; Crow, M.J.; J. S. Milsom, (2005). Sumatra: geology, resources and tectonic evolution. J. Geol. Soc., 31 (**282 pages**).

Beroya-Eitner, M.A.; Aydin A.; Tigloa R.; Lasala M., (2009). Use of microtremor in liquefaction hazard mapping. Eng. Geol., 107: 140–153 (**14 pages**).

Bilham, R., (2009). The seismic future of cities. Bull. Earthquake Eng., 7(4): 839–887 **(49 pages)**.

Boore, D.M., (2004). Estimating Vs (30) (or NEHRP site classes) from shallow velocity models (Depths < 30 m). Bull. Seismol. Soc. Am, 94: 591–597 (**7 pages**).

Chávez-García, F.J.; Kang, T.S., (2014). Lateral heterogeneities and microtremors: limitations of HVSR and SPAC based studies for site response. Eng. Geol., 174: 1–10 **(10 pages)**.

Cho, I., (2019). Two-sensor microtremor SPAC method: potential utility of imaginary spectrum components. Geophys. J. Int., 220(3): 1735-1747 (**13 pages**).

Cho, I.; Tada, T.; Shinozaki, Y., (2004). A new method to determine phase velocities of Rayleigh waves from microseisms. Geophysics. 69(6): 1535–1551 (**17 pages**).

Cho, I.; Tada, T.; Shinozaki, Y., (2006). Centerless circular array method: inferring phase velocities of rayleigh waves in broad wavelength ranges using microtremor records. J. Geophys. Res.: Solid Earth. 111(9): 1-12 (**12 pages**).

Cho, I.; Tada, T.; Shinozaki, Y., (2008). A new method of microtremor exploration using miniature seismic arrays: quick estimation of average shear velocities of the shallow soil. Butsuri-Tansa Geophys. Explor., 61(6): 457–468 (**12 pages**).

Claprood, M.; Asten, M.W.; Kristek, J., (2012). Combining HVSR microtremor observations with the SPAC method for site resonance study of the Tamar Valley in Launceston. Geophys. J. Int., 191(2): 765-780 (**16 pages**).

Culshaw, M.G.; Duncan, S.V.; Sutarto, N.R., (1979). Engineering geological mapping of the Banda Aceh alluvial basin, Northern Sumatra, Indonesia. Bull. Int. Assoc. Eng. Geol., 19(1): 40–47 (**8 pages**).

El-Hady, S.; Ferqany, E.AA.; Othman, A.; Mohamed, G.E.A., (2012). Seismic microzonation of Marsa Alam, Egypt using inversion HVSR of microtremor observations. J. Seismolog., 16(1): 55–66 (**12 pages**).

Forte, G.; Chiocarelli, E.; De Falco, M; Cito, P.; Santo, A.; Lervolino, I., (2019). Seismic soil classification of Italy based on surface geology and shear-wave velocity measurements. Soil Dyn. Earthquake Eng., 122:79–93 (**15 pages**).

Gallipoli, M.R.; Mucciarelli, M.; Galliaccio, S.; Tropeano, M.; Lizza, C., (2004). Horizontal to vertical spectral ratio (HVSR) measurements in the area damaged by the 2002 Molise, Italy, earthquake. Earthquake Spectra. 20(SPEC. 1): 81-93 (**13 pages**).

Goda, K.; Kiota, T.; Fokhrel, R.M.; Chiaro, G.; Katagiri, T.; Sharma, K.; Wilkinson, S., (2015). The 2015 Gorkha Nepal earthquake: insights from earthquake damage survey. Front. Built Environ., 1(8): (**15 pages**).

Gosar, A., (2007). Microtremor HVSR study for assessing site effects in the bovec basin (nw slovenia) related to 1998 Mw5.6 and 2004 Mw5.2 earthquakes. Eng. Geol., 91(2–4): 178–193 (**16 pages**).

Hollender, F.; Cornou, C.; Deschamp, A.; Oghalaei, K.; Renalier, F.; Moufroy, E.; Burnouf, C.; Thomassin, S.; Wathelet, M.; Bard, PY.; Boutin, V.; Desbordes, C.; Isabelle, DB.; Foundotos, L.; Cedric, GB.; Perron, V.; Regnier, J.; Roulle, A.; Langlais, M.; Sicillia, D., (2018). Characterization of site conditions (soil class, VS30, velocity profiles) for 33 stations from the French permanent accelerometric network (RAP) using surface-wave methods. Bull. Earthquake Eng., 16(6): 2337–2365 (**29 pages**).

Idris, Y.; Cummims, P.; Rusydy, I.; Muksin, U.; Syamsidik; Habibie, M.Y.; Meilanda, E., (2019). Post-earthquake damage assessment after the 6.5 Mw earthquake on December, 7th 2016 in Pidie Jaya, Indonesia. J. Earthquake Eng., 1–18 (**18 pages**).

Ito, T.; Gunawan, E.; Kimata, F.; Tabai, T. Simons, M.; Meilano, I.; Agustan; Ohta, Y.; Nurdin, I.; Sugiyanto, D., (2012). Isolating along-strike variations in the depth extent of shallow creep and fault locking on the northern Great Sumatran Fault. J. Geophys. Res. 117(510): 1–16 (**16 pages**).

Jalil, A.; Fathani, T.F.; Satyarno, I.; Wilopo, W., (2020). A study on the Liquefaction potential in Banda Aceh city after the 2004 Sumatera earthquake. International Journal of GEOMATE, 18: 147-155 (**9 pages**).

Kanli, A.I.; Tildy, P.; Pronay, Z.; Pinar, A.; Hermann, L., (2006). Vs30 mapping and soil classification for seismic site effect evaluation in Dinar Region, SW Turkey. Geophys. J. Int., 165(1): 223–235 (**13 pages**).

Maresca, R.; Nardone, L.; Gizzi, F. T.; Potenza, M. R., (2018). Ambient noise HVSR measurements in the Avellino Historical Centre and surrounding area (Southern Italy). Correlation with surface geology and damage caused by the 1980 Irpinia-Basilicata earthquake. Measurement. 130: 211–222 (**12 pages**).

Matsuoka, M.; Wakamatsu, K.; Fujimoto, K.; Midorikawa, S., (2006). Average shear-wave velocity mapping using Japan engineering geomorphologic classification map. Structural Engineering/Earthquake Engineering, 23(1): 58-67 (**10 pages**).

Muksin, U.; Irwandi; Rusydy, I.; Muzli; Erbas, K.; Marwan; Asrillah; Muzakir; Ismail, N., (2018). Investigation of Aceh segment and Seulimeum fault by using seismological data; A preliminary result. J. Phys. Conf. Ser., 1011(1): (**5 pages**).

Muksin, U.; Bauer, K.; Muzli, M.; Ryberg, T.; Nurdin, I.; Masturiyono, M.; Weber, M., (2019). AcehSeis project provides insights into the detailed seismicity distribution and relation to fault structures in Central Aceh, Northern Sumatra. J. Asian Earth Sci., 171: 20–27 (**8 pages**).

Muzli, M.; Muksin, U.; Nugraha, A. D.; Bradley, K. E.; Widiyantoro, S.; Erbas, K.; Jousset, P.; Rohadi, S.; Nurdin, I.; Wei, S., (2018). The 2016 Mw 6.5 Pidie Jaya, Aceh, North Sumatra, earthquake: Reactivation of an unidentified sinistral fault in a region of distributed deformation. Seismol. Res. Lett., 89(5): 1761–1772.

Nakamura, Y. (1989)**.** A method for dynamic characteristics estimation of subsurface using microtremor on the ground surface**.** Railway Tech. Res.Institute, Quarterly Reports, 30(1): 25–33 (**9 pages**).

Nakamura, Y. (1997)**.** Seismic vulnerability indices for ground and structures using microtremor**.** World congress on railway research in Florence, Italy. 16–19 (**4 pages**).

Nakamura, Y. (2000)**.** Clear identification of fundamental idea of Nakamura's technique and its applications. In proceedings of the 12th world conference on earthquake engineering. New Zealand: Auckland. Vol. 2656 (**8 pages**).

Nakamura, Y. (2009)**.** Basic structure of QTS (HVSR) and examples of applications. In increasing seismic safety by combining engineering technologies and seismological data. Springer, Dordrecht. 33–51 (**19 pages**).

Okada, H. (2006). Theory of efficient array observations main of microtremors with special reference to the SPAC method. Explor. Geophys., 59(1): 73–85 (**13 pages**).

Pamuk, E.; Özdag. Ö.C.; Tuchel, A.; Özyalin, S.; Akgun, M., (2018). Local site effects evaluation for Aliağa/İzmir using HVSR (Nakamura technique) and MASW methods. Nat. Hazards. 90(2): 887–899 (**13 pages**).

Park, C.B.; Miller, R.D.; Xia, J., (2007). Multichannel analysis of surface waves (MASW). Geophysics, 64(3): 800–808 (**9 pages**).

Parker, R.N.; Hancox, G.T.; Petley, D.N.; Messey, C.I.; Densmore, A.L.; Rosser, J.N., (2015). Spatial distributions of earthquake-induced landslides and hillslope preconditioning in the northwest South Island, New Zealand. Earth Surf. Dyn., 3(4): 501–525 **(25 pages)**.

Rahman, M.Z.; Kamal, A.S.M.M.; Siddiqua, S., (2018). Near-surface shear wave velocity estimation and V s30 mapping for Dhaka City, Bangladesh. Nat. Hazards. 92(3): 1687–1715 (**29 pages**).

Rusydy, I.; Muksin, U.; Mulkal; Idris, Y.; Akram, M.N.; Syamsidik, (2018). The prediction of building damages and casualties in the Kuta Alam sub district-Banda Aceh caused by different earthquake models. AIP Conf. Proc., 1987, 020012: (**7 pages**).

Rusydy, I.; Idris, Y.; Mulkal; Muksin, U; Cummins, P.; Akram, M.N.; Syamsidik, (2020). Shallow crustal earthquake models, damage, and loss predictions in Banda Aceh, Indonesia. Geoenviron. Disasters, 7(8): 1-16 (**16 pages**).

Ryberg, T.; Muksin, U.; Bauer, K., (2016). Ambient seismic noise tomography reveals a hidden caldera and its relation to the Tarutung pull-apart basin at the Sumatran fault zone, Indonesia. J. Volcanol. Geotherm. Res., 321: 73–84 (**12 pages**).

Scott, J.B.; Rasmussen, T.; Luke, B.; Taylor, W.J.; Wagober, J.L.; Smith, S.B.; Louie, J.N., (2006). Shallow shear velocity and seismic microzonation of the urban Las Vegas, Nevada, basin. Bull. Seismol. Soc. Am., 96(3): 1068–1077 (**10 pages**).

Sieh, K.; Natawidjaja, D., (2000). Neotectonics of the Sumatran fault, Indonesia. J. Geophys. Res.: Solid Earth, 105(B12): 28295–28326 (**32 pages**).

Siemon, B.; Steuer, A., (2010). Airborne geophysical investigation of groundwater resources in northern Sumatra after the tsunami of 2004. The Tsunami Threat - Research and Technology, (May 2014): 575-594 (**20 pages**).

Stanko, D.; Markusic, S.; Strelec, S.; Gazdek, M., (2017) "Equivalent-linear site response analysis on the site of the historical Trakošćan Castle, Croatia, using HVSR method," Environ. Earth Sci., 76:642 (**21 pages**).

Thein, P.S.; Pramumijoyo, S.; Brotopuspito, K.S.; Kiyono, J.; Wilopo, W.; Furukawa, A.; Setianto, A.; Putra, R.R., (2015). Estimation of S-wave velocity structure for sedimentary layered media using microtremor array measurements in Palu City, Indonesia. Procedia Environ. Sci., 28(Sustain, 2014): 595–605 (**11pages**).

Tohari, A.; Sugianti, K.; Syahbana, A.J.; Soebowo, E., (2015). Cone penetration test (CPT)-based liquefaction susceptibility of Banda Aceh city, RISET Geologi dan Pertambangan, 25, 99-110 (**12 pages**).

Tün, M.; Pekkan, E., Ozel, O.; Guney, Y., (2016). An investigation into the bedrock depth in the Eskisehir quaternary basin (Turkey) using the microtremor method. Geophys. J. Int., 207(1): 589–607 (**19 pages**).

Untung M.; Buyung N.; Kertapati E.; Undang; Allen C.R., (1985). Rupture along the Great Sumatran Fault, Indonesia, the earthquakes of 1926 and 1943. Bull. Seismol. Soc. Am., 75(1): 313–317 **(4 pages).**

AUTHOR (S) BIOSKETCHES

Asnawi, Y., Ph.D. Candidate, Assistant Professor, [1]Graduate School of Mathematics and Applied Sciences, Universitas Syiah Kuala, Banda Aceh 23111, Indonesia. [2]Universitas Islam Negeri Ar-Raniry, Banda Aceh 23111, Indonesia. [3]Tsunami and Disaster Mitigation Research Center, Universitas Syiah Kuala, Jl. Prof. Dr. Ibrahim Hasan, Gampong Pie, Indonesia.
- Email: *yusran@ar-raniry.ac.id*
- ORCID: 0000-0003-0806-1716
- Web of Science ResearcherID: NA
- Scopus Author ID: 57217127838
- Homepage: http://tdmrc.unsyiah.ac.id/

Simanjuntak, A.V.H., Ph.D. Candidate, Tsunami and Disaster Mitigation Research Center, Universitas Syiah Kuala, Jl. Prof. Dr. Ibrahim Hasan, Gampong Pie, Indonesia. [4]Meteorological, Climatological, and Geophysical Agency, BMKG, Banda Aceh 23234, Indonesia.
- Email: *andreansimanjuntak@gmail.com*
- ORCID: 0000-0003-0623-0037
- Web of Science ResearcherID: NA
- Scopus Author ID: 57195483722
- Homepage: http://tdmrc.unsyiah.ac.id/

Muksin, U., Ph.D., Associate Professor, Tsunami and Disaster Mitigation Research Center, Universitas Syiah Kuala, Jl. Prof. Dr. Ibrahim Hasan, Gampong Pie, Indonesia.
- Email: muksin.umar@tdmrc.org
- ORCID: 0000-0001-7297-8065
- Web of Science ResearcherID: W-3934-2018
- Scopus Author ID: 55795600300
- Homepage: http://fsd.unsyiah.ac.id/muksinumar/

Okubo, M., Ph.D., Associate Professor, Natural Science Cluster, Science and Technology Unit, Kochi University, Akebono-cho Kochi, Japan.
- Email: *okubo@kochi-u.ac.jp*
- ORCID: 0000-0001-7784-6053
- Web of Science ResearcherID: NA
- Scopus Author ID: 8641817600
- Homepage: https://www.kochi-u.ac.jp/english/academics/science/

Putri, S.I., B.Sc., Tsunami and Disaster Mitigation Research Center, Universitas Syiah Kuala, Jl. Prof. Dr. Ibrahim Hasan, Gampong Pie, Indonesia.
- Email: *izziaputris@gmail.com*
- ORCID: 0000-0001-9331-0099
- Web of Science ResearcherID: NA
- Scopus Author ID: NA
- Homepage: http://tdmrc.unsyiah.ac.id/

Rizal, S., Ph.D., Professor, Graduate School of Mathematics and Applied Sciences, Universitas Syiah Kuala, Banda Aceh 23234, Indonesia.
- Email: *syamsul.rizal@unsyiah.net*
- ORCID: 0000-0002-7691-9449
- Web of Science ResearcherID: V-7627-2017
- Scopus Author ID: 56950902200
- Homepage: http://fsd.unsyiah.ac.id/syamsul_rizal/

Syukri, M., Ph.D., Professor, Graduate School of Mathematics and Applied Sciences, Universitas Syiah Kuala, Banda Aceh 23234, Indonesia.
- Email: *m.syukri@unsyiah.ac.id*
- ORCID: 0000-0003-0405-3145
- Web of Science ResearcherID: NA
- Scopus Author ID: 57217853545
- Homepage: http://fsd.unsyiah.ac.id/m.syukri/

HOW TO CITE THIS ARTICLE

Asnawi, Y.; Simanjuntak, A.; Muksin, U.; Okubo, M.; Putri, S.I.; Rizal, S.; Syukri, M., (2022). Soil classification in a seismically active environment based on shear wave velocity and HVSR data. Global J. Environ. Sci. Manage., 8(3): 297-314.

DOI: 10.22034/gjesm.2022.03.01

url: https://www.gjesm.net/article_247726.html

Global J. Environ. Sci. Manage. 8(3): 315-326, Summer 2022, Serial #31

Global Journal of Environmental Science and Management
(GJESM)

Homepage: https://www.gjesm.net/

ORIGINAL RESEARCH ARTICAL

Enhancement of convolutional neural network for urban environment parking space classification

S. Rahman[1], M. Ramli[2,*], F. Arnia[3], R. Muharar[3], M. Ikhwan[4], S. Munzir[2]

[1] *School of Engineering, Universitas Syiah Kuala, Banda Aceh 23111, Indonesia*

[2] *Department of Mathematics, Universitas Syiah Kuala, Banda Aceh 23111, Indonesia*

[3] *Department of Electrical Engineering, Universitas Syiah Kuala, Banda Aceh 23111, Indonesia*

[4] *Graduate School of Mathematics and Applied Sciences, Universitas Syiah Kuala, Banda Aceh 23111, Indonesia*

ARTICLE INFO

Article History:
Received 29 May 2021
Revised 17 August 2021
Accepted 01 October 2021

Keywords:
Deep learning
Efficient Parking Network
mAlexnet
MobileNet
Parking space

ABSTRACT

BACKGROUND AND OBJECTIVES: The increase in the number of vehicles has several negative impacts, including traffic congestion, air pollution, noise levels, and the availability of parking spaces. Drivers looking for parking spaces can cause traffic jams and air pollution. The solution offered at this time is the development of a smart parking system to overcome these problems. The smart parking system offers a parking availability information feature in a parking area to break up congestion in the parking space. Deep learning is a successful method to solve parking space classification problems. It is known that this method requires a large computational process. Th aims of this study are to modified the architecture of Convolutional Neural Networks, part of deep learning to classify parking spaces. Modification of the Convolutional Neural Networks architecture is assumed to increase the work efficiency of the smart parking system in processing parking availability information.
METHODS: Research is focusing on developing parking space classification techniques using camera sensors due to the rapid advancement of technology and algorithms in computer vision. The input image has 3x3 dimensions. The first convolution layer accepts the input image and converts it into 56x56 dimensions. The second convolution layer is composed in the same way as the first layer with dimensions of 25x25. The third convolution layer employs a 3 x 3 filter matrix with padding of up to 15 and converts it into 10x10 dimensions. The fourth layer is composed in the same way as the third layer, but with the addition of maximum pooling. The software used in the test is Python with a Python framework.
FINDINGS: The proposed architecture is the Efficient Parking Network or EfficientParkingNet. It can be shown that this architecture is more efficient in classifying parking spaces compared to some other architectures, such as the mini–Alex Network (mAlexnet) and the Grassmannian Deep Stacking Network with Illumination Correction (GDSN-IC). EfficientParkingNet has not been able to pass the accuracy of Yolo Mobile Network (Yolo+MobileNet). Furthermore, Yolo+MobileNet has so many parameters that it cannot be used on low computing devices. Selection of EfficientParkingNet as a lightweight architecture tailored to the needs of use. EfficientParkingNet's lightweight computing architecture can increase the speed of information on parking availability to users.
CONCLUSION: EfficientParkingNet is more efficient in determining the availability of parking spaces compared to mAlexnet, but still cannot match Yolo+MobileNet. Based on the number of parameters, EfficientParkingNet uses half of the number of parameters of mAlexnet and is much smaller than Yolo+MobileNet. EfficientParkingNet has an accuracy rate of 98.44% for the National Research Council parking dataset and higher than other architectures. EfficientParkingNet is suitable for use in parking systems with low computing devices such as the Raspberry Pi because of the small number of parameters.

DOI: 10.22034/gjesm.2022.03.02

NUMBER OF REFERENCES	NUMBER OF FIGURES	NUMBER OF TABLES
38	3	10

*Corresponding Author:
Email: *marwan.math@unsyiah.ac.id*
Phone: +62813 9766 8376
ORCID: 0000-0003-1225-9063

Note: Discussion period for this manuscript open until October 1, 2022 on GJESM website at the "Show Article.

INTRODUCTION

Environmental problems often occur in big cities due to urbanization, such as land insecurity, worsening water quality, excessive air pollution, noise, and the problems of waste disposal (Uttara *et al*., 2012). One of the factors causing this problem is vehicles. The increasing number of vehicles can cause air pollution, noise, lack of parking areas, traffic jams, and increased fuel use. Vehicle exhaust is the main source of anthropogenic carbon dioxide (CO_2) in the metropolis that is dangerous to public health (Uttara *et al*., 2012). Emissions and the use of vehicle fuels have also increased (Sukarno *et al*., 2016). Urban planning used to solve various problems in big cities by integrating information technology and communication (ICT) and the internet of things (IoT) technology is called smart cities. Smart parking systems are part of a smart city. Smart parking systems can help drivers avoid traffic jams, use less efficient fuel, avoid vehicle queues, panic, and minimize pollution. Bura *et al*. (2018) stated that 30% of traffic jams are caused by drivers searching for a parking area. Smart parking systems can give direction to vehicles to parking spaces based on the type of vehicle, the appropriate rate, and the available space by selecting the closest route in a short time (Ikhwan *et al*., 2017). Based on the technology, smart parking systems have been developed based on agent-based, fuzzy systems, wireless sensors, global positioning systems (GPS) and computer-based (Mahmud *et al*., 2013). Much research has been developed to improve the reliability of smart parking systems. Some studies related to smart parking systems includes detection of parking space availability, parking meters, integrated vehicle development, simulation and analysis of parking data, and competition in booking available parking spaces. Most implementations of smart parking are focused on sensing technology and mobile application development (Lin *et al*., 2017). One smart camera can monitor multiple parking spaces simultaneously at a lower cost compared to the cost of installing and maintaining sensors in each parking space (Amato *et al*., 2017). Detection of parking spaces' availability is an important part of a smart parking system. It can provide information to drivers in parking spaces about availability for vehicle parking. Detection of parking spaces by using computer vision has been widely developed, including the detection of parking spaces by using image subtraction (Chiang and Knoblock, 2013), marking in the parking area (Rahman *et al*., 2020a; Zhang *et al*., 2018), adaptive approach to space constraint with cube (Masmoudi and Wali, 2019), using feature recognition algorithms such as deep learning (Amato *et al*., 2017) and many others. Deep learning is very effective in solving computer vision problems. Convolutional Neural Network (CNN) is a part of deep learning. It is often used to classify objects in an image (Krizhevsky *et al*., 2012). Some researchers have built CNN models to classify objects in images. CNN model is also known as the pre-trained CNN. Some well-known and widely developed pre-trained CNN such as Alexnet (Krizhevsky *et al*., 2012), VGGNet (Simonyan and Zisserman, 2014), GoogleNet (Szegedy *et al*., 2015), Resnet (He *et al*., 2016), MobileNetV2 (Sandler *et al*., 2018), and ShuffleNet (Ma *et al*., 2018), managed to classify objects well. Pre-trained CNN is designed to classify 1000 objects in an image dataset with high computational and large storage space. For fewer class cases, the researchers exploit CNN, such as transfer learning (Hussain *et al*., 2018), fine-tuning or pruning (Li *et al*., 2016) towards pre-trained CNNs or creating a new CNN architecture. The first CNN models developed specifically to identify parking space availability were mAlexnet and mLenet (Amato *et al*., 2016; 2017). mAlexnet and mLenet are named based on their names, namely Alexnet (Krizhevsky *et al*., 2012) and Lenet (LeCun *et al*., 1998), which are the prunings of the two architectures. mAlexnet has a greater level of accuracy than 90% in classifying PKLot and CNRPark+EXT datasets, and this is better than mLenet. It is known that mAlexnet and Alexnet have the same level of accuracy in several experiments, with a difference of accuracy of 1% (Amato *et al*., 2017). However, if it is measured from the average level of accuracy, mAlexnet is still lower than Alexnet. Increasing the size of the kernel at the convolutional layer of mAlexnet (Rahman *et al*., 2020b) and the activation function of ReLu to LeakyReLu can improve the accuracy of mAlexnet (Rahman *et al*., 2021) on CNRPark A and CNRPark B data. By increasing the kernel size, the number of parameters used will increase. An increasing number of parameters can cause a time increase in training and testing. In this case, CNRPark A and CNRPark B are sub-datasets of CNRPark+EXT. Therefore, an efficient CNN model needs to be developed to increase the accuracy and speed of parking space classification. These quantities are important parts of the smart parking system. In terms of speed, mAlexnet is better than Alexnet in the

Table 1: The Summary of vision-based methods for parking space classification

Methods	Dataset	Accuracy	References
mAlexnet	PKLot and CNRPark	>90%	Amato *et al*., 2017
Background subtraction and SVM	PKLot and CNRPark	Avg Acuracy 96.53%	Varghese and Sreelekha, 2019
Yolo and MobileNet	CNRPark+EXT	99%	Chen *et al*., 2020
GDSN-IC	CNRPark+EXT	97.10%	Connie *et al*., 2021

training and testing process. CNN architecture training is a large computational process and can take a long time (de Gusmao *et al*., 2016). As a result, some researchers focused on speeding up CNN's training time (van Grinsven *et al*., 2016; Yamanaka *et al*., 2017; Zhang *et al*., 2019). Meanwhile, the speed of testing is needed to support real-time information systems. mAlexnet has a speed of 15 seconds in detecting parking spaces on a real-time camera using a Raspberry Pi 3b. The number of parameters of mAlexnet is approximately 1/1340 of the total Alexnet parameters, so it can be applied to low computing devices such as the Raspberry Pi (Amato *et al*., 2017). The CNN architecture proposed in this study is expected to be excellent in accuracy and speed compared to other architectures that have been developed in previous research. This architecture is built by creating a new, better architecture in terms of accuracy and speed. The dataset used for CNN testing is CNRPark-EXT taken from 10 different cameras. The study aims to modify the architecture of Convolutional Neural Networks, part of deep learning, to classify parking spaces. Modification of the Convolutional Neural Networks architecture is assumed to increase the work efficiency of the smart parking system in processing parking availability information. This study is simulated at the Modeling and Simulation Laboratory, Department of Mathematics, Syiah Kuala University, Indonesia in 2021.

MATERIALS AND METHODS

Many researchers are interested in developing a parking system that can be managed by using a smart system. Detection of parking space generally uses two technologies, namely sensor-based and vision-based. The development of technology and algorithms in computer vision has made researchers focus on developing parking space classification techniques using camera sensors. Researchers consider the use of computer vision to be more efficient than using sensors. A camera can monitor multiple parking spaces simultaneously. Computer vision-based parking space detection has been developed using the use of color histograms and Harris corner detection (True, 2007), 3D parking lot models (Huang *et al*., 2013), and the use of background subtraction with a combination of several classification techniques (del Postigo *et al*., 2015; Màrmol and Sevillano, 2016), deep learning, and more. Deep learning becomes one of the solutions used to solve classification problems in computer vision. mAlexNet was first used to classify parking spaces by using CNN (Amato *et al*., 2017). mAlexnet outperforms Support Vector Machine (SVM) accuracy-wise (de Almeida *et al*., 2015) on PKLot dataset. mAlexnet is designed for low computing devices by simplifying the Alexnet architecture. mAlexnet has 45,000 parameters, which is about 1/1340 parameters of Alexnet, so it can be run on a Raspberry Pi. However, the accuracy level of mAlexnet's for classifying parking spaces needs to be improved. Recently, several methods have been developed by researchers to improve the classification accuracy of mAlexnet. These methods include R-CNN (Sairam *et al*., 2020), Bag of Features (Varghese and Sreelekha, 2019), Yolo+MobileNet (Chen *et al*., 2020), and GDSN-IC (Connie *et al*., 2021), as presented in Table 1.

Table 1 shows that Yolo+mobilnet succeeded in increasing the accuracy level in parking space classification to 99%. However, the number of parameters used is around 4 million parameters. This is higher than mAlexnet, which only uses approximately 45,000 parameters. The more parameters used, the greater the computational process gets. As a result, it takes time to classify parking spaces. Parking space classification requires high speed to provide real-time information to parking users. Fine-tuning is a way to increase the accuracy of mAlexnet. Fine-tuning mAlexnet by changing the filter size in the first layer has succeeded in increasing the level of accuracy (Rahman *et al*., 2020b). Furthermore, changing the ReLu activation function to LeakyReLu at each convolution layer can also increase the accuracy level (Rahman *et al*., 2021). Increasing the accuracy level by fine-tuning mAlexnet has not been optimal. Therefore, an architecture with a high level of classification accuracy

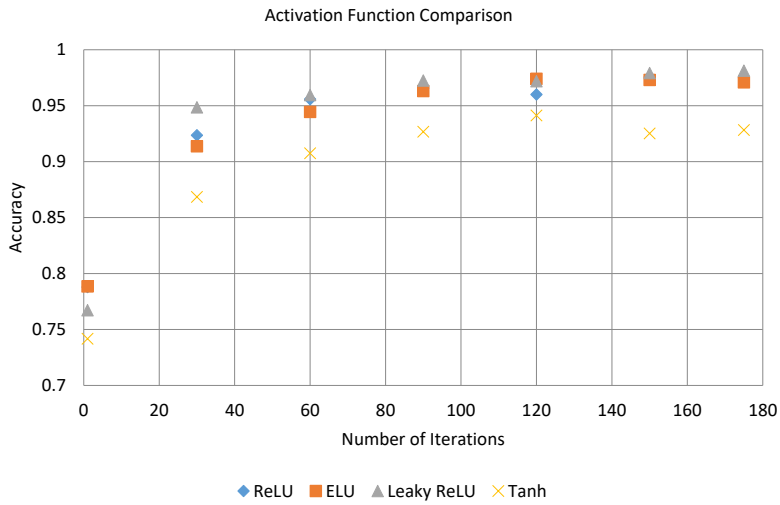

Fig. 1: Comparison of the activation function

and a small number of parameters to produce an efficient architecture is necessary. This study discusses the architecture in question by combining CNN parameters such as convolution layer, kernel, padding, stride, activation function, and fully-connected. Setting CNN parameters in the right order gives good results (Skourt *et al.*, 2021).

CNN architecture for parking space classification

The characteristics of an efficient CNN architecture are balanced convolution on each channel, takes the cost of convolution groups into account, reduces the degree of fragmentation, and reduces element-based operations (Ma *et al.*, 2018). The CNN architecture for parking space classification developed here is called EfficientParkingNet. This architecture is the development of mAlexnet, with added convolution and LeakyReLu used as an activation function. Similar to mAlexnet, EfficientParkingNet does not have branches, it only consists of one channel. In addition, EfficientParkingNet also has a small degree of fragmentation so that the processing cost of each convolution layer is quite low. The use of LeakyReLu as an activation function on mAlexnet can increase the accuracy rate by 0.57% in the CNRPark B subdataset (Rahman *et al.*, 2021). CNRPark B is a small part of the CNRPark+EXT dataset (Amato *et al.*, 2017). The results of the comparison of the activation function on mAlexnet are presented in Fig. 1. LeakyRelu is a better activation function compared to other activation functions as shown in Fig. 1. Based on the number of iterations, Leaky Relu managed to get high accuracy. Leaky Relu succeeded in increasing the accuracy of mAlexnet starting from the 30th iteration, and the value continued to increase to 97.70%.

EfficientParkingNet uses LeakyRelu on each convolution layer. Filter size on each convolution layer uses a filter matrix of 3 x 3 to reduce the number of parameters used. EfficientParkingNet has four convolution layers. This layer is deeper than mAlexnet, which consists of only three layers. The EfficientParkingNet architecture is presented in Fig. 2.

The EfficientParkingNet architecture has four convolution layers as shown in Fig. 2. The input image with a size of 224 x 224 is entered in the first convolution layer. In this case, the first convolution layer uses a filter matrix of 3 x 3, padding 4, and the number of filters 30, followed by the activation functions LeakyRelu, Local Response Normalization (LRN), and Maximum Pooling (MaxPooling) with a filter matrix with padding 2. The second convolution layer has the same composition as the first layer. The third convolution layer uses a filter matrix 3 x 3 with padding of 2 as much as 15, followed by the LeakyRelu activation function, and LRN. The fourth layer has the same composition as the third layer with added MaxPooling. The results of the fourth layer are sent to fully-connected by the platten process. The fully connected (FC1) output has 48 classes with a LeakyReLu activation function and the second fully connected (FC2) has a class binary

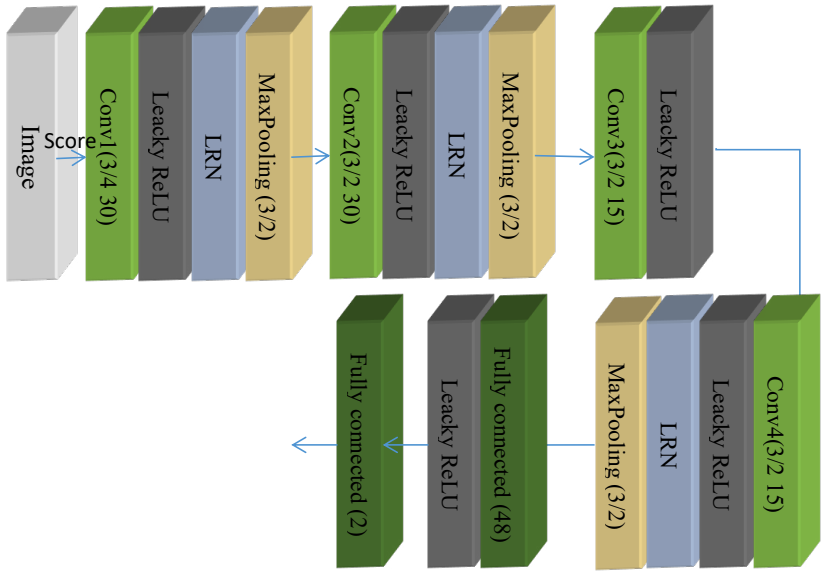

Fig. 2: EfficientParkingNet architecture

output and a softmax activation function. The number of parameters in the convolution layer is determined using Eq. 1.

$$P\_C = \left((F_{Size} - N) + 1\right) \times N\_F, \quad (1)$$

P_C, $F_{\_Size}$, N and N_F states the number of parameters in convolution layer, the filter size used, the number of channels in the previous layer and the number of filters. To determine the number of parameters in the Fully Connected layer, using Eq. 2.

$$P_{Fc} = Cl \times Pl + 1 \times Cl, \quad (2)$$

Where, $P_{\_Fc}$ is the number of parameters in Fully Connected layer, *Cl* is the number of output Current Layer, and *Pl* is the number of output Previous Layer. Next, Activation Shape calculated using Eq. 3.

$$O_{width} = \frac{W - F + 2 * P}{S} + 1, \quad (3)$$

Where, $O_{\_width}$, W, F, p and s represents output width, tensor size, filtersize, number of padding and stride value.

Dataset and tools

The EfficientParkingNet architecture was developed to increase the accuracy of parking space classification in the CNRPark+EXT dataset. CNRPark+EXT consists of CNRPark taken from the parking area of CNR Research in the City of Pisa, Italy. CNRPark consists of 242 full images and 12,584 image spaces captured with two cameras, A and B. CNR-EXT consists of 4,081 full images and 144,965 image spaces captured with nine cameras. CNRPark was taken in sunny weather conditions, while CNR-EXT was taken in three weather conditions, namely sunny, rainy and cloudy. In this case, the entire CNRPark+EXT dataset is cut off and grouped into two groups, namely free and busy. Busy contains images of a parking space containing vehicles, and free contains images of an empty parking space. The various image sizes were converted to a size of 224 x 224. These images are the input for the Convolutional neural network to be classified. Testing was carried out on mAlexnet using the CNRPark+EXT and PKLot datasets. mAlexnet succeeded in classifying the PKLot dataset with an accuracy rate of 99% with an average accuracy rate of 96.77%, for the CNRPark+EXT dataset the accuracy rate reached 97.71%, and the average accuracy rate was 95.70% (Amato *et al.*, 2017). With the CNRPark+EXT dataset has bigger resistance than PKLot in parking space classification. The CNRPark+EXT dataset, mAlexnet has succeeded in detecting parking spaces with a low level of accuracy. Classification of CNRPark+EXT dataset becomes the focus of this study. Therefore, EfficientParkingNet is focused on increasing

Table 2: Dataset details used as training and test data

Subset	Empty slots	Filled slots	Total
CNRPark A	2549	3622	6171
CNRPark B	1632	4781	6413
CNRPark	4181	8403	12584
CNRPark-EXT Train	46877	47616	94493
CNRPark-EXT Train C1 C8	21769	16784	38553
CNRPark-EXT Test	13589	18276	31825
CNRPark+EXT	65658	79307	144965

the accuracy level for tCNRPark+EXT dataset with fewer parameters than mAlexnet. The dataset sharing scheme for training and testing is the same as mAlexnet. In this case the test is added by dividing the CNRPark+EXT data into 2 (two) parts, namely 80% for training and 20% for randomly selected tests. Details of the data used are presented in Table 2. Testing is done by using a computer with the following specifications: 4 GigaByte RAM, Processor Intel(R) core i3-2120 @3.30GHz 3.30GHz, 64-bit operating system. The software used in the test is python with a Python framework.

RESULTS AND DISCUSSION

The CNRPark+EXT dataset as test data is used to compare the performance of EfficientParkingNet to mAlexnet. The tests were carried out based on mAlexnet test scheme. In this case, 3 (three) test schemes were carried out, namely CNRPark, CNRPark-EXT Train C1-C8, and CNRPark+EXT Train as training data. Each test schema uses CNRPark_EXT TEST as test data. The test results are presented in Table 3.

Based on Table 3, it can be seen that EfficientParkingNet's accuracy level is better than each test scheme. EfficientParkingNet is better in the CNRPark dataset by 0.35%,CNRPark+EXT TRAIN C1-C8 excels by 0.97%, and CNRPark+EXT TRAIN is the best by 0.84%. The average accuracy rate of mAlexnet is 95.70% and EfficientParkingNet is 96.42%. EfficientParkingNet's accuracy level is higher with an average of 0.72% compared to mAlexnet's. The low accuracy level is caused by differences between training and the test data, called overfitting or the training data, it does not represent all the underfitting test data (Gavrilov *et al*., 2018). The first test with CNRPark training data and CNRPark-EXT TEST test data shows a low accuracy rate of 93.87%. It is because the training data does not represent the features in the test data. CNRPark was taken from two cameras, namely A and B in sunny weather while CNRPark-EXT TEST was taken from 10 different cameras which were collected randomly under various weather conditions. The difference in weather, location and less training data compared to test data cause overfitting and underfitting. Overfitting and underfitting cause a lower level of validation accuracy in training. This happened in the first test scheme. The comparison results of the training accuracy level and validation accuracy level are presented in Fig. 3.

Based on Fig. 3, it can be seen that there is a difference in accuracy level between training and validation. EffecientParkingNet can study the training dataset, but it cannot recognize the dataset in the test. It is because the difference in features between the training and the test data or the training data does not represent the test data. Hence, designing the dataset is needed to represent all the locations and cameras contained in the CNRPark+EXT dataset. In the implementation of a parking area, an application must be able to classify parking spaces simultaneously. Splitting datasets and training sub-datasets to recognize other sub-datasets is not a solution at the same time. In this study, all the CNRPark+EXT datasets are used and divided randomly. They are 80% for training data and 20% for validation test data. The use of all data is expected to represent the actual state of the parking system in real-time. The test results for the dataset are presented in Table 4.

Based on Table 3, it can be seen that mAlexnet has a better ability to recognize the CNRPark+EXT train dataset compared to other datasets. Furthermore, based on Table 4, the accuracy rate of mAlexnet reaches 98.13% in classifying the CNRPark+EXT dataset. EfficientParkingNet has an accuracy rate of 98.44% or 0.31%. It is better than mAlexnet. Some tests show that EffecientParkingNet is better than mAlexnet. Besides mAlexnet, the results of EfficientParkingNet are also compared with previous studies based on the data used. The results of the comparison of several

Tabel 3: Comparison of mAlexnet accuracy and EfficientParkingNet

Data train	Accuracy rate	
	mAlexnet	EfficientParkingNet
CNRPark	93.52%	93.87%
CNRPark +EXT TRAIN C1-C8	95.88%	96.85%
CNRPark +EXT TRAIN	97.70%	98.54%
Average	95.70%	96.42%

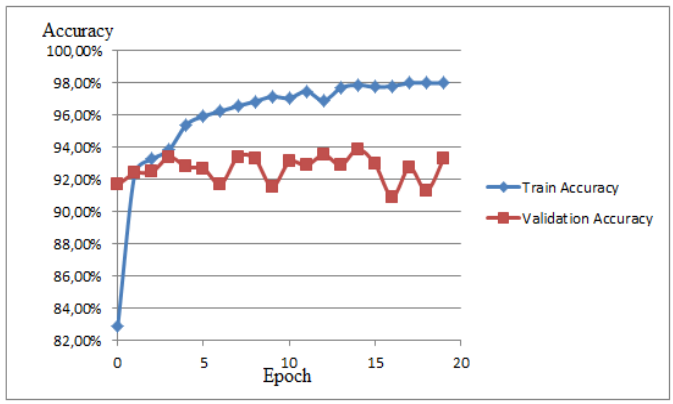

Fig. 3: Training accuracy rate with validation

methods for classifying CNRPark+EXT TEST with CNRPark_EXT TRAIN C1-C8 training data are presented in Table 5.

Based on Table 5, it can be seen that the accuracy level of EffecientParkingNet is better than the two previous studies which classified the sub dataset of CNRPark+EXT Test using CNRPark_EXT TRAIN C1-C8 training data. Furthermore, several researchers claim to have succeeded in increasing the accuracy level with different testing schemes on the CNRPark+EXT dataset by using the Yolo+MobileNet method (Chen *et al.*, 2020) and GDSN-IC (Connie *et al*., 2021). The results of the comparison accuracy level of EffecientParking Net with the results of previous studies are in Table 6.

Based on Table 6, it can be seen that EfficientParkingNet is better than mAlexnet and GDSN-IC. Also, it can also be seen that the results of EfficientParkingNet are close to the results of Yolo+MobileNet. Yolo+MobileNet has a large number of parameters, more than 4 million parameters. It causes a large computational process and takes time. Therefore, Yolo+MobileNet is not suitable to be used on low-computing devices such as the Raspberry Pi. EfficientParkingNet has a number of parameters of 22.0000 or (half of) the number of parameters of mAlexnet. EfficientParkingNet is more suitable for use on low computing devices. The comparison of the number of parameters is presented in Table 7.

Based on Table 7, it can be seen that EfficientParkingNet has fewer parameters than the other two methods. The number of mAlexnet parameters is 1/1340 of Alexnet parameters (Amato *et al*., 2017). The number of parameters of Alexnet is 61 million, so the number of parameters of mAlexnet is 45,522. By using equation 1 and equation 2, the number of parameters of mAlexnet is determined to be 32,648 parameters. Tables 8 and 9 show the number of parameters and activation shapes calculated using Eqs. 1 to 3 for mAlexnet, and EfficientParkingNet, either manually or using Pytorch Code.

Based on Tables 8 and 9, it can be seen that the number of EfficientParkingNet parameters is less than

Table 4: Comparison of the accuracy level all data

Methods	Accuracy rate
mAlexnet	98.13%
EfficientParkingNet	98.44%

Table 5: Comparison of CNRPark+EXT test classifications

Arsitecture	Accuracy Level	References
mAlexnet	95.88%	Amato *et al*., 2017
background subtraction+SVM	96.59%	(Varghese and Sreelekha, 2019)
EfficientParkingNet	96.85%	Proposed method

Table 6: Comparison of accuracy of several architectures

Methods	Level of accuracy	References
mAlexnet	98.13%	Amato *et al*., 2017
Yolo+MobileNet	99%	Chen *et al*., 2020
GDSN-IC	97.10%	Connie *et al*., 2021
EfficientParkingNet	98.44%	Proposed method

Table 7: Comparison of the number of parameters

Architecture	Parameters
mAlexnet	45K
EfficientParkingNet	22K
Yolo+MobileNet	4M

Table 8: The Number of parameters of mAlexnet

Layers	Activation Shape	Activation Size	Parameters
Input Layer	(224,224,3)	150,528	0
Conv1 (11/4 16)	(54,54,16)	46,656	5,824
Pooling (3/2)	(26,26,16)	10,816	0
Conv2 (5/2 20)	(22,22,20)	9,680	8,020
Pooling (3/2)	(10,10,20)	2,000	0
Conv3(3/2 30)	(8,8,30)	1,920	5,430
Pooling (3/2)	(3,3,30)	270	0
FC1 (48)	(48,1)	48	13,230
FC2(2)	(2,1)	2	144
Total			32,648

mAlexnet parameters. The number of parameters for mAlexnet is 33,000, and for EfficientParkingNet is about 22,000. These parameters determine the file size for each architecture. The smaller the file size, the more efficient the storage space, especially on embedded system devices. Table 10 presents the experimental results of the relationship between the number of parameters and file size.

Table 10 shows that the file size of Efficient-ParkingNet is smaller than mAlexnet. Based on the calculation results, EfficientParkingNet has a better accuracy level, a smaller number of parameters, and a smaller file size compared to mAlexnet. Therefore, EfficientParkingNet is suitable to be used on low computing devices and embedded systems.

Table 9: The Number of parameters of EfficientParkingNet

Layers	Activation Shape	Activation Size	Parameters
Input Layer	(224,224,3)	150,528	0
Conv1 (3/4 30)	(56,56,30)	94,080	840
Pooling (3/2)	(27,27,30)	21,870	0
Conv2 (3/2 30)	(25,25,30)	18,750	8,130
Pooling (3/2)	(12,12,30)	4,320	0
Conv3 (3/2 15)	(10,10,15)	1,500	4,065
Conv4 (3/2 15)	(8,8,15)	960	2,040
Pooling (3/2)	(3,3,15)	135	0
FC1 (48)	(48,1)	48	6,615
FC2(2)	(2,1)	2	144
Total			21,834

Table 10: Comparison of parameters and file size

Architecture	Parameters	File Size
mAlexnet	33K	133K
EfficientParkingNet	22K	90K

CONCLUSION

The increased number of vehicles resulted in traffic congestion and pollution. As much as 30% of traffic jams are caused by drivers searching for a parking area. Smart parking systems can direct vehicles to parking spaces based on the type of vehicle, the appropriate rate, and the available space by taking the shortest route. A CNN architecture used to detect parking space named EfficientParkingNet has been developed. It is a “small architecture” which is a development of the mAlexnet architecture, with four layers of convolution and LeakyRelu as an activation function. The low level of accuracy is caused by overfitting. Accuracy is also reduced if the training data does not represent all of the underfitting test data, which is caused by the difference between the training data and the test data. Modifications were also made to the distribution of training data and test data. The first test, which used CNRPark training data and CNRPark-EXT TEST test data, yielded a low accuracy rate of 93.87%. This is due to the fact that the training data does not accurately represent the features in the test data. EffecientParkingNet can analyze the training dataset but not recognize it in the dataset test. In this study, all CNRPark+EXT datasets are used and divided at random, with 80% used for training and 20% used for testing. The use of all data is expected to represent the real-time state of the parking system. An increase in the accuracy level of EfficientParkingNet has been seen, bringing it to 98.44%, higher than the accuracy level of mAlexnet. According to recent research, different Yolo+MobileNet testing schemes have been successful in increasing accuracy. Background subtraction plus SVM and GDSN-IC equals Yolo+MobileNet accuracy level. It can also be seen that the results of EfficientParkingNet are close to the results of Yolo+MobileNet. Yolo+MobileNet has a large number of parameters, more than 4 million parameters. It causes a large computational process. Therefore, Yolo+MobileNet is not suitable to be used on low-computing devices such as the Raspberry Pi. The number of parameters in EfficientParkingNet architecture is 22,000 parameters, or 2/3 of the number of mAlexnet parameters and 1/182 of Yolo+MobileNet parameters. Therefore, EfficientParkingNet is suitable to be used on low computing devices such as the Raspberry Pi. It has an impact on the reduction of implementation costs.

AUTHOR CONTRIBUTIONS

S. Rahman performed the literature review, running the model, analyzed and interpreted the data, prepared the manuscript text, and manuscript edition. M. Ramli performed the literature review, running the model, analyzed and interpreted the data, prepared the manuscript text, and manuscript edition. F. Arnia and R. Muharar performed the literature review, prepared numerical code, prepared the manuscript text, and manuscript edition. M. Ikhwan and S.

Munzir performed the literature review, analyzed and interpreted the data, prepared the manuscript text, and manuscript edition. All authors agreed on the final version of the manuscript.

ACKNOWLEDGEMENT

This study is funded by Professor Research Grant, Universitas Syiah Kuala 2021, with contract number [2/UN11.2.1/PT.01.03/PNBP/2021].

CONFLICT OF INTEREST

The authors declare no potential conflict of interest regarding the publication of this work. In addition, the ethical issues including plagiarism, informed consent, misconduct, data fabrication and, or falsification, double publication and, or submission, and redundancy have been completely witnessed by the authors.

OPEN ACCESS

PUBLISHER'S NOTE

GJESM Publisher remains neutral with regard to jurisdictional claims in published maps and institutional afflictions.

ABBREVIATIONS

%	Percent
Alexnet	Alex Network, network architecture created by Alex Krizhevsky.
Cl	The number of output Current Layer
CNN	Convolutional Neural Networks
CNR	Council of National Research
CNRPark	CNR Parking dataset
CNRPark-EXT	New updated of CNRPark
CO_2	Carbon dioxide
Conv1, Conv2, Conv3, Conv4	Fisrt, second, third, and fourth convolution layer, respectively
ELU	Exponential linear unit
Eq. / Eqs.	Equation / equations
F	Filtersize
$F_{\_Size}$	The filter size used
FC1	The first fully connected
FC2	The second fully connected
Fig.	Figure
GDSN-IC	Grassmannian Deep Stacking Network with Illumination Correction
GoogleNet	Network architecture developed by a team at Google
GPS	Global positioning systems
ICT	Information and Communication Technology
IoT	Internet of things
Lenet	LeCun Network, convolutional neural network structure proposed by LeCun *et al.* (1998)
LeakyReLu	Leaky rectified linear unit
LRN	Local Response Normalization
MaxPooling	Maximum pooling
mAlexnet	mini Alexnet
mLenet	mini Lenet
MobileNet	Mobile Neural Network
MobileNetV2	Version 2 of MobileNet
N	The number of channels in the previous layer
N_F	The number of filters
$O_{\_width}$	Output width
p	The number of padding
P_C	The number of parameters in convolution layer
$P_{\_Fc}$	The number of parameters in Fully Connected layer
PKLot	Parking lot databased
Pl	The number of output Previous Layer
R-CNN	Region CNN

Relu	Rectified linear unit
Resnet	Residual neural network
s	The stride value
ShuffleNet	Shuffle Neural Network
SVM	Support vector machine
Tanh	Hyperbolic tangent
VGGNet	Network architecture that invented by VGG (Visual Geometry Group) from University of Oxford
W	Tensor size
Yolo	You only look once network architecture

REFERENCES

Amato, G.; Carrara, F.; Falchi, F.; Gennaro, C.; Meghini, C.; Vairo, C., (2017). Deep learning for decentralized parking lot occupancy detection. Expert Syst. Appl., 72: 327–334 (**8 pages**).

Amato, G.; Carrara, F.; Falchi, F.; Gennaro, C.; Vairo, C., (2016). Car parking occupancy detection using smart camera networks and deep learning. In 2016 IEEE Symposium on Computers and Communication (ISCC), 1212–1217 (**6 pages**).

Bura, H.; Lin, N.; Kumar, N.; Malekar, S.; Nagaraj, S.; Liu, K., (2018). An edge based smart parking solution using camera networks and deep learning. In 2018 IEEE International Conference on Cognitive Computing (ICCC), 17–24 (**8 pages**).

Chen, L.; Sheu, R; Peng, W.; Wu, J; Tseng, C., (2020). Video-based parking occupancy detection for smart control system. Appl. Sci., 10(3): 1079 (**22 pages**).

Chiang, Y.; Knoblock, C.A., (2013). A general approach for extracting road vector data from raster maps. Int. J. Doc. Anal. Recognit., 16: 55–81 (**27 pages**).

Connie, T.; Goh, M.K.O.; Koo, V.C.; Murata, K.T.; Phon-Amnuaisuk, S., (2021). Improved parking space recognition via grassmannian deep stacking network with illumination correction. In International Conference on Computational Intelligence in Information System, 150–159 (**10 pages**).

de Almeida, P.R.L.; Oliveira, L.S.; Britto Jr, A.S.; Silva Jr, E.J.; Koerich, A.L., (2015). PKLot–A robust dataset for parking lot classification. Expert Syst. Appl., 42: 4937–4949 (**13 pages**).

de Gusmao, P.P.B.; Francini, G.; Lepsøy, S.; Magli, E., (2016). Fast training of convolutional neural networks via kernel rescaling. arXiv Prepr. arXiv1610.03623 (**13 pages**).

del Postigo, C.G.; Torres, J.; Menéndez, J.M., (2015). Vacant parking area estimation through background subtraction and transience map analysis. IET Intell. Transp. Syst., 9: 835–841 (**7 pages**).

Gavrilov, A.D.; Jordache, A.; Vasdani, M.; Deng, J., (2018). Preventing model overfitting and underfitting in convolutional neural networks. Int. J. Softw. Sci. Comput. Intell., 10: 19–28 (**10 pages**).

He, K.; Zhang, X.; Ren, S.; Sun, J., 2016. Deep residual learning for image recognition. In the IEEE Conference on Computer Vision and Pattern Recognition, 770–778 (**9 pages**).

Huang, C.; Tai, Y.; Wang, S., (2013). Vacant parking space detection based on plane-based Bayesian hierarchical framework. IEEE Trans. Circuits Syst. Video Technol., 23: 1598–1610 (**13 pages**).

Hussain, M.; Bird, J.J.; Faria, D.R., (2018). A study on cnn transfer learning for image classification. In UK Workshop on Computational Intelligence, 191–202 (**12 pages**).

Ikhwan, M; Mardlijah, M.; Arif, D.K., (2017). Model predictive parking control on four wheel vehicle with optimum parking space. In International Conference on Electrical Engineering and Informatics, 35-39 (**5 pages**).

Krizhevsky, A.; Sutskever, I.; Hinton, G.E., (2012). Imagenet classification with deep convolutional neural networks. In Advances in Neural Information Processing Systems, 1097–1105 (**9 pages**).

LeCun, Y.; Bottou, L.; Bengio, Y.; Haffner, P., (1998). Gradient-based learning applied to document recognition. Proc. IEEE, 86: 2278–2324 (**10 pages**).

Li, H.; Kadav, A.; Durdanovic, I.; Samet, H.; Graf, H.P., (2016). Pruning filters for efficient convnets. In Proceedings of NIPS Workshop on Efficient Methods for Deep Neural Networks, 1-5 (**5 pages**).

Lin, T.; Rivano, H.; Le Mouël, F., (2017). A survey of smart parking solutions. IEEE Trans. Intell. Transp. Syst. 18, 3229–3253 (**25 pages**).

Ma, N.; Zhang, X.; Zheng, H.; Sun, J., (2018). Shufflenet v2: Practical guidelines for efficient cnn architecture design. In Proceedings of the European Conference on Computer Vision (ECCV), 116–131 (**16 pages**).

Mahmud, S.A.; Khan, G.M.; Rahman, M.; Zafar, H., (2013). A survey of intelligent car parking system. J. Appl. Res. Technol, 11: 714–726 (**13 pages**).

Màrmol, E.; Sevillano, X., (2016). QuickSpot: a video analytics solution for on-street vacant parking spot detection. Multimed. Tools Appl., 75: 17711–17743 (**33 pages**).

Masmoudi, I.; Wali, A., (2019). Vision based approach for adaptive parking lots occupancy estimation. Pattern Recognit. Image Anal., 29: 515–522 (**8 pages**).

Rahman, S.; Ramli, M.; Arnia, F.; Muharar, R.; Luthfi, M.; Sundari, S., (2020a). Analysis and comparison of hough transform algorithms and feature detection to find available parking spaces. J. Phys.: Conf. Ser., 1566: 12092 (**7 pages**).

Rahman, S.; Ramli, M.; Arnia, F.; Muharar, R.; Sembiring, A., (2020b). Convolutional neural network customization for parking occupancy detection. In 2020 International Conference on Electrical Engineering and Informatics, 1-6 (**6 pages**).

Rahman, S.; Ramli, M.; Arnia, F.; Muharar, R.; Sembiring, A., (2021). Performance analysis of mAlexnet by training option and activation function tuning on parking images. IOP Conf. Ser.: Mater. Sci. Eng., 1087: 12084 (**7 pages**).

Sairam, B.; Agrawal, A.; Krishna, G.; Sahu, S.P., (2020). Automated vehicle parking slot detection system using deep learning. In 2020 Fourth International Conference on Computing Methodologies and Communication, 750–755 (**6 pages**).

Sandler, M.; Howard, A.; Zhu, M.; Zhmoginov, A.; Chen, L., (2018). Mobilenetv2: Inverted residuals and linear bottlenecks. In IEEE Conference on Computer Vision and Pattern Recognition, 4510–4520 (**11 pages**).

Simonyan, K.; Zisserman, A., (2014). Very deep convolutional networks for large-scale image recognition. In International Conference on Learning Representations, 1-14 (**14 pages**).

Skourt, B.A.; El Hassani, A.; Majda, A., (2021). Mixed-pooling-dropout for convolutional neural network regularization. J. King Saud Univ. Inf. Sci., 33:1-7 (**7 pages**).

Sukarno, I.; Matsumoto, H.; Susanti, L., (2016). Transportation energy consumption and emissions-a view from city of Indonesia. Futur. Cities Environ., 2: 6 (**11 pages**).

Szegedy, C.; Liu, W.; Jia, Y.; Sermanet, P.; Reed, S.; Anguelov, D.; Erhan, D.; Vanhoucke, V.; Rabinovich, A., (2015). Going deeper with convolutions. In IEEE Conference on Computer Vision and Pattern Recognition, 1–9 (**9 pages**).

True, N., (2007). Vacant parking space detection in static images. Univ. California, San Diego.

Uttara, S.; Bhuvandas, N.; Aggarwal, V., (2012). Impacts of urbanization on environment. Int. J. Res. Eng. Appl. Sci., 2: 1637–1645 (**9 pages**).

van Grinsven, M.J.J.P.; van Ginneken, B.; Hoyng, C.B.; Theelen, T.; Sánchez, C.I., (2016). Fast convolutional neural network training using selective data sampling: Application to hemorrhage detection in color fundus images. IEEE Trans. Med. Imaging, 35: 1273–1284 (**12 pages**).

Varghese, A.; Sreelekha, G., (2019). An efficient algorithm for detection of vacant spaces in delimited and non-delimited parking lots. IEEE Trans. Intell. Transp. Syst., 21: 4052–4062 (**11 pages**).

Yamanaka, J.; Kuwashima, S.; Kurita, T., (2017). Fast and accurate image super resolution by deep CNN with skip connection and network in network. In International Conference on Neural Information Processing, 217–225 (**9 pages**).

Zhang, L.; Li, X.; Huang, J.; Shen, Y.; Wang, D., (2018). Vision-based parking-slot detection: a benchmark and a learning-based approach. Symmetry, 10: 64 (**18 pages**).

Zhang, Yu; Zhang, Yan; Shi, Z.; Zhang, J.; Wei, M., (2019). Design and training of deep CNN-based fast detector in infrared SUAV surveillance system. IEEE Access, 7: 137365–137377 (**13 pages**).

AUTHOR (S) BIOSKETCHES

Rahman, S., Ph.D. Candidate, School of Engineering, Universitas Syiah Kuala, Banda Aceh 23111, Indonesia.
- Email: *sayuti_r@mhs.unsyiah.ac.id*
- ORCID: 0000-0002-4410-4026
- Web of Science ResearcherID: AAE-4070-2021
- Scopus Author ID: 57203457552
- Homepage: *http://dit.unsyiah.ac.id/*

Ramli, M., Ph.D., Professor, Department of Mathematics, Universitas Syiah Kuala, Banda Aceh 23111, Indonesia.
- Email: *marwan.math@unsyiah.ac.id*
- ORCID: 0000-0003-1225-9063
- Web of Science ResearcherID: A-2686-2017
- Scopus Author ID: 57217110324
- Homepage: http://math.unsyiah.ac.id/ind/marwan/

Arnia, F., Ph.D., Professor, Department of Electrical Engineering, Universitas Syiah Kuala, Banda Aceh 23111, Indonesia.
- Email: *f.arnia@unsyiah.ac.id*
- ORCID: 0000-0001-6020-1275
- Web of Science ResearcherID: R-5711-2017
- Scopus Author ID: 14027791000
- Homepage: http://www.fsd.unsyiah.ac.id/fitri.arnia/

Muharar, R., Ph.D., Associate Professor, Department of Electrical Engineering, Universitas Syiah Kuala, Banda Aceh 23111, Indonesia.
- Email: *r.muharar@unsyiah.ac.id*
- ORCID: 0000-0002-5079-4174
- Web of Science ResearcherID: T-9108-2018
- Scopus Author ID: 37085406000
- Homepage: http://fsd.unsyiah.ac.id/rusdha/

Ikhwan, M., Ph.D. Candidate, Graduate School of Mathematics and Applied Sciences, Universitas Syiah Kuala, Banda Aceh 23111, Indonesia.
- Email: *m.ikhwan@mhs.unsyiah.ac.id*
- ORCID: 0000-0002-8162-1479
- Web of Science ResearcherID: D-1570-2018
- Scopus Author ID: 57201743214
- Homepage: http://dmas.unsyiah.ac.id/

Munzir, S., Ph.D., Associate Professor, Department of Mathematics, Universitas Syiah Kuala, Banda Aceh 23111, Indonesia.
- Email: *smunzir@unsyiah.ac.id*
- ORCID: 0000-0003-4717-5521
- Web of Science ResearcherID: ABD-9651-2021
- Scopus Author ID: 57195062107
- Academic or organizational Homepage link: http://fsd.unsyiah.ac.id/smunzir/

HOW TO CITE THIS ARTICLE

Rahman, S.; Ramli, M.; Arnia, F.; Muharar, R.; Ikhwan, M.I.; Munzir, S., (2022). Enhancement of convolutional neural network for urban environment parking space classification. Global J. Environ. Sci. Manage., 8(3): 315-326.

DOI: 10.22034/gjesm.2022.03.02

url: https://www.gjesm.net/article_246490.html

Global J. Environ. Sci. Manage. 8(3): 327-338, Summer 2022, Serial #31

Global Journal of Environmental Science and Management
(GJESM)

Homepage: https://www.gjesm.net/

ORIGINAL RESEARCH ARTICLE

Solid medical waste management practices and awareness in COVID-19 screening stations

S.E. Alzghoul[1,*], O.A. Smadi[1], T.D. Almomani[1], M.B. Alzghoul[2], O.M. Albataineh[1]

[1] *Department of Biomedical Engineering, College of Engineering, The Hashemite University Zarqa, Jordan*

[2] *Department of Basic Medical Veterinary Sciences, College of Veterinary Medicine, Jordan University of Science and Technology, Irbid, Jordan*

ARTICLE INFO

Article History:
Received 18 July 2021
Revised 26 September 2021
Accepted 04 December 2021

Keywords:
Administrative protocols
COVID-19 (Coronavirus disease 2019)
Medical waste management
Solid medical wastes

ABSTRACT

BACKGROUND AND OBJECTIVES: During the Coronavirus disease 2019 pandemic, an effective and efficient medical waste management plan is required to prevent disease transmission from the Coronavirus disease 2019 viral solid wastes. Screening stations are critical locations where solid Coronavirus disease 2019 wastes are created. Solid trash collection and management strategies for screening stations must be studied as they are the first point of origin for solid Coronavirus disease 2019 wastes. The goal of this study is to evaluate the level of healthcare workers' knowledge in the medical waste management field in Jordanian Coronavirus disease 2019 screening stations, with an emphasis on understanding and implementing Jordanian medical waste management protocols, by examining the awareness, perspective, and practice about the many aspects of Coronavirus disease 2019 wastes.

METHODS: A study sample (n = 78) involving technicians, nurses, and physicians working at various screening stations in Jordan's public and private sectors was evaluated. From April 2021 to September 2021, a cross-sectional survey involving questionnaires was carried out. The survey included questions on medical waste management knowledge and awareness among healthcare personnel regarding the Coronavirus 2019 medical waste administrative and collection procedures.

There are various limitations to this cross-sectional study that should be noted. This is a study conducted among health care employees when an overwhelming amount of coronavirus disease cases were being recorded locally and worldwide, affecting transportation ability and minimizing time spent with screening station personnel.

FINDINGS: The outcomes of the first module of the questionnaire revealed a high degree of medical waste management knowledge and awareness among healthcare staff. On the other hand, nurses demonstrated the highest awareness and application of COVID-19 medical waste administrative procedures. Furthermore, the results of the third module revealed that the private sector fails to successfully execute national and international procedures, with the most significant negative responses among other categories.

CONCLUSION: It was concluded that Jordan's solid waste collection and disposal methods were effectively implemented, which might aid in the virus eradication. Even though most Jordanian screening stations have effectively implemented knowledge and awareness regarding solid Coronavirus disease 2019 wastes management practices, there is a need to undertake periodic training and continuous monitoring with a specific focus on the appropriate administrative and collecting processes for both technicians, and private sector stations.

DOI: 10.22034/gjesm.2022.03.03

NUMBER OF REFERENCES	NUMBER OF FIGURES	NUMBER OF TABLES
43	4	3

*Corresponding Author:
Email: *alzghoul@hu.edu.jo*
Phone: +9627 9659 3604
ORCID: 0000-0001-9663-7820

Note: Discussion period for this manuscript open until October 1, 2022 on GJESM website at the "Show Article".

INTRODUCTION

In recent years, public awareness of medical waste management has increased worldwide (Mihai, 2020). Medical waste includes any solid, liquid, or gaseous substance produced by healthcare institutions such as hospitals, medical centers, dental clinics, and medical labs. Before adopting medical waste management rules, medical waste was commonly combined with other municipal wastes and deposited in household trash cans, and inadequate treatment techniques were used (Ilyas *et al.,* 2020). There are two categories of medical waste: normal non-risk trash and hazardous waste. The healthcare sector produces 75–90% of non-risk or general healthcare waste (Prüss *et al.,* 2014). The World Health Organization (WHO) and the United States Environmental Protection Agency (USEPA) classify the remaining 10–25% of healthcare waste as hazardous or particular waste (Prüss *et al.,* 2014). According to the WHO, healthcare waste should be treated as special waste and kept apart from regular garbage. Medical waste could include highly infectious pathological and anatomical waste, genotoxic waste, sharp waste, chemical waste, pharmacological waste, radioactive waste, waste with high heavy metal content, and general healthcare waste, the majority of which are toxic, harmful, or infectious. Despite their small number, contagious and highly infectious medical waste, such as dirty needles and other sharps, can transfer diseases to healthy people. If medical waste management is not correctly done, all the rubbish might become infectious and dangerous (LaGrega *et al.,* 2015). Hazardous chemical wastes can pollute the environment (water, air, and soil), emit unpleasant odors, and spread diseases like cholera, human immunodeficiency virus (HIV), and hepatitis B and C (Babanyara *et al.,* 2013). According to WHO estimates, injection with contaminated syringes caused 21 million hepatitis B infections, 2 million hepatitis C infections, and 260,000 HIV infections in 2000 (Shinee *et al.,* 2008). Because of these hazards, determining acceptable procedures for the safe treatment of medical waste is critical to preserving human health and the environment. The emergence of the Coronavirus disease 2019 (COVID-19) has resulted in an increase in the medical waste throughout the world as well as amounts of household hazardous and plastic trash, suggesting a critical need for proper waste management, which is often overlooked (Sarkodie and Owusu, 2020; Prata *et al.,* 2020). The increased use of personal protection equipment (PPE) has been linked to a considerable rise in pollution load, which has been responded to by different community-based preventive policies and measures (Haque *et al.,* 2021). A good medical waste management system should consider clinical waste generation and disposal options, efficient segregation, handling, storage, safe transportation and treatment, improved monitoring and tracking techniques, emergency plans, and the need for staff training and awareness programs to manage medical wastes effectively. A professional should oversee the medical waste management system to verify that the management plan's criteria are followed (Neumeyer *et al.,* 2020). The epidemic has altered the dynamics of trash creation, posing challenges for governments and waste management personnel (Sharma *et al.,* 2020; Agamuthu and Barasarathi, 2020). During an outbreak, various forms of healthcare and hazardous waste are produced, such as contaminated masks, gloves, and more non-infected goods of the same nature (UNEP, 2020). A record amount of healthcare waste has been documented as a result of the large epidemic; on the other hand, because of many lockdowns throughout the epidemic, air quality was improved, which is seen as a beneficial influence (Isaifan, 2020). The COVID-19 outbreak in China is believed to be increasing healthcare waste from personal protective equipment such as gloves, face masks, and safety goggles due to an increase in personal protective equipment and quick disposal after use. Due to the massive increase in daily waste (over 240 metric tons) and a six-fold increase in hospital discharge trash, the influx of COVID-19 patients allegedly led to the construction of garbage plants and the deployment of 46 mobile waste treatment facilities in China (Sarkodie and Owusu, 2020; Filimonau, 2021). The WHO and the United Nations (UN) Model Regulations categorized COVID-19's medical waste as Category B, which refers to an infectious particle that is not capable of producing serious sickness, life-threatening, or dangerous disease in otherwise healthy animals or people when exposed to it (Gao *et al.,* 2020). Waste is mostly disposed of at hazardous waste dumps in third-world countries, which are regularly frequented by "rag-pickers" with no PPE, which can spread the infection and make contact tracing difficult (Tripathi *et al.,* 2020). As a result, prospective policy responses, and other approaches to trash collection and disposal locations are required for creating strong adaptation and

management of waste disposal amounts produced by various healthcare and home units in this area of the world (Ramteke and Sahu, 2020). On the other hand, governments have recognized the significance of solid waste management during the disease epidemic in developed countries and have developed various strategies to address the problem. For example, to ease the pressure on the local garbage system throughout this epidemic, residents in Austria are being advised to reduce disposal creation and separate waste as much as possible. The British government has released COVID-19 regulatory policy statements for municipal governments and waste collectors. These recommendations focus on prioritizing waste flow, increasing temporary storage capacity, proper disposal, modifying the solid waste incinerator to treat COVID-19 hazardous waste, and communicating with communities (Kulkarni and Anantharama, 2020). Following the COVID-19 epidemic, updated waste management requirements were implemented globally (Kulkarni, 2020). For example, according to the amended Italian standards, the municipal waste streams generated by houses must be classified into two major groups. One group is waste produced by COVID-19 confirmed cases in mandatory quarantine, while the second is waste generated by residences without COVID-19 confirmed persons. First group trash is typically processed by a small number of companies who gather it using standardized containers and adequate sterilization. Those waste standards encourage waste disposal in a double-layer container instead of segregation at the site of the confirmed COVID-19 cases. Furthermore, the second category of waste is being gathered in a different collecting system. Sheets, masks, and disposable gloves should be included in the residual waste stream and transported in double-sealed bags (Singh *et al.,* 2022). The Jordanian Minister of Health adopted local medical waste management legislation in October 2001. The goal of these rules is to keep medical waste management and disposal under control. The critical criteria defined by these regulations are categorizing medical wastes and managing medical wastes inside the healthcare institution. This domain includes medical wastes, separation, collection, storage, transportation, and disposal (JMWMRA, 2001). These instructions describe medical waste as well as the scope of each instruction. According to their classification, the instruction regulates all stages of proper and safe handling of medical wastes from generation to color-coded plastic bags and containers, packing, storing, transporting, and treatment, either by incineration or using alternative environmentally friendly techniques like autoclaving or microwaving. These guidelines establish criteria that all healthcare waste producers must follow to protect public health. Community protection against COVID-19 infection is a top concern for Jordan's government. As a result, medical waste and ordinary garbage from labs, health institutions, quarantine, and isolation centers run the danger of harboring germs that might infect the general population if not correctly disposed of. If the infectious microbe is not effectively confined within the laboratory or if accidents or emergencies occur, then the infected microorganism may be released into the environment. Medical laboratories, quarantine and isolation units, and inspection stations will be obligated to follow specific processes, emphasizing the proper waste management of hazardous substances, sample transport protocols, and workers washing before leaving the workplace and returning to their communities. The Environmental Health Department of the Ministry of Health (MOH) examines each healthcare facility's medical waste management and disposal systems to check if they meet the World Bank Group's standards and the current WHO COVID-19 regulations. Where these processes are not being implemented inside a healthcare facility, the MOH ensures that any necessary technical support or tools will be provided (JMWMRA, 2021). Severe acute respiratory syndrome coronavirus 2 (SARS-CoV-2), specimens are collected from potential COVID-19 patients by swabbing the upper or lower respiratory tract as an initial diagnostic technique. Upper respiratory tract, including nasopharyngeal samples are recommended for most patients while lower respiratory tract samples such as sputum, endotracheal aspirate, and bronchoalveolar lavage are recommended for special clinical circumstances (NCoV-2019, 2019). COVID-19 specimens must be placed into a sterile transport tube containing a viral transport medium as soon as feasible. Good quality diagnostic samples are essential for accurate screening and future study. Therefore, specimens should be obtained by competent professionals. All respiratory specimens should be labeled appropriately and transferred to the laboratory within three days of the collection while remaining at a low temperature (Gao *et al.,* 2020; Abu-

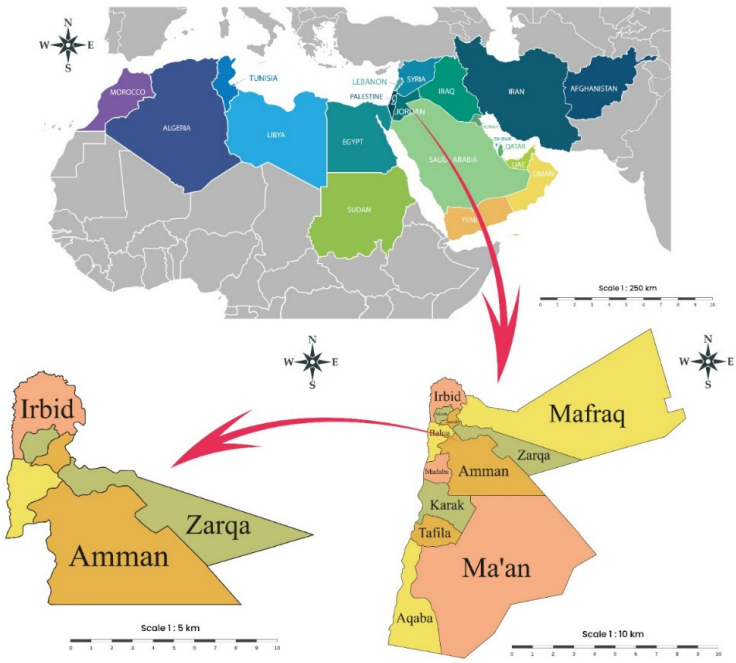

Fig. 1: Geographic location of the study area in the Jordan's central and northern regions in Amman, Zarqa, and Irbid of Jordan

Qdais *et al.,* 2020). Given the severe danger of COVID-19 samples, they must be tested immediately, and it is strongly recommended that the samples collectors contact the medical laboratory or recipients before submitting the specimens, along with a request form, to guarantee correct and efficient handling and treatment (CDC, 2021). The purpose of this study is to assess COVID-19 medical waste knowledge and management in Jordanian screening stations, with a particular focus on understanding and implementing the critical steps of medical waste management. These steps are well-defined and conveyed to technicians, physicians, and nurses who work with patients, medical equipment, and medical waste. This study also intended to verify the knowledge of ostensibly highly skilled medical staff and observe the waste data collection stage (the first stage of waste handling). The survey results will be used to analyze and evaluate the efficiency of medical waste treatment management. Any breach or misinterpretation of these rules and regulations is likely to cause significant issues, such as disease transmission between people and the discharge of dangerous substances into the environment. Furthermore, no significant variations in the answers to the staff of the participating sites are predicted. The objective of this study is to evaluate the level of healthcare workers' knowledge in the medical waste management field in Jordanian Coronavirus disease 2019 screening stations. This study was carried out at COVID-19 screening stations located in the Jordanian governorates of Amman, Zarqa, and Irbid from April 2021 to September 2021.

MATERIALS AND METHODS

The current investigation was carried out in governorates throughout Jordan's central and northern regions. Three governorates were chosen from the total of twelve governorates, namely Amman, Zarqa, and Irbid, and a cross-sectional survey was undertaken to collect data for the current study (Fig. 1). Given that these governorates are hosting about 60% of Jordan's total COVID-19 screening sites (JHC, 2021). The work title distribution of the total healthcare employees at screening station facilities in Jordan is as follows: 60% technicians, 25% nurses, and the remaining amount represents physicians. There are two healthcare workers; one of them is working on the patient's data entry process (outside the screening station), and the other worker is taking COVID-19 swaps within the screening station. In the selected screening stations,

interviews were performed and a survey was conducted to evaluate the degree of awareness, knowledge, and implementation of Jordanians' medical waste management protocols amongst healthcare staff such as physicians, nurses, and laboratory technicians.

The participants' responses were gathered using a designed questionnaire containing closed-ended questions with meticulous consideration to the WHO's 2020 medical waste management regulations and implemented by Jordan's MOH (JMWMRA, 2021). The questionnaire includes information about different variables such as age, gender, education level, job title, smoking, and other details about medical waste handling, awareness, knowledge, and implementation. The data collection tools were created in English and then translated into Arabic. Jordan has about 150 government-run screening facilities and 59 privately run screening stations (JPSSSC, 2021; JHC, 2021). A total of 78 workers from the collecting station sample were chosen randomly to complete the survey (41 males and 37 females, with average age 32.4 years ± 7.5) and 45 government-run and 33 privately run screening stations (20 doctors, 21 nurses, and 37 technicians). Participants in the study were guaranteed of their anonymity and confidentiality. The questionnaire was subdivided into three modules to gather information on various areas of medical waste management. The first module was created to determine the level of COVID-19 knowledge and awareness among healthcare personnel (Table 1). The COVID-19 medical waste administrative procedures (Table 2) focused on the second module, which examined knowledge and implementation. The third module addressed the COVID-19 medical waste collection procedures (Table 3). Responses were given in five different levels and divided into two levels of positive responses ("Very high" and "high") and three levels of negative responses ("Good," Fair," and "Poor."). Positive responses suggest that the person has a high level of knowledge and application of the subject of this topic, while negative responses indicate the reverse (Dell-Kuster *et al.,* 2014).

Data from cross-sectional surveys conducted via interviews at selected COVID-19 screening sites have been entered utilizing the IBM Statistical Package for the Social Sciences (SPSS) version 25.0. IBM SPSS was

Table 1*:* COVID-19 awareness and knowledge among healthcare workers

No.	Question
1	Identify your level of awareness of getting infected of COVID-19.
2	Identify your level of hygiene awareness.
3	Identify your level of commitment to wearing gloves, mask, shield, and coat at the workplace.
4	Identify your level of commitment to wearing gloves and mask out of the workplace.
5	Identify your level of confidence about the safety and effectiveness of the COVID-19 vaccine.
6	After you started working at a COVID-19 screening facility, did you get infected by COVID-19?

Table 2: COVID-19 medical waste administrative processes: Healthcare workers' understanding and implementation inside COVID-19 screening stations Table 3: Healthcare workers' knowledge and implementation of COVID-19 medical waste collection protocols inside COVID-19 screening stations

No.	Question
1	Level of hygiene awareness
2	Speed of screening tests
3	Having warning signs that clarify the hazards of COVID-19 medical wastes
4	Having a clear plan in case there is COVID-19 medical waste emergency pollution
5	Giving periodic training that clarifies the importance of managing COVID-19 wastes
6	Having a fixed schedule for COVID-19 waste removal
7	Having labeled and color-coded containers that identify the content of each container
8	Having a clear and daily record that shows the amount and type of COVID-19 wastes
9	Does your department have spare containers in case the main containers are full?

Table 3: Healthcare workers' knowledge and implementation of COVID-19 medical waste collection protocols inside COVID-19 screening stations

No.	Question
1	Following national and international protocols of separating and managing COVID-19 wastes
2	COVID-19 wastes are treated appropriately
3	A qualified person with the appropriate outfit takes COVID-19 wastes out of your faculty
4	COVID-19 wastes are collected in separate bags based on waste color codes and labels
5	The availability of specific bags and collecting tools at your department
6	The containers are sterilized after waste transportation

used to evaluate the data acquired for item analysis, validity, and reliability of the produced instrument. Descriptive statistics were used to calculate frequency, percentage, average, and variance for study participants' general characteristics. The study's findings were presented in the form of figures and texts as needed. Internal consistency reliability (Cronbach's alpha coefficient) was used to verify the uniformity of questions in this study. Linear regression, multinomial logistic regression (Taber, 2017), and the analysis of variance (ANOVA) were conducted to evaluate the differences between groups. The significance level was set at $p \leq 0.05$.

RESULTS AND DISCUSSION

The reliability statistics for each of the three modules and on the overall questionnaire are discussed as; The first module's Cronbach's alpha coefficient is 0.797 with a Guttman split-half coefficient of 0.674; The second module's Cronbach's alpha coefficient is 0.797 with a Guttman split-half coefficient of 0.68; The third module's Cronbach's alpha coefficient is 0.877 with a Guttman split-half coefficient of 0.788, specifying that the subscale has adequate inter-term reliability; and the entire questionnaire's Cronbach's alpha coefficient is 0.895 with a Guttman split-half coefficient is 0.831, indicating that the subscale has sufficient inter-term reliability. Further analysis revealed that removing any of the items would not significantly increase the alpha level. The questionnaire demonstrates that 99% of participants can recognize more than three COVID-19 symptoms and characterize more than three COVID-19 preventative approaches. In addition, only 5.2% of workers have poor faith in SARS-CoV-2 vaccines, whereas 91% are eager to get vaccinated. The purpose of the first module was to determine the level of knowledge and awareness in medical waste management among healthcare professionals. Fig. 2 depicts the survey findings of several categories. The additive positive replies (the sum of positive answers/ the total number of answers) and additive negative replies (the sum of negative answers/the total number of answers) are summarized in this graph. Different categories represent different replies to the survey's questions. Doctors and government-run screening stations had the highest positive value with a positive average of 0.83 and 0.86, respectively, whereas private sector screening stations had the lowest positive value with an average of 0.78. Nurses and laboratory technicians also showed a lack of personal awareness among other job titles. Nurses and private-sector screening station personnel, in particular, were less likely to commit to wearing gloves and masks outside of the workplace, with p-values of 0.024 and 0.043, respectively. Furthermore, doctors had the highest level of hygiene awareness (p-value 0.042). A five-point Likert scale was used to evaluate module 1, the outcomes were highly satisfying, with a scale value of 4.23 (Lange *et al.,* 2020).

The additive sums of the second module, which focused on COVID-19 medical waste administrative procedures, are shown in Fig. 3.

The results demonstrate that most categories have negative additive sums of answers with a value of 0.27 or greater, with the highest negative averages found for males, technicians, and among doctors. Government-run and private sector stations have nearly identical negative averages of 0.3 and 0.31, respectively. However, multinomial logistic regression (Petrucci, 2009) revealed that government-run screening stations were 2.36 times more likely to have a clear plan in the event of COVID-19 medical waste emergency pollution (p-value 0.044) and were more prepared if the main containers were full by providing spare containers

(p-value 0.001). On the other hand, nurses have the highest rate of correctly applying COVID-19 medical waste administrative procedures, with an average of 0.73. Moreover, they were more confident than other healthcare personnel in performing nasal swaps (the fastest speed of test) with p-value 0.031. Besides, a value of 3.86 on a five-point Likert scale indicates that module 2 overall performance was satisfactory. Fig. 4 depicts the results of the additive sums of answers in the third module, which examines knowledge and application of COVID-19 medical waste collection measures. Males have a lower understanding of waste management methods than females. Furthermore, the private sector fails to execute national and international protocols properly, with a negative average of more than 40%. Nurses, unlike the first and second modules, had the highest positive average of 0.69. Further analysis showed that government-run screening stations employers outperformed private-run screening stations employers in terms of adhering to national and international procedures for separating and handling COVID-19 wastes (p-value 0.028). Females, on the other hand, treated waste better than males (p-value 0.045). Finally, nurses were more concerned with ensuring that containers were sterilized following the waste collection process (p-value 0.023). As expected, the third module has the lowest Likert scale value of 3.8.

The analysis also showed that modules 3 and 2 have a significant positive correlation (R-value = 0.66, p-value < 0.001). However, modules 1 and 3 have weak significant association (p-value = 0.24 and p-value < 0.004, respectively). Finally, between the second and first modules, there is a significant positive correlation (R-value = 0.31, p-value < 0.001). The findings of this investigation revealed that there are no significant medical waste management shortages at the screening stations. Although the results of government screening stations in Jordan are better than those of private-sector screening stations, which require more attention to improve their performance, this is not to say that these hospitals are entirely following the proper and most acceptable medical waste administrative processes and collecting practices. The medical team should be well competent and adequately trained in this field due to the importance and danger of medicinal wastes on both humans and the environment. Figs. 2–4 illustrate that doctors and nurses are the most likely healthcare workers to correctly follow administrative and collection rules. Furthermore, because they have noticed hazardous or unpleasant habits and practices in the collection of medical wastes within screening stations, technicians must pay closer attention to national and international waste management rules.

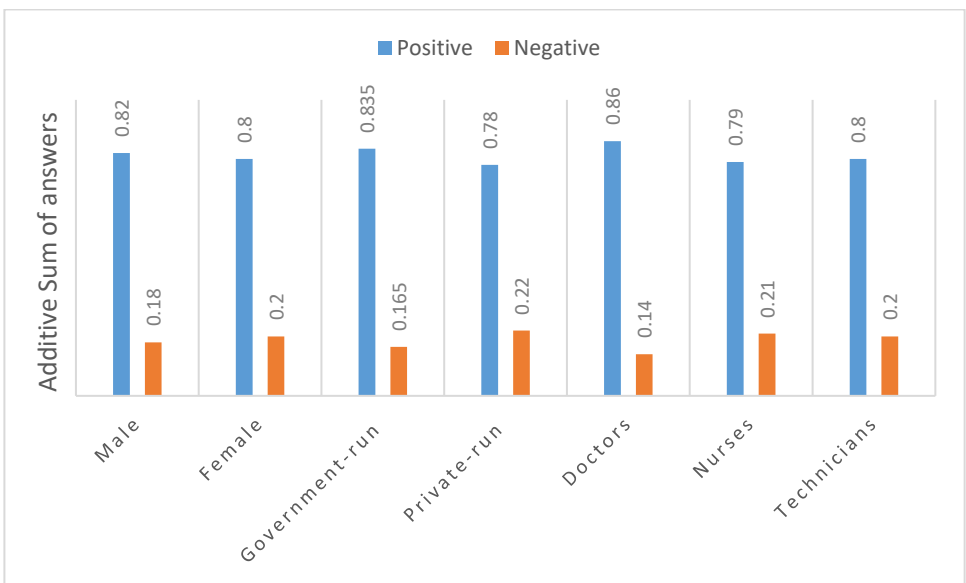

Fig. 2: Module 1 additive sums of positive answers (blue) and negative answers (orange)

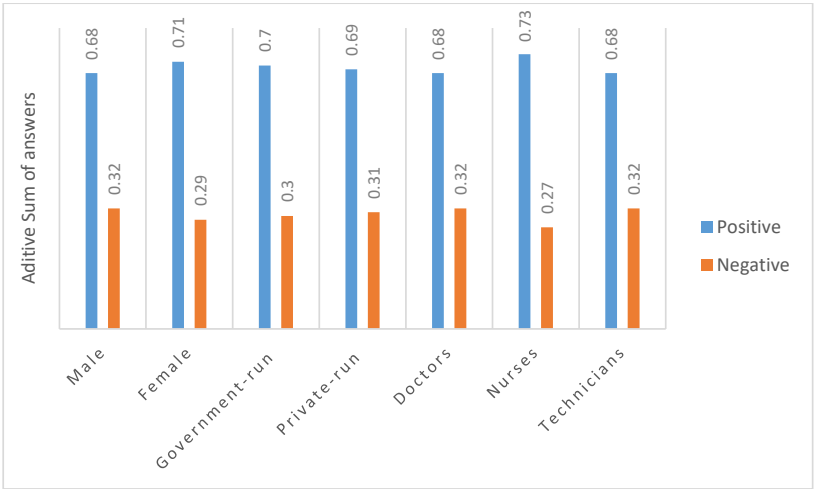

Fig. 3: Module 2 additive sums of positive answers (blue) and negative answers (orange)

Further investigation shows that 46% of participants did not get infected with COVID-19 after they started working in screening stations. After starting working, the average time to get infected is 3.9 months, indicating that most of the staff are applying module 1 correctly. The findings are analyzed and compared with many categories like gender, job title, employer, age, and smoking status via a one-way ANOVA. In the first module, there were no significant differences in any of the category responses. Furthermore, in the module 2 questions, there are no significant differences between the different groups. When the replies to the job title and employer categories are examined in the third module, no significant difference appears in the areas mentioned above as shown in Figs. 2 and 3. The current study found that healthcare practitioners had a high degree of knowledge regarding COVID-19. The average percentage of positive answers was 81.9 %. This is consistent with research undertaken in Egypt, Pakistan, and China (Abdel Wahed *et al.,* 2020; Saqlain *et al.,* 2020; Zhang *et al.,* 2020). Furthermore, a study found that the effect of one's family and society improved the degree of awareness of healthcare personnel (Nabe-Nielsen *et al.,* 2021). Regardless of their profession, the participants in this research had a decent knowledge, particularly about COVID-19 disease prevention methods. With an emphasis on the correct belief that personal hygiene may prevent infection, which was prevalent among physicians, practically all healthcare workers were aware of the proper infection control procedures, which conforms with research from Bangalore and Egypt (Elgibaly *et al.,* 2021). The findings of this investigation demonstrated a very high degree of trust in COVID-19 vaccinations, which is consistent with other study (Shrestha *et al.,* 2021). In contrast, research showed that Iran, Japan, and the United States revealed a low degree of trust in COVID-19 vaccines (Wong *et al.,* 2021; Hou *et al.,* 2021). Additionally, a survey found that 68% of healthcare professionals acknowledged that proper segregation is the most critical stage in waste management, and 82 % of participants working in this setup were familiar with the various color-coded containers used for medical waste separation (Ilyas *et al.,* 2020). Another study showed that the majority of healthcare workers 79.3% were consistently implemented the MOH recommendations for medical waste management, and 69.1% of healthcare workers categorized the color-coded containers used for medical waste disposal according to the kind of waste. While treating COVID-19 patients, about 76.6 % of healthcare personnel always followed infection control procedures (Jalal *et al.,* 2021). In this study, most of the participating healthcare workers (88.3 %) demonstrated a high level of awareness inside screening facilities and adhered to infection control policies while taking nasal swaps from COVID-19 patients. Additionally, 73.1% of screening station workers were able to recognize the labeled and color-coded containers used to identify each container's content. The availability of spare

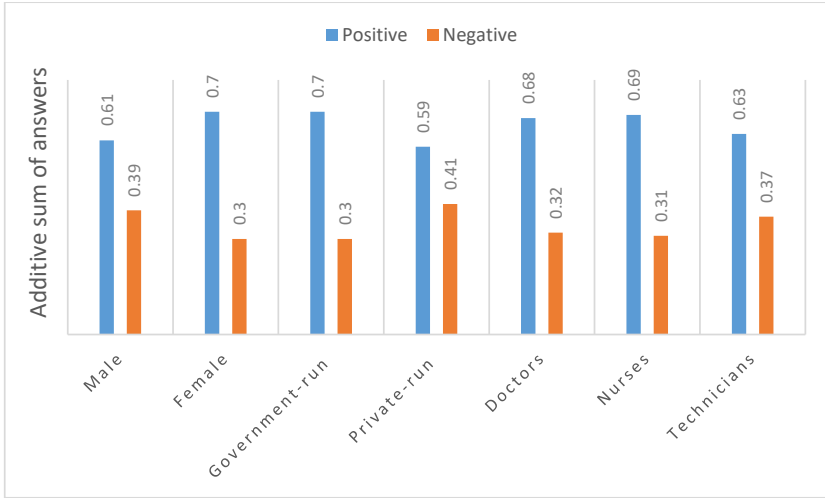

Fig. 4: Module 3 additive sums of positive answers (blue) and negative answers (orange)

containers at screening stations was rated positively by 93.6 % of healthcare workers. Unfortunately, only 48.7% of Jordanian healthcare workers at COVID-19 screening stations received periodic medical waste management training; as a result, policymakers must devote more time and effort to providing health workers with appropriate training. The survey findings also revealed that 69.2 % of healthcare personnel followed local and international (WHO) guidelines for separating and treating COVID-19 wastes, which is greater than the positive response in other countries such as Vietnam and Bangladesh (Tien *et al.,* 2021). A research conducted in Alahsa on the attitudes of healthcare workers toward correctly managing COVID-19 medical wastes revealed that most healthcare professionals agreed that medical wastes must be appropriately handled and that management needs collaboration (Jalal *et al.,* 2021). However, in this study, only 65.4 % of healthcare workers handled COVID 19 medical waste appropriately, which is lower than the proportion of healthcare professionals in Alahsa, Saudi Arabia. Overall, this study found that Jordanian healthcare workers at COVID-19 screening stations demonstrated a high level of knowledge and practice when compared to medical waste treatment guidelines in many countries with emerging and developing economies, which are poorly regulated and frequently disregard WHO recommendation for adequate medical waste treatment (Singh *et al.,* 2021).

CONCLUSION

This study reports the results of a survey of personnel in several COVID-19 screening sites located across Jordan. The key criteria listed in the WHO and MOH rules released following the epidemic were covered in this study. These requirements include healthcare personnel's expertise and awareness, administrative processes, and collecting techniques. The research survey focused on personal medical waste knowledge and awareness, medical waste administrative procedures which were applied by the healthcare workers inside COVID-19 screening stations, and applying national and international COVID-19 medical waste administrative and collection standards inside COVID-19 screening sites. According to the study, 99 % can identify more than three COVID-19 symptoms and define more than three COVID-19 preventative procedures. Furthermore, 5.2 % have little confidence in SARS-CoV-2 vaccinations, whereas 91% are ready to be immunized. For the first module, all categories provided highly satisfactory responses, but the private sector screening stations, females, nurses, and laboratory technicians, among others, showed a lack of personal awareness. The results of the second module revealed that the majority of categories have unfavorable responses in terms of awareness and application of COVID-19 medical waste administrative processes inside screening stations. However, the overall performance of the second module was

adequate. The results of the third module, which examined knowledge and application of COVID-19 medical waste-collecting procedures inside screening stations by health care workers, revealed that males have a lower knowledge of waste management methods than females. Furthermore, the private sector fails to implement national and international protocols fully. As a result, Jordan's medical waste management system are effective, although it needs further attention. Although the Jordanian government is paying close attention to this issue, some who work with hazardous waste are ignorant of the actual implications. Furthermore, the management of these institutions should pay greater attention to how medical waste is treated and disposed of at all levels. More thorough studies will be necessary in the future. This study did not calculate the quantity of medical waste generated in various medical institutions. Contaminants of various sorts were not calculated as well.

AUTHOR CONTRIBUTIONS

S.M. Alzghoul conducted the literature review, statistical analysis of the gathered data, data analysis and interpretation, paper preparation, and manuscript edition. O. Smadi compiled the data analysis and helped with paper preparation, literature review, and manuscript editing. M.B. Alzghoul assisted with the literature review, data interpretation, and paper writing. T.D. Almomani conducted the literature review, analyzed the acquired data statistically, and manuscript edition. O. Albataineh edited and prepared the text, as well as analyzed the data.

ACKNOWLEDGMENT

The authors are appreciative to Mrs. Alaa Mofleh Alzghoul for her help in data collection, to the staff at COVID 19 screening sites for supplying the data required for this study's development, and to The Hashemite University for its support.

CONFLICT OF INTEREST

The authors declare no potential conflict of interest regarding the publication of this work. In addition, the ethical issues including plagiarism, informed consent, misconduct, data fabrication and, or falsification, double publication and, or submission, and redundancy have been completely witnessed by the authors.

ABBREVIATIONS

%	Percent
ANOVA	The analysis of variance
COVID-19	Coronavirus disease 2019
Fig.	Figure
HIV	Human immunodeficiency virus
MOH	Ministry of Health
n	Number of samples
PPE	Personal protection equipment
p-value	Probability value
SARS-CoV-2	Severe acute respiratory syndrome coronavirus 2
SPSS	Statistical package for the social sciences
UN	United Nations
USEPA	United States Environmental Protection Agency
WHO	World Health Organization

REFERENCES

Abdel Wahed, W.Y.; Hefzy, E.M.; Ahmed, M.I.; Hamed, N.S., (2020). Assessment of knowledge, attitudes, and perception of health

care workers regarding COVID-19. A cross sectional study from Egypt. J. Community Health. 45(6): 1242-1251 **(10 pages)**.

Abu-Qdais, H.A.; Al-Ghazo, M.A.; Al-Ghazo, E.M., (2020). Statistical analysis and characteristics of hospital medical waste under novel Coronavirus outbreak. Global J. Environ. Sci. Manage., 6 (Special Issue in Covid-19): 21-30 **(10 pages).**

Agamuthu, P.; Barasarathi, J., (2020). Clinical waste management under COVID-19 scenario in Malaysia. Waste Manage., Res., 39(1): Suppl. 18-26 **(9 pages)**.

Babanyara Y.Y.; Ibrahim, D.B.; Garba T.; Bogoro, A.G.; Abubakar, M.Y., (2013). Poor medical waste management (MWM) practices and its risks to human health and the environment: A Literature Review, World Academy of Science, Engineering and Technology, Open Science Index 83, Int. J. Health Med. Eng., 7(11): 780 - 787 **(8 pages).**

CDC, (2020). Interim Laboratory Biosafety Guidelines: COVID-19. Centers for Disease Control and Prevention.

Dell-Kuster, S.; Sanjuan, E.; Todorov, A.; Weber, H.; Heberer, M.; Rosenthal, R., (2014). Designing questionnaires: healthcare survey to compare two different response scales. BMC Med. Res. Methodol., 14(1) **(13 pages)**.

Elgibaly, O.; Daef, E.; Elghazally, S.; Hassan, H.; ElsaidTash, R.; Bahgat, S.; ELantouny, N.; Zarzour, A.; Othman, M.; El-Sokkary, R., (2021). Knowledge, perception, and confidence of healthcare workers about COVID-19 preventive measures during the first wave of the pandemic: a cross-sectional study from Egypt. GERMS. 11(2): 179-188 **(10 pages)**.

Filimonau, V., (2021). The prospects of waste management in the hospitality sector post COVID-19. Resour. Conserv. Recycl., 168: 105272 **(9 pages)**.

Gao, F.; Tao, L.; Ma, X.; Lewandowski, D.; Shu, Z., (2020). A study of policies and guidelines for collecting, processing, and storing coronavirus disease 2019 patient biospecimens for biobanking and research. Biopreserv. Biobanking. 18(6): 511 **(6 pages)**.

Haque, M.S.; Uddin, S.; Sayem, S.M.; Mohib, K.M., (2021). Coronavirus disease 2019 (COVID-19) induced waste scenario: a short overview. J. Environ. Chem. Eng., 9(1): 104660 **(14 pages)**.

Hou, Z.; Tong, Y.; Du, F.; Lu, L.; Zhao, S.; Yu, K.; Piatek, S.; Larson, H.; Lin, L., (2021). Assessing COVID-19 vaccine hesitancy, confidence, and public engagement: a global social listening study. J. Med. Internet Res., 23(6): **(11 pages)**.

Ilyas, S.; Srivastava, R.R.; Kim, H., (2020). Disinfection technology and strategies for COVID-19 hospital and bio-medical waste management. Sci. Total Environ., 749: 141652 **(11 pages)**.

Isaifan, R.J., (2020). The dramatic impact of Coronavirus outbreak on air quality: has it saved as much as it has killed so far. Global J. Environ. Sci. Manage., 6(3): 275-288 **(14 pages)**.

Jalal, S.; Akhter, F.; Abdelhafez, A.; Alrajeh, A., (2021). Assessment of knowledge, practice and attitude about biomedical waste management among healthcare professionals during COVID-19 Crises in Al-Ahsa. Healthcare., 9(6): **(13 pages)**.

JHC, (2021). Jordanian Healthcare Centers. Ministry of Health.

JPSSSC, (2021). Jordanians' Privet Sector Screening Stations for COVID-19.

JMWMRA, (2001). Jordanian Medical Waste Management Regulations Act. Ministry of Health.

JMWMRA, (2021). Jordanian Medical Waste Management Regulations Act (2021) Ministry of Health.

Kulkarni, B.; Anantharama, V., (2020). Repercussions of COVID-19 pandemic on municipal solid waste management: challenges and opportunities. Sci. Total Environ., 743: 140693 **(8 pages)**.

Kulkarni, B.N., (2020). Environmental sustainability assessment of land disposal of municipal solid waste generated in Indian cities: a review. Environ. Dev., 33: 100490 **(15 pages)**.

LaGrega, M.D.; Buckingham, P.L.; Evans, J.C., (2015). Hazardous waste management. New Delhi, India. Medtech.

Lange, T.; Kopkow, C.; Lützner, J.; Günther, K.; Gravius, S.; Scharf, H.; Stöve, J.; Wagner, R.; Schmitt, J., (2020). Comparison of different rating scales for the use in Delphi studies: different scales lead to different consensus and show different test-retest reliability. BMC Med. Res. Methodol., 20(1) **(11 pages)**.

Mihai, F.C., (2020). Assessment of covid-19 waste flows during the emergency state in Romania and related public health and environmental concerns. Int. J. Environ. Res. Public Health. 17(15): 5439 **(18 pages)**.

Nabe-Nielsen, K.; Nilsson, C.J.; Juul-Madsen, M.; Bredal, C.; Hansen, L.O.P.; Hansen, Å.M., (2021). COVID-19 risk management at the workplace, fear of infection and fear of transmission of infection among frontline employees. Occup. Environ. Med., 78(4): 248-254 **(7 pages)**.

NCoV-2019, (2019). Laboratory testing for 2019 novel coronavirus in suspected human cases 2020.

Neumeyer, X.; Ashton, W.S.; Dentchev, N., (2020). Addressing resource and waste management challenges imposed by COVID-19: an entrepreneurship perspective. Resour. Conserv. Recycl., 162: 105058 **(4 pages)**.

Petrucci, C., (2009). A primer for social worker researchers on how to conduct a multinomial logistic regression. J. Soc. Serv. Res., 35(2): 193-205 **(13 pages)**.

Prata, J.C.; Silva, A.L.P.; Walker, T.R.; Duarte, A.C.;Rocha-Santos, T., (2020). COVID-19 pandemic repercussions on the use and management of plastics. Environ. Sci. Technol., 54(13): 7760-7765 **(6 pages)**.

Prüss, A.; Emmanuel, J.; Stringer, R.; Pieper, U.; Townend, W.; Wilburn, S.; Chantier, Y.; World Health Organization. (2014). Safe management of wastes from health-care activities, Handbook, 2nd. Ed. World Health Organisation, Geneva.

Ramteke, S.; Sahu, B.L., (2020). Novel coronavirus disease 2019 (COVID-19) pandemic: considerations for the biomedical waste sector in India. Case Stud. Chem. Environ. Eng., 2: 100029 **(6 pages)**.

Saqlain, M.; Munir, M.M.; Rehman, S.U.; Gulzar, A.; Naz, S.; Ahmed, Z.; Tahir, A.H.; Mashhood, M., (2020). Knowledge, attitude, practice and perceived barriers among healthcare workers regarding COVID-19: a cross-sectional survey from Pakistan. J. Hosp. Infect., 105(3): 419-423 **(5 pages)**.

Sarkodie, S.; Owusu, P., (2020). Impact of COVID-19 pandemic on waste management. Environ. Dev. Sustain., 23(5): 7951-7960 **(10 pages)**.

Sharma, H.B.; Vanapalli, K.R.; Cheela, V.S.; Ranjan, V.P.; Jaglan, A.K.; Dubey, B.; Goel, S.; Bhattacharya, J., (2020). Challenges, opportunities, and innovations for effective solid waste management during and post COVID-19 pandemic. Resour. Conserv. Recycl., 162: 105052 **(12 pages)**.

Shinee, E.; Gombojav, E.; Nishimura, A.; Hamajima, N.; Ito, K., (2008). Healthcare waste management in the capital city of Mongolia. Waste Manage., 28(2): 435-441 **(7 pages)**.

Shrestha, A.; Thapa, T.; Giri, M.; Kumar, S.; Dhobi, S.; Thapa, H.;

Dhami, P.; Shahi, A.; Ghimire, A.; Rathaur, E., (2021). Knowledge and attitude on prevention of COVID-19 among community health workers in Nepal-a cross-sectional study. BMC. Public. Health. 21(1): **(13 pages)**.

Singh, E.; Kumar, A.; Mishra, R.; Kumar, S., (2022). Solid waste management during COVID-19 pandemic: Recovery techniques and responses. Chemosphere. 288: 132451 **(15 pages)**.

Singh, N.; Ogunseitan, O.; Tang, Y., (2021). Medical waste: Current challenges and future opportunities for sustainable management. Crit. Rev. Environ. Sci. Technol., 1-23 **(23 pages)**.

Taber, K., (2017). The use of cronbach's alpha when developing and reporting research instruments in science education. Res. Sci. Educ., 48(6): 1273-1296 **(24 pages)**.

Tien, T.; Tuyet-Hanh, T.; Linh, T.; Hai Phuc, H.; Van Nhu, H., (2021). Knowledge, attitudes, and practices regarding COVID-19 prevention among Vietnamese healthcare workers in 2020. Health. Serv. Insights., 14: 1-7 **(7 pages)**.

Tripathi, A.; Tyagi, V.K.; Vivekanand, V.; Bose, P.; Suthar, S., (2020). Challenges, opportunities and progress in solid waste management during COVID-19 pandemic. Case Stud. Chem. Environ. Eng. , 2: 100060 **(7 pages)**.

UNEP, (2020). COVID-19 waste management factsheets, (2020). UNEP - UN Environment Program.

Wong, L.; Alias, H.; Danaee, M.; Ahmed, J.; Lachyan, A.; Cai, C.; Lin, Y.; Hu, Z.; Tan, S.; Lu, Y.; Cai, G.; Nguyen, D.; Seheli, F.; Alhammadi, F.; Madhale, M.; Atapattu, M.; Quazi-Bodhanya, T.; Mohajer, S.; Zimet, G.; Zhao, Q., (2021). COVID-19 vaccination intention and vaccine characteristics influencing vaccination acceptance: a global survey of 17 countries. Infect. Dis. Poverty., 10(1): **(14 pages)**.

Zhang, M.; Zhou, M.; Tang, F.; Wang, Y.; Nie, H.; Zhang, L.; You, G., (2020). Knowledge, attitude, and practice regarding COVID-19 among healthcare workers in Henan, China. J. Hosp. Infect., 105(2): 183-187 **(5 pages)**.

AUTHOR (S) BIOSKETCHES

Alzghoul, S.E., Ph.D., Assistant Professor, Department of Biomedical Engineering, College of Engineering, The Hashemite University Zarqa, Jordan.
- Email: *alzghoul@hu.edu.jo*
- ORCID: 0000-0001-9663-7820
- Web of Science Researcher ID: ABE-5425-2021
- Scopus Author ID: 56898948300
- Homepage: https://staff.hu.edu.jo/CV_e.aspx?id=BzkMMqslw/g=

Smadi, O.A., Ph.D., Associate Professor, Department of Biomedical Engineering, College of Engineering, The Hashemite University Zarqa, Jordan.
- Email: *othman.smadi@hu.edu.jo*
- ORCID: 0000-0002-9586-3743
- Web of Science Researcher ID: NA
- Scopus Author ID: 25229175900
- Homepage: https://staff.hu.edu.jo/CV_e.aspx?id=11urcy5NPpw

Almomani, T.D., Ph.D., Professor, Department of Biomedical Engineering, College of Engineering, The Hashemite University Zarqa, Jordan.
- Email: *thakir2000@hu.edu.jo*
- ORCID: 0000-0003-3638-079X
- Web of Science Researcher ID: ABB-6410-2020
- Scopus Author ID: 23970168800
- Homepage: https://staff.hu.edu.jo/CV_e.aspx?id=RJIAZT7evUs=

Alzghoul, M.B., Ph.D., Professor, Department of Basic Medical Veterinary Sciences, College of Veterinary Medicine, Jordan University of Science and Technology, Irbid, Jordan.
- Email: *alzghoul@just.edu.jo*
- ORCID: 0000-0003-4404-2889
- Web of Science Researcher ID: ABE-8281-2021
- Scopus Author ID: 14029872600
- Homepage: https://www.just.edu.jo/eportfolio/Pages/Default.aspx?email=alzghoul

Albataineh, O.M., Ph.D., Associate Professor, Department of Biomedical Engineering, College of Engineering, The Hashemite University Zarqa, Jordan.
- Email: *osamam@hu.edu.jo*
- ORCID: 0000-0002-6572-7695
- Web of Science Researcher ID: NA
- Scopus Author ID: 6507553713
- Homepage: https://www.iau.edu.sa/sites/default/files/cv/cv_template_-_englishosama.pdf

HOW TO CITE THIS ARTICLE

Alzghoul, S.E.; Smadi, O.A.; Almomani, T.D.; Alzghoul, M.B.; Albataineh, O.M., (2022). Solid medical waste management practices and awareness in COVID-19 screening stations Global J. Environ. Sci. Manage., 8(3): 327-338.

DOI: 10.22034/gjesm.2022.03.03

url: https://www.gjesm.net/article_247732.html

Global J. Environ. Sci. Manage. 8(3): 339-352, Summer 2022, Serial #31

Global Journal of Environmental Science and Management
(GJESM)

Homepage: https://www.gjesm.net/

ORIGINAL RESEARCH PAPER

Flood hazard simulation and mapping using digital elevation models with different resolutions

G.R. Puno[1,*], R.C.C. Puno[2], I.V. Maghuyop[2]

[1]*Department of Forest Resources Management, College of Forestry and Environmental Science, Central Mindanao University, Musuan, Maramag, Bukidnon, Philippines*

[2]*Department of Environmental Science, College of Forestry and Environmental Science, Central Mindanao University, Musuan, Maramag, Bukidnon, Philippines*

ARTICLE INFO

Article History:
Received 04 September 2021
Revised 09 November 2021
Accepted 14 January 2022

Keywords:
Bathymetry
Calibration
Floodplain
Remote sensing
Two-dimensional map

ABSTRACT

BACKGROUND AND OBJECTIVES: Fine topographic information is a key input parameter for a detailed flood simulation and mapping. This study aimed to compare the accuracy statistics of the flood models developed using the digital elevation datasets with different resolutions from the light detection and ranging and interferometric synthetic aperture radar systems.

METHODS: The study applied the Hydrologic Engineering Center-Hydrologic Modeling System and Hydrologic Engineering Center-River Analysis System models workable within the geographic information system to simulate and map flood hazards in Maapag Watershed. The models' validity and accuracy were tested using the confusion error matrix, f-measurement, and the root means square error statistics.

FINDINGS: Results show that using the light detection and ranging dataset, the model is accurate at 88%, 0.61, and 0.41; while using the interferometric synthetic aperture radar dataset, the model is accurate at 76%, 0.34, 0.53; for the error matrix, f-measurement, and root mean square error; respectively.

CONCLUSION: The model developed using the light detection and ranging dataset showed higher accuracy than the model developed using the interferometric synthetic aperture radar. Nevertheless, the latter can be used for flood simulation and mapping as an alternative to the former considering the cost of model implementation and the smaller degree of accuracy residual error. Hence, flood modelers particularly from local authorities prefer to use coarser datasets to optimize the budget for flood simulation and mapping undertakings.

DOI: 10.22034/gjesm.2022.03.04

NUMBER OF REFERENCES	NUMBER OF FIGURES	NUMBER OF TABLES
39	5	3

*Corresponding Author:
Email: *grpuno@cmu.edu.ph*
Phone: +9166 918 259
ORCID: 0000-0002-7170-641X

Note: Discussion period for this manuscript open until October 1, 2022 on GJESM website at the "Show Article".

INTRODUCTION

Food hazard research has since been important in the last two decades and continues to be relevant in future climate scenarios to develop realistic solutions to disaster risk problems (Pinos and Quesada-Roman, 2022). For more detailed and accurate outputs, studies on flood hazards are conducted through simulations using high-resolution digital elevation models (DEMs) such as those derived from the light detection and ranging (LiDAR) and interferometric synthetic aperture radar (IfSAR) systems. DEM, as a representation of the natural and man-altered ground surface, is valid for any three-dimensional and topographic visualization. It is excellent as an input dataset in flood modeling and simulation for risk management strategies (Li *et al.,* 2017; Guidolin *et al.,* 2016). High-resolution DEM is sought in flood hazard modeling studies to give a quality result as it determines specific areas where inundation might occur in the particular watershed (Alivio *et al.,* 2019; Hawker *et al.,* 2018). Highly detailed DEMs are the most preferable datasets in hydrologic modeling and simulations where accurate flood hazard maps are sought. Appropriate DEM specification is an essential factor to enhance flood simulation accuracy and reliability. Enhanced simulations reliability is important in generating detailed information that contributes to the cost-effective approaches in the reduction and prevention of damages and economic losses caused by flood hazards (Demir and Kisi, 2016). Two of the fastest-growing remote sensing technologies that provide satisfactory resolution DEMs are light detection and ranging (LiDAR) and interferometric synthetic aperture radar (IfSAR) (Hawker *et al.,* 2018). LiDAR and the IfSAR systems offer high-resolution DEMS suitable for developing hydrologic models with more refined and accurate model outputs. Theoretically, LiDAR DEM offers more advantages than IfSAR DEM as it provides a flood hazard map with more detailed and precise information. Airborne LiDAR is also an emerging remote sensing state-of-the-art system design, technology and application (Li *et al.,* 2020). LiDAR is capable of providing highly accurate spatial data and information widely used for hazard assessment, disaster risk assessment and flood modeling. The advancement of LiDAR technology systems facilitated and improved flood applications (Muhadi *et al*., 2020). It is the most useful elevation dataset for mapping small regions with high accuracy. However, acquiring LiDAR DEM is costly especially for large-area applications. Thus, LiDAR data is limited in areas with wider coverage due to expensive acquisition operations (Khalid *et al*., 2016). High acquisition cost is a hindrance in using LiDAR datasets in some developing countries (Muhadi *et al*., 2020). IfSAR, also termed InSAR, on the other hand, is considered a relatively cheaper and complementary 3-D mapping technology with varying applications in many fields including flood simulations and mapping flood hazards (Lu *et al*., 2007). It is more cost-effective compared to LiDAR and is readily available for use in flood modeling with quality and accuracy of results higher than other satellite systems (Gopal, 2010). Nevertheless, LiDAR is generally the most preferred technology for deriving DEM despite its high cost (Hashim *et al*., 2014). In a disaster-prone country like the Philippines, billions worth of local funds had been allocated for research projects on flood hazard management particularly mapping and monitoring in some priority river basins using LiDAR technologies. The project allocated the highest bulk of the cost for the acquisition of LiDAR datasets (Mateo, 2013; Ronda, 2013). Meanwhile, the government has also acquired IfSAR DEM which covers the whole country (Belen, 2015). The desire for effective flood hazard maps at the onslaught of disaster in recent years instigated the use of high-resolution DEMs from LiDAR and IfSAR technologies for flood modeling and simulation studies (Talisay *et al*., 2019). The accuracy of the results in such studies is generally acceptable due to the good topographic representation of both DEMs. However, LiDAR is still more preferred than other digital elevation datasets as it provides higher flood simulation accuracy with minimal errors (Ogania *et al*., 2019). But still, in any project requirements and resources, the cost and economic feasibility perpetually remain the critical factors (Chen and Hill, 2007). Previous studies on the comparison of LiDAR and IfSAR datasets on flood simulations focus only on the predictive accuracy and precision of the model without expounding the degree of difference and the economic considerations. The computer application software used in the study includes the Hydrologic Engineering Center-Hydrologic Modeling System (HEC-HMS) and the Hydrologic Engineering Center-River Analysis System (HEC-RAS) models of the U.S. Army Corps of Engineers (USACE, 1964).

HEC-HMS and HEC-RAS models are workable within the geographic information systems (GIS) environment with HEC-GeoHMS and HEC-GeoRAS as their geospatial extension, respectively. The developed cost-sensitive model with acceptable accuracy performance is essential to enhance the management capability of pertinent government and non-government organizations in implementing the programs and projects regarding urban flood risk reduction and management both at the national and local levels. This study aimed to compare the accuracy statistics of the flood models developed using the digital elevation datasets with different resolutions from the light detection and ranging and interferometric synthetic aperture radar systems. Furthermore, this study aimed to investigate the applicability of IfSAR DEM as an alternative to LiDAR DEM based on the residual error of accuracies of the two models using the three statistical tests, namely the confusion error matrix, f-measurement, and the root mean square error (RMSE). By doing so, this study generates information helpful in formulating a science-based and cost-sensitive policy statement specific to the application of appropriate datasets for flood simulation and mapping necessary in the economically-sound implementation of disaster risk mitigation and management. This study was conducted in the Maapag Watershed, Valencia City, Bukidnon, Philippines from 2017 to 2019.

MATERIALS AND METHODS

Study watershed

This study covered the Maapag Watershed with geographical coordinates of 7° 45' 55.77" to 7° 56' 10.27" north and 125° 4' 40.03" to 125° 16' 25.51" east. The watershed extends at a width of 15 km and a length of 16.80 km with approximately 251.20 km^2. The majority of the watershed area falls under the jurisdiction of Valencia City, Bukidnon, Mindanao, Philippines (Fig. 1). Some tributaries, specifically the southern portion of the watershed, fall within the Municipality of Quezon, Bukidnon. Maapag Watershed drains to Mindanao River Basin, the second largest river basin in the country. The vast expanse of the Maapag floodplain is dominantly cultivated for rice production and for settlement areas that are regularly flooded, especially during heavy rainfalls with waters coming from the upstream terrains. Most often, the local government authorities warn the communities within the floodplain to be prepared during heavy rain to mitigate the negative impacts of flood hazards on human lives and properties (Cantal-Albasin, 2017).

DEM description

DEM is a computer graphic representation of elevation data in three-dimensional coordinates

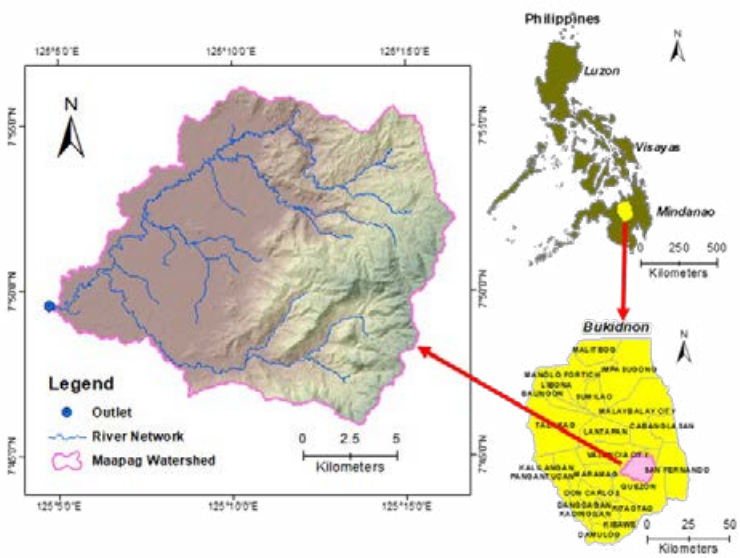

Fig. 1: Geographic location of the study area in Maapag Watershed, Valencia City of Bukidnon, Mindanao, Philippines

usually used in geographic information systems to visualize the terrain of the ground surface (Gandhi and Sarkar, 2016). Acquiring the DEMs can be done through photogrammetry like the LiDAR and IfSAR technologies. LiDAR technique uses airborne sensors emitting lasers to the Earth deriving DEM with a resolution of 1 m. The produced DEM has a vertical accuracy ranging from ±5 to 15 cm and horizontal accuracy of less than 1 m (Wedajo, 2017). The uses of LiDAR enable grain-scale surface roughness and provide highly accurate ground and urban landscape topographic datasets, which are essential characteristics for efficient simulation of the flood (Puno *et al*., 2019). In the Philippines, the LiDAR data was made available through the Data Acquisition Component (DAC) of the University of the Philippines-Disaster Risk and Exposure Assessment for Mitigation (UP-DREAM) and Phil-LiDAR Programs of the UP Training Center for Applied Geodesy and Photogrammetry (UP-TCAGP) supported by the Department of Science and Technology (DOST) (Makinano-Santillan *et al*., 2019). On the other hand, the IfSAR technology utilizes a Synthetic Aperture Radar (SAR) system of two or more images of the same extracted area (Lu *et al*., 2007). The data is formed from two radar images of the recorded phase and amplitude using microwave echoes, a combination of conventional SAR and interferometry techniques (Smith, 2002). The interaction of electromagnetic waves measures the precise distance between satellite antenna and ground resolution elements, deriving landscape topography of subtle elevation changes (Lu *et al*., 2007). The available IfSAR data in the Philippines from the National Mapping and Resource Information Authority (NAMRIA) has a resolution of 5 m with 1 m RMSE vertical accuracy and 2 m RMSE horizontal accuracy (Belen, 2015). Table 1 presents the comparison of the two digital elevation models used in the study.

DEM processing and preparation

Activities for DEM processing followed the workflows within the GIS environment involving data editing, mosaicking, calibration, and bathymetric data burning. The LiDAR datasets from the DREAM and Phil-LiDAR Programs were available in a form of spatial coordinates in American standard code for information interchange (ASCII) format file and drawing exchange format (DXF). ArcTeam toolbar developed by the UP Diliman Data Processing Component was utilized in generating DEM formats, particularly in the form of a digital terrain model (DTM). DEM editing included filling data gaps in the flight mission with no data using the FillDataGaps toolbar. The process also involved interpolation and object retrieval techniques to edit the DEM by omitting unnecessary objects in the DTM, ensuring unobstructed water flow in river systems, and filling of missed portions using a secondary DTM layer. These two processes served as the cleaning and refining of DTM. Adjacent edited flight missions were then mosaicked with edges smoothened. DTMs calibration was done through actual field surveys using ground validation points reckoned from mean sea level (MSL) gathered from the survey. The team conducted a resampling of the initially 5-meter resolution IfSAR DEM into 1 m and edited it following similar processes as that of LiDAR DEM. Scrutinizing the processed and mosaicked DTMs was also done for quality checking. The method also involved bathymetric data burning to integrate river morphology to DTM. This process fills the gaps created from LiDAR due to the inability of its laser pulse to penetrate the water surface and the inaccurate river bed elevations data from IfSAR. Conducting the bathymetric survey to acquire the desired data involves the collection of actual heights and coordinate points and the river geometry using the high-precision global navigation satellite system (GNSS) instrument applied with real-time kinematic

Table 1: Comparison of the two digital elevation models

Descriptions	LiDAR	IfSAR
Radar systems	Airborne	Airborne/Spaceborne
Vertical accuracy	<0.15 m	1 m
Horizontal accuracy	< 1 m	2 m
Resolution/pixel size	1 m	5 m
Model	DTM/DSM	DTM/DSM
Availability	Upon request	Upon request
Source	UP-DREAM	NAMRIA

(RTK) techniques. The process enabled the generation of a new raster using the inverse distance weighted (IDW) interpolation method of the Spatial Analyst tool of ArcGIS 10.2.2 version.

Basin model development, calibration and evaluation

The hydrologic models applied in this flood modeling and simulation studies are the HEC-HMS and HEC-RAS of the US Army Corps of Engineers. HEC-HMS was utilized to simulate the hydrologic processes while HEC-RAS was for the simulation of two-dimensional unsteady flow hydraulic analysis (Santillan and Makinano-Santillan, 2016). Both are open-source computer programs extensively utilized in modeling researches and studies involving hydrological processes (Divin and Mikita, 2016). The study team developed the hydrologic basin model of Maapag Watershed using the HEC-GeoHMS extension of ArcGIS 10.2.2. Within the HEC-HMS version 3.5 workflows, the team calibrated the Maapag basin model using the actual event data collected on November 20-22, 2017, caused by the tail-end of a cold front and northeast monsoon. Calibration of the model involved manual adjustment and fine-tuning of parameters such as the soil and land cover through the "trial and error" method to fit the simulated values to the observed hydrograph. Model performance to simulate flooding events was evaluated by calculating the efficiency criteria such as the root mean square error (*RMSE*) to the standard deviation (*STDEV*) of measured data ratio (*RSR*), Nash-Sutcliffe efficiency (*NSE*), and percent bias (*PBIAS*) statistics. The *RSR* values range from 0 which indicates a perfect prediction or zero *RMSE* to a large positive value. It follows the lower *RSR*, the lower the *RMSE*, the optimal or better the model simulation performance. *RSR* is computed using Eq. 1. (Moriasi *et al*., 2007).

$$RSR = \frac{RMSE}{STDEV_O} = \frac{\sqrt{\sum_{i=1}^{n}\left(Y_i^o - Y_i^s\right)^2}}{\sqrt{\sum_{i=1}^{n}\left(Y_i^o - Y^m\right)^2}}, \quad (1)$$

where *RMSE* is the root mean square error to the standard deviation of the observed data ($STDEV_o$) ratio (*RSR*), where Y_i^o is the i^{th} observation for the evaluated variable, Y_i^s is the i^{th} simulated value for the evaluated variable, Y^m is the mean of observed data for the evaluated variable, and *n* is the total number of observations. *NSE*, on the other hand, is a test of model performance that indicates how well the plot of observed versus simulated data fits the 1:1 line. Values between 0.0 and 1.0 are generally viewed as acceptable levels of performance, whereas values <0.0 indicate an unacceptable model performance. Following the same symbols used in Eq. 1, NSE is computed using Eq. 2 (Moriasi *et al*., 2007).

$$NSE = 1 - \frac{\sum_{i=1}^{n}\left(Y_i^o - Y_i^s\right)^2}{\sum_{i=1}^{n}\left(Y_i^o - Y^m\right)^2}, \quad (2)$$

PBIA is another test of model performance that assesses the average tendency of the predicted results to overestimate or underestimate the field observed data. A PBIAS of 0.0 indicates an accurate model performance. A positive and negative PBIAS value indicates underestimation and overestimation, respectively. With the same symbols used from the previous equations, PBIAS is calculated using Eq. 3 (Moriasi *et al*., 2007).

$$PBIAS = \frac{\sum_{i=1}^{n}\left(Y_i^o - Y_i^s\right)}{\sum_{i=1}^{n} Y_i^o} 100 \quad (3)$$

With acceptable statistical results, the calibrated and evaluated model of Maapag enabled simulation of flood depth and extent covering the floodplain of the river basin using the rainfall data from the tropical storm on December 21-23, 2017.

Flood simulation

For the hydraulic simulation, the team established the model using the HEC-GeoRAS extension tool in ArcGIS 10.2.2. The team also prepared the following datasets as the 2-dimensional (2D) area; land use/ land cover (LULC) map with incorporated Manning's *n* values; break lines shapefile of roads, riverbanks and the sudden change of elevation; and terrain data of LiDAR and IfSAR. A discharge hydrograph of the tropical storm simulated by the calibrated model was used for the unsteady flow analysis of hydraulic simulation. Flow data were inputted in each boundary condition identified as points for discharge inflows. A constant value of 0.01 was assigned for the standard depth and the outlet of the 2D domain area. Precipitation data from the calibrated HMS for

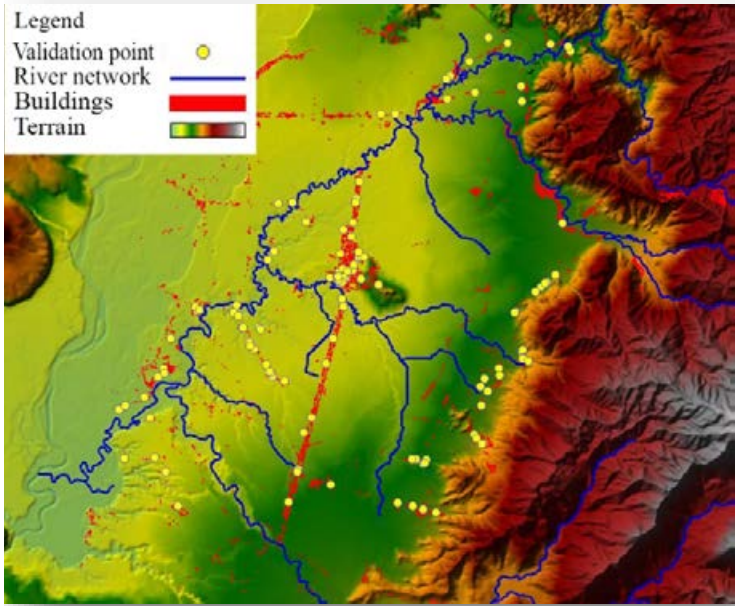

Fig. 2: Validation points in the floodplain of the watershed

the same event was added as an additional boundary condition covering the whole 2D domain area extent. Two separate unsteady flow analyses using the LiDAR and IfSAR DEMs were consequently performed in HEC-RAS version 5.0.

Flood validation

Around 120 points randomly scattered in the floodplain of Maapag were established for flood validation (Fig. 2). Each point represents a random household in the floodplain as determined by the extracted building features using the LiDAR-derived digital surface model (DSM), which portrays above-surface features such as buildings (Sharma *et al*., 2010). Flood information consisting of flood height, flood duration, and other relevant information were collected from each point through personal interviews. These points were then loaded in ArcGIS and plotted against the simulated flood depths using the LiDAR and IfSAR DEMs.

Three statistical tests, namely the error matrix or accuracy, f-measurement, and root mean square error, were run to measure the accuracy and validity of the simulated flood using the two DEMs. These statistical metrics are the common standard procedures for determining the similarity of maps in various mapping and model performance evaluation studies (Timbadiya *et al*., 2011). The accuracy statistic of the simulated flood depths was computed using Eq. 4 (Cabrera and Lee, 2019).

$$Accuracy\% = \frac{(A+B)}{N} \tag{4}$$

where *A* is the number of correctly predicted flooded points, *B* is the number of correctly predicted not flooded points, and *N* is the total number of collected points. The f-measurement was computed using Eq. 5 (Jung *et al*., 2014).

$$F = \frac{A}{(A+B+C)} \tag{5}$$

where *A* is the same as described in equation 4, *B* is the number of points predicted by the model as flooded but not flooded in reality, and *C* is the number of points that are predicted by the model as not flooded but flooded in reality. The RMSE statistics for models' validity and reliability test were computed using Eq. 6 (Timbadiya *et al*., 2011).

$$RMSE = \sqrt{\frac{\sum_{i=1}^{n}(X_{mo} - X_o)^2}{n}} \tag{6}$$

where X_{mo} is the modeled values, X_o is the observed

values at a time/place *i*., *n* is the number of points.

Flood exposure analysis

This process quantifies the number of exposed buildings based on two simulated flood hazards developed using LiDAR and IfSAR DEMs, respectively. The initial process involved the extraction of building features from LiDAR DSM. Determining the number of exposed buildings was done through superimposing separately the building features map layers with the flood hazard maps derived from the simulation models using LiDAR and IfSAR datasets.

RESULTS AND DISCUSSION

Processed DEMs

Fig. 3 illustrates the processed DEMs of the 1 meter-resolution, LiDAR, and 5 meter-resolution, IfSAR, integrated with bathymetric data. A more detailed DEM, as characterized by smaller stream networks, is evident in the LiDAR DEM. This observation confirmed the findings from previous studies where LiDAR DEM is capable of offering detailed elevation data that can be used to improve flood-model input and consequently increase the accuracy of the flood modeling results (Leitao and de Sousa, 2018). Meanwhile, IfSAR DEM appears more coarse and is unable to capture other tributary streams. Moreover, the two DEMs have a minimal difference when it comes to elevation ranges. The 2D area boundary of the two DEMs, which sets the extent of simulation, has the same highest elevation of 992 m. On the other hand, the lowest elevation is 275 m and 283 m for LiDAR and IfSAR DEMs, respectively.

Hydrologic basin model

The delineation of the basin boundary along with the river network or reaches was accomplished during basin model preparation using the HEC-GeoHMS extension tool. Calibrating the HMS model involved fitting the simulated discharge with the observed discharge hydrograph. Calibration was through manual adjustment of parameters and visual evaluation of the fitted lines of the observed and simulated values in the hydrographs. After closely fitting the hydrographs, model performance was subsequently evaluated using the validation guidelines of Moriasi *et al*. (2007). The initial result of evaluation before calibration showed acceptable model performance considered as „good" for both RSR and NSE and „satisfactory" for PBIAS. After calibration, the model performance result shows „very good" for the three statistical tests. Fig. 4 shows the observed hydrograph against the calibrated and

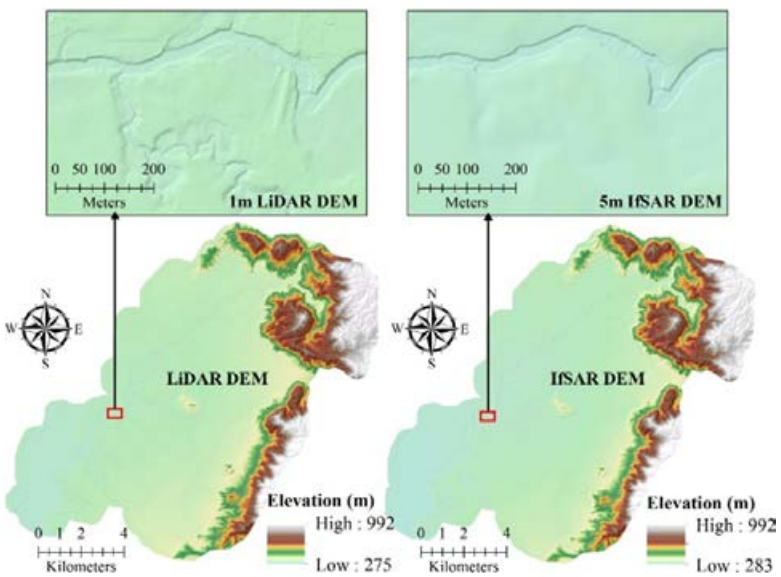

Fig. 3: Processed LiDAR and IfSAR DEMs

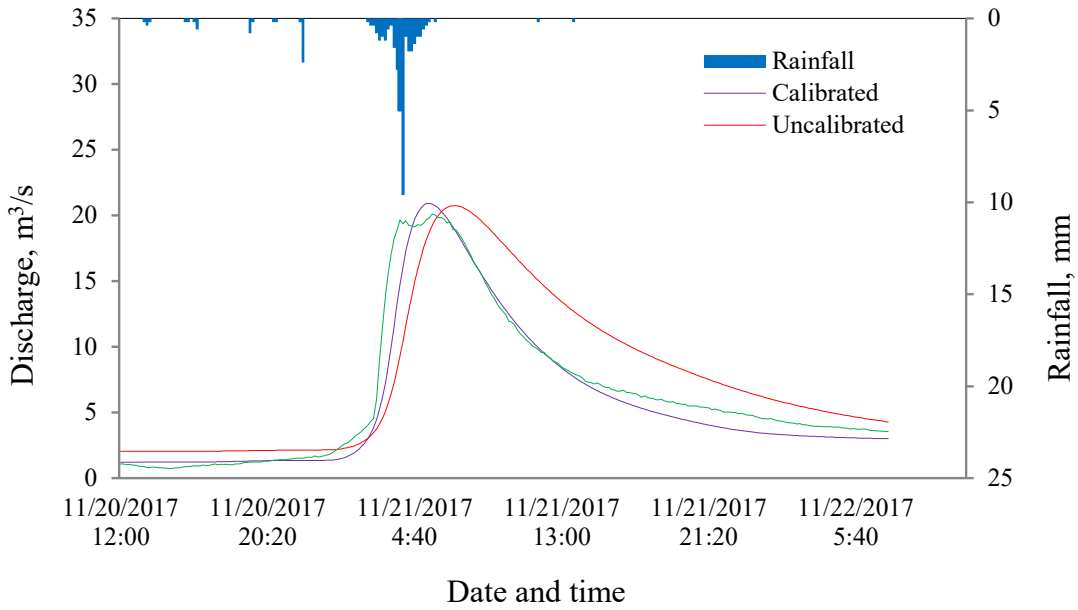

Fig. 4: Calibrated and uncalibrated simulated hydrographs against actual discharge

Table 2: Statistical analysis of model performance

Statistical matrices	Pre-calibration		Post calibration	
	Value	Remarks	Value	Remarks
RSR	0.56	Good	0.23	Very Good
NSE	0.68	Good	0.95	Very Good
PBIAS	-22.39	Satisfactory	8.61	Very Good

uncalibrated simulated hydrographs, while Table 2 shows the statistical model performance before and after calibration. The calibrated model was used to reconstruct the flood event that occurred last December 21-23, 2017.

Flood simulation and mapping

The geometric data consists of a 2D domain area that determines the simulation extent with model boundary conditions corresponding to the baseflow depth, precipitation boundary, and the flow hydrograph conditions which contained the simulated discharge data of the calibrated HMS model. Fig. 5 depicts the result of the simulated flood using the 5 m IfSAR and 1 m LiDAR DEM with the terrain models overlaid with extracted features of building structures from LiDAR DSM. A closer look reveals that the differences in topographic details resulted in varying flood propagation in both IfSAR and LiDAR simulations. Moreover, the model developed with IfSAR has recognizable clamped inundations due to the less intricate of smaller tributaries. It was also unable to capture the inundated channels and its floodplain, which are barely flooded, unlike LiDAR DEM-based simulation. Comparatively, LiDAR and IFSAR DEMs yielded the simulated flood areas of 35.82 km^2 and 35.59 km^2, respectively, showing a slight difference of 0.23 km^2. The LiDAR-based simulation has wider inundation which may be due to a broader extent of the flat terrain of lower elevations occupied by floodwaters. Varying observations were noted in some related studies. Chen and Hill (2007) concluded that due to the relatively smooth terrain of coarser DEM, there are few terrain details restraining water dispersion and reducing the area of inundation. In contrast, Md Ali *et al*. (2015),

observed a wider flood extent in DEM with coarser resolution. Simulation using LiDAR and IfSAR DEMS revealed different maximum flood depths of 23.66 m and 19.54 m, respectively. As reported, flood model simulation results show differences in water depths and inundation when using detailed DEMs (Muhadi *et al*., 2020). Furthermore, in comparing the two flood simulations of different DEMs, the building features had not accurately occupied the actual locations, particularly with IfSAR DEM compared to LiDAR DEM. Such observation is expected since exposure datasets which consist of building structures, were extracted from LiDAR DSM only.

Flood validation and accuracy

Information on the historic flood experiences included the 120 locations within the 2D domain flood simulation area. Each point represented by a household is either flooded or not flooded during the event. Flood height was measured in each flooded point. Following the spatial analyst tool of ArcGIS workflow, the simulated flood depths using the two DEMs were extracted and the outputs of which were used to calculate the accuracy metrics. Table 3 shows the validation results of the simulated flood event using the three accuracy metrics.

Comparing the two flood models developed with LiDAR and IfSAR DEM datasets using the error matrix approach, the former yielded a more accurate result with a difference of 12% accuracy. Error matrix is influenced by the number of correctly predicted flooded and not-flooded points by the model simulation and is interpreted as the overall reliability (Cabrera and Lee, 2019). For both simulations, the number of correctly predicted flooded and not-flood points is greater than the incorrectly predicted points. Simulation using LiDAR DEM mainly attained a high percentage which passed the acceptable value of 85% for the overall accuracy as reported by Foody (2008). On the other hand, the simulation using IfSAR failed to satisfy the acceptable prescribed percentage overall accuracy. Test of accuracy using f-measurement revealed an intermediate fit for the simulation using LiDAR and a bad fit for the model using IfSAR. Based on Breilh *et al*. (2013), flood simulated using LiDAR DEM is

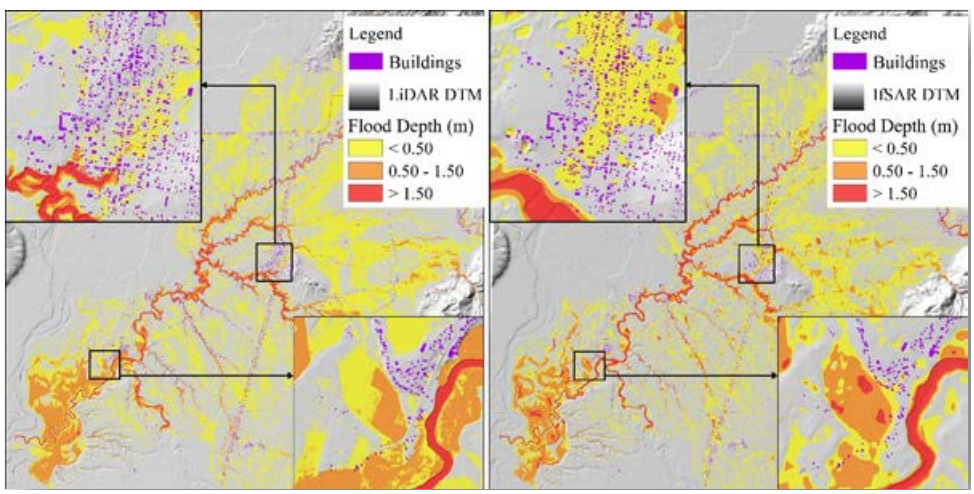

Fig. 5: Simulated flood using LiDAR and IfSAR DEMs

Table 3: Accuracy tests of flood simulation models using LiDAR and IfSAR DEMs

Accuracy metrics	LiDAR DEM-based model	IfSAR DEM-based model
Error Matrix	88%	76%
F-measurement	0.61	0.34
RMSE	0.41	0.53

acceptable after attaining an f-measure of above 0.5. This accuracy metric reveals that several incorrectly predicted flooded and not flooded points are few for the model using LiDAR but too numerous for the simulation using IfSAR. Comparatively, the IfSAR simulation showed an overestimation of flooding than the LiDAR DEM simulation. The RMSE metric explains the differences between the predicted and observed data, with the significant errors affecting the rating (Najafi and Salam, 2016). The test showed a low RMSE for LiDAR simulation but high RMSE for IfSAR. Specifically, the simulation using IfSAR DEM has a more significant error compared to LiDAR DEM as indicated by the higher RMSE value. Between the two, the flood model using LiDAR falls within the acceptable level of RMSE, which is below 0.5. Coarser DEM contains more errors in elevation which tend to overestimate hazard levels and underestimate flooded areas. Overall, the LIDAR DEM-based flood model has statistically yielded a better result than IfSAR DEM-based model. However, LiDAR data has some issues that need to be addressed regarding filtering processes and data density resulting in a longer computational time to simulate flood models (Muhadi, *et al*., 2020). Besides, the high cost of LiDAR data acquisition has been a constraint for its availability and operational use (Hudak *et al.,* 2011). Thus, the application of IfSAR DEM in flood modeling studies is still preferred (Mokhtar *et al*., 2018).

Flood exposure analysis

This analysis allows the calculation of the building features exposed to risk according to the simulated flood using the two kinds of DEMs categorized into three hazard levels namely „low", „medium", and „high" with flood depth of <0.5 m, 0.5-1.5 m, and >1.5 m, respectively. For both simulations, the majority of the flooded buildings were under the „low" hazard level, followed by „medium" and the „high". The IfSAR-based simulation consistently showed a lower number of flooded buildings under the „low" and „medium" hazard category levels. In LiDAR-based simulation, the total number of flooded buildings is 3580 (38%) of the total buildings in the floodplain. On the other hand, the IfSAR simulation inundates a total of 2896 (30%) buildings. A difference of 684 or 8% more flooded building features, the majority of which are residential, were extracted using the LiDAR-based flood hazard maps. In the aspect of disaster operations and management, there is an underestimation of flooded buildings using IfSAR. This generated information is necessary as it serves as a basis for making an optimal decision on the exact location and coverage of hazards in the localities that need immediate rescue and response operations during flood disasters.

CONCLUSION

The flood simulation model using LiDAR DEM passed the three statistics of accuracy tests showing more precise results. The simulated flood using IfSAR DEM yielded near to acceptable results but failed to statistically satisfy the overall prescribed accuracy tests. Flood simulation shows differences in flood depth with LiDAR DEM-based model having the deeper inundation indicating more detailed results. In the infrastructure feature extraction, both models showed similar trends where the majority of the flooded buildings were under the low hazard level indicating the applicability of both DEMs in the process. Generally, the LiDAR DEM dataset revealed to be advantageous than IfSAR DEM and is more appropriate when it comes to the accurate estimation of flood impacts up to the household level. However, difficulty in terms of data storage that results in a longer processing time to simulate flood models is one of its drawbacks. Additionally, the cost of LiDAR DEM data acquisition is relatively high. An agency or the local government units may limit the coverage to focus on the highly populated areas to minimize the LiDAR data acquisition cost. Thus, in flood-prone agricultural lands where critical analysis is unnecessary, IfSAR can be used for flood simulation. Areas covered with other land uses may be represented by IfSAR and mosaicked with the available LiDAR datasets on specific floodplains. Overall, this study presents the benefit of using fine-resolution DEM such as a LiDAR over coarser DEM such as IfSAR, especially when seeking a more detailed and accurate flood model simulation. However, with the issues and concerns about LiDAR data acquisition, processing and storage, the IfSAR system is still preferred as it offers a more cost-sensitive DEM dataset for use in the process of flood simulation model development and updating which are necessary for the economically-optimal implementation of flood hazards monitoring and management.

AUTHOR CONTRIBUTIONS

G.R. Puno acted as the project leader of the study and prepared the manuscript main file, GIS and other databases, layout design, and graphs. R.C.C. Puno acted as the research associate of the project and was involved in several activities such as data collection, flood simulation, and hazard mapping, and land use/land cover map generation using satellite images. I.V. Maghuyop was involved in the manuscript preparation and editing.

ACKNOWLEDGMENTS

This study is a product of the Geo-Informatics for the systematic assessment of flood effects and risks in Northern Mindanao and Cotabato, Philippines (Geo-SAFER Northern Mindanao/Cotabato) Project No. 2, funded by the Department of Science and Technology-Philippine Council for Industry, Energy, and Emerging Technology Research and Development (DOST-PCIEERD) with a financial account [Grant number 1-416-154]; and the Provincial Government of Bukidnon with a financial account [Grant number 116-164]. The authors also acknowledge the administration of Central Mindanao University and the local government units of Valencia City for the logistics.

CONFLICT OF INTEREST

The authors declare no potential conflict of interest regarding the publication of this work. Also, the ethical issues including plagiarism, informed consent, misconduct, data fabrication and, or falsification, double publication and, or submission, and redundancy have been completely witnessed by the authors.

OPEN ACCESS

PUBLISHER'S NOTE

ABBREVIATIONS

%	Percent
0	Degrees
'	Minutes
"	Seconds
Σ	Summation sign
>	Greater than
<	Less than
2D	Two-dimensional
A	Number of correctly predicted flooded points
ArcGIS	Geographic information system software product
ASCII	American standard code for information interchange
B	Number of correctly predicted not flooded points
C	Number of points predicted as not flooded but flooded in reality
DAC	Data acquisition component
DEM	Digital elevation model
DOST	Department of Science and Technology
DREAM	Disaster Risk and Exposure Assessment for Mitigation
DSM	Digital surface model
DTM	Digital terrain model
DXF	Drawing exchange format
Eq	Equation
F	F-measurement
Fig.	Figure

Geo-SAFER	Geo-Informatics for the Systematic Assessment of Flood Effects and Risks
GIS	Geographic information system
GNSS	Global navigation satellite system
HEC-GeoHMS	Hydrologic engineering center-hydrologic modeling system GIS interface
HEC-GeoRAS	Hydrologic engineering center-river analysis system GIS interface
HEC-HMS	Hydrologic engineering center-hydrologic modeling system
HEC-RAS	Hydrologic engineering center-river analysis system
IDW	Inverse distance weighted
IfSAR	Interferometric synthetic aperture radar
i^{th}	Ith number
km	kilometer
Km^2	Kilometer squared
LiDAR	Light detection and ranging
LULC	Land use or land cover
m	Meter
mm	Millimeter
m^3/s	Cubic meter per second
MSL	Mean sea level
n	Total number of observations
N	Total number of collected points
n	Number of points
NAMRIA	National Mapping and Resource Information Authority
PBIAS	Percent bias
PCIEERD	Philippine Council for Industry, Energy, and Emerging Technology Research and Development
Phil-LiDAR	Philippine-Light Detection and Ranging
RMSE	Root mean square error
RSR	RMSE-observation standard deviation ratio
RTK	Real-time kinematic
SAR	Synthetic aperture radar
$STDEV_o$	The standard deviation of the observed data
UP	University of the Philippines
TCAGP	Training Center for Applied Geodesy and Photogrammetry
US	United States
USACE	United States Army Corps of Engineers
X_{mo}	Modeled values
X_o	Observed values
Y^m	Mean of the observed value of the evaluated variable
Y^o	Observed value of the evaluated variable
Y^s	Simulated value of the evaluated variable

REFERENCES

Alivio, M.B.T.; Puno, G.R.; Talisay, B.A.M., (2019). Flood hazard zones using 2d hydrodynamic modeling and remote sensing approaches. Global J. Environ. Sci. Manage., 5(1): 1-16 (**16 pages**).http://dx.doi.org/10.22034/gjesm.2019.01.01

Belen, R.D.M., (2015). Mapping of the typhoon Haiyan affected areas in the Philippines using geospatial data and very high-resolution satellite images. In 20th United Nations Regional Cartographic Conference for Asia and the Pacific. Jeju, Islands, 6-9 October.

Breilh, J.F.; Chaumillon, E.; Bertin, X.; Gravelle, M., (2013). Assessment of static flood modeling techniques: Application to contrasting marshes flooded during Xynthia (western France). Nat. Nat. Hazards Earth Syst. Sci., 13(6): 1595-1612 (**18 pages**).

Cabrera, J.S.; Lee, H.S., (2019). Flood-prone area assessment using GIS-based multi-criteria analysis: A case study in Davao Oriental, Philippines. Water, 11(11): 1-23 (**23 pages**).

Cantal-Albasin, G., (2017). Valencia City under state of calamity. Sun Star Philippines.

Chen, J.; Hill, A., (2007). Modeling urban flood hazard: just how much does DEM resolution matter? In Applied Geography Conferences. Indianapolis, 30: 372-379 (**8 pages**).

Demir, V.; Kisi, O., (2016). Flood hazard mapping by using geographic information system and hydraulic model: Mert River, Samsun, Turkey. Adv. Meteorol., 2677 (**9 pages**).

Divin, J.; Mikita, T., (2016). Effects of land use changes on the runoff in the landscape based on hydrological simulation in HEC-HMS and HEC-RAS using different elevation data. Acta Univ. Agric. Et Silviculturae Mendelianae Brunensis, 64(3): 759-768 (**10 pages**).

Foody, G.M., (2008). Harshness in image classification accuracy assessment. Int. J. Remote Sens., 29(11): 3137-3158 (**22 pages**).

Gandhi, S.M.; Sarkar, B.C., (2016). Essentials of Mineral Exploration and Evaluation. In: Catena, Walker and Willgossse, Digital elevation models.

Gopal, S., (2010). IFSAR: Mapping geospatial intelligence. Geospatial World.

Guidolin, M.; Chen, A.S.; Ghimire, B.; Keedwell, E.C.; Djordjevic, S.; Savic, D.A., (2016). A weighted cellular automata 2D inundation model for rapid flood analysis. Environ. Model. Software, 84: 378-394 (**17 pages**).

Hashim, S.; Naim, W.M.; Mohd, W.; Adnan, N.; Sadek Said, E.; Md Sadek, E.; Hashim, S.M.N.; Wan Mohd, W.; Md Sadek.; Á., (2014). Evaluation of vertical accuracy of airborne IFSAR and open-source digital elevation models (DEMs) for flood inundation mapping. In Regional Conference on Science, Technology and Social Sciences. Singapore, January. Springer.

Hawker, L.; Bates, P.; Neal, J.; Rougier, J., (2018). Perspectives on digital elevation model (DEM) simulation for flood modeling in the absence of a high-accuracy open access global DEM. Front. Earth Sci., 6(233): 1-9 (**9 pages**).

Hudak, A.T.; Uebler, E.H.; Falkowski, M.J., (2011). A Comparison of accuracy and cost of LiDAR versus stand exam data for landscape management on the Malheur National Forest. J. For., 109(5): 267-273 (**6 pages**).

Jung, Y.; Kim, D.; Kim, D.; Kim, M.; Lee, S.O., (2014). Simplified flood inundation mapping based on flood elevation-discharge rating curves using satellite images in gauged watersheds. Water, 6(5): 1280-1299 (**20 pages**).

Khalid, N.F.; Din, A.H.M.; Omar, K.M.; Khanan, M.F.A.; Omar, A.H.; Hamid, A.I.A.; Pa'suya, M.F., (2016). Open-source Digital Elevation Model (DEMs) Evaluation with GPS and LiDAR Data. Int. Arch. Photogramm. Remote Sens. Spatial Inf. Sci., XLII-4/W1: 299–306 (**8 pages**).

Leitao, J.P.; de Sousa, L.M., (2018). Towards the optimal fusion of high-resolution Digital Elevation Models for detailed urban flood assessment. J. Hydrol., 561: 651-661 (**11 pages**).

Li, X.; Liu·C.; Wang, Z.; Xie, X.; Li, D.; Xu, L., (2020). Airborne LiDAR: state-of-the-art of system design, technology and application. Meas. Sci. Technol., 32(3).

Li, X.; Shen, H.; Feng, R., Li, J.; Zhang, L., (2017). DEM generation from contours and a low-resolution DEM. ISPRS J. Photogramm. Remote Sens., 134(2017): 135-147 (**13 pages**).

Lu, Z.; Kwoun, O.; Rykhus, R., (2007). Interferometric synthetic aperture radar (InSAR): Its past, present and future. Photogramm. Eng. Remote Sens., 73(3): 217-221 (**5 pages**).

Makinano-Santillan, M.; Serviano, J.; Rubillos, C.K.; Amora, A.; Santillan, J.R.; Morales, E.M.; Marqueso, J.T.; Gingo, A.L., (2019). Near-real time hazard monitoring and information dissemination through integration of remote sensing, GIS, numerical modelling, web applications and social media. ISPRS Ann. Photogramm. Remote Sens. Spatial Inf. Sci., IV-3/W1: 25-32 (**8 pages**).

Mateo, J., (2013). UP allots P40M for NOAH project. Philstar Global. Philippines.

Md Ali, A.; Solomatine, D.P.; Di Badldassarre, G., (2015). Assessing the impact of different sources of topographic data on 1-D hydraulic modelling of floods. Hydrol. Earth Syst. Sci., 19(1): 631-643 (**13 pages**).

Mokhtar, E.S.; Pradhan, B.; Ghazali, A.H.; Shafri, H.Z.M., (2018). Assessing flood inundation mapping through estimated discharge using GIS and HEC-RAS model. Arab. J. Geosci., 11(682): 1-20 (**20 pages**).

Moriasi, D.N.; Arnold, J.G.; Van Liew, M.W.; Bingner, R.L.; Harmel, R.D.; Veith, T.L., (2007). Model evaluation guidelines for systematic quantification of accuracy in watershed simulations. Trans. Am. Soc. Agric. Biol. Eng., 50(3): 885-900 (**16 pages**).

Muhadi, N.A.; Abdullah, A.F.; Bejo, S.K.; Mahadi, M.R.; Mijic, A., (2020). The use of LiDAR-derived DEM in flood applications: A review. Remote Sens., 12(14), 1-20.

Najafi, S.; Salam, Z., (2016). Evaluating Prediction Accuracy for Collaborative Filtering Algorithms in Recommender Systems. Kth Royal Institute of Technology School of Computer Science and Communication, Stockholm, Sweden.

Ogania, J.L.; Puno, G.R.; Alivio, M.B.T.; Taylaran, J.M.G., (2019). Effect of digital elevation model's resolution in producing flood hazard maps. Global J. Environ. Sci. Manage., 5(1): 95-106 (**12 pages**).

Pinos, J.; Quesada-Roman, A., (2002). Flood Risk-Related Research Trends in Latin America and the Caribbean. Water, 14(1): 1-14 (**14 pages**).

Puno, G.R.; Amper, R.A.L.; Opiso, E.M.; Cipriano, J.A.B., (2019). Mapping and analysis of flood scenarios using numerical models and GIS techniques. Spatial Inf. Res., 28: 215-226 (**12 pages**).

Ronda, R.A., (2013). DOST project gets P2.4-B fund. ABS-CBN News, Manila.

Santillan, J.R.; Amora, A.M.; Makinano-Santillan, M.; Marqueso, J.T.; Cutamora, L.C.; Serviano, J.L.; Makinano, R.M., (2016). Assessing the impacts of flooding caused by extreme rainfall events through a combined geospatial and numerical modeling approach. Int. Arch. Photogramm. Remote Sens. Spatial Inf. Sci., XLI-B8: 1271–1278 (**8 pages**).

Sharma, M.; Paige, G.B.; Miller, S.N., (2010). DEM development from ground-based LiDAR data: a method to remove non-surface objects. Remote Sens., 2(11): 2629-2642 (**14 pages**).

Smith, L.C., (2002). Emerging applications of interferometric synthetic aperture radar (InSAR) in geomorphology and hydrology. Ann. Am. Assoc. Geogr., 92(3): 385-398 (**14 pages**).

Talisay, B.A.M.; Puno, G.R.; Amper, R.A.L., (2019). Flood hazard mapping in an urban area using combined hydrologic-hydraulic models and geospatial technologies. Global J. Environ. Sci. Manage., 5(2): 139-154 (**16 pages**).

Timbadiya, P.V.; Patel, P.L.; Porey, P.D., (2011). Calibration of HEC-RAS model on prediction of flood for lower Tapi river, India. J. Water Resour. Prot., 3(11): 805-811 (**7 pages**).

USACE, (1964). Hydrologic Engineering Center-Hydrologic Modeling System (HEC-HMS). The U.S. Army Corps of Engineers.

Wedajo, G.K., (2017). LiDAR DEM data for flood mapping and assessment; opportunities and challenges: A review. J. Remote Sens. Geog. Inf. Syst., 6(4): 1-4 (**4 pages**).

AUTHOR (S) BIOSKETCHES

PUNO, G.R., Ph.D., Professor, College of Forestry and Environmental Science, Central Mindanao University, Musuan, Bukidnon, Philippines.
- Email: grpuno@cmu.edu.ph
- ORCID: 0000-0002-7170-641X
- Web of Science ResearcherID: F-2553-2017
- Scopus Author ID: 56955824400
- Homepage: https://www.cmu.edu.ph/academic-units/forestry-and-environmental-science/

PUNO, R.C.C., M.Sc., Instructor, College of Forestry and Environmental Science, Central Mindanao University, Musuan, Maramag, Philippines
- Email: *rccpuno@cmu.edu.ph*
- ORCID: 0000-0001-7798-1335
- Web of Science ResearcherID: AAA-1038-2022
- Scopus Author ID: 57188870850
- Homepage: https://www.cmu.edu.ph/academic-units/forestry-and-environmental-science/

Maghuyop, I.V., M.Sc., Instructor, College of Forestry and Environmental Science, Central Mindanao University, Musuan, Maramag, Philippines
- Email: *ivmcfes@cmu.edu.ph*
- ORCID: 0000-0002-5035-8495
- Web of Science ResearcherID: AAA-2256-2022
- Scopus Author ID: NA

Homepage: https://www.cmu.edu.ph/academic-units/forestry-and-environmental-science/

HOW TO CITE THIS ARTICLE

Puno G.R., Puno R.C.C., Maghuyop I.V. (2022). Flood hazard simulation and mapping using digital elevation models with different resolutions. Global J. Environ. Sci.Manage., 8(3): 339-352.

DOI: 10.22034/gjesm.2022.03.04

url: https://www.gjesm.net/article_249008.html

Global J. Environ. Sci. Manage. 8(3): 353-368, Summer 2022, Serial #31

Global Journal of Environmental Science and Management
(GJESM)

Homepage: https://www.gjesm.net/

ORIGINAL RESEARCH ARTICLE

Impact of tropical Cyclone Marcus on ocean subsurface and surface layers

A.F. Koropitan*, M.H.I. Khaldun, Y. Naulita

Department of Marine Science and Technology, Faculty of Fisheries and Marine Science, IPB University, Kampus IPB Dramaga, Bogor 16680, Indonesia

ARTICLE INFO

Article History:
Received 02 September 2021
Revised 29 November 2021
Accepted 20 December 2021

Keywords:
Chlorophyll-a
Cyclone Marcus
Ocean temperature
Southeast Indian Ocean
Subsurface and surface layers
Eddy

ABSTRACT

BACKGROUND AND OBJECTIVES: The southeast Indian Ocean is one of the areas where tropical cyclones formed. A comprehensive understanding of the cyclone impact in the Southeastern Indian Ocean is needed to anticipate future changes due to the warming trend. The present study investigates the influence of Cyclone Marcus on oceanographic processes in the subsurface and surface layers and its impact on temperature and Chlorophyll-a in the Southeastern Indian Ocean. The present study applies the Argo Float data located near the peak of the Cyclone Markus path and could capture the subsurface layer vertically that has never been reported previously.
METHODS: This study performs Copernicus data set and Argo Float data to analyze the oceanographic feature of the region before, during, and after Cyclone Marcus.
FINDINGS: The average surface current velocity increased almost two times during Cyclone Marcus, and the eddy was formed in the clockwise direction following the surface wind pattern. The Argo Float data presents that Cyclone Marcus could induce surface divergence (clockwise eddy) where the cold water and high salinity waters pumped up to the surface layer, starting 1 day after the peak of Cyclone Marcus, resulting in cooling surface temperature by 1.7 °C and deepening mixed layer depth up to 60 m. It implies that the lifted nutrient-rich water stays in the mixed layer depth for 11 days, and sea surface Chlorophyll-a concentration increase with time lags of 2.5 days and 5.6 days, respectively. The Chlorophyll-a concentration increases 2.5 times, and since then starts to decrease its 'normal concentration' within two weeks.
CONCLUSION: Cyclone Marcus triggers the entrainment between the subsurface layer and the sea surface, forcing a phytoplankton growth, particularly in the path area. The future cyclone could increase in the category in the study area, as the warming trend in the Indian Ocean.

DOI: 10.22034/gjesm.2022.03.05

NUMBER OF REFERENCES	NUMBER OF FIGURES	NUMBER OF TABLES
35	9	2

*Corresponding Author:
Email: *alan@apps.ipb.ac.id*
Phone: +62 251 8623644
ORCID: 0000-0001-5794-094X

Note: Discussion period for this manuscript open until October 1, 2022 on GJESM website at the "Show Article".

INTRODUCTION

The Southeast Indian Ocean is one of the areas where tropical cyclones (TCs) formed. Generally, tropical cyclone seeds form in the Arafura Sea and the waters of Northern Australia, which continue to move southwest (Hoque *et al.*, 2017). The intensity of TCs will continue to move increasingly until their energy becomes extinct. The increase in cyclone intensity is forced by ocean temperature, where the relatively warm waters in the surface ocean could be a source of energy for TCs to maintain their existence (Pillay and Fitchett, 2021). The trend of the Indian Ocean warming, as reported by Roxy *et al.* (2015), is expected to affect the number and intensity of TCs. The temperature increase in a tropical ocean area could provide a low-pressure centre or a tropical depression that becomes the seed of TCs. A comprehensive understanding of the TCs impact in the Southeastern Indian Ocean is needed to anticipate future changes due to the warming trend. The negative impact of TCs, such as extreme weather, could cause material losses and casualties in the impacted coastal areas. Another encouraging impact was reported by Yu *et al.* (2013) that after the TCs Goni and Koppu, there was an increase in the abundance of fish offshore for up to eight days in the South China Sea. Yu *et al.* (2014) showed that TCs Chanthu, Vicente, and Kai-tak could increase catch per unit effort (CPUE) for up to three weeks in the Northwest of the South China Sea. The increased CPUE is closely related to the increase in Chlorophyll-a (Chl-a) after TCs. A similar thing could happen in the Southeastern Indian Ocean. Previous studies suggested a decrease in temperature and an increase in primary productivity triggered by TCs. Lü *et al.* (2020) reported that the phenomenon was due to the vertical entrainment that pumped up the relatively cold and nutrient-rich waters from the subsurface to surface layers. TCs will form eddies in the surface ocean along the cyclone path. The pressure difference in the surface ocean due to the lower centre of the cyclone will be filled by a water mass from the subsurface to surface layers (upwelling). The upwelling implied ocean fertility. Chacko and Zimik (2018) revealed that TCs could affect a surface mixed layer down to 100 m depth. The biological responses in the surface ocean can be different along the cyclone path, depending on the upwelling magnitude and the availability of nutrients in the water. The increase in primary productivity caused by TCs is temporary. After some time, primary productivity will decrease again at different intervals (Lü *et al.*, 2020). Comprehensive studies on the impact of TCs on ocean dynamics in the subsurface layer have been elaborated. The response of the water column in the subsurface was shown in the form of increasing mixed layer depth (MLD), which becomes deeper due to the turbulent mixing. Cyclone Phailin in the Bay of Bengal caused a MLD of 29 m (Vidya *et al.*, 2017). Cyclone Trami in the northwest Pacific Ocean showed a mixed layer change by 94 m (Chai *et al.*, 2021). A review paper by (Zhang, *et al.*, 2021) highlighted that the upper ocean response usually recovers in several days to several weeks, depending on the intensity, translation speed and size of the TCs. Environmental parameters are also important, such as ocean stratification and eddies. The ocean dynamics in the subsurface layer of the Southeast Indian Ocean influenced by TCs still need to be studied further. Most of the previous studies only report the oceanographic processes in the surface, as presented in Tabel 1.

The impact of TCs is quite significant on the surface and subsurface layers. What are the oceanographic characteristics in subsurface and surface layers of the Southeast Indian Ocean during and after TCs? The mechanism and impact on oceanographic processes in the subsurface layer that affect Chl-a and temperature in the surface layer of the Southeast Indian Ocean have not been studied previously. The present study aims to investigate in detail the influence of Cyclone Marcus on oceanographic processes in the subsurface and surface layers and its impact on SST and surface Chl-a in the Southeastern Indian Ocean in 2018. The present study applies the Argo Float data, which has stations simultaneously near the peak of the Cyclone Markus path. The Argo Float data could capture the oceanographic processes in the subsurface layer vertically that has never been reported previously in the Southeastern Indian Ocean.

MATERIALS AND METHODS

Description of the study area and data collection

Tropical Cyclone Marcus was an intense tropical cyclone in 2018 with a category 5 *Saffir-Simpson* scale where the TCs data were collected from the Australian Bureau of Meteorology (BOM). Cyclone Marcus seedlings formed in northern Australian

waters on 14 March 2018 and became extinct on 24 March 2018. Information and images of the trajectory of Cyclone Marcus are shown in Fig. 1. This study used oceanographic data set or derivative works from Copernicus Marine Service Information. The SST data are adopted from the Operational Sea Surface Temperature and Sea Ice Analysis (OSTIA) data. OSTIA uses satellite data provided by Group for High-Resolution Sea Surface Temperature (GHRSST) using field observations and satellite data that uses infrared and microwaves to determine the SST data. The use of microwaves can overcome the effects of

Table 1: Previous studies in the Southeastern Indian Ocean

No.	Tropical cyclones and references	Period	Category (*Saffir-Simpson* scale)	Data Set	Findings (highlighted in the abstract)
1	Ernie (Efendi *et al.*, 2018)	6-10 April 2017	4	Sea Surface Temperature (SST) and	SST decrease and Chl-a increase after the cyclone.
2	Seroja (Avrionesti *et al.*, 2021)	4-12 April 2021	2	SST (satellite data), Chl-a, MLD and sea surface height (E.U. Copernicus Marine Service Information), sea surface wind (satellite data).	SST decrease, Chl-a increase, sea surface height anomaly decrease, and MLD increase after the cyclone.
3	Seroja (Setiawan *et al.*, 2021)	4-12 April 2021	2	SST and Chl-a (satellite), sea surface wind (Cross-Calibrated Multi-Platform).	SST decrease and Chl-a increase after the cyclone.
4	Cempaka (Aditya *et al.*, 2021)	25-27 November 2017	1	SST and Chl-a (satellite), sea surface wind (Cross-Calibrated Multi-Platform).	SST decrease and Chl-a increase after the cyclone.
5	Dahlia (Aditya *et al.*, 2021)	27 November to 2 December	2	SST and Chl-a (satellite), sea surface wind (Cross-Calibrated Multi-	SST decrease and Chl-a increase after the cyclone.

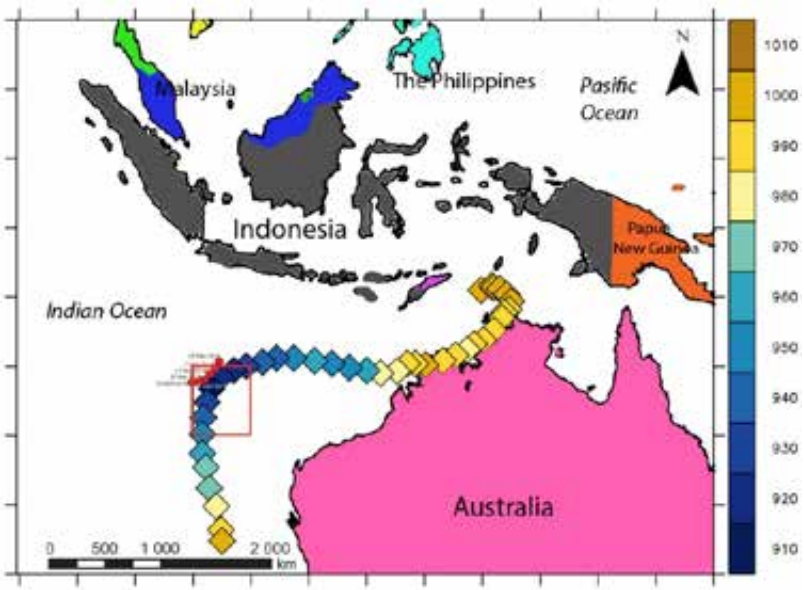

Fig 1: Path of Cyclone Marcus during 14-24 March 2018 and pressure (color in hPa), while the red dots indicate the position of Argo Float stations. The red box shows the study area indicating the highest intensity (low-pressure area) of Cyclone Marcus

clouds that form during TCs. SST data have a spatial resolution of 0.05° by 0.05° and daily temporal resolution (Donlon *et al.,* 2012). MLD data were obtained from a 3 dimension multi-observations product of the ocean (ARMOR3D) with a spatial resolution of 0.25° by 0.25° and a weekly temporal resolution (Guinehut *et al.,* 2012; Mulet *et al.,* 2012). Surface wind data has a spatial resolution of 0.25° by 0.25° and a temporal resolution of six hours, while ocean current data has a spatial resolution of 0.25° by 0.25° and a daily temporal resolution (Rio *et al.,* 2014). The Chl-a concentration data are based on the merging of the sensors Sea-viewing Wide Field-of-view Sensor (SeaWiFS), Moderate Resolution Imaging Spectroradiometer (MODIS), Medium Resolution Imaging Spectrometer (MERIS), The Visible and Infrared Imager/Radiometer Suite (VIIRS), the Suomi National Polar-orbiting Partnership (S-NPP), The Joint Polar Satellite System (JPSS), and Ocean and Land Color Instrument (OLCI) sensor. The Chl-a concentration data has a spatial resolution of 4 km by 4 km and a daily temporal resolution. Subsurface observations were examined using the Argo Float Commonwealth Scientific and Industrial Research Organization (CSIRO) Australia. The Argo Float is operational with a thermistor, conductivity sensor, and pressure gauge to record temperature, salinity, and depth, respectively, every ten days in the Southeastern Indian Ocean. The Argo Float data was chosen because of its location (17 March 2018 at 107.08°E and 15.68°S; 27 March 2018 at 106.72°E 15.92°S), which was on the path of Cyclone Marcus when it reached its lowest pressure peak so that it can provide information before and after the cyclone passes that location at 21-24 March 2018.

Data analysis

Spatial analysis is divided into three phases, namely before Cyclone Marcus (11-17 March 2018), during Cyclone Marcus (18-25 March 2018), and after Cyclone Marcus (26-31 March 2018). Spatial analysis is the average of each phase on each variable, using in Eq. 1.

$$\overline{x} = \frac{\sum_{i=1}^{n} x_i}{n} \quad (1)$$

where $\overline{x}$ is the average value of each phase, x_i is the sample's value, and n is the amount of data.

Accumulated Cyclone Energy (ACE) is a method to measure or quantify tropical cyclone phenomena based on the strength and timing of TCs in a particular area or time (Collins, 2018). The ACE value is obtained from the estimated maximum wind speed during the life of a tropical cyclone with 6-hour intervals. As for the calculation of ACE, using Eq. 2.

$$ACE = 10^{-4} \sum v^2_{max} \quad (2)$$

where v_{max} is the maximum constant wind speed at 6-hour intervals (m/s). *Ekman* pumping velocity (EPV) forced by TCs was calculated using Eqs. 3 and 4 (Chacko and Zimik, 2018).

$$\text{wind stress } (\tau) = \rho_{air} C_d U^2 \quad (3)$$

$$EPV = Curl(\tau) / \rho_w xf \quad (4)$$

where ρ_{air} is the density of air (1.25 kg/m^3), C_d is wind drag coefficient (1.3 x 10^{-3}), which is a dimensionless quantity, U is the wind speed, ρ_w is the density of seawater (1025 kg/m^3), and f is the *Coriolis* parameter. A positive (negative) value indicates an upwelling (downwelling) event. The relationship between SST, Chl-a, and ACE was analyzed using a wavelet transformation, which is a *Morlet* wavelet (Grinsted *et al.*, 2004).

RESULTS AND DISCUSSION

Surface ocean response to Cyclone Marcus

The response of the layer above sea level is often determined by observing changes in wind speed and current speed. During the peak of Cyclone Marcus (Fig. 2a), the lowest pressure occurs in the eye, where surface wind speed reached 20 m/s in a clockwise direction due to the Coriolis effect. The average surface wind speed before the occurrence of Cyclone Marcus (11–17 March 2018) was around 4-6 m/s in the study area (Fig. 2b). The average surface wind speed during Cyclone Marcus (18–25 March 2018) was in the range of 11-18 m/s in the study area (Fig. 2c). Besides that, Cyclone Marcus began to re-curvature to the South. The surface winds will accelerate as the intensity of TCs increases (Zhang *et al.,* 2020). After the cyclone reached the extinction

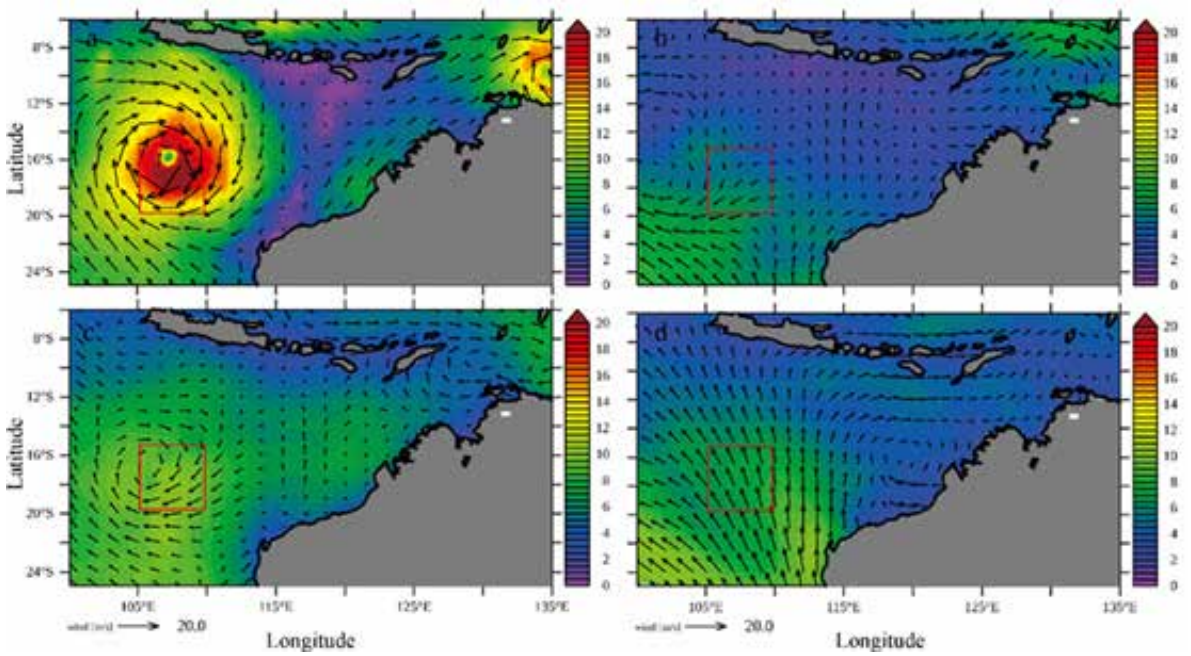

Fig. 2: The wind pattern (color in m/s): (a) during the peak of Cyclone Marcus on 22 March 2018, (b) before Cyclone Marcus (11-17 March 2018), (c) during Cyclone Marcus (18-25 March 2018), (d) after Cyclone Marcus (26-31 March 2018)

phase (26–31 March 2018), the average surface wind speed in the study area of Cyclone Marcus ranged 1-10 m/s (Fig. 2d). The surface wind speed decreased significantly, presumably because the post-tropical cyclone causes calmer weather with cold SST. SST cooling weakens the cyclone system because of no energy source (Sillmann *et al.,* 2021; Guo *et al.,* 2020).

Ocean flow patterns also show a significant response to Cyclone Marcus, particularly in the study area. During the peak of Cyclone Marcus (Fig. 3a), the eddy was formed in the clockwise direction following the surface wind pattern where surface current velocity reached 0.7 m/s. Before the cyclone, the average surface current velocity was around 0.19-0.23 m/s in the study area (Fig. 3b). The average surface current velocity during the occurrence of Cyclone Marcus ranged from 0.21-0.45 m/s in the study area (Fig. 3c), which is in line with the movement direction of the cyclone towards the South. The movement of surface currents changed significantly, while the currents increased as the cyclone intensity was high. The current velocity decreased close to normal after the cyclone, with its average value ranging at 0.2-0.23 m/s in the study area (Fig. 3d). The decrease in currents is not as significant as that in the wind since the currents are not directly related to TCs and only receive the influence of energy transfer from wind friction (Zhang *et al.,* 2020).

The response of temperature and salinity in the subsurface

Cyclone Marcus affects the sea surface layer and the subsurface layer as indicated by a response of physical and biological parameters (Chacko and Zimik, 2018). The present study performs the Argo Float data located near the trajectory of Cyclone Marcus that shows temporal changes in temperature and salinity below the surface, particularly at depths of 4 m to 100 m, as presented in Fig. 4. The water temperature in the surface layer before Cyclone Marcus showed a value of 28.53 °C, which continued to increase to 29.49 °C (Fig. 4a). Before the cyclone, the value of 27.79 °C at 30 m depth continued to increase by 28.91 °C during the cyclone, where the turbulent mixing and upwelled water from the subsurface to surface layers occurred. This mechanism subsequently decreased the temperature on the surface after the cyclone. Fig. 4a shows the temperature at 52 m depth

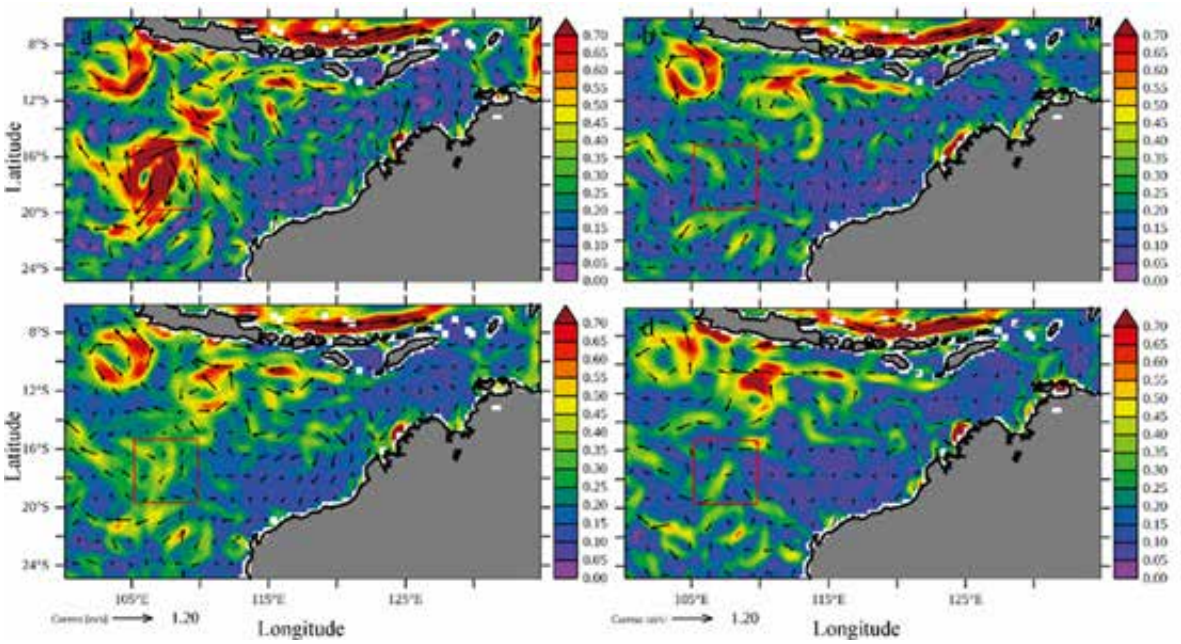

Fig. 3: The ocean flow pattern (color in m/s): (a) during the peak of Cyclone Marcus on 22 March 2018, (b) before Cyclone Marcus (March 11-17), (c) during Cyclone Marcus (March 18-25), (d) after Marcus (March 26-31)

reached 28.28 °C as the cyclone became extinct. The temperature at a depth layer of 4 – 52 m is relatively similar, indicating an increase in temperature. This response is due to temperature inversion below the surface. The temperature inversion causes an increase in the surface layer temperature. The temperature inversion significantly increases the temperature in the subsurface before the cyclone and later increases SST (Chacko and Zimik, 2018). Fig. 4b shows the salinity changes in the subsurface. Before the cyclone, salinity at a depth layer of 0-22m showed a low salinity <34.25 PSU. During the cyclone, the vertical mixing caused a significant increase in salinity, reaching 34.668 PSU at 46 m depth. After the cyclone was extinct, it took time to return to normal, which varies from a few days to a few weeks (Chacko and Zimik, 2018; Yan *et al.,* 2017). Fig. 4b clearly shows an upwelling event during the cyclone, which ended ten days after the cyclone. The occurrence of upwelling is the consequence of the clockwise eddy that triggers surface divergence. Turbulent mixing also changes MLD in the study area, where the MLD before the cyclone was counted around 22 – 26 m depths (Fig. 5a). During the cyclone, MLD ranged between 20 until 25 m depths (Fig. 5b). After the cyclone, MLD has seen around 18 – 40 m depths (Fig. 5c). In comparison with Fig. 4a, a MLD before the cyclone of 30 m depth and after the cyclone of 60 m depth. The MLD in Fig. 5 was adopted from ARMOR3D (Copernicus data set), while the MLD in Fig. 4a was an estimation from the vertical temperature profile of the Argo Float Data.

Sea surface temperature response

The SST response to TCs is clearly illustrated by the relatively low SST values, where the spatially averaged SST in the study area was 28.04 °C before Cyclone Marcus (Fig. 6a) and decreased to around 27.5 °C during Cyclone Marcus (Fig. 6b). Table 2 presents the comparison of SST as reported in the previous studies. This mechanism is presumably due to the influence of water mass mixing, upwelling, and heat release. About 85% of the causes of SST cooling due to TCs are caused by upwelling or entrainment processes, in addition to the heat release process used by TCs as energy to maintain their existence (Sillmann *et al.,* 2021). The initially warm SST value will be the heat intake used by the cyclone as an energy source to maintain its existence for more prolonged movements. Each tropical cyclone has a different SST threshold value, and the threshold depends on

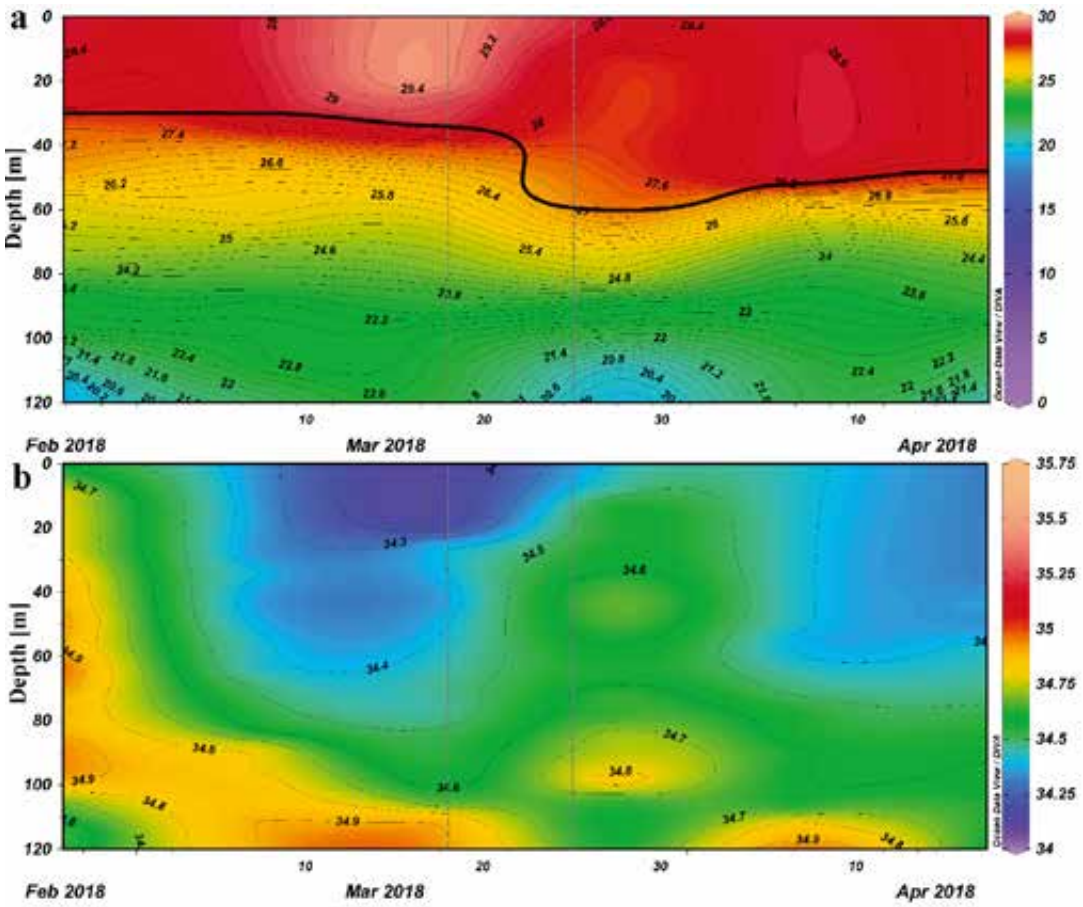

Fig. 4: Vertical profile of temperature (color in °C) (a), and salinity (color in PSU) (b) at Argo Float stations. The thick contour-line in (a) indicates a MLD. A thick vertical dash-line indicates the occurrence of Cyclone Marcus between 18 and 25 March 2018. Data interpolation among the Argo Float stations and visualization was carried out using Ocean Data View with DIVA (Data Interpolating Variational Analysis) method (Schlitzer, 2021)

the lifetime of the cyclone (Tory and Dare., 2015) so that each tropical cyclone has an SST value that varies in experiencing intensification (increase in energy), de-intensification (decrease in energy), re-curvature, and even dissipation (Chacko and Zimik, 2018). The spatially averaged SST value after Cyclone Marcus in the study area was around 27.11 °C (Fig. 6c). The dissipation stage started after the cyclone, as seen by slowly increased SST until 27.34 °C. That means the ocean response was indicated to restore SST to an original or stable condition. During pre-and post- Cyclone Marcus, the SST difference reached 1.7 °C. The magnitude of SST difference caused by the cyclone is strongly influenced by its intensity which causes vertical mixing in the surface ocean. The SST variability can determine the intensity of TCs (Xu *et al.,* 2016; Thanh *et al.,* 2019).

Biological response

The spatial and temporal response of Chl-a in the sea surface affected by Cyclone Marcus showed an increased concentration along the cyclone path. The present study focuses on the Chl-a response in the area where the peak intensity (category 5) occurred. The Chl-a concentration before Cyclone Marcus was around 0.065-0.081 mg/m^3 in the study area (Fig. 7a). The present results correspond with previous research conducted by Li *et al.* (2012) regarding the vertical distribution of Chl-a in the Indian Ocean, which shows the concentration of Chl-a in the surface layer in the East Indian Ocean is less than 0.10 µg/L (equal to mg/m^3). The concentration of Chl-a during

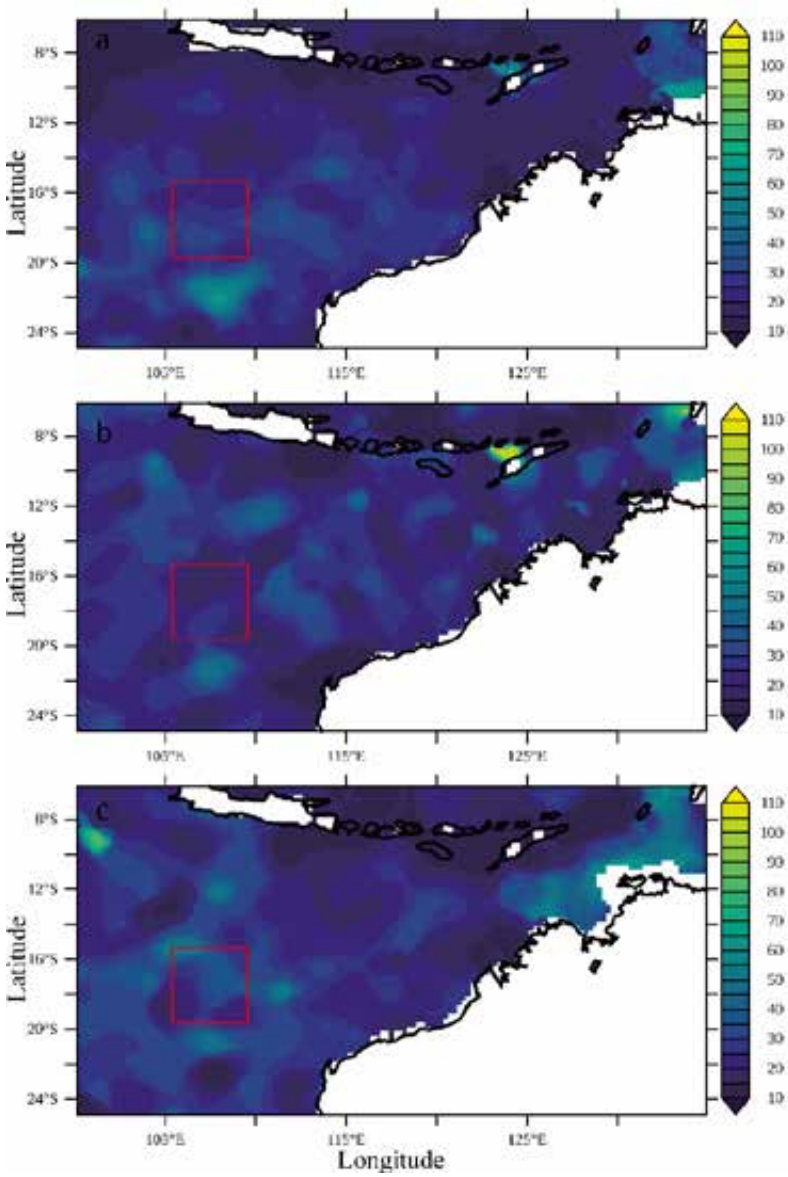

Fig. 5: Distribution of weekly MLD (color in m): (a) before Cyclone Marcus (11-17 March 2018), (b) during Cyclone Marcus (18-25 March 2018), (c) after Cyclone Marcus (26-31 March 2018)

Cyclone Marcus showed an increase of 0.072- 0.14 mg/m^3 in the study area (Fig. 7b) and continued to increase after the cyclone with a range of 0.114- 0.186 mg/m^3 in the study area (Fig. 7c). As for comparison, the Chl-a concentrations from the previous studies are shown in Table 2. The response of Chl-a showed the most significant increase in concentration on 27 March 2018, which reached 0.186 mg/m^3 or 2.5 times greater than the average concentration of 0.075 mg/m^3 before the cyclone. The present study confirms a time lag of the Chl-a response during the occurrence of Cyclone Marcus and the nutrient enrichment process around the cyclone path.

Several factors might influence the process of increasing Chl-a in the sea surface layer. The present study highlights that wind-induced EPV plays a

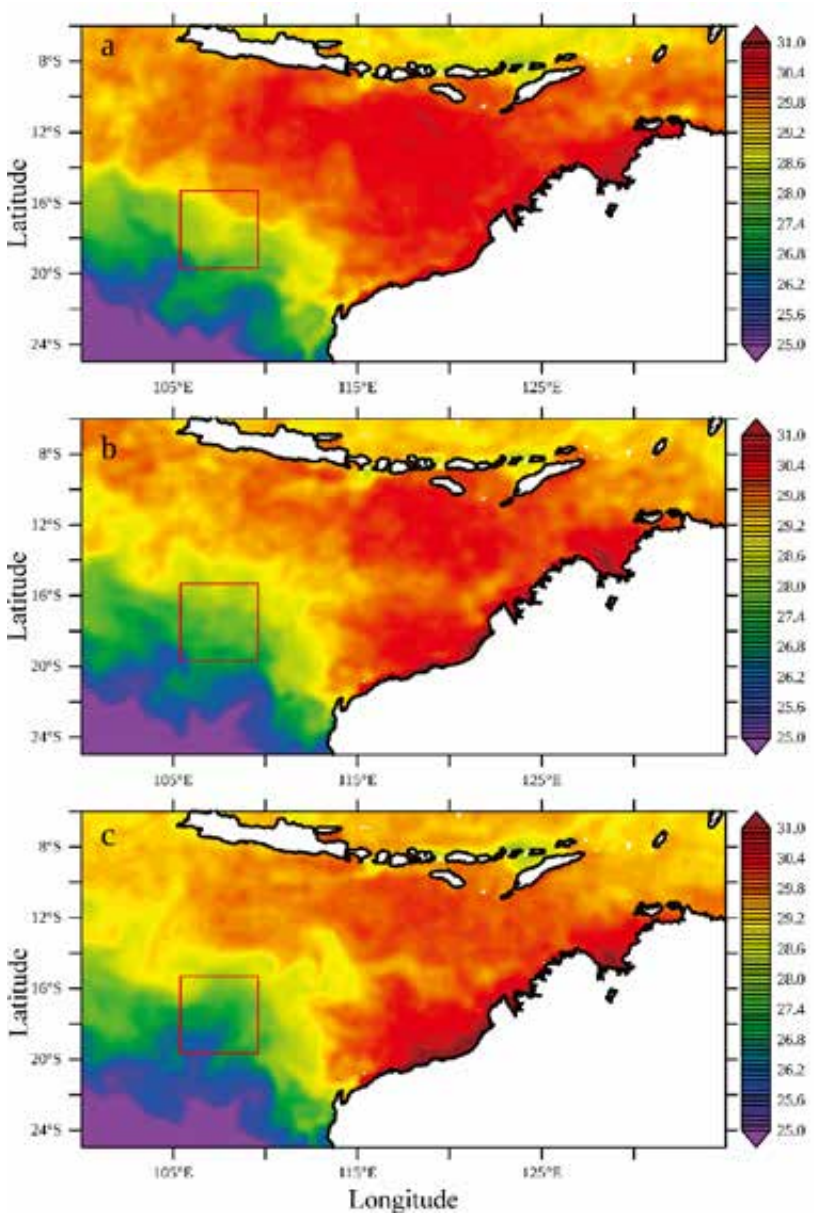

Fig. 6: Distribution of SST (color in °C): (a) before Marcus (11-17 March 2018), (b) during Marcus 18-25 March 2018), (c) after Marcus (26-31 March 2018)

significant role in determining the upwelling. The wind generated by Cyclone Marcus produces a positive (negative) value, indicating an upwelling (downwelling) event, as shown in Fig. 8. The increase in Chl-a concentration is consequently affected by the upwelling process that causes a nutrient-rich water mass to pump up to the surface (Chacko and Zimik, 2018; Efendi *et al.*, 2018). As discussed previously, Cyclone Marcus can mix up 60 m depth. Li *et al.* (2012) reported that the Depth Chl-a Maximum (DCM) was at 55.6 m to 91 m depths in the East Indian Ocean. The nutrients and Chl-a concentrations in DCM were carried to the surface and increased the concentration of Chl-a. The increase in Chl-a after the cyclone was

Table 2: SST and sea surface Chl-a of the previous studies in the Southeastern Indian Ocean

No.	TCs and references	Period	Category (*Saffir-Simpson* scale)	SST (°C)		Chl-a (mg/m^3)	
				Before TCs	After TCs	Before TCs	After TCs
1	Ernie (Efendi *et al.*, 2018)	6-10 April 2017	4	30 - 32	24 -27	0.08	0.15
2	Seroja (Avrionesti *et al.*, 2021)	4-12 April 2021	2	29.72	26.32	Not available	2.57
3	Seroja (Setiawan *et al.*, 2021)	4-12 April 2021	2	29.8	<28	Not available	>12
4	Cempaka (Aditya *et al.*, 2021)	25-27 November 2017	1	29.3	28.2	0 - 0.12	0.15 - 0.2
5	Dahlia (Aditya *et al.*, 2021)	27 November - 2 December 2017	2	28 - 32	26 - 27	0 - 0.12	0.2 - 0.35

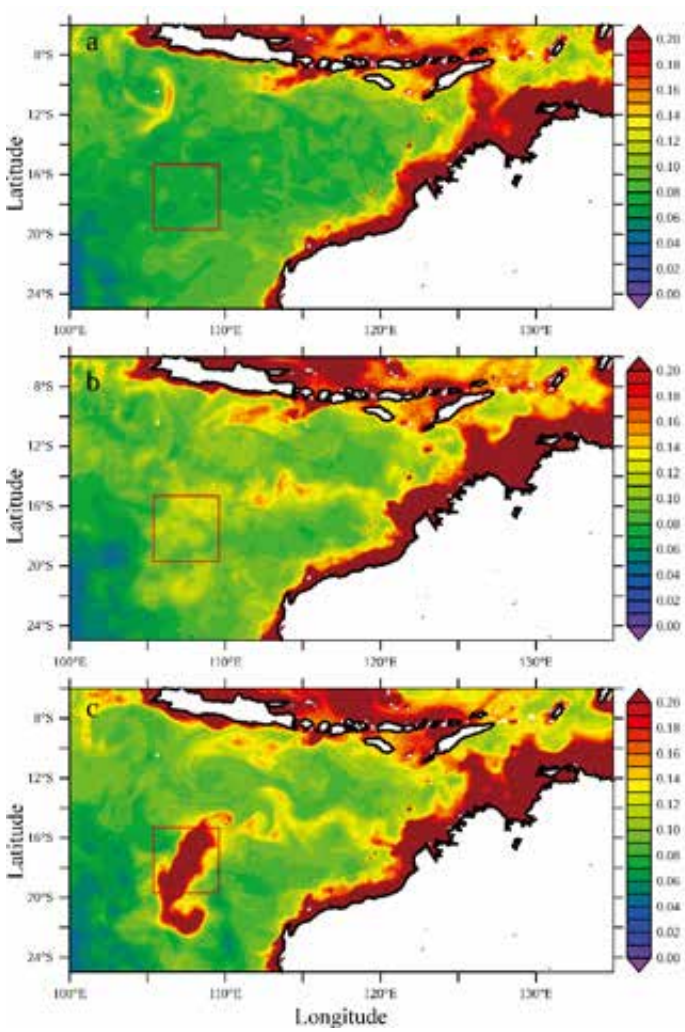

Fig. 7: Distribution of sea surface Chl-a (color in mg/m^3): (a) before Cyclone Marcus (11-17 March 2018), (b) during Cyclone Marcus (18-25 March 2018), (c) after Cyclone Marcus (26-31 March 2018)

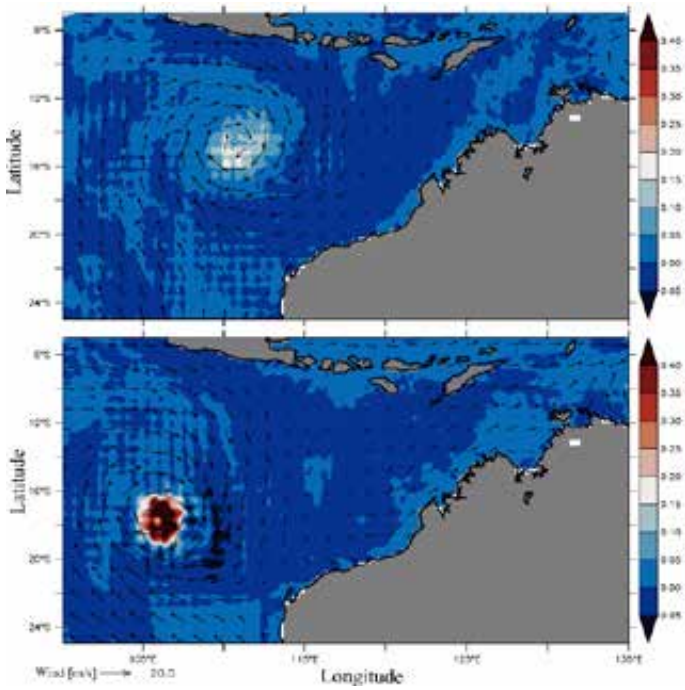

Fig. 8: Distribution of EPV [color in x10^{-5} m/s] during: (a) Cyclone Marcus category 4 (21 March 2018), (b) Cyclone Marcus category 5 (22 March 2018)

due to the shallowing MLD and thermocline depth, which subsequently provided nutrient enrichment in the surface layer (Chakraborty *et al.,* 2018). After 27 March 2018, the Chl-a concentration continued to decrease until its concentration reached the monthly average without the cyclone effects on 10 April 2018. The present finding presents that Cyclone Marcus could induce surface divergence (clockwise eddy) where the cold water and high salinity waters pumped up to the surface layer, starting from 23 March (1 day after the peak of Cyclone Marcus) to 4 April 2018 (Fig. 4). It implies that the lifted nutrient-rich water stays in the MLD for 11 days, and a Chl-a increases two weeks after the cyclone. A similar phenomenon was also found by Lü *et al.* (2020), with the Chl-a concentration increase persisting for up to ten days, while Mandal *et al.* (2018) found up to eight days. Chakraborty *et al.* (2018) and Efendi *et al.* (2018) reported that the Chl-a concentration increase could last two to three weeks after a storm. As affected SST, the speed and intensity of the cyclone affect the vertical mixing and upwelling processes (Fig. 8a and Fig. 8b). The present study found that category four or intensity four of the cyclone resulted in EPV value around 2.6 x 10^{-6} m/s, while in category five, the EPV value increased significantly by 3.01 x 10^{-4} m/s. The speed and intensity of the cyclone will subsequently increase the concentration of nutrients and trigger the growth of phytoplankton and increase the Chl-a concentration (Chacko and Zimik, 2018; Lin, 2012; Mei *et al.,* 2015).

Relationship between SST, Chl-a, and ACE

The response of SST and sea surface Chl-a concentration during the formation of TCs showed a strong relationship around the path of TCs. Our findings showed that the SST decreased and the Chl-a concentration increased along the cyclone path. Increasing (decreasing) Chl-a concentration (SST) depended on the intensity of TCs caused by the wind speed that forced mixing in the surface layer. The wavelet transforms cross-correlation between SST, Chl-a, and ACE (represents wind speed) in the study area during 2017-2018, as shown in Fig. 9. The present study found an increasing value of the wavelet spectrum from the end of March 2018 to the beginning of April 2018 with ten days. The phase relationship between variables is indicated by the

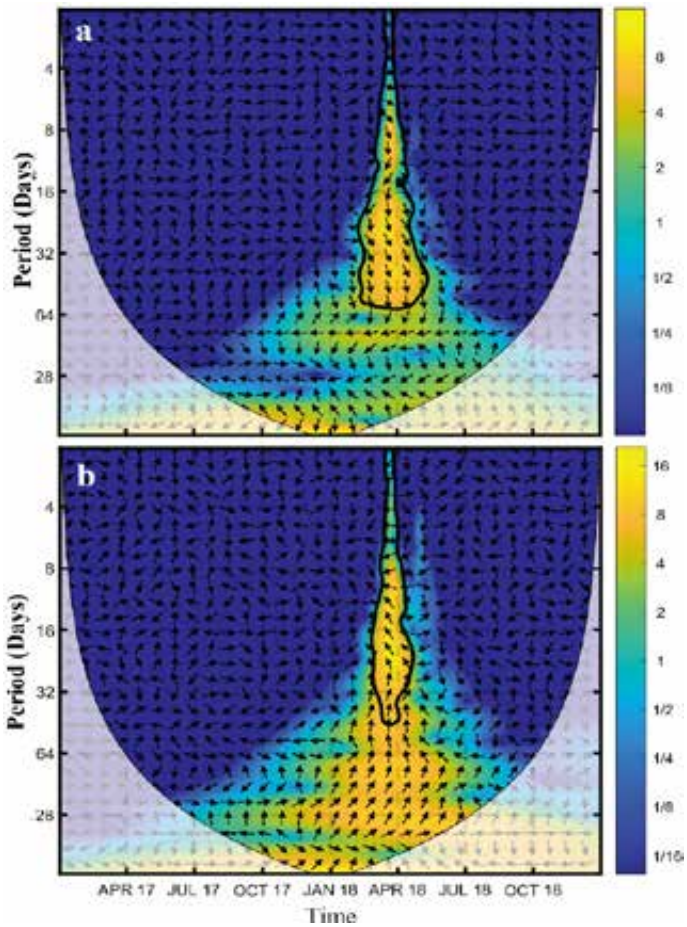

Fig. 9: Wavelet cross transformations in the study area where the thick black contours show a 95% confidence level for: (a) ACE and SST, (b) ACE and Chl-a. The wavelet calculation and visualization were carried out using MatLab R2020b

direction of the arrow in the wavelet analysis, where the arrow indicates the in-phase (anti-phase) to the right (left). The direction of the arrow starts from the right arrow to represent a time lag between the two variables. In this case, the arrows pointing to the lower right or upper left indicate the variable-1 (ACE) occurs first, while the arrows pointing to the upper right or lower left indicate that the variable-2 (SST and Chl-a) occurs first (Fig. 9). The time lag between the peak of Cyclone Marcus and the SST decrease was about 2.5 days (Fig. 9a). The coherence value for SST during the cyclone is 0.8, indicating that the two variables have a strong relationship. The present study also found that the time lag corresponds with the *Ekman* pumping response of 2.3 days, where the maximum EPV shows a value of 3.01 x 10^{-4} m/s consistent with the highest intensity in the study area. The water-mass entrainment from the lowest depth of MLD, which is 60 m, to the sea surface requires 2.3 days. The time lag between the peak of Cyclone Marcus and the Chl-a concentration increase was about 5.6 days (Fig. 9b). The coherence value for Chl-a during the cyclone shows a strong relationship among the two variables, which is 0.8. The present findings suggest that the mixing process due to upwelling would produce a different time lag for SST and Chl-a responses according to the wavelet analysis. In this case, the SST response is shorter than Chl-a because of the direct response of this SST parameter in the sea surface. It is different for the Chl-a parameter that needs a pre-response for nutrient enrichment in the surface from the subsurface layer before a

photosynthesize process for phytoplankton growth (Chl-a increase). Kämpf and Chapman (2016) stated that the movement of water masses from the water column takes several days to a week, which is sufficient time to lift the water mass to a vertical distance of 100 m or more. The difference in TCs intensity may cause a different time lag for the Chl-a response (Parker *et al.,* 2017). The Chl-a response relates to the pyramidal structure of the ecosystem in the upwelling regions, where primary, secondary and small pelagic fish productivities have a different time for their growths.

CONCLUSION

Cyclone Marcus in 2018 was one of TCs with high intensity of category 5 in the Southeastern Indian Ocean. The present study investigates the influence of Cyclone Marcus on oceanographic processes in the subsurface and surface layers and its impact on SST and surface Chl-a in the study area. The average surface wind speed increased by three times during Cyclone Marcus in a clockwise direction and decreased significantly after the cyclone reached the extinction phase due to SST cooling in the study area, resulting in no energy source for the cyclone. The average surface current velocity increased almost two times during Cyclone Marcus, and the eddy was formed in the clockwise direction following the surface wind pattern. The decrease in post-cyclone currents was not as drastic as the wind because the ocean friction limited energy transfer from the wind. The Argo Float data presents that Cyclone Marcus could induce surface divergence (clockwise eddy) where the cold water and high salinity waters pumped up to the surface layer, starting 1 day after the peak of Cyclone Marcus. It implies that the lifted nutrient-rich water stays in the MLD for 11 days, and a Chl-a increases two weeks after the cyclone. Wind-induced eddy and EPV play a significant role in determining the upwelling. Cyclone Marcus can mix up 60 m depth where the nutrients and Chl-a concentrations in DCM were carried to the surface and increased the concentration of Chl-a. The increase in Chl-a after the cyclone was due to the shallowing MLD and thermocline depth, which subsequently provided nutrient enrichment in the surface layer. Significant findings in this research show a SST difference of 1.7 °C, MLD deepening up to 60 m, and an increase in Chl-a almost three times in responding to the cyclone. The future TCs could increase in the category in the study area, as the warming trend in the Indian Ocean. Besides its negative impacts, future research could focus on the marine food chain as the phytoplankton blooming (Chl-a) after the cyclone.

AUTHOR CONTRIBUTIONS

A.F. Koropitan performed the literature review, research design, analyzed and interpreted the data, prepared the manuscript text and manuscript edition. M.H.I. Khaldun performed the literature review, data analysis and visualization, and manuscript preparation. Y. Naulita enriched the literature review and manuscript preparation.

ACKNOWLEDGEMENT

The authors wish to acknowledge the use of the PyFerret and Ocean Data View softwares for analysis and graphics in this paper. *PyFerret* is a product of NOAA's Pacific Marine Environmental Laboratory. The authors are grateful to Randi Firdauss for helping us in wavelet analysis using MatLab. This study has been conducted at Big Data and Ocean Modeling (BiOM) Laboratory, Department of Marine Science and Technology, IPB University.

CONFLICT OF INTEREST

The author declares that there is no conflict of interests regarding the publication of this manuscript. In addition, the ethical issues, including plagiarism, informed consent, misconduct, data fabrication and/or falsification, double publication and/or submission, and redundancy have been completely observed by the authors.

PUBLISHER'S NOTE

GJESM Publisher remains neutral with regard to jurisdictional claims in published maps and institutional affiliations.

ABBREVIATIONS

%	Percent
<	Less than
°	Degree
°C	Degree celsius
°E	Degree east
°S	Degree south
τ	Wind stress
µg/L	Microgram per liter
ACE	Accumulated cyclone energy
ARMOR3D	A 3 dimension multi-observations product of the ocean
BiOM	Big data and ocean modeling
BOM	Bureau of meteorology
C_d	Wind drag coefficient
Chl-a	Chlorophyll-a
CPUE	Catch per unit effort
CSIRO	Commonwealth scientific and industrial research organization
DCM	Depth chlorophyll maximum
DIVA	Data interpolating variational analysis
EPV	*Ekman* pumping velocity
Eq	Equation
f	*Coriolis* parameter
Fig	Figure
GHRSST	Group for high-resolution sea surface temperature
hPa	Hectopascal
JPSS	Joint polar satellite system
kg/m³	Kilogram per cubic meter
Km	Kilometers
m	Meter
m/s	Meter per second
MERIS	Medium resolution imaging spectrometer
mg/m³	Milligram per cubic meter
MLD	Mixed layer depth
MODIS	Moderate resolution imaging spectroradiometer
n	Amount of data
OLCI	Ocean and land color instrument
OSTIA	The operational sea surface temperature and sea ice analysis
ρ_{air}	Density of air
ρ_w	Density of seawater
PSU	Practical salinity unit
S-NPP	Suomi national polar-orbiting partnership
SeaWiFS	Sea-viewing wide field-of-view sensor
SST	Sea surface temperature
TCs	Tropical cyclones
U	Wind speed
v	Maximum constant wind speed
VIIRS	Visible and infrared imager/radiometer suite
v_{max}	Maximum constant wind speed at 6-hour intervals
$\bar{x}$	Average value of each phase
xi	Sample's value

REFERENCES

Aditya, H.N.; Wirasatriya, A.; Kunarso.; Ismunarti, D.H.; Yusuf, M.; Rifai, A.; Purwanto.; Ismanto, A.; Widiaratih, R., (2021). Impact of tropical cyclones Cempaka and Dahlia to the variability of chlorophyll-a and sea surface temperature in the seas southern coast of Java Island. Ecol. Environ. Cnsev., 27: 379-387 **(9 pages).**

Avrionesti.; Khadami, F.; Purnaningtyas, D.W., (2021). Ocean response to tropical cyclone Seroja at East Nusa Tenggara waters. IOP Conference Series: Earth and Environmental Science, 925: 1-9 (**9 pages**).

Chacko, N.; Zimik, L., (2018). Effect of cyclone Thane in the Bay of

Bengal explored using moored buoy observations and multi-platform satellite data. J. Indian Soc. Remote Sens., 46: 821–828 (**8 pages**).

Chai, F.; Wang, Y.; Xing, X.; Yan, Y.; Xue, H.; Wells, M.; Boss, B., (2021). A limited effect of sub-tropical typhoons on phytoplankton dynamics. Biogeosciences. 18: 849–859 (**10 Pages**).

Chakraborty, K.; Nimit, K.; Akhand, A.; Prakash, S.; Paul, A.; Ghosh, J.; Udaya Bhaskar, T.V.S.; Chanda, A., (2018). Modeling the enhancement of sea surface chlorophyll concentration during the cyclonic events in the Arabian Sea. J. Sea Res., 140: 22–31 (**10 pages**).

Collins, D.J., (2018). Worldwide tropical cyclone activity measured using the actuaries climate index® methodology. Casualty Actuar. Soc. E-Forum., 2: 1 (**32 pages**).

Donlon, C.J.; Martin, M.; Stark, J.; Roberts-Jones, J.; Fiedler, E.; Wimmer, W., (2012). The Operational sea surface temperature and sea ice analysis (OSTIA) system. Remote Sens. Environ., 116: 140–158 (**19 pages**).

Efendi, U.; Fadlan, A.; Hidayat, A.M., (2018). Chlorophyll-a variability in the southern coast of Java Island, Indian Ocean: corresponding to the tropical cyclone of Ernie. IOP Conference Series: Earth and Environmental Science, 162: 1-12 (**12 pages**).

Grinsted, A.; Moore, J.; Jevrejeva S., (2004). Application of the cross wavelet transform and wavelet coherence to geophysical time series. Nonlinear Processes Geophys., 11(4): 561–566 (**6 pages**).

Guinehut, S.; Dhomps, A.L.; Larnicol, G.; Le Traon, P.Y., (2012). High resolution 3-d temperature and salinity fields derived from in situ and satellite observations. Ocean Sci., 8: 845–857 (**13 pages**).

Guo, T.; Sun, Y.; Liu, L.; Zhong, Z., (2020). The impact of storm-induced sst cooling on storm size and destructiveness: results from atmosphere–ocean coupled simulations. J. Meteorolog. Res., 34(5): 1068-1081 (**14 pages**).

Hoque, M.A.A.; Phinn, S.; Roelfsema, C., (2017). A systematic review of tropical cyclone disaster management research using remote sensing and spatial analysis. Ocean Coast. Manage., 146: 109–120 (**12 pages**).

Kämpf, J.; Chapman, P., (2016). Upwelling Systems of the World: A scientific journey to the most productive marine ecosystems. Switzerland, Swiss. Spinger International Publishing Switzerland.

Li, G.; Lin, Q.; Ni, G.; Shen, P.; Fan, Y.; Huang, L.; Tan, Y., (2012). Vertical patterns of early summer chlorophyll a concentration in the Indian Ocean with special reference to the variation of deep chlorophyll maximum. J. Mar. Biol., 2012: 1–6 (**6 pages**).

Lin, I.I., (2012). Typhoon-induced phytoplankton blooms and primary productivity increase in the western North Pacific subtropical ocean. J. Geophys. Res. C: Oceans., 117: 1-15 (**15 pages**).

Lü, H.; Zhao, X.; Sun, J.; Zha, G.; Xi, J.; Cai, S., (2020). A case study of a phytoplankton bloom triggered by a tropical cyclone and cyclonic eddies. PLoS One, 15: 1–18 (**18 pages**).

Mandal, S.; Sil, S.; Shee, A.; Venkatesan, R., (2018). Upper ocean and subsurface variability in the Bay of Bengal during cyclone ROANU: a synergistic view using in situ and satellite observations. Pure Appl. Geophys., 175: 4605–4624 (**20 pages**).

Mei, W.; Lien, C.C.; Lin, I.I.; Xie, S.P., (2015). Tropical cyclone-induced ocean response: a comparative study of the South China Sea and tropical Northwest Pacific. J. Clim., 28: 5952–5968 (**17 pages**).

Mulet, S.; Rio, M.H.; Mignot, A.; Guinehut, S.; Morrow, R., (2012). A new estimate of the global 3d geostrophic ocean circulation based on satellite data and in-situ measurements. Deep Sea Res. Part II., 77–80: 70-81 (**12 pages**).

Parker, C.; Lynch, A.; Spera, S.; Spangler, K., (2017). The relationship between tropical cyclone activity, nutrient loading, and algal blooms over the Great Barrier reef. Biogeosci. Discuss., 1–35 (**35 pages**).

Pillay, M.T.; Fitchett, M.T., (2021). On the conditions of formation of southern hemisphere tropical cyclones. Weather Clim. Extremes, 34(100376): 1-12 (**12 pages**).

Rio, M.H.; Mulet, S.; Picot, N., (2014). Beyond GOCE for the ocean circulation estimate: synergetic use of altimetry, gravimetry, and in situ data provides new insight into geostrophic and Ekman currents. Geophys. Res. Lett., 41: 8918–8925 (**8 pages**).

Roxy, M.K.; Ritika, K.; Terray, P.; Murtugudde, R.; Ashok, K.; Goswami, B.N., (2015). Drying of Indian subcontinent by rapid Indian Ocean warming and a weakening land-sea thermal gradient. Nat. Commun., 1-6 (**6 pages**).

Schlitzer, R., (2021). Ocean data view user 's guide.

Setiawan, R.Y.; Susanto, R.D.; Wirasatriya, A.; Alifdini, I.; Puryajati, A.D.; Maslukah, L.; Nurdin, N., (2021). Impacts of tropical cyclone Seroja on the phytoplankton chlorophyll-a and sea surface temperature in the Savu Sea, Indonesia. IEEE Access, 21: 152938-152944 (**7 pages**).

Sillmann, J.; Daloz, A.S.; Schaller, N.; Schwingshackl, C., (2021). Climate change 3rd ed: observed impacts on planet earth. United States. Elsevier Inc, USA.

Thanh, N. T.; Cuong, H. D.; Hien, N. X.; Kieu, C., (2019). Relationship between sea surface temperature and the maximum intensity of tropical cyclones affecting Vietnam's coastline. Int. J. Climatol., 40: 2527–2538 (**12 pages**).

Tory, K. J.; Dare, R. A., (2015). Sea surface temperature thresholds for tropical cyclone formation. J. Clim., 28(20): 8171–8183 (**13 pages**).

Vidya, P.J.; Das, S.; Murali.R, M., (2017). Contrasting chl-a responses to the tropical cyclones Thane and Phailin in the Bay of Bengal. J. Mar. Syst., 165: 103-114 (**12 pages**).

Xu, J.; Wang, Y.; Tan, Z., (2016). The relationship between sea surface temperature and maximum intensification rate of tropical cyclones in the North Atlantic. J. Atmos. Sci., 73: 4979-4988 (**10 pages**).

Yan, Y.; Li, L.; Wang, C., (2017). The effects of oceanic barrier layer on the upper ocean response to tropical cyclones. J. Geophys. Res. C: Oceans., 122: 4829–4844 (**16 pages**).

Yu, J.; Tang, D.; Chen, G.; Li, Y.; Huang, Z.; Wang, S., (2014). The positive effects of typhoons on the fish CPUE in the South China Sea. Cont. Shelf Res., 84: 1–12 (**12 pages**).

Yu, J.; Tang, D.; Li, Y.; Huang, Z.; Chen, G., (2013). Increase in fish abundance during two typhoons in the South China Sea. Adv. Space Res., 51: 1734–1749 (**16 pages**).

Zhang, H.; He, H.; Zhang, W.; Tian, D., (2021). Upper ocean response to tropical cyclones: a review. Geosci. Lett., 8(1): 1-12 (**12 pages**).

Zhang, H.; Liu, X.; Wu, R.; Chen, D.; Zhang, D.; Shang, X.; Wang, Y.; Song, X.; Jin W.; Yu, L.; Qi, Y.; Di Tian, D.; Zhang, W., (2020). Sea surface current response patterns to tropical cyclones. J. Mar. Syst., 208(103345): 1-16 (**16 pages**).

AUTHOR (S) BIOSKETCHES

Koropitan, A.F., Ph.D., Associate Professor, Department of Marine Science and Technology, Faculty of Fisheries and Marine Science, IPB University, Kampus IPB Dramaga, Bogor 16680, Indonesia.
- Email: *alan@apps.ipb.ac.id*
- ORCID: 0000-0001-5794-094X
- Web of Science ResearcherID: ABE-7099-2021
- Scopus Author ID: 23135214600
- Homepage: https://itk.ipb.ac.id/~itkipb/dr-alan-frendy-koropitan-s-pi-m-si/

Khaldun, M.H.I., M.Sc., Department of Marine Science and Technology, Faculty of Fisheries and Marine Science, IPB University, Kampus IPB Dramaga, Bogor 16680, Indonesia.
- Email: *mhikhaldun@gmail.com*
- ORCID: 0000-0003-2161-8136
- Web of Science ResearcherID: ABF-1690-2021
- Scopus Author ID: 57202966767
- Homepage:https://ipb.ac.id/faculty/index/faculty-of-fisheries-and-marine-science/department-of-marine-science-and-technology

Naulita, Y., Ph.D., Associate Professor, Department of Marine Science and Technology, Faculty of Fisheries and Marine Science, IPB University, Kampus IPB Dramaga, Bogor 16680, Indonesia.
- Email: *naulita@ipb.ac.id*
- ORCID: 0000-0002-4931-3783
- Web of Science ResearcherID: ABF-9349-2021
- Scopus Author ID: 54781750900
- Homepage: https://itk.ipb.ac.id/~itkipb/dr-ir-yuli-naulita-m-si/

HOW TO CITE THIS ARTICLE

Koropitan, A.F.; Khaldun, M.H.I.; Naulita, Y., (2022). Impact of tropical cyclone Marcus on ocean subsurface and surface layers. Global J. Environ. Sci. Manage., 8(3): 353-368.

DOI: 10.22034/gjesm.2022.03.05

url: https://www.gjesm.net/article_248202.html

Global J. Environ. Sci. Manage. 8(3): 369-388, Summer 2022, Serial #31

Global Journal of Environmental Science and Management
(GJESM)

Homepage: https://www.gjesm.net/

ORIGINAL RESEARCH PAPER

Connectivity of vegetation diversity, carbon stock, and peat depth in peatland ecosystems

R. Garsetiasih, N.M. Heriyanto, W.C. Adinugroho, H. Gunawan, I.W.S. Dharmawan*, R. Sawitri, I. Yeny, N. Mindawati, Denny

Forest Research and Development Center, Ministry of Environment and Forestry, Bogor, West Java, Indonesia

ARTICLE INFO

Article History:
Received 27 August 2021
Revised 08 Nivember 2021
Accepted 12 December 2021

Keywords:
Carbon stock
Connectivity
Diversity
Peat depth
Sustainability

ABSTRACT

BACKGROUND AND OBJECTIVES: Peat swamp forest ecosystems are fragile ecosystems with different peat depths according to the level of peat formation. Moreover, a peat swamp forest can have diverse vegetation and high carbon stocks. Thus, caution should be taken in the sustainable management of a peat swamp forest. However, the connection between vegetation diversity, carbon stocks, and peat depths has not been widely studied in efforts to conserve vegetation and peatlands. This study aimed to analyze the connection between vegetation diversity, carbon stocks, and peat depths in the Kahayan Sebangau Peat Hydrology Unit.

METHODS: Plots at the peat depths of four sites were studied: site 1 (<50 cm), site 2 (393-478 cm), site 3 (479-564 cm), and site 4 (565-649 cm).

FINDINGS: : This study discovered that diverse vegetation at the tree, sapling, and seedling levels and the species richness at different peat depths were significantly different due to various nutrient contents and distances from the river. The number of species found varied at various peat depths, with 20, 28, 32, and 19 species at peat depths of 565 cm, 479-<565 cm, 393-<479 cm, and <50 cm, respectively. In addition, the highest carbon stock was 95.2 ± 19.52 Mg C/ha, which was found at a peat depth of 479 – 564 cm and a vegetation diameter of ≥10 cm. The tree species *Combretocarpus rotundatus* (Miq.) Danser, *Maclurodendron porteri* (Hook. f.) T.G. *Hartley, Tetramestra glabra* Miq, and *Horsfieldia irya* (Gaertn.) Warb. had high survival rates and grew at a peat depth of <50 cm. The study results confirmed that peat thickness could not directly affect the vegetation dynamic in terms of vegetation diversity. The vegetation changes were influenced directly by changing other characteristics of peat hydrology, peat chemistry, and peat organic matter.

CONCLUSION: All Pearson correlation values between peat depth, vegetation diversity, and carbon stock were positive with each other. This shows that peat depth, vegetation diversity, and carbon stock are interdependent and connected to one another.

DOI: 10.22034/gjesm.2022.03.06

NUMBER OF REFERENCES	NUMBER OF FIGURES	NUMBER OF TABLES
47	9	8

*Corresponding Author:
Email: *salifa03@yahoo.co.id*
Phone: +6282173073981
ORCID: 0000-0002-7007-393X

Note: Discussion period for this manuscript open until October 1, 2022 on GJESM website at the "Show Article".

INTRODUCTION

Peat swamp forests in Indonesia are scattered across Riau, Jambi, South Sumatra, Southeast Sulawesi, Kalimantan Island, and Maluku Island, with a total area of 149,056 km^2 (Warren *et al.,* 2017). Peat swamps are important ecosystems, providing environmental services, creating diversity among the tree species and wildlife, and contributing to the mitigation of climate change and thus to a reduction in global warming (Osaki *et al.,* 2021). Climate change also affects hydrological aspects of peatland forests. Peat swamps are important ecosystems globally because their functions are primarily related to hydrology, carbon cycling, and biodiversity regarding tree species and wildlife and they contribute to climate change mitigation, thus reducing global warming (Hirano *et al.,* 2014; Osaki *et al.,* 2021; Sefidi *et al.,* 2015). They are also especially sensitive to climate dynamics, such as changes in precipitation and the flood regime (Fenner and Freeman, 2011). These environmental factors are interrelated and interact, which ultimately affect the composition and pattern of vegetation diversity (Afrianto *et al.,* 2016). These areas possess a unique and fragile ecosystem with certain characteristics. One of the functions of forests, such as peat swamps, is carbon cycling by absorbing or sinking carbon dioxide (CO_2) from the air. Carbon dioxide storage is closely correlated with standing biomass (Dargie *et al.,* 2017). The amount of biomass in an area is obtained by calculating the biomass density and number of tree species. Peat swamp forests, especially in Kalimantan, have been significantly degraded and fragmented from 1990 to 2010 (Dohong *et al.,* 2017) because peat swamp forests have been extracted since the establishment of forest concession rights (Miettinen and Liew, 2010). The most degrading factors of this peat forest are illegal logging, land conversion, and forest fire. The conversion of peat swamps increases the amount of carbondioxide (CO_2). According to Hooijer *et al.* (2010), emissions related to changes in peat swamp use and management are estimated to be 50% of Indonesia's total national emissions. Tree growth in tropical regions is generally faster than that in sub-tropical regions (Russel and Raich, 2012). Therefore, developed countries are highly concerned about tropical forest preservation because forests can absorb gas emissions and prevent climate change (Harrison *et al.,* 2019). The third-largest tropical forest in the world is located in Indonesia, after those in Brazil and Kenya (Kusmana and Hikmat, 2015), so we must obtain basic data about how much carbon can tropical forests absorb, especially lowland peat swamp forests. Peat swamp is a soil material not easily weathered and consists of organic materials mostly not decomposed and accumulated in aerobic conditions (Dommain *et al.,* 2015). Peat swamp forests have an important global ecological function as carbon sinks and stocks and significantly contribute to global carbon cycles (Osaki *et al.,* 2021). On the other hand, logging and fires threaten biodiversity loss in peat swamp forests (Posa *et al.,* 2011). These two reasons are the triggers for this research, which investigates tree species and carbon stocks at various peat depths. In this regard, the research gaps were found between vegetation diversity, carbon stock, and peat depth in the peatland forest ecosystem. Rieley *et al.* (1996); Page *et al.* (1999); Lahteenoja *et al.* (2009a, 2009b); Astiani *et al.* (2016) stated that varying responses to local gradients in hydrology, nutrient availability, and depth of peat affect vegetation changes. Meanwhile, more in-depth analyses between vegetation diversity and its connection to carbon stock and peat depth are needed. Specifically, this study aims to investigate the vegetation diversity and carbon stock at several peat depths as well as to analyze the connection/correlation between vegetation diversity, carbon stock, and peat depths to provide recommendations for peat swamp forest conservation. This study was carried out in the peat hidrology unit (PHU) of Kahayan, Sebangau River, Pulang Pisau Regency, Central Kalimantan Province, in 2020.

MATERIALS AND METHODS

Description of the study area and context

The study location is categorized as a peat swamp forest by the Peat Hidrology Unit (PHU) of Kahayan, Sebangau River, Pulang Pisau Regency, Central Kalimantan Province. In this research, the location is divided into four sites: site 1 (2° 28'55.04 " S and 114° 7'15.13" E), site 2 (2° 21 ' 6.18 " S and 114 ° 2'6.77" E), site 3 (2° 21'8.25" S and 114° 5'29.86" E), and site 4 (2° 22'48.05 " S and 114° 9'4.70 " E). These sites are presented in Fig. 1.

The study sites are located ± 7-25 m above

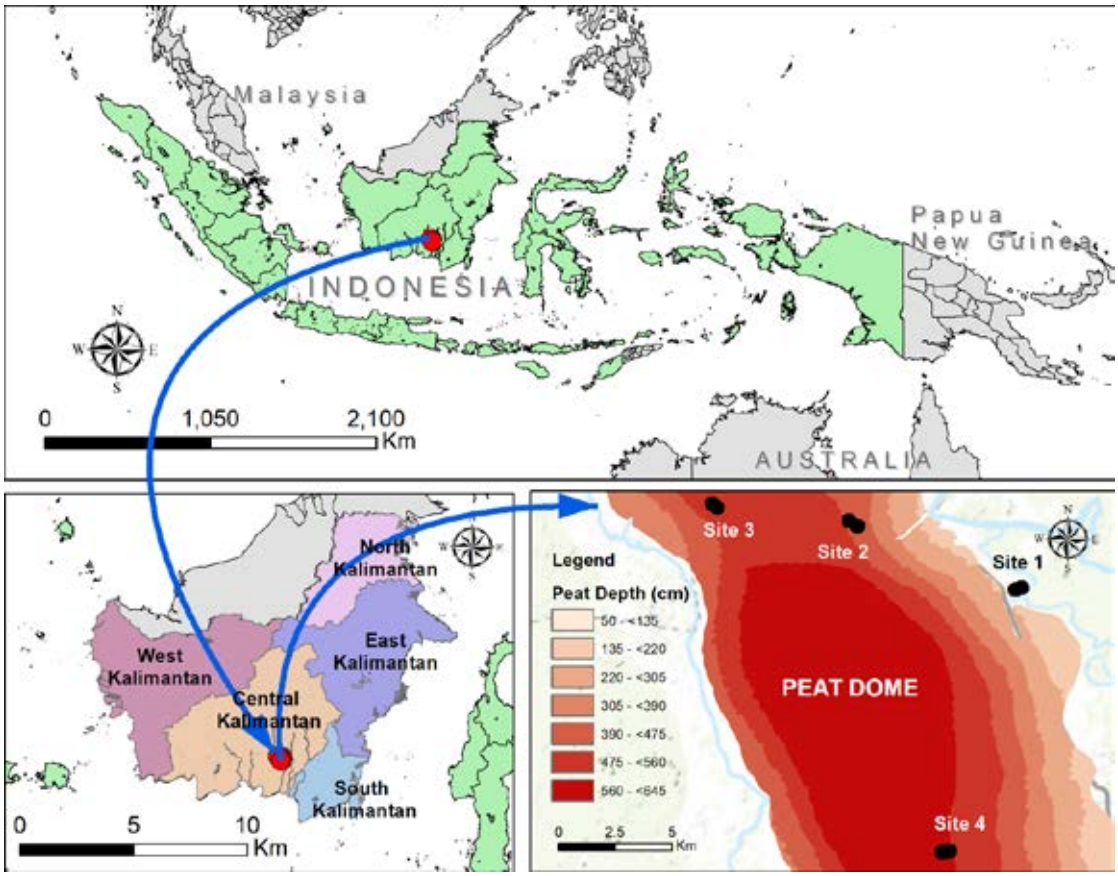

Fig. 1: Geographic location of the study area in the Kahayan Sebangau Peat Hydrology Unit in Indonesia.

sea level, and their topography is flat, with slopes between 0 and 8%. The soil of the study sites include Tropochemist, Troposaprist, and Tropofibrist/Saprik Peat, which continuously rot and are made of old alluvium materials. The stone components including clay, silt, gravel, plant debris, and sand are dark brown to black, and when they are squeezed, their fiber content is less than 15% (Soil Survey Staff, 2014). For an illustration of the study methodology from preparation until data analysis, a flow diagram for the overall methodology in this study is shown in Fig. 2. The approach used in this research was a field survey, which was then analyzed quantitatively using a statistical approach. The study used primary data and a number of relevant secondary data. The primary data consist of measurement data for the forest stand parameters, namely diameter, height, and species obtained through measurements on an observation plot.

Survey and sampling designs

The vegetation diversity and carbon stock were analyzed on sample sites from peat domes to shallow peats. The study used stratified random sampling in the research design. The research location was stratified by peat category, namely shallow peat (edge), between shallow and peat dome, and peat dome. Then, the sampling plots were determined randomly for each stratum in several classes of peat depth based on the peat depth map issued by the Peatland Restoration Agency. In each of the shallow peat and peat dome strata, 10 observation plots were made, while between the shallow peat and peat dome, 20 observation plots were made. Site 1 was at a peat depth < 50cm (shallow peat), and then, 2 sites are shallow peat to peat domes, namely site 2 (393-478 m) and site 3 (479 – 564 m), while site 4 was a peat dome with a depth of 565 – 649 m (Fig. 1). The sample unit was a square with

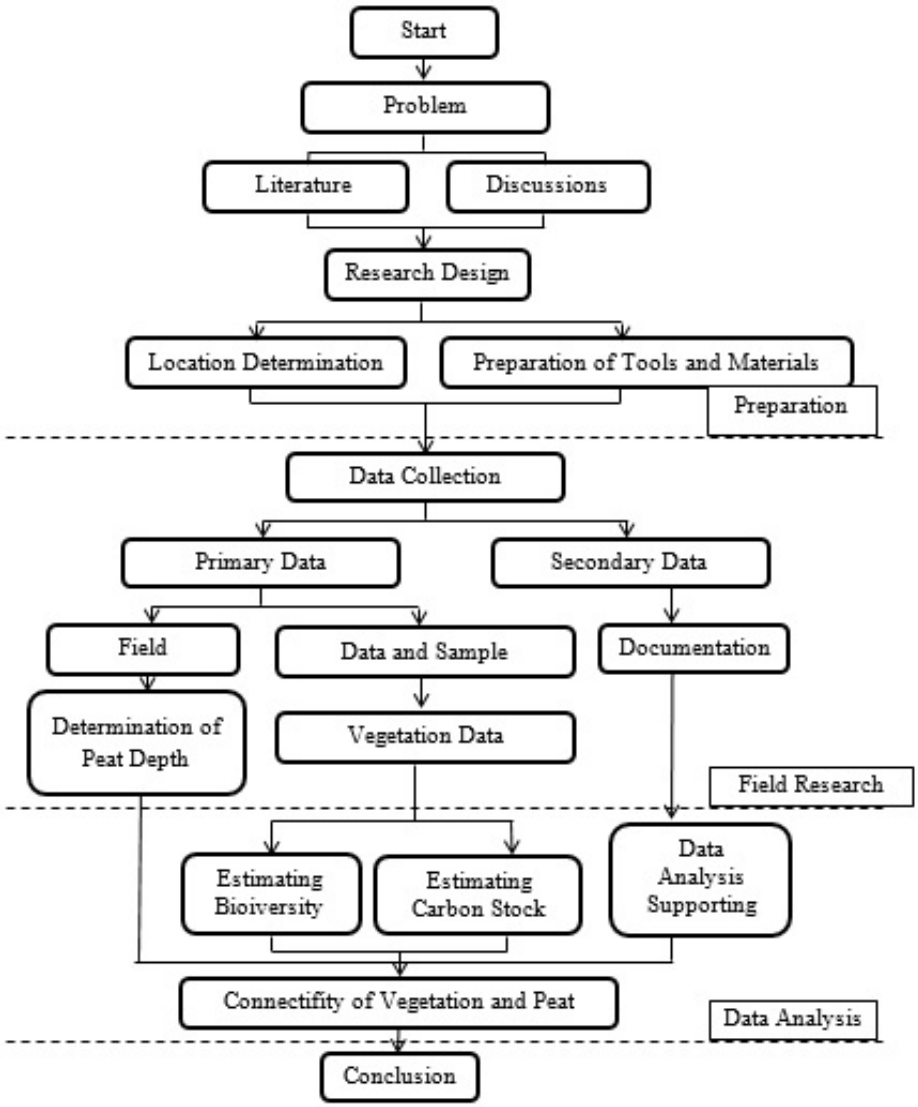

Fig. 2: Flow diagram for the overall methodology

a size of 20 m x 20 m (0.04 ha) and nested with a different size plot for different growth stages. The plots were repeated ten times at each site. A plot of 20 m x 20 m was established for the tree inventory, a plot of 5 m x 5 m for the sapling inventory, and a plot of 2 m x 2 m for seedlings inventory (Haryadi *et al.,* 2019). These plots are presented in Fig. 3. This study employed a global positioning system (GPS) to measure devices, tape diameters, plastic ropes, tree height measurement tools, and herbarium tool kits. The diameters, height, and species of all trees and saplings were recorded, while species' numbers and names were recorded for seedlings. These kinds of materials were sampled and identified at the Herbarium Laboratory of Forest Research and Development Center, Bogor. The criteria for tree, sapling, and seedling are as follows (Mansur and Kartawinata, 2017). The trees' diameter was 1.3 m ≥10 cm at breast height. If they contained a buttress, the diameter was measured 20 cm above the buttress. Those criteria were recorded in the plot size of 20 m x 20 m (Afzanizam *et al.,* 2019).

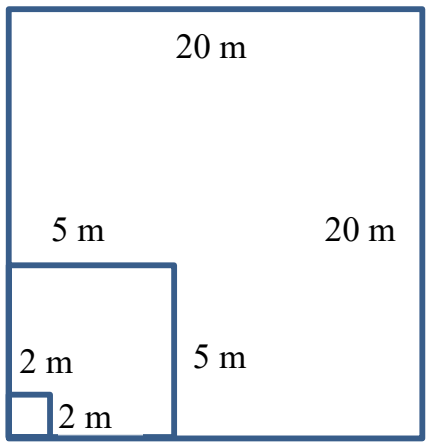

Fig. 3: Measurement plots.

Saplings, namely natural regeneration with a height of > 1.5 m to a young tree with a diameter <10 cm, were recorded in a plot size of 5 m x 5 m. Seedlings, natural regeneration from sprouts to <1.5 m high, were recorded in a plot size of 2m x 2m (Haryadi *et al.,* 2019).

Estimating peat depth

The peat depth information was obtained based on the peat depth map issued by the Peatland Restoration Agency. The plot coordinates from the survey determined using GPS were then overlaid with a peat depth map to determine the peat depth in the plot observation. The peat depth map was generated from sampling measurements of the peat depth in the field. The peat depth was estimated using peat auger until the mineral soil was reached. The depth of peat was estimated from the length of the peat auger (6 m extension rods plus sampler) inserted into the mineral soil surface. When the peat depth exceeded the length of the extension rod, one meter was added to the measured depth.

Estimating biodiversity

Data of the vegetation analyses were calculated to obtain values for relative frequency, relative density, and relative dominance; they were then summed into an index of importance value (Mueller-Dombois and Ellenberg, 2016). The important value index (IVI) and its components (relative density (D_R), relative frequency (F_R), and relative dominance (Dom_R)) are shown in Eqs. 1, 2, 3, and 4, respectively.

$$D_R = \frac{ni}{N} 100\% \quad (1)$$

$$F_R = \frac{Fi}{\sum Fi} 100\% \quad (2)$$

$$Dom_R = \frac{Gi}{G} 100\% \quad (3)$$

$$IVI = D_R + F_R + Dom_R \quad (4)$$

where *ni* is the number of individuals for a species, *N* is the total number of individuals for all species in the plot, *Fi* is the frequency of a species, *Gi* is the total base area of a species, and *G* is the total base area of all species.

The density of the trees describe the forest structures from the diameter classes 0-10 cm, 10-20 cm, 20-30 cm, and above 30 cm. The diversity parameter consists of Shannon's diversity index, Simpson's diversity index, Fisher's alpha, Rarefied species richness, and Pielou's evenness; those diversity parameters were calculated using R v. 3.6.3 (R Core Team, 2020). The diversity parameter consists of Shannon's diversity index, Simpson's diversity index, Fisher's alpha index, Pielou's evenness index, and Rarefied species richness (R), provided in Eqs. 5, 6, 7, 8, and 9, respectively.

$$H' = -\sum_{i=1}^{T} pi\, lnpi \quad (5)$$

$$D = \sum_{i=1}^{T} \frac{ni(ni-1)}{N(N-1)} \quad (6)$$

$$S = \alpha ln\left(1 + \frac{N}{\alpha}\right) \quad (7)$$

$$e = \frac{H'}{\ln S} \quad (8)$$

$$R = \frac{S}{\sqrt{N}} \quad (9)$$

where *H'* is Shannon's diversity index, *D* is Simpson's diversity index, *S* is Fisher's alpha index, *e* is Pielou's evenness index, *R* is the Rarefied species richness, *pi* is the number of individuals for a species over the total number of individuals, *ni* is the number of individuals for a species, *N* is the total number of individuals, and *S* is the number of different species.

Non-metric multidimensional scaling (MDS) with the vegan package was used to analyze the response of plant species composition to peat depth (Oksanen et al., 2019). To analyze whether species composition, species richness, and species diversity were statistically different among depth categories, a multivariate permutation analysis of variance (n = 1000) was performed using the vegan package. Ordination was performed using a species matrix containing several plant species in each plot, using the default mono MDS function, which included the double-Wisconsin square root transformation and the Bray–Curtis difference index. The ordination was presented graphically using the package ggplot (Wickham, 2016), and a visual display of each plot was color-coded based on the levels of each peat depth.

Estimating carbon stock

The biomass of a live tree was estimated using the allometric equations for mixed species of Indonesian peat swamp forests using Eq. 10 (Manuri *et al.*, 2017).

$$Y = 0.088 \text{ x } \left(\left(D^2\right) \text{x } H \text{ x } WD\right)^{0.954} \quad (10)$$

where *Y* is the aboveground biomass (kg), *D* is the diameter at breast height (cm), *H* is the height (m), and *WD* is the wood density (g/cm^3).

The total aboveground tree biomass for each plot was calculated by adding up all of the estimated aboveground biomass values of each tree in the plot expressed in Mega gram (Mg). The root biomass was calculated using the allometric model using Eq. 11 (Niiyama *et al.*, 2010).

$$Y = 0.02186 \text{ x } D^{2.487} \quad (11)$$

where *Y* is the belowground biomass/roots (kg) and *D* is the diameter at breast height (cm).

Carbon pools that are not measured directly are thought to use the relationship between aboveground tree biomass and other carbon pools that have been developed from previous research. The aboveground biomasses for understorey, litter, and deadwood were estimated using the ratio to aboveground biomass from previous research in Central Kalimantan by Krisnawati *et al.* (2021). The estimated ratio value of understorey biomass, litter, and deadwood to aboveground tree biomasses were 2.4%, 1.6%, and 18.5%, respectively.

The carbon contained in the aboveground biomass was approximately 47% or Mg biomass = 0.47 Mg C (Manuri *et al.*, 2017). In contrast, those in the the roots were approximately 39% and 50% for litter and deadwood. Carbon stocks in the organic soil carbon pools (Mg C/ha) were calculated using a fixed depth method, using Eq. 12.

$$C_{peat} = BD \text{ x } h \text{ x } C \quad (12)$$

where *BD* is the peat bulk density (g/cm^3), *h* is the peat depth (cm), and *C* is the peat carbon content (%). The values of BD and carbon content of peat at the research sites were 0.14 g/cm^3 and 41.73%, respectively.

The total carbon in the peat swamp forests was estimated as the amount of carbon aboveground biomass, belowground biomass/roots, litter, deadwood, and soil. Their values were equivalent to the carbon dioxide values in the atmosphere by multiplying the carbon stocks by a factor (44/12). The depth categories, analysis of variance, and comparison of mean values were performed

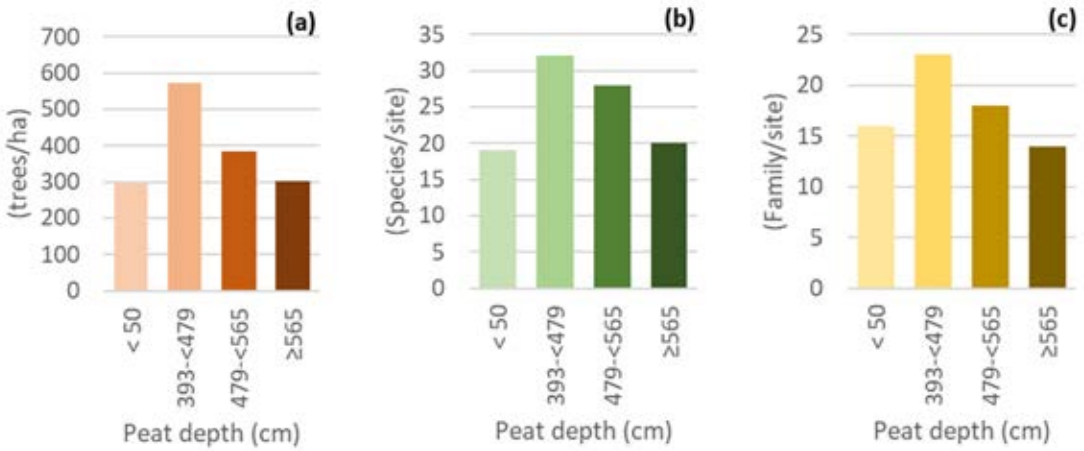

Fig. 4: Number of trees per hectare (a), species (b), and family (c) at the study sites

to determine whether the carbon stocks were statistically different.

RESULTS AND DISCUSSION

Species composition

Vegetation observations were used to identify the species and families of plants at the research sites. The identification of plant species and families at the research sites is presented in Fig. 4.

Fig. 4 shows that 23 families are in the forest with a peat depth of 393-478 cm, dominated by Lauraceae. Meanwhile, 28 families are in the forest with a peat depth of 479-564 cm and with a peat

depth 565 – 649 cm, and 19 families are in the forest with a peat depth <50. Myrtaceae dominated all peat depths. The diverse species of Lauraceae and Myrtaceae represent anthropogenic disturbance and degraded, previously burnt, peat swamp forests (Kalima *et al.,* 2020). At the research sites, the peat depths of 565-649 cm and 393-478 cm were dominated by *Combretocarpus rotundatus* (Miq.) Danser (IVI = 66.85% and 89.80%), the peat depths of 479-564 cm were dominated by *Mezzettia umbellata* Becc. (IVI = 47.78%), and the peat depths <50 cm were dominated by *Macaranga pruinosa* (Miq.) Muell. Arg. (IVI = 58.31%). The species potentially replacing future stands were sapling-level stands, and the peat depths of 565-649 cm were dominated by *Angelesia splendens* Korth. (IVI = 24.99%) and *Baccaurea polyneura* Hook.f. (IVI = 22.68%). The peat forests with 479-564 cm were dominated by *Mezzettia umbellata* Becc. (IVI = 67.23%) and *Stemonurus scorpioides* Becc. (IVI = 51.17%). Peat depths of 393-478 cm were dominated by *Combretocarpus rotundatus* (Miq.) Danser (IVI = 40.20%) and *Horsfieldia crassifolia* (Hook. Fil. and Thoms.) Warb. (IVI = 29.73%). The peat depth <50 cm was dominated by *Tetramerista glabra* Miq. (IVI = 120.19%) and *Dyera polyphylla* (Miq.) Steenis (IVI = 26.61%). These species, especially *Combretocarpus rotundatus* (miq.) Danser and anthropogenic peat swamp fragmentations such as *Callophyllum inophyllum,* indicated highly degraded forests due to forest fires (Nelson *et al.,* 2021; Astiani, 2016). The peat depth significantly affected the peat swamp forest species composition. The ordinance analysis discovered a large difference among peat depths of <50 cm, 393-<479 cm, 479-<565 cm, and ≥ 565 cm. The community composition among plots (points) became less similar because their distance increases stress by 0.15. These results are presented in Fig. 5.

Species richness, diversity, and evenness

Biodiversity plays several important roles in the biosphere and is usually measured by proxy indexes to reveal changes in ecosystems. A biodiversity index is the simplest way to describe the richness of biota and challenges ecologists to explain the diversity of an area (Kusmana and Hikmat, 2015). In its development, several indices can be used to analyze an area's biodiversity, such as the species richness, rarefied richness index, Shannon index,

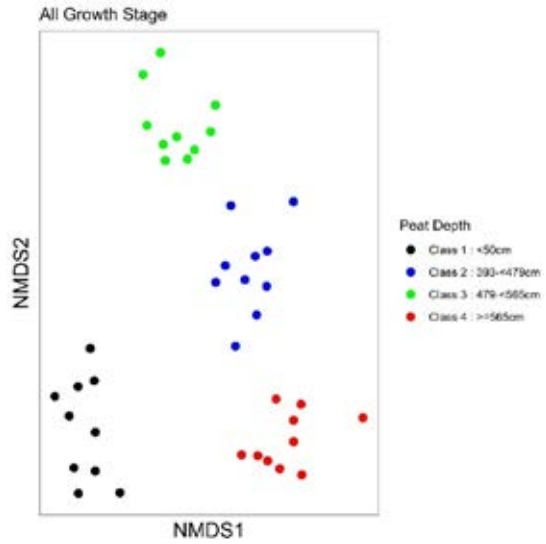

Fig. 5: The non-metric multidimensional scaling (NMDS) plot for the composition of tree species at peat depths of <50 cm, 393-<479 cm, 479-<565 cm, and ≥565 cm

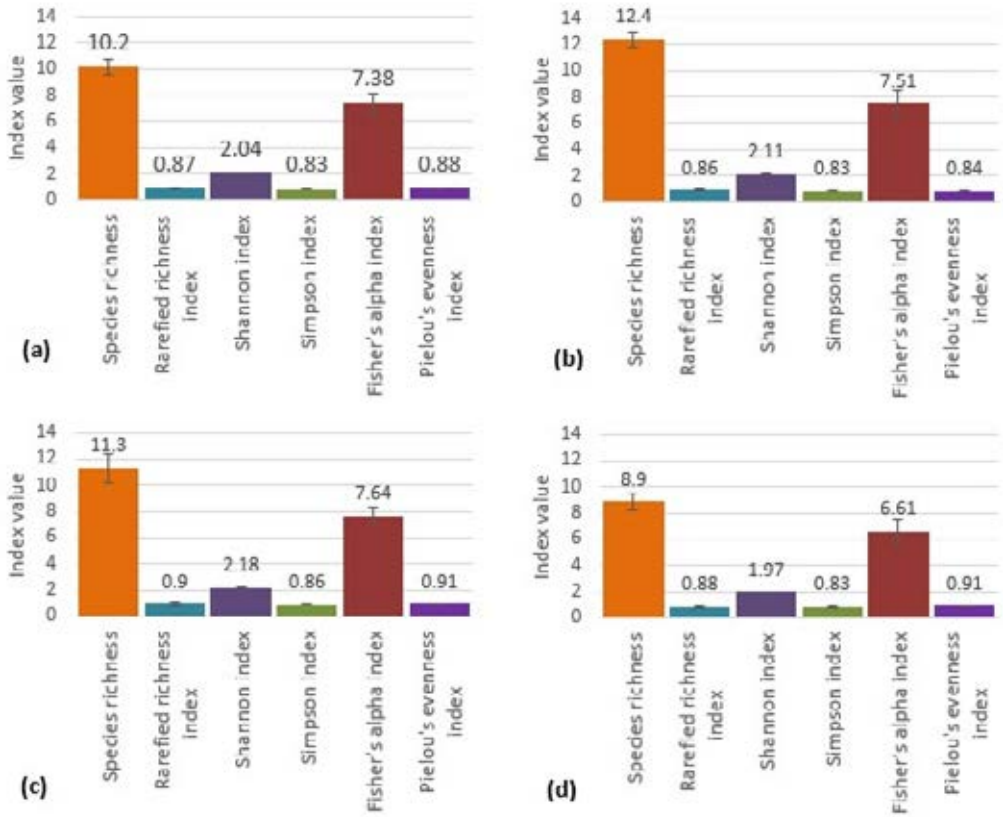

Fig. 6: Species richness, rarefied richness, Shannon index, Simpson index, Fisher's alpha, and evenness in the peat depths of <50 cm (a), 393-<479 cm (b), 479-<565 cm (c), and ≥565 cm (d) (error bars represent std. errors of means).

Table 1: F-values of multivariate diversity in different taxons and peat depths.

Diversity indexes	Species		Genus		Family	
	F-values	Pr(>F)	F-values	Pr(>F)	F-values	Pr(>F)
Species richness	3.984	0.015*	3.79	0.0185*	3.041	0.0413*
Rarefied richness index	1.358	0.271	0.477	0.7	0.465	0.709
Shannon index	1.455	0.243	0.896	0.452	0.692	0.563
Simpson index	0.91	0.446	0.132	0.94	0.106	0.956
Fisher's alpha index	0.262	0.853	0.514	0.676	0.557	0.647
Pielou's evenness index	4.517	0.00866**	2.433	0.0808	2.144	0.112

Table 2: F-values of multivariate diversity at different growth stages and peat depths.

	Trees		Sapling		Seedling	
	F-values	Pr (>F)	F-values	Pr (>F)	F-values	Pr (>F)
Species richness	8.836	0.00016***	5.04	0.00511**	2.275	0.097
Rarefied richness index	6.056	0.0019**	1.533	0.223	4.82	0.00651**
Shannon index	8.325	0.000246***	4.388	0.00989**	2.578	0.0692
Simpson index	5.407	0.00356**	3.452	0.0264*	3.325	0.0307*
Fisher's alpha index	1	0.404	0.667	0.578	1.568	0.214
Pielou's evenness index	6.884	0.000879***	0.473	0.703	0.957	0.425

Table 3: Nutrient availabilities at various peat depths.

No.	Peat depths (cm)	Distance from rivers (m)	Nutrient availability					Ash content (%)
			Mg	Ca	K	P	C-organic	
			mg/100 g	mg/100 g	mg/100 g	mg/100 g	(%)	
1	<50	< 200	5.13	9.60	6.01	1.83	41.15	20.91
2	393 - 478	2800 - 3000	1.68	0.39	0.14	0.33	51.37	1.26
3	479 – 564	400 - 600	1.65	0.50	0.15	0.34	51.52	1.00
4	565 – 649	1000 - 1600	1.86	0.62	0.15	0.35	51.61	0.80

Simpson index, Fisher's alpha index, and Pielou's evenness index. The biota diversity at the research sites is presented in Fig. 6.

Generally, Fig. 6 and further variant analyses discovered that peat depths had significantly different species richness index, and the Pielou's evenness index was significantly different (Table 1). Vegetation diversity at the tree, sapling, and seedling levels of the peat depths was significantly different (Table 2). This difference showed that the peat depths of various nutrient contents and distances from the river (Table 3) influenced the diversity of vegetation at the tree, sapling, and seedling levels, and that condition makes vegetation more adaptable (Minayeva *et al.,* 2017). The distance from the river affects the role of hydrology,

which is related to the flow of water to peatlands. In this study, the furthest distance of a plot from the river was 3000 m, and still, it obtained water flow from the river. Pages *et al.* (1999) stated that the peat gradient in a peatland distance from the river < 5500 m in the Sebangau Peatland Forest, Central Kalimantan, still allows the flow of water from the river to the peatland to run well. The water supply from this river carries the river's alluvial soil deposits along with seeds that allow various types of plants to grow so that it increases vegetation diversity, the growth of biomass, and carbon stock (Aravind *et al.*, 2015). The continuity in the water flow allows the thickness of the peat as well as the peat mass to be maintained properly. The relationship between hydrology, vegetation composition, and peat depth is closely related to restoration efforts. The study by Schulte *et al.* (2019) reinforced the assumption that, the wetter the peat, the deeper the peat thickness. In addition, during the rainy season, peatland also receives river floodwater containing dissolved nutrient components. The nutrient content provides nutrient inputs for vegetation development from seedling to the tree levels. This condition agrees with the results of the research by Astiani *et al.* (2016), stating that various responses to the local gradients in hydrology, nutrient availability, and peat depths affect vegetation changes. This evidence strengthens the research results of Page *et al.* (1999), confirming that peat thickness could not directly affect the vegetation dynamic. The vegetation changes were influenced directly by changing other characteristics of peat hydrology, peat chemistry, and peat organic matter (Morton and Heinemeyer, 2019). The research sites have various nutrient availabilities according to the peat depths, as shown in Table 3.

The decreasing contents of Mg, Ca, K, and P at deeper peat depths are associated with alluvial mineral soil deposits from the river. A peat depth < 50 m has a river distance of < 200 meters, and a mixture of many alluvial soils at the peat depth is assumed as the ash content is higher. The peat depth < 50 cm has an ash content of 20.91%, declining to 0.80% at a depth of 565 – 649 cm. In contrast, the smaller the ash content, the higher the organic C in the deeper peat depth. This fact is in line with the findings of Page *et al.* (1999) in the Sebangau Peatland Forest, where the contents of Mg, Ca, K, and P decreases with deeper peat depths.

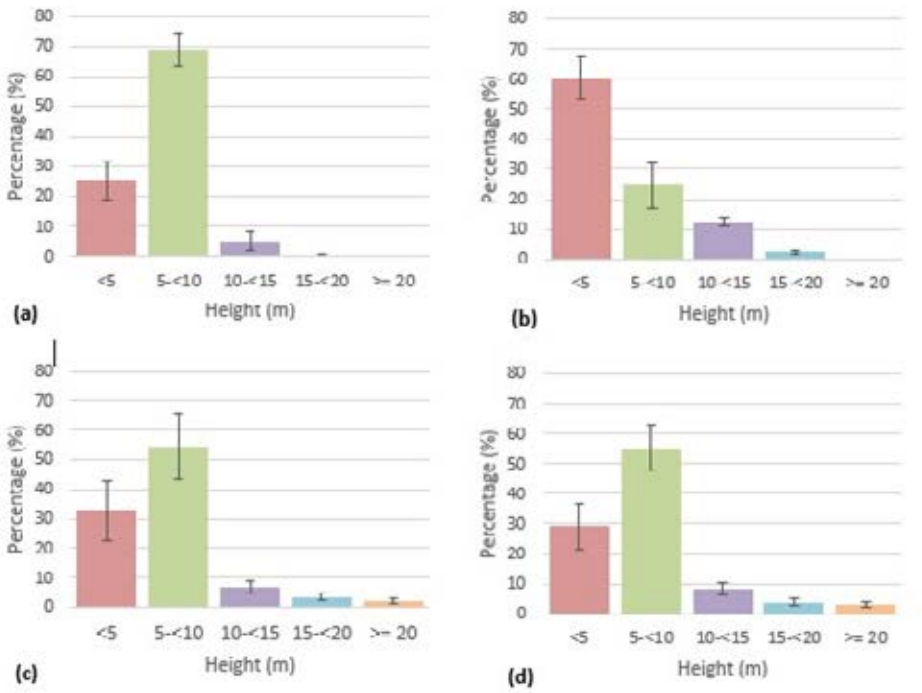

Fig. 7: Height distributions of stands at peat depths of <50 cm (a), 393-<479 cm (b), 479-<565 cm (c), and ≥565 cm (d) (error bars represent std. errors of means).

Stand structure and regeneration

Forest stand structures constitute the distribution of individual plants in the crown layer and can be illustrated as the tree distribution in each area with various diameters (Laumonier *et al.,* 2010). The canopy structure and vertical distribution are significant components of the dynamics of a forest ecosystem and appropriate habitat. Various vegetation structures indicate that they are interdependent with peat thickness and related to the physical, chemical, and hydrological properties of peat conditions. Fig. 7 shows the distribution of the vegetation canopy height at several peat depths.

The dominant species were *Combretocarpus rotundatus, Cratoxylum glaucum, Syzygium* spp., *Tristaniopsis* sp., and *Calophyllum* sp, as shown

Table 4: Dominant trees by height at the research sites

	Peat depth and tree species			
Tree height (m)	Peat depth 565-649 cm	Peat depth 479-564 cm	Peat depth 393-478 cm	Peat depth <50 cm
>20	*Combretocarpus rotundatus* *Syzygium zeylanicum*	*Callophillum sclerophyllum* *Mezzetia umbellate*	*Shorea teysmanniana* *Horsfieldia crassifolia*	--
>15	*Horsfieldia irya*/kumpang *Syzygium zeylanicum*	*Mezzetia umbellate* *Diospyros borneensis*	*Shorea teysmanniana* *Combretocarpus rotundatus*	*Combretocarpus rotundatus* *Syzygium zeylanicum*
>10	*Calophyllum sclerophyllum* *Lithocarpus dasystachyus*	*Shorea teysmanniana* *Gonystylus bancanus*	*Campnosperma coriaceum* *Cratoxylum glaucum*	*Cratoxylum glaucum* *Maclurodendron porter*
<10	*Combretocarpus rotundatus* *Litsea* sp.	*Dyera polyphylla* *Gonystylus bancanus*	*Garcinia bancana* *Combretocarpus rotundatus*	*Tetramerista glabra* *Macaranga pruinosa*

Table 5: Dominant trees by diameter at the research sites

	Peat depth and tree species			
Diameter class (cm)	Peat depth 565-649 cm	Peat depth 479-564 cm	Peat depth 393-478 cm	Peat depth <50 cm
10-19	*Combretocarpus rotundatus* *Xylopia fusca*	*Mezzetia umbellate* *Stemonurus scorpioides*	*Combretocarpus rotundatus* *Cratoxylum glaucum*	*Macaranga pruinosa* *Tetramerista glabra*
20-29	*Callophillum sclerophyllum* *Baccaurea polyneura* Hook.f.	*Mezzetia 5mbellate* *Gonystylus bancanus*	*Cratoxylum glaucum* *Combretocarpus rotundatus*	*Macaranga pruinosa* *Melaleuca leucadendra*
30-39	*Syzygium zeylanicum* *Litsea* sp.	*Mezzetia umbellate* *Callophillum sclerophyllum*	*Combretocarpus rotundatus* *Cratoxylum glaucum*	*Combretocarpus rotundatus* *Eugenia paludosa*
40-49	*Combretocarpus rotundatus* *Shorea smithiana*	*Combretocarpus rotundatus* *Horsfieldia crassifolia*	*Shorea teysmanniana* *Maclurodendron umbellate*	*Dyera polyphylla*
≥50	*Combretocarpus rotundatus* *Litsea* sp.	*Combretocarpus rotundatus* *Callophillum sclerophyllum*	*Garcinia bancanus*	--

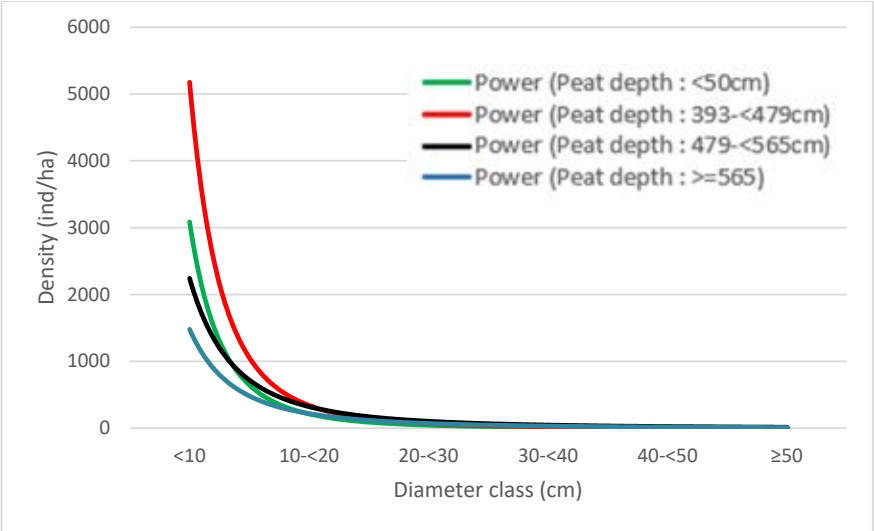

Fig. 8: Diameter distributions of stands at the peat depths of <50 cm, 393-<479 cm, 479-<565 cm, and ≥565 cm

in Tables 4 and 5. The presence of those species show that the studied area is a disturbed/degraded peat swamp forest (Graham and Page, 2014). The presence of Shorea, Eugenia, Calophyllum, Tetramerista, Gonystylus, and Diospyros indicated that the forest in this area is a mixed peat swamp forest. The pioneer species in the studied area are native species. Therefore, they can be used to restore degraded peat swamp forests, such as *Shorea teysmannia*. The density distribution according to diameter could describe the vegetation structures, as shown in Fig. 8. The distribution of diameters also showed whether the forest regeneration process was running normally or disturbed because the trees had different abilities in utilizing solar energy, nutrients, minerals, and water as well as in natural competition. Consequently, the trees in the forest stand had various diameters and the forest stand structures at the study location were generally dominated by *Combretocarpus rotundatus* and *Mezzetia umbellate*.

In natural forests, the small diameter class is more dominant than the large diameter class. Species such as *Combretocarpus rotundatus* and *Mezzetia umbellate* have a wide and dominant distribution until the peat depth of 649 cm. Similarly, the *Combretocarpus rotundatus* species is the dominant species in Central and East Kalimantan and in West Kalimantan in peatlands after fires; thus, this species can be used to enrich, rehabilitate, and restore peatlands. *Combretocarpus rotundatus* species can grow in peat depths of up to 10 m and is the main species that grows on the peat swamplands of Kalimantan (Qirom and Lestari, 2016). Regeneration is an organism's mechanism for maintaining and continuing its presence, and forest stands are reflected by complete profiles of individuals along with a gradient of diameters from seedlings to trees, with the largest diameter. The dominant species of complete plant regeneration, presented in each stratum of trees, saplings, and seedlings, are presented in Table 6.

The species present are strongly affected by their place of growth, including peat depths. Table 6 shows different types of plants at each peat depth and their regeneration. The tree species *Combretocarpus rotundatus* (Miq.) Danser, *Maclurodendron porteri* (Hook. f.) T.G. Hartley, *Tetramestra glabra* Miq, and *Horsfieldia irya* (Gaertn.) Warb. had high survival rates and growth in a peat depth of <50 cm.

Biomass and carbon stock

Important carbon pools of forest ecosystems include biomass, dead organic matter, and soil organic matter. A credible approach to calculating changes in biomass and carbon stock is to consider all relevant carbon pools, including AGB, BGB (roots), DOM (deadwood), litter, and soil (Lepotin

Table 6: Tree species with complete regeneration at the research sites.

Location/sites	Botanical names	Family	IVI (%)		
			Seedlings	Saplings	Trees
Peat depths of 565-649 cm					
1	*Horsfieldia sp*.	Myristicaceae	6.28	32.96	13.94
2	*Horsfieldia irya* (Gaertn.) Warb.	Myristicaceae	15.44	12.34	33.06
3	*Syzygium zeylanicum* (L.) DC.	Myrtaceae	10.56	10.65	10.83
Peat depth 479-564 cm					
1	*Syzygium zeylanicum* (L.) DC.	Myrtaceae	31.42	14.98	2.29
Peat depth 393-478 cm					
1	*Garcinia bancana* (Miq.) Miq./Manggis Hutan	Clusiaceae	14.15	11.69	10.51
2	*Horsfieldia crassifolia* (Hook. fil. and Thoms.) Warb.	Myristicaceae	8.34	29.73	20.15
3	*Campnosperma coriaceum* (Jack) Hallier f.	Anacardiaceae	3.54	8.92	21.83
Peat depth <50 cm					
1	*Combretocarpus rotundatus* (Miq.) Danser	Anisophylleaceae	8.76	24.99	41.03
2	*Maclurodendron porteri* (Hook. f.) T.G. Hartley	Rutaceae	12.76	18.58	39.60
3	*Tetramerista glabra* Miq.	Tetrameristaceae	23.94	120.19	37.84

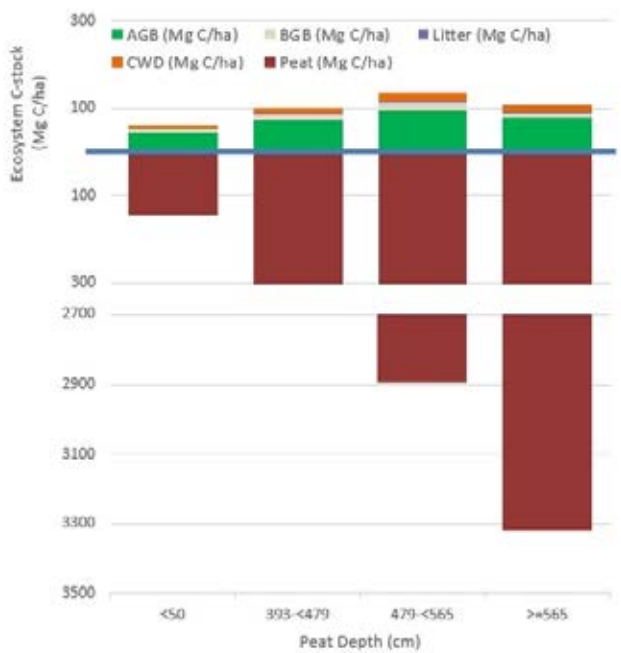

Fig. 9: Profiles of ecosystems of carbon stock at different peat depths.

Table 7: Carbon stock (Mg C/ha) in each carbon pool at different peat depths.

Peat Depth (cm)	AGB (Mg C/ha)	BGB (Mg C/ha)	Litter (Mg C/ha)	CWD (Mg C/ha)	Peat (Mg C/ha)
<50	42.4±7.05	9.8±1.78	0.7±0.12	8.2±1.35	146.1±0
393-<479	73.7±7.93	12.3±1.45	1.2±0.13	14.2±1.52	2642.4±19.78
479-<565	95.2±19.52	19±5.74	1.6±0.32	18.3±3.75	2894.2±2.49
>=565	79.2±17.41	10±2.18	1.3±0.29	15.2±3.35	3317.8±11.03

*Values in means, ± se

et al., 2019). The carbon stock profiles at various peat depths of the research sites are presented in Fig. 9. The contributions to the carbon pools from peat include the peat swamp forests' carbon stock, 71-97%; that from AGB, 2-20%; and those from the roots, litter, and deadwood, the remainder. Roots and deadwood significantly contributed to shallow peat (<50 cm), by 4-5%. In general, the carbon stock in peats and at peat depths increased, and this condition impacted the diversity of carbon pools contributing to the carbon stock ecosystems. Novita *et al.* (2020) investigated peat swamp forests in Tanjung Putting, Central Kalimantan, and found the C stock total to be 1038 Mg C/ha at the Pesalat site (peat depth = 155 cm) and 2502 Mg C/ha in Beguruh (peat depth = 290 cm). The average amount of carbon stock in each carbon pool at various peat depths in KHG Kahayan, Sebangau, is presented in Table 7.

The highest carbon stock in the AGB carbon pool was found at a peat depth of 479-<565 cm (95.2 ± 19.52 Mg C/ha). In contrast, the smallest was found at a peat depth of <50cm (42.4 ± 7.05 Mg C /ha). However, the one-way ANOVA analysis showed that peat depths did not significantly affect the carbon stock in the AGB carbon pool ($F\text{-}_{value}$ = 2.4498, $P\text{-}_{value}$ = 0.0793). The amount of carbon stock in AGB was influenced by the basal area of the stands that make up the ecosystems and had a basal area ranging from 18.6 to 32 m^2/ha. This study found that the carbon stock estimation of the AGB carbon pool was slightly lower than that of Krisnawati *et al.* (2021), who investigated the same KHG location. Krisnawati *et al.* (2021) reported that the carbon stock of the AGB carbon pool in primary peat swamp forests in Tumbang Nusa was 105.5-125.7 Mg C/ha. Meanwhile, the secondary forest was affected by the frequency of fires and logging, and the secondary length of undisturbed forests was 79.9-126.9 Mg C/ha. The carbon stocks in other carbon pools, besides peats, insignificantly contribute to the carbon stock ecosystem. The belowground biomass/roots carbon pools have the highest carbon stocks, 19±5.74 Mg C/ha, at a peat depth of 479-<565 cm. The carbon pools for litter and CWD were 1.6±0.32 Mg C/ha and 18.3±3.75 Mg C/ha, respectively. Generally, the smallest carbon stock was found in thin peat depths <50cm. Relatively deep peat with a high concentration of C produced a high soil carbon stock, while shallow peat depths with a lower concentration of C produced a lower soil carbon stock of C. This finding shows the importance of considering peat depths and utilizing peat swamp forests. Deeper peats produced higher carbon stocks. The risk of exploitation occurred because carbon stocks were potentially released. A peat dome is a critical area that must be protected because it has the largest carbon stock, and this study found more than 3000 Mg C ha^{-1} in these areas.

Connection between vegetation diversity, carbon stock, and peat depth

The deeper the peat, the greater the diversity of vegetation and carbon stock. Deeper peats make peat vegetation grow optimally because those plants will have greater adaptation. Shallow peat is dominated by shrubs so the vegetation is less diverse and the carbon stock value is smaller. On the other hand, plants that grow optimally on deeper peats produce higher carbon stock values than shallow peat. The connection between vegetation diversity, carbon stock, and peat depth assessed through Pearson correlation values between those parameters is shown in Table 8. All correlation values between peat depth, vegetation diversity, and carbon stock are positive with each other. This shows that peat

Table 8: Pearson correlation values between peat depth, vegetation diversity, and carbon stock.

Parameter	Depth (cm)	Car-bon stock (Mg C/ha)	Species richness	Shannon index	Simpson index	Rarefied richness index	Fisher's alpha index	Pielou's evenness index
Depth (cm)	1	0.994**	0.449**	0.424**	0.372*	0.332*	0.084	0.127
Carbon stock (Mg C/ha)		1	0.485**	0.451**	0.390*	0.339*	0.063	0.129
Species richness			1	0.915**	0.763**	0.662**	0.037	0.437**
Shannon index				1	0.953**	0.901**	0,074	0.741**
Simpson index					1	0.975**	0.121	0.846**
Rarefied richness index						1	0.237	0.907**
Fisher's alpha index							1	0.223
Pielou's evenness index								1

* Correlation is significant at the 0.05 level (two-tailed).
** Correlation is significant at the 0.01 level (two-tailed).

depth, vegetation diversity, and carbon stock are interdependent and connected to one another. In this study, a peat depth that is maintained properly is one of the ecological characteristics that has an important role in ensuring the sustainability of biodiversity as well as carbon stock. In maintaining peatland forests in good condition, protecting and conserving carbon stock and its ecosystem structure, including biodiversity and peat depth conditions, is necessary. This is confirmed by the results of research by Kareksela *et al.* (2015), which states that the recovery of conditions for increasing carbon stock/sequestration and ecosystem structure is very necessary in order to support restoration activities.

Implications for conservation

The landscape of peat swamp forests is fragile. The slightest disturbance in vegetation and hydrology can have an adverse effect (Anshari, 2021). The peat swamp forest ecosystem is currently facing threats from forest exploitation and use for cultivation. The exploitation and conversion of peat swamp forests can increase carbon emissions into the atmosphere. Therefore, carefully utilizing peat swamps, for example, to develop food estates extensively, is necessary. Besides preventing recurring peat swamp fires and avoiding bigger disasters, the Indonesian government has set a moratorium on peat swamp forest exploitation and designated peat swamp forests as protected areas. Moreover, the government has issued various regulations to improve peat governance through the implementation of rewetting, revegetation, revitalization of local livelihoods, and institutional strengthening to achieve peatland sustainability (Yuwati *et al.*, 2021). This study shows that the Kahayan-Sebangau landscape has secondary peat swamp forest vegetation that also need to be regulated before sustainability can be achieved. Of the four observation plots at different peat depths, some areas still have good vegetation and need to be maintained as protected areas, especially

peats with depths of four and six meters. A heavily degraded area is indicated by low species diversity due to frequent fires or intensive use and can be rehabilitated. Peatlands can be rehabilitated by revegetating or replanting, conducting silviculture, creating agroforestry, enriching species, rewetting, and building dams in fire-prone areas (Yuwati *et al.,* 2021), whereas heavily degraded peatlands must be restored. The alternative is to rehabilitate degraded shallow peatlands and to develop productive agricultural cultivation through recommended paludiculture techniques (Triadi, 2020). In selecting the species, the dominant species around the area or local species with a high index value must be considered to successfully grow and quickly adapt to the local environment. Using local species for peat rehabilitation and restoration can be promoted due to similar benefits, especially in biodiversity and ecosystem services (Lof *et al.,* 2019). To improve an environment's sustainability, the degraded areas of peatland need to be restored with types of vegetation that are suitable for each peat depth as well as improved hydrology condition by maintaining ground water level as height as the ground level and can store/absorb of carbon. Carbon stock can be improved by maintaining plant diversity and planting native plant species. Paludiculture is an alternative solution for sustainable peatland management. The types of species that are suitable for peatland can be seen in areas that have not been degraded. To maintain these areas, especially medium peat depth and peat dome areas, they need to be protected. Restoring heavily damaged peat can maintain and save biodiversity, reduce emissions, increase carbon sequestration, and improve people's living standards.

CONCLUSION

The diverse vegetation at the tree, sapling, and seedling levels and the species richness of the peat depths were significantly different due to the various nutrient contents and distances from the river. This study revealed several species with various peat depths: 20 species with a peat depth of 565 cm, 28 species with 479-<565 cm, 32 species with 393-<479 cm, and 19 species with <50 cm. The tree species *Combretocarpus rotundatus* (Miq.) Danser, *Maclurodendron porteri* (Hook. f.) T.G. Hartley, *Tetramestra glabra* Miq, and *Horsfieldia irya* (Gaertn.) Warb. had high survival rates and grew at a peat depth of <50 cm. Those species could be used for rehabilitation in degraded peatland forest as pioneer species. The presence of Shorea, Eugenia, Calophyllum, Tetramerista, Gonystylus, and Diospyros indicated that the forest in a certain area was a mixed peat swamp forest. In addition, the highest carbon stock was 95.2 ±19.52 Mg C/ha, found at a peat depth of 479-564 cm and a vegetation diameter of ≥10 cm. The study results confirmed that peat thickness could not directly affect the vegetation dynamic in terms of vegetation diversity. The vegetation changes were influenced directly by changing other characteristics of peat hydrology, peat chemistry, and peat organic matter. All Pearson correlation values between peat depth, vegetation diversity, and carbon stock are positive with each other. This shows that peat depth, vegetation diversity, and carbon stock are interdependent and are connected with one another. The deeper the peat, the greater the diversity of vegetation and carbon stock. Deeper peats make peat vegetation grow optimally because those plants have higher adaptation levels. The diverse vegetation as well as carbon stock in peatland forests must be conserved to maximize the environmental services they provide humans in the future. Therefore, protecting this forest from unsustainable use, encroachment, and forest fires is necessary. The connection between vegetation diversity, carbon stock, and peat depth can be applied as indicators of whether to protect or rehabilitate peatland forests. With high diversity, high carbon stock, and deeper peatlands, protection efforts are needed. However, with low diversity, low carbon stock, and shallow peatland, rehabilitation efforts are needed.

AUTHOR CONTRIBUTIONS

R. Garsetiasih performed the conception and design. N.M. Heriyanto performed the analyze and interpreted the data, and drafting of the manuscript literature review. W.C. Adinugroho performed the analyze and interpreted the data, and drafting of the manuscript. H. Gunawan performed the literature review, analyzed and interpreted the data. I.W.S. Dharmawan performed the literature review, analyzed and interpreted the data, and preparation of the manuscript text. R. Sawitri performed analyzed and interpreted the data, and literature

review. I. Yeny performed analyzed and interpreted the data, and literature review. N. Mindawati performed literature review and interpreted the data. D. Denny performed the literature review and compiled the data.

ACKNOWLEDGEMENT

The authors would like to thank to the Head of Forest Research and Development Center, Head of Forest the Central Kalimantan Provincial Office and the Communities around the peat land ecosystem block C, Pulang Pisau District.

CONFLICT OF INTEREST

The authors declare no potential conflict of interest regarding the publication of this work. In addition, the ethical issues including plagiarism, informed consent, misconduct, data fabrication and, or falsification, double publication and, or submission, and redundancy have been completely witnessed by the authors.

ABBREVIATIONS

%	Percent
AGB	Above Ground Biomass
BD	Bulk Density
BGB	Below Ground Biomass
C	Carbon
Ca	Calsium
cm	centimeter
CO_2	Carbondioxide
CWD	Coarse Woody Debris
D	Diameter at breast height
D	Simpson's diversity index
DOM	Dead Organic Matter
e	Pielou's evenness index
eq	equivalent
Fi	frequency of a species
Fig.	Figure
Gi	total base area of a species and *G* is total base area of all species
g	gram
g/cm^3	gram per centimeter cubic
GPS	Global Positioning System
Gt	Giga ton
H'	Shannon's diversity index
H	Height
HPH	Hak Pengusahaan Hutan (Concessionaries)
IVI	Important Value Index
K	Kalium
KHG (PHU)	Kawasan Hidrologi Gambut (Peat Hidrology Unit)
kg	kilogram
km^2	kilometer square
m	meter
Mg	Mega gram
Mg	Magnesium
Mg C/ha	Mega gram Carbon per hectare
N	total number of individuals of all species in the plot
ni	number of individuals of a species

P	Phosporus
pi	number of individuals of a species over total number of individuals
PLG	Proyek Lahan Gambut (Peatland Project)
R	Rarefied species richness
S	Fisher's alpha index
WD	Wood Density
Y	Above-ground/below-ground biomass

REFERENCES

Afrianto, W.F.; Hikmat A.; Widyatmoko, D., (2016). Florist and succession community vegetation after the 2010 eruption at Mount Merapi, Central Java. J. Indonesian Biol., 12(2):265-276 **(12 pages).**

Afzanizam, M.M.; Philip, E.; Shahrul, A.B.; Haniff, H.M., (2019). Biomass and carbon stock assessment of peat swamp forest ecosystem: a case study in permanent forest reserve Pekan Pahang, Malaysia. Int. Res. J. Eng. Technol., 6(1): 21-31 **(11 pages).**

Anshari, G., (2021). Circularity and singularity of tropical peat swamp forest ecosystems, in: Osaki, M., Tsuji, N., Foead, N., Rieley, J. (Eds). Tropical peatland eco-management. Springer, Singapore.

Aravind, J.; Kanmani, P.; Sudha, G.; Balan, R., (2016). Optimization of chromium (VI) biosorption using gooseberry seeds by response surface methodology. Global J. Environ. Sci. Manage., 2 (1); 61-68 **(8 Pages)**.

Astiani, D., (2016). Tropical peat swamp tree-species diversity altered by forest degradation. Biodivers. J., 17(1): 102-109 **(8 pages).**

Dargie, G.C.; Lewis, S.L.; Lawson, I.T.; Mitchard, E.T.A.; Page, S.E.; Bocko, Y.E.; Ifo, S.A., (2017). Age, extent and carbon storage of the Central Congo Basin peat swamp complex. Nature, 542: 86–90 **(5 pages).**

Dohong, A.; Aziz, A.A.; Dargush, P., (2017). A review of the drivers of tropical peat swamp degradation in South - East Asia. Land Use Policy. 69: 349-360 **(12 pages).**

Dommain, R.; Cobb, A.R.; Joosten, H.; Glaser, P.H.; Chua, A.F.L.; Gandois, L.; Kai, F.M.; Noren, A., Salim, K.A.; N. Salihah, H.; Su'ut, N.S.H.; Charles, F.; Harvey, C.F., (2015). Forest dynamics and tip-up pools drive pulses of high carbon accumulation rates in a tropical peat dome in Borneo (Southeast Asia). J. Geophys. Res. Biogeosci., 120: 617–640 **(24 pages).**

Fenner, N.; Freeman, C., (2011). Drought-induced carbon loss in peatlands. Nat. Geosci., 4: 895–900 **(6 pages).**

Graham, L.L.B.; Page, S.E., (2014). Forest restoration in degraded tropical peat swamp forest, in: Bossano, M., Jalonene, R., Boshier, D., Gallo, L., Cavers, S., Bordacs, S., Smith, P., Loo, J. (Eds)., The State of the world's forest genetic resources – thematic study: genetic considerations in ecosystem restoration using native tree species. FAO, Rome.

Harrison, M. E.; Ottay, J. B.; D,Arcy, L. J.; Cheyne, S. M.; Anggodo; Belcher, C.; Cole, L.; Dohong, A.; Ermiasi, Y.; Feldpausch, T.; Gallego-Sala, A.; Gunawan, A.; Hoing, A.; Husson, S. J.; Kulu, I. P.; Soebagio, S. M.; Mang, S.; Mercado, L.; Morrogh-Bernard, H. C.; Page, S. E.; Priyanto, R.; Capilla, B. R.; Rowland, L.; Santos, E. M.; Schreer, V.; Sudyana, I. N.; Taman, S. B. B.; Thorton, S. A.; Upton, C.; Wich, S. A.; van Veen, F. J. F., (2019). Tropical forest and peat swamp conservation in Indonesia: Challenges and directions. People nat., 2(04): 1-25 **(25 pages).**

Haryadi; Sunarto; Sugiyarto., (2019). Vegetation analysis of the secondary forest area in Cangkringan Resort, Mount Merapi National Park. Biodjati, 4(1): 50-57 **(8 pages).**

Hirano, T.; Kusin, K.; Limin, S.; Osaki, M., (2014). Carbon dioxide emissions through oxidative peat decomposition on a burnt tropical peat swamp. Glob. Change Biol., 20(2):555-565 **(11 pages).**

Hooijer, A.; Page, S.; Canadell, J.G.; Silvius, M.; Kwadijk, J.; Wösten, H.; Jauhiainen, J., (2010). Current and future CO2 emissions from drained peat swamps in Southeast Asia. Biogeosciences, 7(5): 1505–1514 **(10 pages).**

Kalima, T.; Suharti, S.; Sumarhani; Trethowan, L.A., (2020). Tree species diversity and ethnobotani of degraded peat swamp forest in Centarl Kalimantan. Reinwardtia, 19(1): 27-54 **(28 pages).**

Kareksela, S.; Haapalehto, T.; Juutinen, R.; Matilainen, R.; Tahvanainen, T.; Kotiaho, J.S., (2015). Fighting carbon loss of degraded peatlands by jump-starting ecosystem functioning with ecological restoration. Sci. Total Environ., 537:268-276 **(9 pages).**

Krisnawati H.; Adinugroho; W.C.; Imanuddin, R.; Suyoko; Weston, C.J.; Volkova, L., (2021). Carbon balance of tropical peat forests at different fire history and implications for carbon emissions, Sci. Total Environ, 779: **(9 pages).**

Kusmana, C.; Hikmat, A., (2015). Diversity of flora in Indonesia. J. Nat. Environ. Manage., 5(2): 187–198 **(12 pages).**

Lähteenoja, O.; Ruokolainen, K.; Schulman, L.; Alvarez, J., (2009a). Amazonian floodplains harbour minerotrophic and ombrotrophic peat- lands. Catena., 79(2):140–145 **(6 pages).**

Lähteenoja, O.; Ruokolainen, K.; Schulman, L.; Oinonen, M., (2009b). Amazonian peatlands: An ignored C sink and potential source, Glob. Change Biol., 15(9):2311–2320 **(10 pages).**

Laumonier, Y.; Edin, A.; Kanninen, M.; Munandar, A.W., (2010). Landscape-scale variation in the structure and biomass of the hill dipterocarp forest of Sumatra: Implications for carbon stock assessments. For. Ecol. Manage., 259(3): 505–513 **(9 pages).**

Lof, M.; Madsen, P.; Metslaid, M.; Witzell, J.; Jacobs, D.F., (2019). Restoring forests : regeneration and ecosystem fungtion for the future. New For., 50(2): 139-151 **(13 pages).**

Lepotin, J.; Kattetenborn, T.; Galleguillos, M.; Perez-QueZada, J.F.; Schmidtlein, S., (2019). Using aboveground vegetation attributes as proxes for mapping peatland belowground

carbon stocks. Remote Sens. Environ., 231(111217): 1-26 **(26 pages).**

Mansur, M.; Kartawinata, K., (2017). Phytosociology of a lower montane forest on Mt. Batulanteh, Sumbawa, Indonesia. Reinwardtia, 16(2): 77–92 **(16 pages).**

Manuri, S.; Brack, C.; Rusolono, T.; Noor'an F.; Verchot L.; Maulana, S.I.; Adinugroho, W.C.; Kurniawan, H.; Sukisno, D.W.; Kusuma, G.A.; Budiman, A.; Anggono, R.S.; Siregar, C.A.; Onrizal, Yuniati, D.; Soraya, E., (2017). Effect of species grouping and site variables on aboveground biomass models for lowland tropical forests of the Indo-Malay region. Ann. For. Sci., 74(23): 1-14 **(14 pages).**

Miettinen, J.; Liew, S.C., (2010). Degradation and development of peatlands in Peninsular Malaysia and in the islands of Sumatra and Borneo since 1990. Land Degrad. Dev. 21(3): 285-296 **(12 pages).**

Minayeva, T.; Bragg, O.; Sirin, A., (2017). Toward ecosystem based restoration of peatland biodiversity. Mires Peat., 17(01): 1-36 **(36 pages).**

Morton, P.A.; Heinemeyer, A., (2019). Bog breathing: The extent of peat shrinkage and expansion on blanket bogs in relation to water table, heather management and dominant vegetation and its implications for carbon stock assessments. Wetl. Ecol. Manag., 27(2): 467-482 **(16 pages).**

Mueller-Dombois, D.; Ellenberg, H., (2016). Vegetation ecology: Objectives and methods (translation of aims and methods of vegetation ecology by K. Kartawinata & R. Abdulhadi). LIPI Press and Yayasan Pustaka Obor, Jakarta.

Nelson, K.; Thompson, S.; Hopkinson, C.; Petrone, R.; Chasmer L., (2021). Peatland-fire interactions: A review of wildland fire feedbacks and interactions in Canadian boreal peatlands. Sci. Total Environ., 769(145212): 1-14 **(14 pages).**

Niiyama, K.; Kajimoto, T.; Matsuura, Y.; Yamashita, T.; Matsuo, N.; Yashiro, Y.; Ripin, A.; Kassim, A.R.; Noor, N.S., (2010). Estimation of Root biomass based on excavation of individual root systems in a primary dipterocarp forest in Pasoh Forest Reserve, Peninsular Malaysia. J. Trop. Ecol., 26(3): 271-284 **(14 pages).**

Novita, N.; Kauffman, J.B.; Hergoualc'h, K.; Murdiyarso, D.; Tryanto, D.H.; Jupesta, J., (2020). Carbon stocks from peat swamp forest and oil palm plantation in Central Kalimantan, Indonesia, in: Djalante, R., Jupesta, J., Aldrian E. (Eds.), Climate change research, policy and actions in Indonesia. Springer Climate. Springer, Cham.

Oksanen, J.; Blanchet, F.G.; Friendly, M.; Kindt, R.; Legendre, P.; McGlinn, D.; Minchin, P.R.; O'Hara, R.B.; Simpson, G.L.; Solymos, P.; Stevens, M.H.H.; Szoecs E.; Wagner, H., (2019). Vegan: Community ecology package. R package version 2.5-6.

Osaki, M.; Kato, T.; Takashi, K.; Hidenori, T.; Akira, H.; Kazuo,Y.; Nobuyuki, T.; Satomi, S.; Joeni, S.R.; Tika, D.A.; Ayako, O.; Kayo, M.; Rahmawati, I.W.; Sisva, S., (2021). in: Osaki, M., Tsuji, N., Foead N., Rieley J. (Eds.)., Tropical peat swamp eco-management. Basic information about tropical peat swamp ecosystems. Springer, Singapore.

Page, S.E; Rieley, J.O.; Shotyk, O.W.; Weiss, D., (1999). Interdependence of peat and vegetation in a tropical peat swamp forest. Phil. Trans. R. Soc. Lond. B., 354(1391): 1885-1897 **(13 pages).**

Posa, M.R.C.; Wijedasa, L.S.; Corlett, R.T., (2011). Biodiversity and conservation of tropical peat swamp forests. BioScience, 61(1): 49–57 **(9 pages).**

Qirom, M.A.; Lestari, N.S., (2016). Diversity of plant species at various peat depts in Kalimantan. In National Conference of Wetland. South Kalimantan, Republic of Indonesia. Lembaga Penelitian dan Pengabdian kepada Masyarakat, Universitas Lambung Mangkurat: South Kalimantan.

R Core Team, (2020). R: A language and environment for statistical computing. R Foundation for Statistical Computing, Vienna, Austria.

Rieley, J.O.; Ahmad-Shah, A.A.; Brady, M.A., (1996). The extent and nature of tropical peat swamps, in: Maltby E., Immirzi, C.P., Safford, R.J. (Eds). Tropical peatlands of Southeast Asia. International Union for Conservation of Nature.

Russell, A.E.; Raich, J.W., (2012). Rapidly growing tropical trees mobilize remarkable amounts of nitrogen, in ways that differ suprisingly among species. Proc. Natl. Acad. Sci USA, 109(26):10398-10402 **(4 pages).**

Schulte, M.L.; McLaughlin, D.L.; Wurster, F.C.; Balentine, K.; Speiran, G.K.; , Aust, W.M.; Stewart, R.D.; Varner, J.M.; Jone, C.N., (2019). Linking ecosystem function and hydrologic regime to inform restoration of a forested peatland. J. Environ. Manage., 233:342-351 **(10 pages).**

Sefidi, K.; Copenheaver, C.A.; Kakavand, M.; Behjou, F.K., (2015). Structural diversity within mature forests in Northern Iran: A case study from a relic population of persian ironwood (Parrotia persica CA Meyer). For. Sci., 61(2): 258-265 **(8 pages).**

Soil Survey Staff, (2014). Keys to soil taxonomy, 12th Edition. USDA Natural Resources Conservation Service: US.

Triadi, L.B., (2020). Restorasi lahan rawa gambut melalui metode pembasahan (sekat kanal) dan paludikultur (Restoration of peat swamp through rewetting (canal blocking) and paludiculture method). J. Sumber Daya Air., 16(2): 103-118 **(6 pages).**

Warren, M.; Hergoualc'h.; Kauffman, J.B.; Murdiyarso, D.; Kolka, R., (2017). An appraisal of Indonesia's immense peat carbon stock using national peat swamp maps: Uncertainties and potential losses from conversasion. Carbon Balance Manage., 12(12): 1-12 **(12 pages).**

Wickham, H., (2016). GGplot2: Elegant graphics for data analysis. Springer-Verlag: New York.

Yuwati, T.W.; Rachmanadi, D.; Pratiwi; Turjaman, M.; Indrajaya, Y.; Nugroho, H.Y.S.H.; Qirom, M.A.; Narendra, B.H.; Winarno, B.; Lestari, S.; *et al.,* (2021). Restoration of degraded tropical peatland in Indonesia: a review. Land. 10(11): 1-31 **(31 pages).**

AUTHOR (S) BIOSKETCHES

Garsetiasih, R., Ph.D., Professor, Forest Research and Development Center, Ministry of Environment and Forestry, Bogor, West Java, Indonesia.
- Email: *garsetiasih@yahoo.com*
- ORCID: 0000-0002-5886-0279
- Web of Science ResearcherID: 4807773
- Scopus Author ID: 57209804820
- Academic Homepage: http://puslitbanghut.or.id

Heriyanto, N.M., M.Sc., Forest Research and Development Center, Ministry of Environment and Forestry, Bogor, West Java, Indonesia.
- Email: *nurmheriyanto88@yahoo.com*
- ORCID: 0000-0002-1098-7641
- Web of Science ResearcherID: 4809758
- Scopus Author ID: NA
- Academic Homepage: http://puslitbanghut.or.id

Adinugroho, W.C., M.Sc., Forest Research and Development Center, Ministry of Environment and Forestry, Bogor, West Java, Indonesia.
- Email: *wahyuk2001@yahoo.com*
- ORCID: 0000-0003-0687-5679
- Web of Science ResearcherID: 59462020
- Scopus Author ID: 57193552889
- Academic Homepage: http://puslitbanghut.or.id

Gunawan, H., Ph.D., Professor, Forest Research and Development Center, Ministry of Environment and Forestry, Bogor, West Java, Indonesia.
- Email: *hendragunawan1964@yahoo.com*
- ORCID: 0000-0002-2855-801X
- Web of Science ResearcherID: 4807323
- Scopus Author ID: 57216983705
- Academic Homepage: http://puslitbanghut.or.id

Dharmawan, I.W.S., Ph.D., Forest Research and Development Center, Ministry of Environment and Forestry, Bogor, West Java, Indonesia.
- Email: *salifa03@yahoo.co.id*
- ORCID: 0000-0002-7007-393X
- Web of Science ResearcherID: 4807546
- Scopus Author ID: 57267722400
- Academic Homepage: http://puslitbanghut.or.id

Sawitri, R., M.Sc., Forest Research and Development Center, Ministry of Environment and Forestry, Bogor, West Java, Indonesia.
- Email: *sawitri_reny@yahoo.com*
- ORCID: 0000-0002-6080-7805
- Web of Science ResearcherID: 4809875
- Scopus Author ID: 57193732162
- Academic Homepage: http://puslitbanghut.or.id

Yeny, I., M.Sc., Forest Research and Development Center, Ministry of Environment and Forestry, Bogor, West Java, Indonesia.
- Email: *irmayeny.kemenhut@yahoo.com*
- ORCID: 0000-0002-3450-7913
- Web of Science ResearcherID: 4807972
- Scopus Author ID: 57219414393
- Academic Homepage: http://puslitbanghut.or.id

Mindawati, N., Ph.D., Professor, Forest Research and Development Center, Ministry of Environment and Forestry, Bogor, West Java, Indonesia.
- Email: *ninapulp@yahoo.co.id*
- ORCID: 0000-0001-7368-1351
- Web of Science ResearcherID: 75602021
- Scopus Author ID: 104404844009
- Academic Homepage: http://puslitbanghut.or.id

Denny, M.Sc., Forest Research and Development Center, Ministry of Environment and Forestry, Bogor, West Java, Indonesia.
- Email: *dennybppn@gmail.com*
- ORCID: 0000-0003-0800-0956
- Web of Science ResearcherID: 4809845
- Scopus Author ID: NA
- Academic Homepage: http://puslitbanghut.or.id

HOW TO CITE THIS ARTICLE

Garsetiasih, R.; Heriyanto, N.M.; Adinugroho, W.C.; Gunawan, H.; Dharmawan, I.W.S.; Sawitri, R.; Yeny, I.; Mindawati, N.; Denny., (2022). Connectivity of vegetation diversity, carbon stock, and peat depth in peatland ecosystems. Global J. Environ. Sci. Manage., 8(3): 369-388.

DOI: 10.22034/gjesm.2022.03.06

url: https://www.gjesm.net/article_247902.html

Global J. Environ. Sci. Manage. 8(3): 389-402, Summer 2022, Serial #31

Global Journal of Environmental Science and Management
(GJESM)

Homepage: https://www.gjesm.net/

ORIGINAL RESEARCH PAPER

Fuzzy entropy type II method for optimizing clean and renewable solar energy

M. Ramli[1,*], M. Mardlijah[2], M. Ikhwan[3], K. Umam[4]

[1] *Department of Mathematics, Universitas Syiah Kuala, Banda Aceh 23111, Indonesia*

[2] *Department of Mathematics, Institut Teknologi Sepuluh Nopember, Surabaya 60111, Indonesia*

[3] *Graduate School of Mathematics and Applied Sciences, Universitas Syiah Kuala, Banda Aceh 23111, Indonesia*

[4] *Department of Mathematics Education, Universitas Syiah Kuala, Banda Aceh 23111, Indonesia*

ARTICLE INFO

Article History:
Received 16 August 2021
Revised 03 November 2021
Accepted 22 December 2021

Keywords:
Altitude tracker
DC motor
Fuzzy logic control
Sliding mode control
Solar energy

ABSTRACT

BACKGROUND AND OBJECTIVES: A solar panel is a device that converts solar rays into electricity. It is a step to reduce emissions from fossil energy, which is to replace it with renewable energy. It requires a control system to ensure that the position of the solar panel is always perpendicular to the sun's rays. This study aims to modify the fuzzy set based on fuzzy entropy in the control system that has been developed. The modifications made are expected to increase the efficiency of solar panels in harvesting energy.

METHODS: Type II fuzzy sliding mode control is used, along with a modified fuzzy set based on the entropy value. Before modification, the system containing the fuzzy set generates a histogram of entropy and voltage performance, which is the initial value and the comparison value. The algorithm alters the footprint of the uncertainty limit. This change results in a new fuzzy set, which results in a new histogram and voltage. The final step is to compare the initial and final parameters based on the results of the modifications.

FINDINGS: The solar panels require only 7.3x10-5 degrees of movement per second. This is a very slow movement for a dc motor with a maximum voltage of 12 volts. The simulation produced a stable speed of 7.297x10-5 on the unmodified system and 7.295x10-5 on the modified system. The modified system experiences a slight delay towards the stable point because the fuzzy entropy method reduces the dominance of set point positions in the system.

CONCLUSION: The modified fuzzy set is good at controlling the solar panel driving motor based on the output voltage value. On both controllers under consideration, the voltages follow the same pattern. However, it experienced a control mismatch at the point towards the set point. Finally, by changing the foot of uncertainty and adjusting it proportionally according to control needs, the control system based on fuzzy sets with fuzzy entropy can be further developed.

DOI: 10.22034/gjesm.2022.03.07

NUMBER OF REFERENCES	NUMBER OF FIGURES	NUMBER OF TABLES
35	7	2

*Corresponding Author:
Email: *marwan.math@unsyiah.ac.id*
Phone: +62 813-9766-8376
ORCID: 0000-0003-1225-9063

Note: Discussion period for this manuscript open until October 1, 2022 on GJESM website at the "Show Article".

INTRODUCTION

Renewable energy-based power generation has the potential to reduce greenhouse gas emissions. Subsidizing the tariffs imposed on renewable energy can encourage energy generation, which leads to job creation through renewable energy generation. Renewable energy sources are very promising in Nigeria, Cameroon, Ghana, and South Africa, but government interest and policies are still low (Ibrahim *et al.,* 2021; Akinbami *et al.,* 2021). Governments in the former Soviet bloc play an active role in their renewable energy policies, including revising existing market-based instruments by imposing feed-in tariffs and offering tax incentives for renewable energy projects (Karatayev *et al.,* 2021). The use of renewable energy has become a separate issue in some countries, namely the rise in electricity costs. In Guatemala, more than a third of urban housing could see an increase in monthly energy expenditure (Henry *et al.,* 2021). The Indonesian government's goal is to increase the use of renewable energy in the National Energy Mix by 23% by 2025. This statement is found in Government Regulation No. 79 of 2014, which relates to National Energy Policy. Indonesia is expected to be able to use 31% renewable energy by 2050 (Rahman *et al.,* 2021). Solar energy is one type of renewable energy that is readily available in Indonesia. Indonesia's geographical location at the equator is one of the factors assisting in meeting the country's renewable energy targets. In Indonesia, the average intensity of solar radiation is quite high, around 4.8 kWh/m^2 per day (Ikhwan *et al.,* 2019). The development of solar energy harvesting technology has resulted in a reduction in carbon dioxide emissions. The operation of the Mohammed bin Rashid Al Maktoum Solar Park in Dubai has saved 6.5 million tonnes of carbon dioxide equivalent, and this plant is expected to rise once all phases are completed and operational (Obaideen *et al.*, 2021). The control system on the solar panel drive system is being researched to ensure that the angle of the solar panel is facing the direction of the sun's rays. Many active and passive methods have been tried, but there is still a significant gap in the accuracy of the solar panel angle. The angle of incidence of sunlight on a sun tracker is known to be nearly equal to the active method (Sharma and Rohilla, 2021). This accuracy is affected by the light dependent resistor light sensor on the solar panel (Stefenon *et al.*, 2020). The passive drive system relies on the hypothesis that is built, so the set point approach is considered the most appropriate way to determine tracking accuracy. A fairly good approach at the set point can increase the amount of energy absorbed from solar radiation by 35.91% to 45.45% from systems that do not have controllers (Ayamolowo *et al.*, 2021). The application of a modified fuzzy system with a sliding surface yielded a very small error value (Ghiasi *et al.*, 2017). The addition of entropy value to fuzzy sets is a novel development in the production of control systems. The updated control system considers the difference in light intensity obtained as well as the timeliness of the setting. The system automatically returns the solar panel's position to face the sun. The energy absorbed by the solar panel can be maximized by keeping the angle facing the solar panel. This system can be used in other units that require precise sun positioning, such as navigation and location. Solar panels, which are currently being mass-produced, are used in the solar energy harvesting process. The solar tracking system ensures that the solar panels receive sunlight. Another study was successful in comparing proportional, integral and derivative (PID) and Type II fuzzy sliding mode control (T2FSMC) and producing data on the angular position of the motor based on constant angular speed (Mardlijah *et al.,* 2017). T2FSMC has many advantages, including good control performance with a wide range of parameters and a faster response time (Hamzaoui and Al-Khazraji, 2011). T2FSMC was implemented on a one-axis sun tracker by Mardlijah *et al.* (2018), who used the firefly algorithm for optimization. The T2FSMC development method is proposed in this study, but it has the limitation of forming fuzzy sets (Mardlijah *et al.,* 2019). The T2FSMC method uses the fuzzy entropy type II (hereinafter referred to as fuzzy entropy) metaheuristic algorithm described by Oliva *et al.* (2019). Fuzzy entropy seeks the best value for each fuzzy set used to control solar panels. Fuzzy entropy is known as a physical concept of a vulnerability assessment model based on pattern recognition. Fuzzy entropy is clearer, and the evaluation results are reasonable and credible (Zhou *et al.,* 2022). At the Equator, a local control system was developed during the first year. Within one degree of freedom, the control system follows the direction of motion. The assumption is that the sun's motion follows an angle ranging from 0° to 180° circle

angles. Previously, research on the solar panel drive system was conducted using one axis and two axes of the sun's movement. However, there is still an angle error between the solar panel and the sun in these studies, which reduces the efficiency of solar energy absorption. This research proposes a new control system to improve the error performance between the sun's angle and the angle of the solar panel. Fuzzy Type-II Entropy Sliding Mode Control (T2FESMC) was developed. This method evolved from the FSMC and T2FSMC methods. In the previous control, the entropy value was used as an element of optimizing fuzzy sets in this study. This study is simulated at the Modeling and Simulation Laboratory, Department of Mathematics, Syiah Kuala University, Indonesia in 2021.

MATERIALS AND METHODS

The investigation begins with determining the reference angle, which is followed by the output of the control system. The control system began with SMC control and evolved into T2FSMC and T2FESMC. To determine the error value between the angle of the solar panel and the angle of the sun, simulations are run. System validation employs an integral time absolute error (ITAE) statistical measurement tool to detect and correct errors.

The reference angles

The reference angle is the angle of movement of the sun as seen from an object on the earth's surface. This angle is used as a reference to be followed by the developed control system. The reference angle is calculated using two methods: sensors and models. Because the focus of this study is on the model as a basis for control, no sensor data is required. Divide the semicircle by the amount of time the sun has moved to get the angular motion of one axis using Eqs. 1 and 2.

$$0 \le \theta \le \pi \tag{1}$$

$$\omega = \frac{\pi}{12\,\text{hours}} = 7.27 \times 10^{-5}\ \text{rad/s} \tag{2}$$

Where, θ in radians represents the sun's angle of movement and ω is the angular velocity of the reference being followed.

Fuzzy entropy

The application of fuzzy entropy type II can be seen in maximizing the entropy value for each possible fuzzy set which is formulated using Eq. 3 (Oliva et al., 2019), and Eqs. 4 and 5 (Zamri and Abdullah, 2013).

$$\max Tfe_k\left(\text{FOU}\right) = \sum_{k=1}^{nl+1} Fe_k \tag{3}$$

Where;

$$Fe_k = -\sum_{i=1}^{L-1}\left(\frac{h_i * \left(\mu_k^{high}(i) - \mu_k^{low}(i)\right)}{P_k}\right) * \ln\left(\frac{h_i * \left(\mu_k^{high}(i) - \mu_k^{low}(i)\right)}{P_k}\right), \quad k = \{1,\ldots,nl+1\} \tag{4}$$

$$P_k = \sum_{i=0}^{L-1}\left(h_i * \left(\mu_k^{high}(i) - \mu_k^{low}(i)\right)\right), k = \{1,\ldots,nl\} \tag{5}$$

By maximizing the total entropy, the value of each footprint of uncertainty becomes the solution using Eq. 2.

T2FESMC

The T2FESMC system is made up of three systems: sliding mode control (SMC), type II fuzzy (T2F), and type II fuzzy entropy (T2FE). SMC has long been recognized as an excellent controller for systems with uncertain values, such as solar panel models (Kchaou *et al.*, 2017). The SMC variable for fuzzy type II has the value using Eq. 6.

$$S_p = \frac{\dot{e} + \lambda e}{\sqrt{1+\lambda^2}} \text{ and } d = \sqrt{|e|^2 - S_p^2} \tag{6}$$

The use of SMC also has a good effect on research that uses the error value e and its derivative e as a variable that determines the amount of voltage to follow the sun's reference angle (Abadi *et al.*, 2015; 2020). The values of S_p and d are then entered into fuzzy type II. Both of these variables can be measured for each driving motor and the limits used can be

Table 1: The "and" relation between S_p and d parameters

d \ S_p	NB	NM	NS	NZ	PZ	PS	PM	NB
B	PB	PB	PB	PB	NB	NB	NB	NB
M	PB	PB	PB	PM	NM	NB	NB	NB
S	PB	PB	PM	PS	NS	NM	NB	NB
Z	PB	PM	PS	PZ	NZ	NS	NM	NB

updated for different types of DC motors. S_p and d are connected by the relation in Table 1.

Where, NB = negative big, NM = negative medium, NS = negative small, NZ = negative zero, PB = positive big, PM = positive medium, PS = positive small, PZ = positive zero. These rules are used to determine the range of membership functions S_p and d. The next step is to update the footprint value on the S_p and d variables by using entropy. Entropy is used for the optimization method described in Eq. 2. Accordingly, this method has been updated to T2FESMC which contains optimizations in it.

Simulation and validation

Simulation is carried out at one reference angle or the whole. However, in this study, the angular velocity becomes the reference because the angle followed changes with the same value every time. Any change in the angle of the sun's altitude must be followed by the pitch angle of the solar panels. The angular difference formed on the solar panel is referred to as the angular error, while the unstable angular velocity is referred to as the angular velocity error. The error value is the difference between the angle of the sun and the angle of the solar panel. Furthermore, validation is carried out using Eq. 7 (Rao *et al.,* 2020).

$$\mathrm{ITAE} = \int_{t=0}^{\infty} t\left|e(t)\right| dt \tag{7}$$

Where, ITAE is integral time absolute error, the value of *e(t)* is the difference y_i dan y, y_i is the angle of the sun and y is the external angle of the solar panel with the amount of n in the simulation time span *t*. If the ITAE value is very small, then the control system has succeeded in following the sun, but on the contrary, the MAE value is large enough, then the control system is repaired again with a larger entropy value. The value of y is obtained from the following motor system using Eqs. 8 and 9 (Ikhwan *et al.,* 2018).

$$\frac{di(t)}{dt} = \frac{1}{L}\left(E(t) - Ri(t) - K_b\omega(t)\right) \tag{8}$$

$$\frac{d\omega(t)}{dt} = \frac{1}{J}\left(K_m i(t) - B_f\omega(t)\right) \tag{9}$$

Where, the parameters used in Eqs. 8 and 9 are presented in Table 2.

RESULTS AND DISCUSSION

Recent development and analysis

The development is carried out using a combination of methods that are robust against existing disturbance conditions. A fuzzy logic controller and sliding mode control system has been introduced which is claimed to have robust properties compared to high calculation methods such as predictive control models. Mardlijah *et al.,* (2017) and Mardlijah *et al.* (2018) evaluated T2FSMC with two optimization methods, namely the firefly algorithm and the bisection approach. Both of them have small error values of $9.816\text{x}10^{-5}$ and $9.805\text{x}10^{-5}$, respectively. Comparison of the two can be traced by remaking the system and simulated fairly. The system formed by the firefly algorithm is shown in Fig. 1.

Fig. 1 shows the fuzzy set used to control the solar panels. The vertical axis represents the membership function of the fuzzy set, while the horizontal axis represents the input parameter S_p in Fig.1(a), parameter *d* in Fig.1(b), and voltage output parameter *U* in Fig. 1(c). In Fig. 1(a) and (b), the outputs of SMC in the form of S_p and d are categorized as linguistic variables. The process continues by translating the previous two images into fuzzy output, namely in Fig. 1(c). The pre-set rules force two fuzzy sets for S_p and d to transform into voltage U. In this regulated system, only the variable voltage U is able to change the position of the solar panel so that it faces the

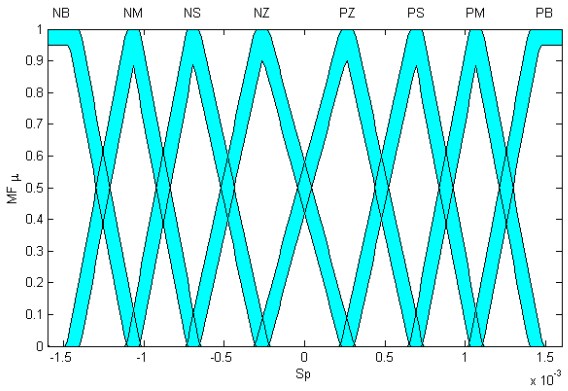

(a)

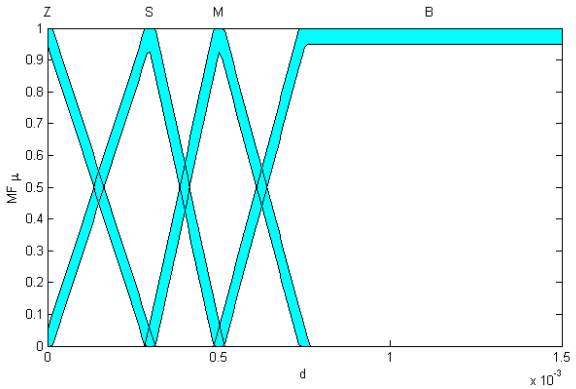

(b)

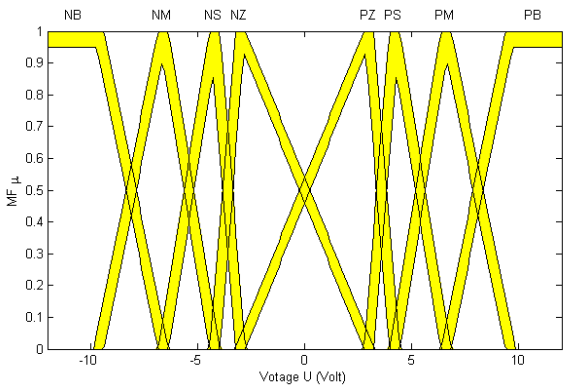

(c)

Fig. 1: T2FSMC with firefly algorithm

sun. The translation failure in Fig. 1(c) causes errors in the position and performance of the set of Fig. 1(a) and (b) must be modified again. The system formed in this control is not yet completely independent of the firefly algorithm. It is because of the effect of the gain magnifying parameter, which is set based on the smallest error value; it uses ITAE for this error value. The modified new control is the combination that produces the least ITAE. The novelty of this system is the reduction in the steady-state error value, but

the computations required are lengthy because it is dependent on the distance of the parameter range. The resulting ITAE has a minimum value of 9.816×10^{-5} degrees and follows the sun's position perfectly. This development, however, cannot be regarded as the best combination. The performance of the fuzzy combination must still be analyzed and compared to the performance of other algorithm combinations.

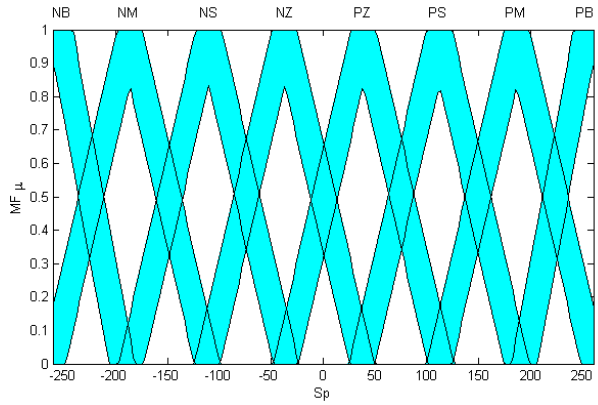

(a)

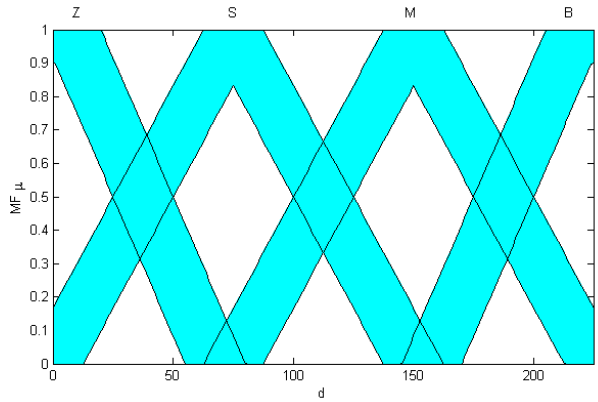

(b)

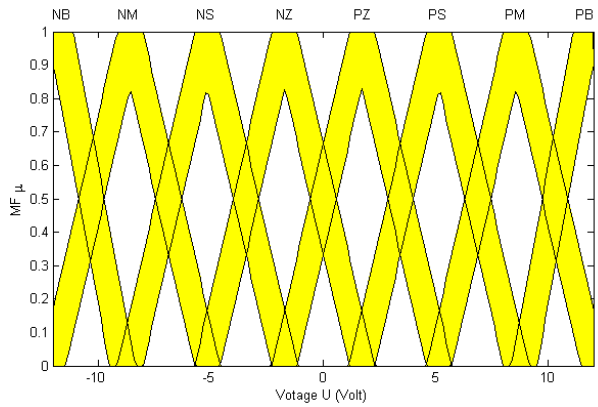

(c)

Fig. 2: T2FSMC with bisection algorithm

Fig. 2 of the article reintroduces T2FSMC with a very fair and simple algorithm.

The workings of Fig. 1 are also adopted for Fig. 2. In fuzzy set planning, the assumption used is a proportional change in the entire system. Fig. 2 is made up of a fair distribution with the area of each fuzzy set not being differentiated. This even distribution is only seen as a set that can be enlarged and shrunk as needed. Mardlijah *et al.* (2017) measured and calculated both S_p and d values in real conditions, so that the two fuzzy sets in Fig. 2(a) and Fig. 2(b) are not subject to the bisection algorithm. The voltage output to the dc motor, however, is the main focus. The solar panels require only $7.3x10^{-5}$ degrees of movement per second. This is a very slow movement for a dc motor with a maximum voltage of 12 volts. It is important to note that if the voltage value remains high, the system will be inefficient and may even cause equipment damage. Starting from the range of values [0.1], the article proposes a reduction point using a bisection algorithm. The obtained value is 0.00012, allowing the sun's position to be tracked smoothly. Furthermore, the performance analysis of the two systems that have been formed is carried out on the error values Sp, d, and U. Figs. 3 and 4 are presented with a simulation that is fair and in accordance with the output of each algorithm.

Although the ITAE value is higher in the bisection algorithm, Fig. 3 on the left is more accurate. This is compared to the highest possible value for each error. Both S_p and d have a similar shape but differ in value to an accuracy of $1x10^{-7}$. Although the method is the same, changes in the forming algorithm cause the accuracy value to change. Fig. 4 output is not significantly different from that of Fig. 3. The voltage produced by the firefly algorithm is more stable and lower in magnitude than the voltage produced by the bisection algorithm. Previous research (Mardlijah *et al.*, 2013) with a trial-and-error method resulting in a combination of fuzzy sets that direct the error value to be close to NZ and PZ is the main cause of this stable and small. That is, the other fuzzy sets have MF=0 and have no effect on the system's dynamics. This supports the results of the firefly algorithm, which show that the NZ and PZ areas are prioritized beginning with the second iteration, namely S_p and d errors.

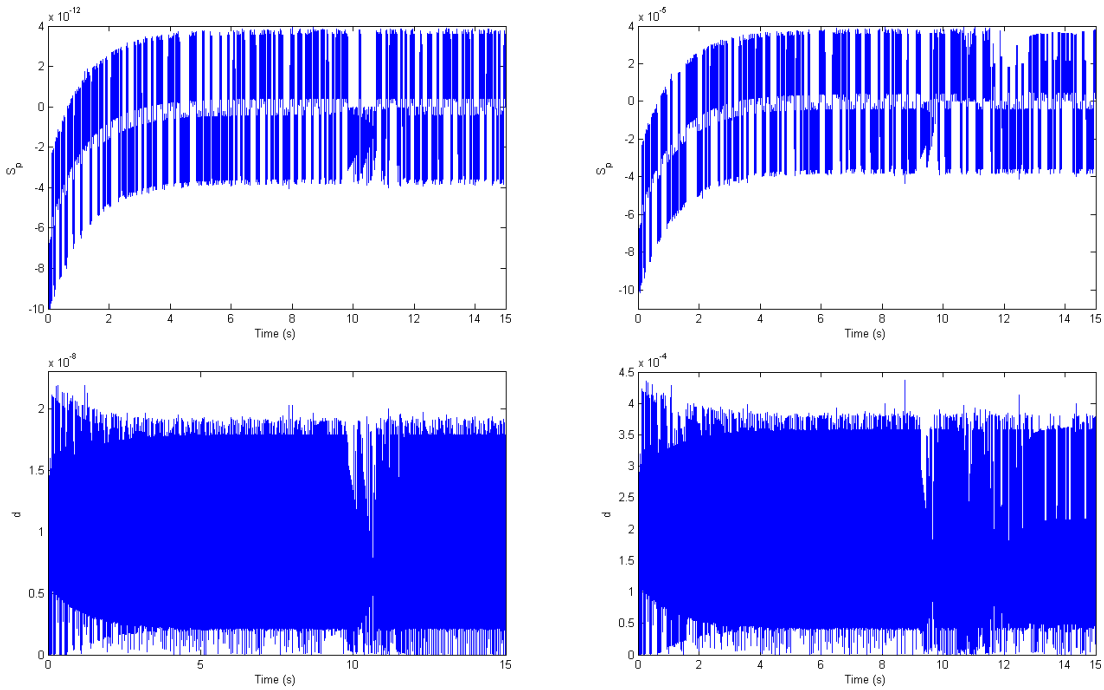

Fig. 3: S_p and d error values on T2FSMC (the firefly algorithm (left side) and the bisection algorithm (right side))

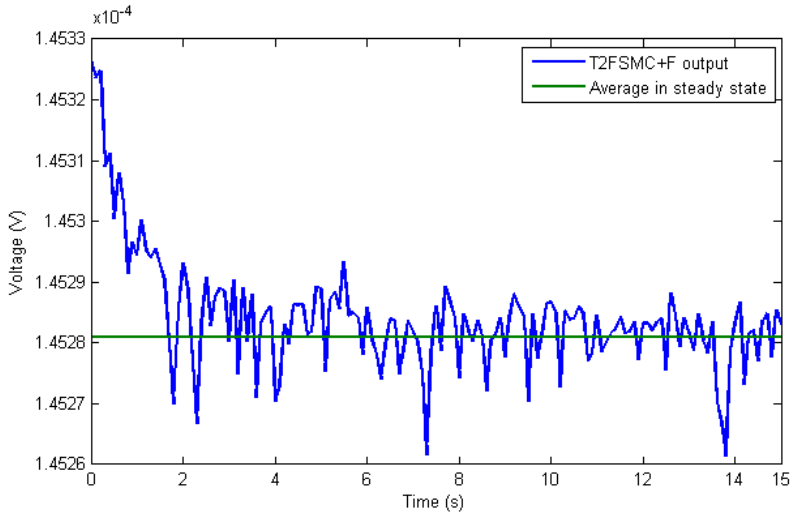

(a)

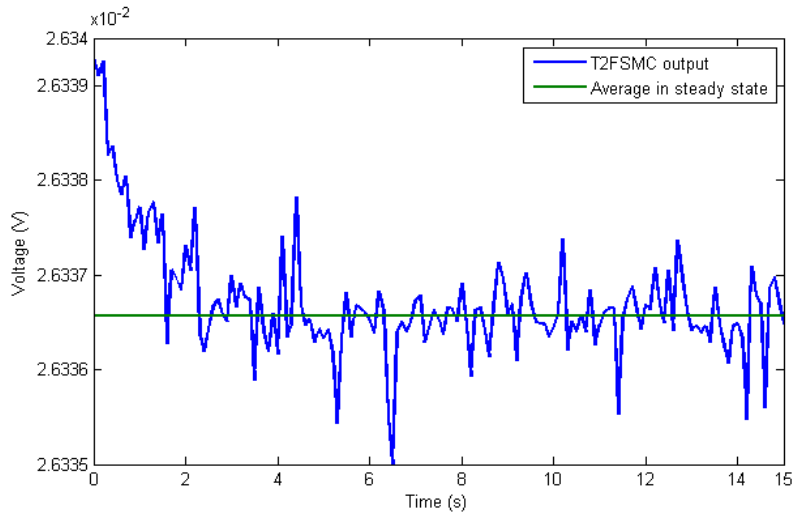

(b)

Fig. 4: Voltage output on T2FSMC (a) firefly algorithm, (b) bisection algorithm

Fuzzy entropy analysis

The analysis was performed on the previously discussed fuzzy set. This method has been modified because feature extraction adjustments are required. Fuzzy entropy can be used to calculate a new threshold for dividing the gray histogram on a grayscale image. The histogram division in the control problem, on the other hand, is in different ranges, namely [0 $7.3x10^{-5}$] with stepsize $1x10^{-7}$. When the range is divided, a minimum of 729 new histogram data are obtained, which are included in Eq. (4) and Eq. (5). Prior to optimizing the entropy value, a fuzzy inference system was built to reference the histogram value h(i) and the membership function of each histogram. Starting with the previously discussed entropy value of T2FSMC, the results are very satisfying, with the total fuzzy entropy T_{fe} = $5.4x10^{-5}$. This value denotes those irregularities and uncertainties have values ranging from 5.4 to 12 Volts. Furthermore, the analysis is refined by gradually incorporating the footprint of uncertainty into the

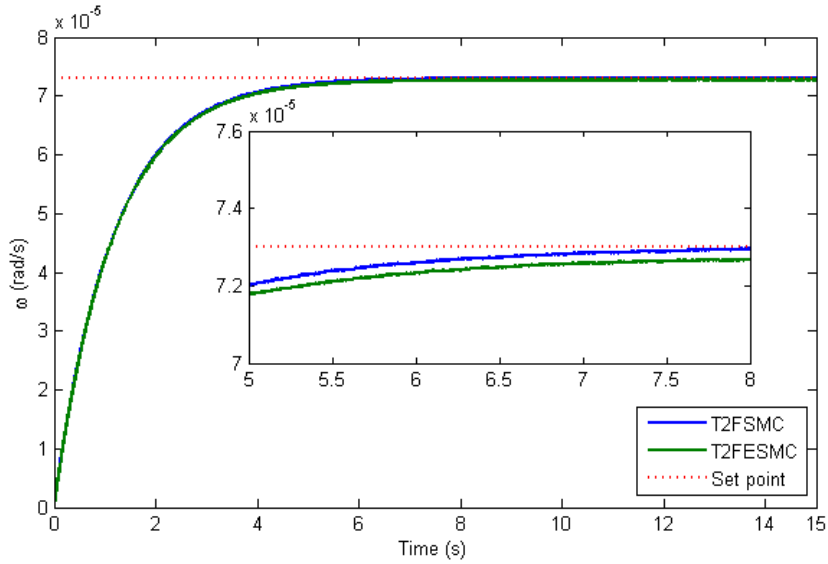

Fig. 5: Simulation of the new fuzzy inference system with the dc motor equation.

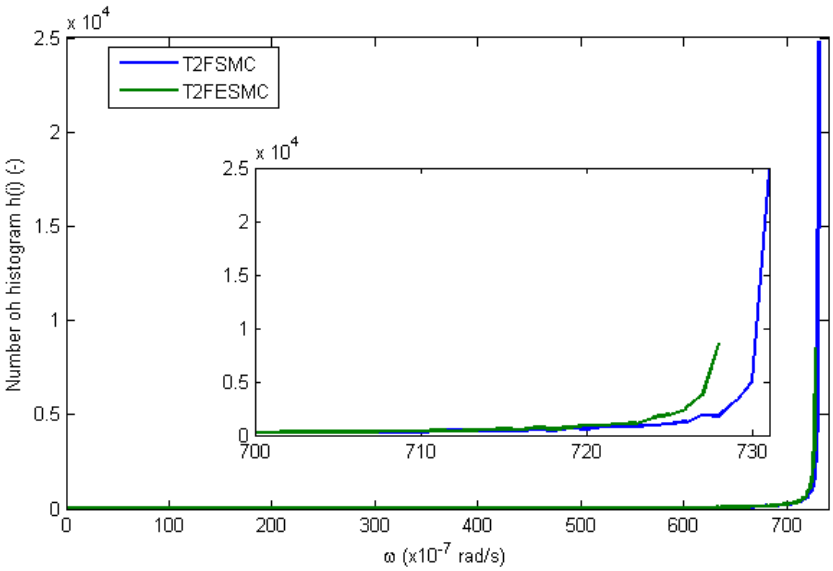

Fig. 6: The number of histograms h(i) in the conversion range [0.73x10^{-5}] with stepsize 1x10^{-7}

fuzzy set's legs. Fig. 5 depicts the simulation results of T2FSMC and T2FESMC after modification.

As a candidate control system, this system has succeeded in simulating and controlling the solar panel drive motor without using complicated calculations and only based on fuzzy set adjustments. The adjustment of the fuzzy set only takes two iterations due to the decrease in the total fuzzy entropy value which reaches 0.5x10^{-5}. The simulation is designed with a stop if there is a decrease in the total fuzzy entropy. The total fuzzy entropy obtained in the final iteration is 4.95x10^{-5}. This simulation generates a new histogram that can be analyzed. Fig. 6 explains that in the second iteration the total fuzzy

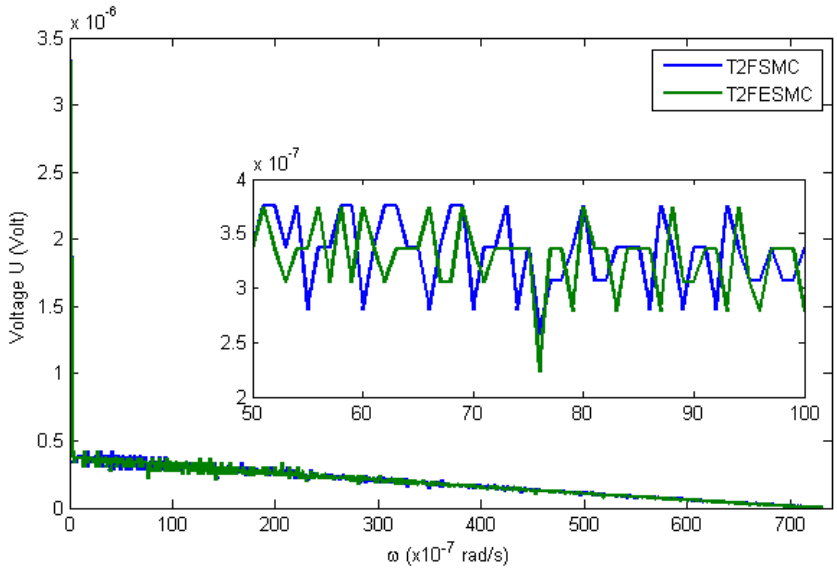

Fig. 7: Output voltage

Table 2: DC motor system parameters (Mardlijah *et al.,* 2018)

Parameter	Symbol	Value
Resistance	R	18.2214 Ω
Infuctance	L	0.000866 Henry
emf constant	K_b	0.030941093 V/(rad/s)
back-emf constant	K_m	0.030941093 N m/Ampere
Rotor inertia	J	0.00009 Kg m^2
Viscous friction coefficient	B_f	0.000025 N m s

entropy value decreases due to the decrease in the histogram close to the set point. This value is also influenced by the number of histograms before the peak. The T2FESMC is capable of matching histograms at low to moderate angular velocities. However, at high angular speeds, T2FESMC suffers from a lack of histograms. The number of histograms for T2FSMC is more than T2FESMC.

Reduction of the high value histogram on fuzzy entropy treatment is caused by incompatibility with the solar panel drive system. In the discussion of color histograms in black and white images, the application of fuzzy entropy is based on the dominant histogram division in the image (Mahajan *et al.,* 2021). The threshold that is formed eliminates the minor histogram by combining it with the nearby major histogram. While several major histograms that are close together, one of them is chosen to be the new threshold. This is different from the way solar panels work, which tries to be at set points. At the beginning of the simulation the position of the solar panels is far from the set point, so the system considered is a system that already has a major histogram at the set point as discussed in the bisection method at the beginning of this subsection. In this study, several major histograms that are already near the set point should produce a threshold that is at the set point. The fuzzy entropy algorithm does not accommodate this, so the set threshold is further from the set point.

The output voltage is the center of attention because the results in Fig. 7 are very similar. In addition to the decreasing fuzzy total value and the relatively low number of histograms, performance still has advantages in both systems. The fuzzy set used succeeded in producing the same voltage for both T2FSMC and the proposed system T2FESMC. The dynamics shown also have a range that is not much different and in the same trend. The resulting accuracy

is also quite good reaching $1x10^{-7}$ and better than in Fig. 4. This voltage output can be used separately in all types of solar panels with the same parameters or close to the parameters in Table 2. In the end this comparison produces two different voltage outputs have the same trend so that the irregularities in the simulation can be handled properly. This system can also be digitized so that it can be easily applied to the prototype by taking a larger stepsize for the resulting voltage output.

CONCLUSION

The two previous control systems have been compared with their fuzzy entropy values. Both managed to control the solar panels according to the direction of the sun's rays. Although different optimization methods, both systems are known as former T2FSMC. Fuzzy entropy method is proposed to optimize the former T2FSMC, hereinafter referred to as T2FESMC. The results obtained are in accordance with the control requirements with a similar trend between the system that has been used and the proposed system. Based on the angular velocity as a set point, the modified fuzzy entropy lags slightly compared to T2FSMC. T2FSMC is faster towards the set point and then it oscillates slightly at steady state. T2FESMC is a bit late, but still keeps pace with T2FSMC. There is a slight change in the position of the solar panels compared to T2FSMC. In fuzzy entropy analysis, the total fuzzy entropy in T2FSMC is better than T2FESMC. It is due to the missing histogram division at values near the set point. Fuzzy entropy has an algorithm to determine a new threshold so that certain features can be eliminated. In this case, T2FESMC obtains a threshold value which causes the histogram to decrease near the set point value. In the iteration process, this algorithm does not eliminate histograms with large errors, but the histograms are removed proportionally from small errors to large errors. It means that the modification of fuzzy sets with fuzzy entropy does not guarantee that a more reliable control system will be obtained. The modified fuzzy set is very good at controlling the solar panel driving motor based on the generated voltage value. Voltages follow the same pattern in both controllers under consideration. The weakness of the modified system is that the shot is not strong at the beginning of the simulation, so the process to get to the set point is slower. However, when compared to the former T2FSMC, the applied voltage is similar and is still in a stable condition. Finally, the modification of the control system based on fuzzy sets with fuzzy entropy can be further developed by changing the foot of uncertainty and adjusting it proportionally according to control needs. A further challenge is the calculation of the energy obtained from the modified system and before the modification. Insignificant changes usually have little effect on the results that can be obtained. A faster computational process is also able to have a positive impact on controlling solar panels, so that the energy obtained can help substitute renewable energy. The modified control system applies not only to solar panels. The motor equation used in this study can generally be used for all types of systems that use a driving motor for solar tracking.

AUTHOR CONTRIBUTIONS

M. Ramli performed the literature review, running the model, analyzed and interpreted the data, prepared the manuscript text, and manuscript edition. M. Mardlijah performed the literature review, analyzed and interpreted the data, and manuscript edition. M. Ikhwan performed the literature review, prepared numerical code, prepared the manuscript text, and manuscript edition. K. Umam performed the literature review, analyzed and interpreted the data, and manuscript edition. All authors agreed on the final version of the manuscript.

ACKNOWLEDGEMENT

This study is funded by Ministry of Education, Culture, Research and Technology, Republic of Indonesia in term of '*Penelitian Dasar*', under contract number: [20/UN11.2.1/PT.01.03/DPRM/2021].

CONFLICT OF INTEREST

The authors declare no potential conflict of interest regarding the publication of this work. In addition, the ethical issues including plagiarism, informed consent, misconduct, data fabrication and, or falsification, double publication and, or submission, and redundancy have been completely witnessed by the authors.

PUBLISHER'S NOTE

ABBREVIATIONS

%	Percent
°	Degrees (circle angles)
λ	Constant parameter
μ	Membership function
ω	rotor angular velocity (rad/sec)
ω_d	desired rotor angular velocity (rad/sec)
θ	Sun's angle of movement
B	Big
B_f	viscous friction coefficient (N-m/rad/sec)
d	distance between normal vector and sliding surface
E	Error
$\dot{e}$	First derivative of error
Eq /Eqs.	Equation
Fe_k	Fuzzy entropy on k index
Fig.	Figure
FSMC	Fuzzy sliding mode control
FOU	Footprint of uncertainty
H	Histogram
$i_a(t)$	armature current (Ampere)
ITAE	Integral time absolute error
J	rotor inertia (Kg-m^2)
$K_b(t)$	back-emf constant (Volt-sec/rad)
$K_m(t)$	torque constant (N-m/Ampere)
kWh/m^2	Kilowatt hours per square meter
L	Length of histogram
$L_a(t)$	armature inductance (Henry)
M	Medium
MW	Megawatt
No.	Number
NB	Negative big
NM	Negative medium
NS	Negative small
NZ	Negative zero
PB	Positive big
PM	Positive medium
PS	Positive small
PZ	Positive zero
$R_a(t)$	armature resistance (Ohm)
rad	Radians
rad/s	Radian per second
S	Small
S_p	distance between state vector and sliding
SMC	Sliding mode control
$T_m(t)$	load torque (N-m)
T2F	Type II fuzzy
T2FE	Type II fuzzy entropy
T2FESMC	Type II fuzzy entropy sliding mode control

T2FSMC	Type II fuzzy sliding mode control
Tfe_k	Total fuzzy entropy on k index
y	the external angle of the solar panel
y_i	The angle of the sun
Z	Zero

REFERENCES

Abadi, I.; Musyafa, A.; Soeprijanto, A., (2015). Design and implementation of active two axes solar tracking system using particle swarm optimization based fuzzy logic controller. Int. Rev. Model. Simul., 8(6): 640–652 (**13 pages**).

Abadi, I.; Uyuniyah, Q.; Fitriyanah, D.N.; Jani, Y.; Abdullah, K., (2020). Performance study of maximum power point tracking (mppt) based on type-2 fuzzy logic controller on active dual axis solar tracker. E3S Web of Conferences. 190: 00016 (**16 pages**).

Akinbami, O.M.; Oke, S.R.; Bodunrin, M.O., (2021). The state of renewable energy development in south africa: an overview. Alex. Eng. J., 60(6): 5077–5093 (**17 pages**).

Ayamolowo, O.J.; Manditereza, P.T.; Kusakana, K., (2021). Investigating the potential of solar trackers in renewable energy integration to grid. J. Phys.: Conf. Ser., 2022**:** 012031 (**9 pages**).

Baculi, J.; Ayoubi, M.A., (2017). Fuzzy attitude control of solar sail via linear matrix inequalities. Acta Astronaut., 138: 233–241 (**9 pages**).

Ballabel, A.; Mahfouz, A.; Salem, F.A., (2013). Design and performance of solar tracking photo-voltaic system. Int. J. Control. Autom. Syst., 1(2): 49-55 (**7 pages**).

Cánovas, J.; Kupka, J., (2016). On fuzzy entropy and topological entropy of fuzzy extensions of dynamical systems. Fuzzy Sets Syst., 1: 1–26 (**26 pages**).

Ganesh, N.J.; Maniprakash, S.; Chandrasekaran, L.; Srinivasan, S.M.; Srinivasan, A.R., (2011). Design and development of a sun tracking mechanism using the direct sm actuation. Trans. ASME. J. Mech. Des., 133(7): 1-14 (**14 pages**).

Ghiasi, M.I.; Golkar, M.A.; Hajizadeh, A., (2017). Lyapunov based-distributed fuzzy-sliding mode control for building integrated-dc microgrid with plug-in electric vehicle. IEEE Access, 5: 7746–7752 (**7 pages**).

Hamzaoui, A.; Al-khazraji, A., (2011). Robust tracking control of uncertain dynamic nonlinear systems via type-2 fuzzy sliding mode approach. IFAC Proc. Vol., 44(1): 4181–4185 (**5 pages**).

Henry, C.L.; Baker, J.S.; Shaw, B.K.; Kondash, A.J.; Leiva, B.; Castellanos, E.; Wade, C.M.; Lord, B.; Van Houtven, G.; Redmon, J.H., (2021). How will renewable energy development goals affect energy poverty in guatemala? Energy Econ., 104: 105665 (**22 pages**).

Ibrahim, I.D.; Hamam, Y.; Alayli, Y.; Jamiru, T.; Sadiku, E.R.; Kupolati, W.K.; Ndambuki, J.M.; Eze, A.A., (2021). A review on africa energy supply through renewable energy production: Nigeria, Cameroon, Ghana and South Africa as a case study. Energy Strategy Rev., 38: 100740 (**13 pages**).

Ikhwan, M.; Mardlijah; Imron, C., (2018). Model predictive control on dual axis solar tracker using matlab/simulink simulation. 2018 International Conference on Information and Communications Technology (ICOIACT), 784–788 (**5 pages**).

Ikhwan, M.; Rizal, S.; Ramli, M.; Muchlisin, Z.A.; Mardlijah, (2019). Wind disturbance elimination on dual axis solar tracker using fuzzy logic control. IOP Conf. Ser.: Earth Environ. Sci., 364: 012038 (**7 pages).**

Ishikawa, A.; Mieno, H., (1979). The fuzzy entropy concept and its application. Fuzzy Sets Syst., 2: 113–123 (**11 pages**).

Karatayev, M.; Lisiakiewicz, R.; Gródek-Szostak, Z.; Kotulewicz-Wisińska, K.; Nizamova, M., (2021). The promotion of renewable energy technologies in the former soviet bloc: why, how, and with what prospects? Energy Reports. 7: 6983–6994 (**12 pages**).

Kchaou, A.; Naamane, A.; Koubaa, Y.; M'sirdi, N., (2017). Second order sliding mode-based mppt control for photovoltaic applications. Sol. Energy. 155: 758–769 (**12 pages**).

Mahajan, S.; Mittal, N.; Pandit, A.K., (2021). Image segmentation using multilevel thresholding based on type II fuzzy entropy and marine predators algorithm. Multimed. Tools. Appl., 80(13): 19335–19359 (**25 pages**).

Mardlijah, M.; Jazidie, A.; Santoso, A.; Widodo, B., (2013). Design of t2fsmc controller with minimum gain scale factor by optimizing membership function using firefly algorithm on mobile inverted pendulum. Int. Rev. Autom. Control. 6(4): 431–440 (**10 pages**).

Mardlijah; Rinanto, N.; Soemarsono, A.R., (2017). Type 2 fuzzy sliding mode control (t2fsmc) controller on solar panel prototype using the most representative parameters. J. Theor. Appl. Inf. Technol., 95(20): 5562-5570 (**9 pages**).

Mardlijah, M.; Zuhri, Z., (2018). Solar panel control system using an intelligent control: t2fsmc and firefly algorithm. Telecommun. Comput. Electron. Control. 16(6): 2988 (**11 pages**).

Mardlijah; Zhai, G.; Adzkiya, D.; Mardianto, L.; Ikhwan, M., (2019). Modified t2fsmc approach for solar panel systems. Syst. Sci. Control Eng., 7(1): 189–197 (**9 pages**).

Obaideen, K.; AlMallahi, M.N.; Alami, A.H.; Ramadan, M.; Abdelkareem, M.A.; Shehata, N.; Olabi, A.G., (2021). On the contribution of solar energy to sustainable developments goals: case study on mohammed bin rashid al maktoum solar park. Int. J. Thermofluids.12: 100123 (**14 pages**).

Oliva, D.; Abd Elaziz, M.; Hinojosa, S., (2019). Metaheuristic algorithms for image segmentation: theory and applications. Springer Nature. Switzerland.

Rahman, A.; Dargusch, P.; Wadley, D., (2021). The political economy of oil supply in indonesia and the implications for renewable energy development. Renew. Sustain. Energy Rev., 111027 (**14 pages**).

Rani, P.; Singh, O.; Pandey, S., (2018). An analysis on arduino based single axis solar tracker. 5th IEEE Uttar Pradesh Section International Conference on Electrical, Electronics and Computer Engineering. 1–5 (**5 pages**).

Rao, C.S.; Santosh, S.; Ram, V.D., (2020). Tuning optimal pid controllers for open loop unstable first order plus time delay systems by minimizing itae criterion. IFAC-PapersOnLine. 53(1): 123-128 (**6 pages**).https://www.sciencedirect.com/science/article/pii/S2405896320300392

Sawant, A.; Bondre, D.; Joshi, A.; Tambavekar, P.; Deshmukh, A., (2019). Design and analysis of automated dual axis solar tracker based on light sensors. Proceedings of the International Conference on I-SMAC (IoT in Social, Mobile, Analytics and Cloud), I-SMAC 2018, 454–459 (**6 pages**).

Sharma, S.; Rohilla, Y., (2021). A study-level dual-axis active solar tracker. International Conference on System, Computation, Automation and Networking (ICSCAN 2021), 1-6 (**6 pages**).

Stefenon, S.F.; Kasburg, C.; Freire, R.Z.; Ferreira, F.C.S.; Bertol, D.W.; Nied, A., (2020). Photovoltaic power forecasting using wavelet neuro-fuzzy for active solar trackers. J. Intell. Fuzzy Syst., 40: 1–14 (**14 pages**).

Tomson, T., (2008). discrete two-positional tracking of solar collectors. Renew. Energy. 33: 400-405 (**6 pages**).

Yan, K.; Zeng, F., (2018). Conditional fuzzy entropy of fuzzy dynamical systems. Fuzzy Sets Syst., 342: 138 - 152 **(15 pages**).

Yu, H.; Zhi, X.; Fan, J., (2015). Neurocomputing image segmentation based on weak fuzzy partition entropy. Neurocomputing, 168: 994-1010 (**17 pages**).

Zamri, N.; Abdullah, L., (2013). A new linguistic variable in interval type-2 fuzzy entropy weight of a decision making method. Procedia Comput. Sci., 24: 42–53 (**12 pages**).

Zhou, R.; Jin, J.; Cui, Y.; Ning, S.; Bai, X.; Zhang, L.; Zhou, Y.; Wu, C.; Tong, F., (2022). Agricultural drought vulnerability assessment and diagnosis based on entropy fuzzy pattern recognition and subtraction set pair potential. Alex. Eng. J., 61(1): 51–63 (**13 pages**).

AUTHOR (S) BIOSKETCHES

Ramli, M., Ph.D., Professor, Department of Mathematics, Universitas Syiah Kuala, Banda Aceh 23111, Indonesia.
- Email: *marwan.math@unsyiah.ac.id*
- ORCID: 0000-0003-1225-9063
- Web of Science ResearcherID: AAB-8015-2019
- Scopus Author ID: 57217110324
- Homepage: http://math.unsyiah.ac.id/ind/marwan/

Mardlijah, M., Ph.D. Professor, Department of Mathematics, Institut Teknologi Sepuluh Nopember, Surabaya 60111, Indonesia.
- Email: *mardlijah@matematika.its.ac.id*
- ORCID: 0000-0002-2867-407X
- Web of Science ResearcherID: ABF-2537-2021
- Scopus Author ID: 53980121800
- Homepage: https://www.its.ac.id/matematika/en/lecturer-and-staff/list-of-lecturers/mardlijah/

Ikhwan, M., Ph.D. Candidate, Graduate School of Mathematics and Applied Sciences, Universitas Syiah Kuala, Banda Aceh 23111, Indonesia.
- Email: *m.ikhwan@mhs.unsyiah.ac.id*
- ORCID: 0000-0002-8162-1479
- Web of Science ResearcherID: D-1570-2018
- Scopus Author ID: 57212382115
- Homepage: http://dmas.unsyiah.ac.id/

Umam, K., Ph.D. Candidate, Department of Mathematics Education, Universitas Syiah Kuala, Banda Aceh 23111, Indonesia.
- Email: *khumam77@unsyiah.ac.id*
- ORCID: 0000-0003-3884-181X
- Web of Science ResearcherID: ABF-2533-2021
- Scopus Author ID: 57268953200
- Homepage: http://fsd.unsyiah.ac.id/umam/

HOW TO CITE THIS ARTICLE

Ramli, M.; Mardlijah, M.; Ikhwan, M.; Umam, K., (2022). Fuzzy entropy type II method for optimizing clean and renewable solar energy. Global J. Environ. Sci. Manage., 8(3): 389-402.

DOI: 10.22034/gjesm.2022.03.07

url: https://www.gjesm.net/article_248316.html

Global J. Environ. Sci. Manage. 8(3): 403-418, Summer 2022, Serial #31

Global Journal of Environmental Science and Management
(GJESM)

Homepage: https://www.gjesm.net/

CASE STUDY

Soil fertility in agricultural production units of tropical areas

S. Rodelo-Torrente[1], A.C. Torregroza-Espinosa[2,*], M. Moreno Pallares[3], D. Pinto Osorio[1], A. Corrales Paternina[2], A. Echeverría-González[4]

[1] *Departamento de Civil y Ambiental, Universidad de la Costa, 080002 Barranquilla, Colombia*

[2] *Departamento de Productividad e Innovación, Universidad de la Costa, 080002 Barranquilla, Colombia*

[3] *Departamento de Biología, Universidad del Atlántico, 081001 Puerto Colombia, Colombia*

[4] *Departamento de Ciencias Empresariales, Universidad de la Costa, 080002 Barranquilla, Colombia*

ARTICLE INFO

Article History:
Received 03 August 2021
Revised 13 November 2021
Accepted 20 December 2021

Keywords:
Soil nutrients
Soil physicochemical properties
Soil quality
Soil texture
Tropical soils

ABSTRACT

BACKGROUND AND OBJECTIVES: Soil is the most important basic natural resource for the support of agricultural production systems. Productivity maintenance in these ecosystems depends on their physicochemical. However, there are no significant studies on the current status of soil fertility and quality in tropical areas vulnerable to climate change and lacking management practices. The purpose of this study was to assess the physical and chemical properties of the soil to propose guidelines on soil handling and management in tropical areas.
METHODS: Data on texture, macronutrients, micronutrients, and cation ratios were collected at 200 farms in the Sucre Department of Northern Colombia. Correlation analysis and principal component analysis were performed on the resulting data set, and a soil quality index was calculated.
FINDINGS: Macronutrients N, P, K, S, Ca, Mg, and Na displayed average values of 21.65 ± 10.65 part per million, 40.35 ± 67.21 part per million, 0.46 ± 0.43 meq/100g, 7.94 ± 28.35 part per million, 15.63 ± 17.30 meq/100 g, 5.63 ± 3.58 meq/100g, 0.19 ± 0.20 meq/100g, respectively. Micronutrients Cu, Fe, Zn, and Mn displayed average values of 2.20 ± 1.66 part per million, 48.05 ± 37.87 part per million, 1.16 ± 1.26 part per million, 14.22 ± 12.24 part per million, respectively. The predominant texture among assessed soils was sandy clay loam. A significant correlation was found between (Ca/Mg) K-Ca/K, (Ca/Mg) K-Mg/K, Fe-Cu, and Ca-cation exchange capacity. The soil quality index of the soils assessed in the Department of Sucre indicates a high level of quality, which is strongly influenced by the indicators S, P, Mn (≥ 0.90) Fe, Zn, Cu, K, Na (≥ 0.80).
CONCLUSION: The macronutrients displayed a deficiency of potassium. It is therefore recommended to monitor these soils and apply fertilization plans according to the needs of each assessed soil. Lastly, this study provides relevant information for proposing guidelines for crop improvement.

DOI: 10.22034/gjesm.2022.03.08

NUMBER OF REFERENCES	NUMBER OF FIGURES	NUMBER OF TABLES
46	4	7

*Corresponding Author:
Email: *atorregr4@cuc.edu.co*
Phone: +30176 62812
ORCID: 0000-0001-8077-8880

Note: Discussion period for this manuscript open until October 1, 2022 on GJESM website at the "Show Article".

INTRODUCTION

The contribution of soils is essential for agricultural productivity, water regulation, climate regulation, and the environmental cycling of energy, carbon and nutrients, as well as the sustainment of biodiversity (van Leeuwen *et al.*, 2019). The importance of soil quality is associated with its functional capacity within ecological and land-use limits, while maintaining productivity and plant health (Martínez-Mera et al., 2017). Soil quality is a complex functional concept that cannot be measured directly in the field or laboratory but can only be inferred through a combination of physical, chemical, and biological indicators providing key information on the soil's composition, structure, and function (Paz-Ferreiro and Fu, 2016). The most noteworthy of these indicators is soil fertility, which refers to the soil's capacity to sustain plant growth by producing the required nutrients (León-Moreno, 2019). Soil fertility decrease is a major problem in many regions of the planet and a persistent limitation for agricultural production, particularly in low-potential areas. Therefore, declining soil fertility represents a major threat to food safety and development of small farmer communities (Vanlauwe *et al.*, 2017). Soil degradation implies a decline in soil quality, together with an associated reduction in ecosystem functions and services. One of the main types of soil degradation is chemical degradation (Lal, 2015). Soil chemical degradation includes processes such as acidification, salinization, nutrient depletion, reduced cation exchange capacity (CEC), increased Al or Mn toxicities, Ca, or Mg deficiencies, leaching of NO_3-N or other essential plant nutrients, or contamination by industrial wastes or by-products (Lal, 2015). At the same time, different human activities are producing physical changes, increased concentrations of chemical residues, and accumulation of materials (Muñoz-Rojas, 2018). Due to the above, it is important to assess the physicochemical quality of the soil as an indicator of its fertility and therefore of its environmental condition. Thus, a mathematical or statistical framework was put forward in the early 1990s to estimate soil quality index (SQI) (Mukherjee and Lal, 2014). It is also necessary to assess soil fertility, in order to develop suitable fertilization strategies. Soil management is one of the main factors influencing the improvement or degradation of soil quality (Lal, 2015). Soil health is a key component for addressing the global challenges of food safety, simultaneously ensuring environmental sustainability in view of a growing human population (Kurgat *et al.*, 2018). Several studies have been carried out on the evaluation of physicochemical characteristics in soils (Martínez-Mera et al., 2019). Table 1. provides examples of recent research on soil quality around the globe. In Colombia, studies have been mainly developed in the Atlántico (Martínez-Mera *et al.*, 2019) and Córdoba departments (Marrugo-Negrete *et al.*, 2017). Some of the most important physicochemical characteristics for the assessment of soil fertility and health include its texture (Bünemann *et al.*, 2018), organic carbon (OC/OM), total N, total P, macronutrients, micronutrients, CEC, potential of hydrogen (pH), exchangeable ions, cation ratios, and mineralization rate (Obriot *et al.*, 2016; Karbassi and Heidari, 2015; Karbassi and Pazoki, 2015). Sustainable soil management is an urgent matter worldwide: 25% of the world's population depends directly on degraded soils (Zhang *et al.*, 2011), mainly in tropical and subtropical areas of developing countries. However, there are no significant studies on the current status of soil fertility and quality in tropical areas vulnerable to climate change and lacking management activities, as is the case in northern Colombia. This study aims to determine soil quality in agricultural units through the analysis of its physical and chemical properties. Research was carried out in 200 properties, owned by small farmers, in five prioritized municipalities (San Onofre, San Marcos, Morroa, Corozal, and Majagual) of the Sucre Department, northern Colombia. Field measurements and laboratory analysis for this study were carried out in 2020.

MATERIALS AND METHODS

The methods employed in this research is summarized in Fig. 1. Soil samples were collected and sent to the laboratory to determine their physical and chemical properties. Relationships between cations were estimated, and statistical analyzes were carried out in order to assess soil. This methodology used allowed to determine which physical and chemical properties are the most significant for soil quality in the region.

Study area

The Sucre Department, located in the Caribbean plains of northern Colombia (Fig. 2), encompasses an area of 10670 km^2, equivalent to 0.9% of the total area

Table 1: Summary of different recent studies about soil quality.

Location	Relevant aspects	References
South-West Cameroon	Assessed two soil fertility approaches in paddy fields for rice cultivation, in order to develop a user-friendly and credible soil fertility index (SFI). According to the two methods used in the study, most of the study area was classified as moderately suitable for rice cultivation. The results of the parametric and fuzzy methods also demonstrated that the most important limiting factors were drainage and the thickness of the plow layer. The other limiting factors were texture, pH, OM, and coarse fragment	Delsouz Khaki *et al.* (2017)
Sub-Saharan Africa	Performed different analyses on various datasets demonstrated the direct impact of physicochemical properties of soil and derived soil fertility parameters on major constraints for plant growth and optimal crop production such as water retention capacity, roots development, soils aeration, nutrients availability, nutrients abundance, and cations balance Based on physicochemical soil properties, fertility parameters and Soil Quality Index (SQI), four soil fertility classes were identified: (*i*) very good fertility soils; (*ii*) good fertility soils; (*iii*) fairly good fertile soils; (*iv*) poorly fertile soils. The principal indicators controlling soil are Ca, Mg, pH water, OM, available P, total Nitrogen, and CEC. Four of the seven indicators (Ca, pH, OM, and P) were also identified as important indicators for assessing the fertility status of the different soil groups	Nguemezi *et al.* (2020)
South-Western China	Calculated a soil quality index found that soil organic carbon, total nitrogen, potassium, and free iron are the most important indicators of soil quality in tropical acidic red soils. Deforestation and corn cultivation related to significant decreases in SQI	Huang *et al.* (2021)
Review paper (around the world)	Revealed how soil quality assessment has changed through time in terms of objectives, tools and methods, and overall approach. Main objectives included: suitability for crop growth, productivity, environment, multi-functionality, ecosystem services, resistance, and resilience. Total organic matter/carbon and pH are the most frequently proposed soil quality indicators, followed by available phosphorus, various indicators of water storage, and bulk density (all mentioned in > 50% of reviewed indicator sets). Texture, available potassium, and total nitrogen are also frequently used (> 40%)	Bünemann *et al.* (2021)

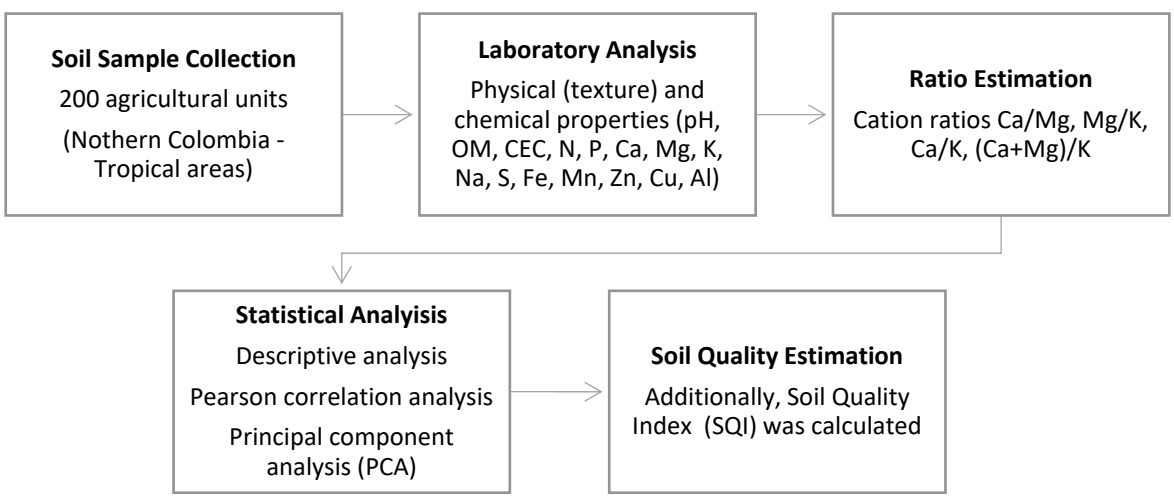

Fig. 1: Scheme of the methodology used in this study.

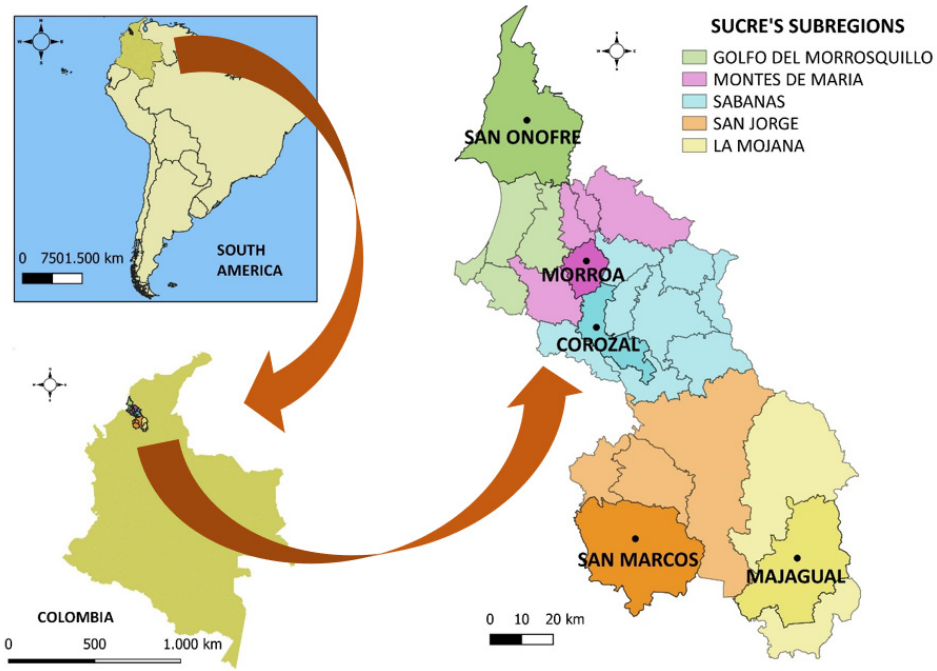

Fig. 2: Geographic location of the study area in the Department of Sucre in northern Colombia

of Colombia and 8.5% of the Colombian Caribbean region (Bustamante *et al.,* 2003). The weather in the region features a marked gradient of heavier rainfall from north to south (IDEAM, 2018). There are five subregions within the Sucre Department, the relevant characteristics of which are described in Table 2. In each subregion, a municipality was prioritized due to differences in precipitation, soil type, vegetation, and crop type. In addition, Sucre has the greatest percentage of area with land use conflicts among Colombian departments. Approximately 78% of the department area is affected by conflict of use, 42% (approximately 446000 Hectares) is affected by overuse, and 36% by underutilization. Proper use of soil, that is, productive systems where natural covers have not been affected, is present in only 22% of the department area. There are two trends of land use in Colombia: one is the use of some soils for agriculture and livestock when they have a different vocation, such as forestry or agroforestry. Another is the underutilization of soils, that is, abandoned or wasted lands that are not used for their true calling (DNP, 2003). Colombia is rich and diverse in soil resources. The Geographical Institute Agustin Codazzi (IGAC, for its initials in Spanish) recognizes 8 types of soils in Colombia, based on their vocation and capacity for use, productivity, and conservation (IGAC, 2021). Class 1, 2, and 3 soils, the most suitable for agricultural developments and controlled livestock, are widely distributed in areas of the Caribbean (northern) region of Colombia. Soils in these classes can support transitory crops and intensive livestock with high-yield pastures, with practices such as fertilization, waxing, watering, and drainage. Class 4, also found in the department of Sucre, includes soils with low fertility and high Al content. This class is suitable for agricultural, and livestock uses, but due to its limitations, it requires agricultural management practices. According to IGAC (2016), soils in the sampled municipalities of Sucre represent the orders Alfisols, Inceptisols, Mollisols, Ultisols, Vertisols, and Histosols.

Sample collection and laboratory analysis

Soil samples were collected at 200 farms in the five prioritized municipalities: 40 samples in Morroa (Montes de María subregion); 40 samples in Corozal (Sabana subregion); 40 samples in San Onofre (Gulf

Table 2: Characteristics of the five subregions and municipalities sampled in the department of Sucre in northern Colombia (Agronet, 2021).

SR/area	Mun	Av T /Av A	AP	Localization	Vegetation	Soil texture	Soil type (Order)	Crops
Montes de María (6466 km^2)	Morroa	26.8ºC 160 masl	1000-1200 mm	9º 20' 42" N 75º 18' 21" W	Tropical dry forest, mountain landscape	Sandy loam, Sand, Clay loam	Alfisols, Inceptisols	Cassava, corn, tropical yam, watermelon, beans, sweet pepper, rice, melon, pumpkin, white cucumber, purple sweet potato, eggplant
Sabana (2101 km^2)	Corozal	27ºC 143 masl	990-1275 mm	9º 19' 3" N 75º 17' 29" W	Tropical dry forest, hills landscape, extensive grassland area	Sand, Sandy loam, Clay loam	Mollisols	Cassava, tropical yam, corn, beans, plantain, watermelon
Golfo de Morrosquillo (1886 km^2)	San Onofre	27.4ºC 17 masl	900-1300 mm	9º 43' 59" N 75º 31' 59" W	Tropical dry forest, anthropic grasslands, hills landscape, mangrove forest	Clay, Clay loam	Mollisols Ultisols	Rice, cassava, tropical yam, corn, plantain, sweet pepper, beans, watermelon, pumpkin, sesame.
San Jorge (2934 km^2)	San Marcos	28ºC 25 masl	1300-2300 mm	8º 40' 1" N 75º 7' 59" W	Tropical humid forest, tropical dry forest, natural grassland	Sand, Clay	Mollisols, Vertisols	Corn, rice, cassava, tropical yam, watermelon.
Mojana (2337 km^2)	Majagual	28ºC 28 masl	2320-3000 mm	8º 32' 9" N 74º 39' 23" W	Tropical humid forest, wetland area	Clay loam	Mollisols, Histosols	Rice, corn, cassava, plantain, pumpkin, sugarcane, watermelon.

SR: Sub-region; Mun: Municipality; Av T: Average Temperature; Av A: Average Altitude; AP: Annual Precipitation.

of Morrosquillo subregion); 40 samples in San Marcos (San Marcos subregion); and 40 samples in Majagual (Mojana subregion) (Fig. 2). Samples were taken in crop fields, on flat terrain, mainly from Mollisols and Alfisols. Average farm area was 3 hectares; within each farm, one hectare was chosen for sampling. 15 subsamples were taken along zigzag transects, making V shaped cuts in the soil at a depth of 30 cm. The external portions of samples were discarded to avoid contamination. Each subsample was placed in a sterile plastic container in order to mix all subsamples and obtain a composite sample weighing 500 g. Sample collection followed the guidelines of Colombian Technical Standard (NTC) 3656 (ICONTEC, 2004). All samples were collected by triplicate to determine the precision of tests. The samples were analyzed at the environmental laboratory Zona Costera S.A.S., which is certified for environmental characterizations by the Institute of Hydrology, Meteorology and Environmental Studies (IDEAM). At the laboratory, physical (e.g., texture) and chemical (e.g., pH, OM, CEC N, P- total phosphorus -, Ca, Mg, K, Na, S, Fe, Mn, Zn, Cu, and Al) characteristics were determined (Table 3).

Data analysis

Descriptive statistics (e.g., minimum, maximum, mean, and standard deviation values) were performed on all physicochemical variables, followed by tests of normality and homogeneity of variance. Pearson correlation analyses were performed to test the relationships between physicochemical variables. Lastly, a principal component analysis (PCA) was performed to examine the contribution of each physicochemical variable to the overall variance of the studied soils. All statistical analyses and plots were performed using the R software package (R Core Team, 2020). Additionally, SQI was calculated for each farm production unit, by assigning unique values to each physicochemical variable by means of a weighted average (Nguemezi *et al.,* 2020). The Nv was calculated using Eq. 1.

$$Nv = 1 - \left(\frac{Im - Imin}{Imax - I\,min}\right) \quad (1)$$

Where Nv = is the normalized value, Im = indicator mean, Imax = indicator maximum value, Imin = indicator minimum value. The SQI was calculated using the simple additive method (Mukherjee and Lal, 2014). The SQI was interpreted using a transformation scale of five classes of soil quality (Nguemezi *et al.,* 2020): Very high quality 0.80 – 1.00; High quality 0.60 – 0.79; Average quality 0.40 – 0.59; Low quality 0.20 – 0.39; Very low quality 0.00 – 0.19.

RESULTS AND DISCUSSION

Predominant textures in assessed soils were sandy clay loam (SCL: 26%), clay loam (CL: 13%), clay (C: 12%), loamy sand (LS: 12 %), silt loam (SL: 11%), and loam (L: 10%). Average OM was 1.05 ± 0.51 % (Fig. 3). Loam texture and their products were the most abundant in soil samples. Loam soils generally contain more nutrients, moisture, and humus than sandy soils, have better drainage and infiltration of water and air than silt and clay-rich soils, and are easier to till than clay soils (Moraru *et al.,* 2020). Texture and OM are inherent properties of soil and crops, as well as indicators of soil health; affecting the availability of some macronutrients and micronutrients in the soil (Coblinski *et al.,* 2021). Amsili *et al*. (2021) found that physical and biological indicators were affected both by soil texture and cropping system. According to the classification of Villasanti *et al.* (2013), the content of OM was low in the studied soils. OM content is considered high above 2.8%, medium between 1.2 and 2.8%, and low below 1.2%. Low levels of organic matter are a threat to soil fertility Ndung'u *et al.* (2021). To improve the availability of organic matter, burning of vegetation should be avoided and compost from food waste and animal manure should be added to the soil. OM values in this work are consistent, and sometimes even lower, than those previously reported in other sites of northern Colombia (Martínez-Mera *et al.,* 2019).

Regarding macronutrients average values of N, P, K, S, Ca, Mg, and Na were 21.65 ± 10.65 parts per million (ppm), 40.35 ± 67.21 ppm, 0.46 ± 0.43 meq/100g, 7.94 ± 28.35 ppm, 15.63 ± 17.30 meq/100g, 5.63 ± 3.58 meq/100g, and 0.19 ± 0.20 meq/100g, respectively. For the case of the micronutrients Cu, Fe, Zn, and Mn, average values of 2.20 ± 1.66 ppm, 48.05 ± 37.87 ppm, 1.16 ± 1.26 ppm, and 14.22 ± 12.24 ppm, respectively. Average soil pH was 6.05 ± 0.80, with a maximum of 7.68 and a minimum of 4.19. Acid soils (average pH = 4.68) have been previously reported in Andean soils of Colombia. Average soil CEC was 22.84 ± 10.23

Table 3: Methods used to analyze the physical and chemical properties.

Variable	Method	Reference values		
PHYSICAL				
Texture	Bouyoucos NTC ISO 11464 (1975-11-24)	% Sand	% Silt	% Clay
CHEMICAL				
		Under	Medium	High
OM (%)	OM = Organic carbon x 1,724 (1.724 constans)	<1.49	1.5-3	>3.01
N (ppm)	NOM-021-SEMARNAT-2000, 7.1.8 AS-08 – Volumetry	0.09	0.1-0.199	>0.2
P (ppm)	Bray II extraction – Spectrophotometry	<9.99	10-20	>20.01
Ca (meq/100 g)	Extraction ammonium acetate 1 M, pH 7,0 – A.A spectrometry	<2.99	3-6	>6
Mg(meq/100 g)	Extraction ammonium acetate 1 M, pH 7,0 – A.A spectrometry	<1.5	1.5-3	>3
K (meq/100 g)	Extraction ammonium acetate 1 M, pH 7,0 – A.A spectrometry	<0.15	0.15-0.3	>0.301
Na (meq/100 g)	Extraction ammonium acetate 1 M, pH 7,0 – A.A spectrometry	< 1 Normal	>1 Problem	
S (ppm)	Extraction with calcium monophosphate 0,008 M - Turbidimetry	<10	10-20	>20
Fe (ppm)	NTC-5526 Method A. DTPA/ A.A spectrometry	<20	20-50	>50
Mn (ppm)	NTC-5526 Method A. DTPA/ A.A spectrometry	<10	10-30	>30
Zn (ppm)	NTC-5526 Method A. DTPA/ A.A spectrometry	<1	1-2	>2
Cu (ppm)	NTC-5526 Method A. DTPA/ A.A spectrometry	<1	1-2	>2
Al (meq/100 g)	IN-EE-081: NTC ISO 11464:1995, Extraction KCl 1 M - Volumetry	<= 1 Acid	>3 Problem	
$pH_{1:1, soil:water}$	EPA SW-846 9045 D /Electrometric	<5.5 Acid	5.5-6.5 neutral	> 6.5 alkaline
CEC (mEq/100 g)	Extraction with ammonium acetate 1 M, pH 7,0 – Volumetry	< 10	10-20	>20
$EC_{1:5, soil:water}$	NTC 5596:2008 / Electrometric	<0.8	0.8-1.6	>1.6
CATION RATIOS				
Ca/Mg	Estimate	<1	Calcium deficiency	
		1-2	Low level of with respect to Mg	
		2-5	Ideal	
		>5	Mg deficiency	
Mg/k	Estimate	<1	Mg deficiency	
		1-3	Acceptable	
		3	Ideal	
		3-18	Acceptable	
		>18	K deficiency	
Ca/k	Estimate	<30	Suitable	
		>30	K deficiency	
(Ca/Mg)k	Estimate	<40	K suitable	
		>40	K deficiency	

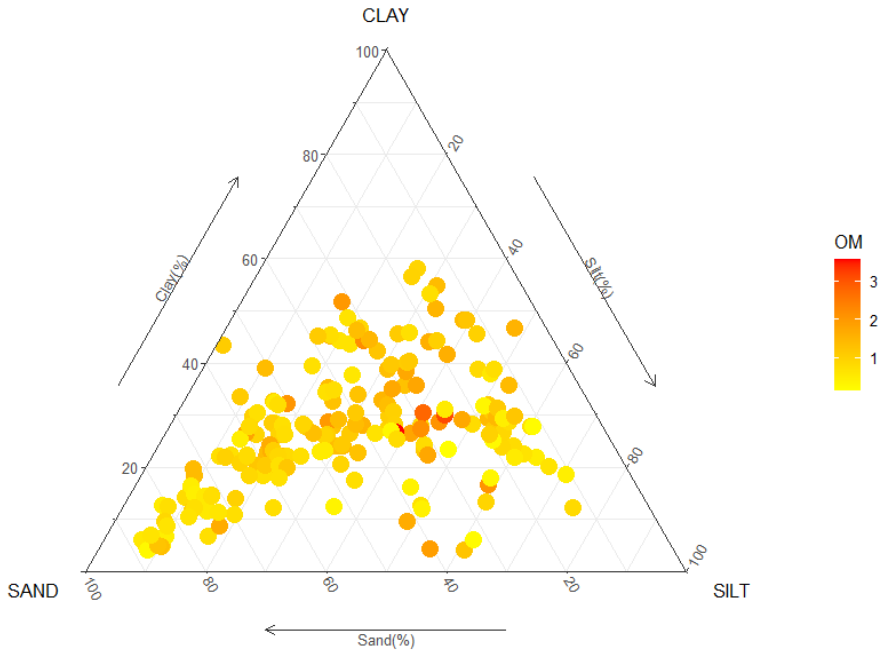

Fig. 3: Texture and OM of the studied soils.

Table 4: Summary for the physicochemical parameters analyzed in agricultural soils of the study area

Parameter	Maximum	Mínimum	Mean	SD
N (ppm)	63.20	5.40	21.65	10.65
P (ppm)	401.49	2.60	40.35	67.21
Ca (meq/100 g)	213.35	0.13	15.63	17.30
Mg(meq/100 g)	18.01	0.07	5.63	3.58
K (meq/100 g)	2.94	0.02	0.46	0.43
Na (meq/100 g)	0.98	0.02	0.19	0.20
S (ppm)	344.00	0.06	7.94	28.35
Fe (ppm)	319.24	2.74	48.05	37.87
Mn (ppm)	131.58	0.50	14.22	12.24
Zn (ppm)	8.35	0.19	1.16	1.26
Cu (ppm)	10.28	0.23	2.20	1.66
Al (meq/100g)	1.97	0.00	0.32	0.48
$pH_{1:1,\ soil:water}$	7.68	4.19	6.05	0.80
CEC (meq/100g)	50.84	4.61	22.84	10.23
$EC_{1:5,\ soil:water}$ (mS/cm)	0.17	0.01	0.05	0.03

P: total phosphorus, CEC: cation exchange capacity, EC: electrical conductivity

meq/100g, and average EC was 0.05 ± 0.03 mS/cm (Table 4). Values of pH and EC found in this study are below the maximum limit established by the Canadian Soil Quality Guidelines for Agriculture (CCME, 2014). Land use significantly influenced the change in CEC values. P content of soil can be altered by crop removal (approximately 80% is absorbed by plants), water erosion, and OM mineralization (Novello and Quintero, 2009). In the studied soils, macronutrients P and Ca displayed high values, whereas S displayed a low value. Phosphorus is essential for plant development and interacts with other nutrients such as C and N (Torri *et al.*, 2017). Continuous application of P from agrochemicals increases the potential risk

Table 5: Summary of the calculated cation ratios by the municipality.

Cation ratios	Municipiality				
	Corozal	Majagual	Morroa	San Marcos	San Onofre
Ca/Mg (Estimate)	2.86±1.48	2.63±5.16	3.94±2.24	2.46±1.40	2.96±0.83
Mg/K (Estimate)	18.53±7.56	36.92±18.37	9.52±5.96	10.31±7.61	14.52±6.41
Ca/K (Estimate)	47.09±19.26	75.68±68.25	29.27±11.09	22.58±16.21	40.83±16.35
(Ca+Mg)/K (Estimate)	65.62±23.65	112.60±73.30	38.79±14.25	32.89±21.94	55.35±21.12

of leaching into surface water through runoff, and underground water contamination via lixiviation (Silva-Leal *et al.,* 2021). In addition, high Ca values in soil are mediated by soil origin materials, as well as by the degree in which weathering and lixiviation have influenced soil formation processes (Chang *et al.,* 2020). In moderate quantities, $CaCO_3$ is beneficial for soil structure, and is often used to neutralize acid pH in soils. However, when high Ca levels are present, this nutrient combines with other components, creating non-soluble compounds that are difficult to absorb by plants. Therefore, an excess of Ca may restrict plant availability of P, B, and Fe (FAO, 2021).

Cation ratios Ca/Mg, Mg/K, Ca/K, and (Ca+Mg)/K, displayed average values of 2.97 ± 2.72, 17.96 ± 14.29, 43.09 ± 38.14, 61.05 ± 46.77, respectively. In all the assessed municipalities, an ideal Ca/Mg cation ratio was found, whereas the Mg/K ratio indicated a deficiency of K. Ca/K and (Ca+Mg)/K ratios displayed suitable values only in the municipalities of San Marcos and Morroa (Table 5). On the other hand, calculated cation ratios Mg/K, Ca/K, and (Ca+Mg)/K indicated a deficiency of K in most assessed samples, with average values > 18 in the ratio Mg/K, > 30 in the ratio Ca/K and > 40 in the ratio (Ca+Mg)/K. K is essential for plant physiological processes and is vital for the receptors of tolerance to hydric stress (Ruan *et al.,* 2014). In addition, hydric stress is a main limiting factor affecting plant growth and production. In arid and semi-arid regions, water scarcity limits crop productivity (Bader *et al.,* 2021). Consequently, it is essential to carry out studies in the area to propose management actions to improve the reported K deficiency. Previous studies of acid, low CEC soils in Colombian localities revealed the difficulty to adjust the relationships between exchangeable cations, due to the relationship between base saturation and soil pH (León, 1994). In general terms, it can be argued that very high Ca^{2+} and Mg^{2+} concentrations decrease K^+ absorption, and high K^+ levels may aggravate Mg^{2+} deficiency. However, it is worth noting that plants have a large capacity for adaptation, and their growth would be affected only under extreme conditions.

Pearson analysis found statistically significant correlations between most variables assessed (*p-value* ≤ 0.05), excepting for P, which did not correlate to other parameters. On the other hand, S was correlated only to Ca (*p-value* ≤ 0.05). High, positive correlations were found for (Ca/Mg)K-Ca/K (R^2=0.93, *p-value* ≤ 0.05), (Ca/Mg)K-Mg/K (R^2=0.61, *p-value* ≤ 0.05), Fe-Cu (R^2=0.53, *p-value* ≤ 0.05) and Ca-CEC (R^2=0.64, *p-value* ≤ 0.05). A high negative correlation was also found between soil textures Silt-Sand (R^2=0.52, *p-value* ≤ 0.05) and Sand-Clay (R^2=0.48, *p-value* ≤ 0.05) (Table 6). Similar correlations between cation ratios and Ca were previously reported by Bonomelli *et al.* (2020). Correlation analyses indicate that Fe is interacting with Cu, as well as Ca is interacting with CEC. Iron oxyhydroxides are natural, mineral constituents that are widely distributed, particularly in very mature soils that have been formed over very long periods (Cornell and Schwertmann, 2006). Cu exerts a strong control on the mobility and bioavailability of OM, Fe oxides, and Mn within the soil. It may also precipitate as hydroxide, carbonate, or phosphate (Yu *et al.,* 2016). Yu *et al.* (2014) found that cation exchanges in the soil can reduce the saturation of Ca hydroxide in the soil.

The first two principal components of the PCA accounted for 40% of the variance in the data set. The variables K, Ca, CEC, EC, and silt texture displayed the highest factor loads for the first principal component (PC_1). For the case of PC_2, the variables with the highest factor loads were the cation ratios Mg/K, Ca/K, and (Ca/Mg)K, together with Mg and clay texture (Fig. 4). It was also found that the percentage of sand was not related to any of the assessed variables, whereas the percentage of silt was related to OM, and EC is related

Table 6: Correlation between the physicochemical properties of soil in the department of Sucre, in northern Colombia.

Parameter		Silt	Sand	Clay	OM	N	P	Ca	Mg	K	Na	S	Fe	Mn	Zn	Cu	$pH_{1:1}$	CEC	$EC_{1:5}$	Ca/Mg	Mg/K	Ca/K	(Ca/Mg)K
		p - value																					
Silt	Correlation coefficient		0.00	0.93	0.00	0.41	0.65	0.00	0.03	0.00	0.01	0.66	0.45	0.70	0.01	0.00	0.00	0.00	0.00	0.00	0.00	0.05	0.01
Sand		**-0.72**		0.00	0.00	0.69	0.57	0.00	0.00	0.00	0.00	0.32	0.04	0.66	0.42	0.00	0.02	0.00	0.00	0.46	0.21	0.11	0.10
Clay		0.01	**-0.70**		0.41	0.78	0.73	0.00	0.00	0.11	0.00	0.33	0.02	0.30	0.15	0.00	0.38	0.00	0.53	0.03	0.08	0.76	0.73
OM		0.45	-0.37	0.08		0.35	0.93	0.00	0.00	0.00	0.19	0.58	0.63	0.72	0.14	0.09	0.05	0.00	0.00	0.28	0.01	0.01	0.00
N		-0.08	0.04	0.03	0.09		0.20	0.15	0.25	0.82	0.41	0.95	0.01	0.20	0.20	0.00	0.12	0.47	0.04	0.38	0.81	0.52	0.56
P		0.04	-0.05	0.03	0.01	-0.12		0.37	0.97	0.80	0.96	0.63	0.90	0.81	0.69	0.19	0.12	0.56	0.68	0.55	0.49	0.13	0.16
Ca		0.49	-0.58	0.32	0.39	0.13	-0.08		0.00	0.00	0.02	0.04	0.42	0.29	0.31	0.25	0.00	0.00	0.00	0.00	0.02	0.08	0.58
Mg		0.20	-0.52	0.55	0.29	0.11	0.00	0.51		0.00	0.00	0.17	0.06	0.05	0.31	0.01	0.75	0.00	0.27	0.00	0.00	0.99	0.19
K		0.48	-0.45	0.15	**0.60**	0.02	-0.02	0.55	0.29		0.12	0.22	0.51	0.86	0.27	0.18	0.00	0.00	0.00	0.01	0.00	0.00	0.00
Na		0.24	-0.50	0.48	0.12	0.08	-0.01	0.21	0.44	0.14		0.83	0.40	0.30	0.63	0.13	0.66	0.00	0.05	0.24	0.81	0.11	0.25
S		0.04	-0.09	0.09	0.05	0.01	-0.04	0.19	0.13	0.11	-0.02		0.35	0.61	0.96	0.64	0.53	0.10	0.25	0.76	0.50	0.70	0.60
Fe		0.07	-0.19	0.21	0.05	-0.23	-0.01	-0.08	0.17	-0.06	0.08	-0.09		0.03	0.09	0.00	0.10	0.69	0.03	0.01	0.08	0.75	0.74
Mn		-0.04	-0.04	0.10	0.03	-0.12	0.02	-0.10	0.18	-0.02	0.10	0.05	0.20		0.73	0.54	0.63	0.20	0.31	0.00	0.00	0.87	0.23
Zn		0.23	-0.08	-0.13	0.14	-0.12	0.04	-0.09	-0.09	0.10	-0.04	0.00	0.16	-0.03		0.00	0.46	0.49	0.70	0.73	0.05	0.06	0.04
Cu		0.40	-0.48	0.28	0.16	-0.32	0.12	0.11	0.24	0.13	0.14	-0.04	**0.73**	0.06	0.28		0.87	0.15	0.13	0.20	0.68	0.53	0.72
$pH_{1:1}$		0.37	-0.21	-0.08	0.18	0.14	-0.14	0.34	-0.03	0.33	0.04	0.06	-0.15	-0.05	-0.07	0.02		0.03	0.00	0.00	0.00	0.94	0.28
CEC		0.42	-0.59	0.42	0.42	0.07	-0.05	**0.80**	**0.63**	0.56	0.38	0.15	0.04	0.12	-0.06	0.13	0.20		0.00	0.01	0.25	0.85	0.60
$EC_{1:5}$		0.48	-0.30	-0.06	0.45	0.19	-0.04	0.47	0.10	**0.61**	0.18	0.11	-0.20	-0.09	0.04	-0.14	0.37	0.37		0.00	0.00	0.00	0.00
Ca/Mg		0.29	-0.07	-0.20	0.10	0.08	-0.06	0.54	-0.37	0.25	-0.11	0.03	-0.23	-0.27	-0.03	-0.12	0.40	0.24	0.38		0.00	0.04	0.69
Mg/K		-0.32	0.12	0.16	-0.25	0.02	-0.06	-0.22	0.37	-0.59	0.02	-0.06	0.16	0.30	-0.18	0.04	-0.29	-0.11	-0.47	-0.55		0.00	0.00
Ca/K		-0.18	0.15	-0.03	-0.25	0.06	-0.14	0.16	0.00	-0.56	-0.15	-0.04	-0.03	0.02	-0.17	-0.06	-0.01	-0.02	-0.26	0.19	0.59		0.00
(Ca/Mg)K		-0.24	0.15	0.03	-0.28	0.05	-0.13	0.05	0.12	**-0.62**	-0.11	-0.05	0.03	0.11	-0.19	-0.03	-0.10	-0.05	-0.36	-0.04	**0.78**	**0.96**	

OM: Organic Matter, CEC: cation exchange capacity, EC: electrical conductivity

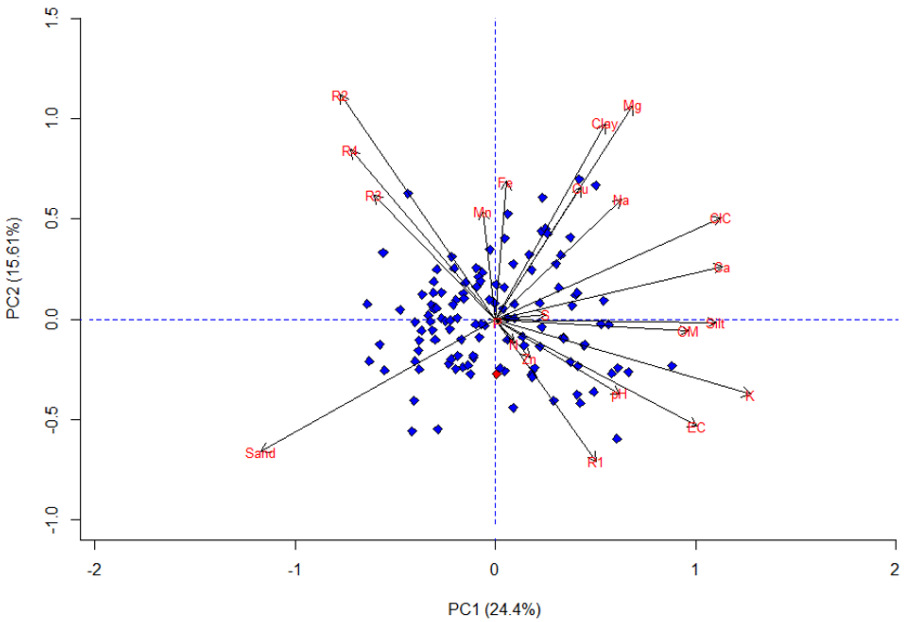

Fig. 4: Principal component analysis. R1= Ca/Mg, R2= Mg/K, R3= Ca/K, R4= (Ca/Mg) K.

Table 7: SQI in the department of Sucre (Northern Colombia).

Physicochemical Characteristics (Indicator)	Im	Nv
Silt	27.07	0.57
Sand	42.83	0.55
Clay	30.10	0.52
OM	1.17	0.74
N	23.26	0.69
P	40.35	0.91
Ca	19.74	0.61
Mg	6.70	0.67
K	0.62	0.82
Na	0.21	0.81
S	7.95	0.98
Fe	37.70	0.89
Mn	14.23	0.90
Zn	1.08	0.89
Cu	1.98	0.84
pH	6.40	0.38
CEC	26.87	0.52
EC	0.05	0.73
SQI		**0.72**

to pH. The percentage of clay is related to Mg and Cu. The PCA indicated that crop physiological processes depend on a balance between the parameters K, Ca, CEC, EC, Mg and the cation ratios Mg/K, Ca/K a,nd (Ca/Mg)K. A PCA analysis by Bonomelli *et al.* (2020) found that the variance was mostly determined by K, Mg, N, and Ca.

Calculated indicators and soil quality index values are shown in Table 7. The calculated SQI was 0.72, indicating that assessed soils in the Department of Sucre are of high quality. SQI value in the study is strongly influenced by the indicators S, P, Mn (Nv ≥ 0.90) and Fe, Zn, Cu, K, Na (Nv ≥ 0.80), whereas the indicator pH exerted very little influence. However, previous research has shown that soil quality should be determined by analyzing both physicochemical and biological soil characteristics. Therefore, contamination levels should be incorporated into the SQI valuation in those agricultural regions exposed to anthropogenic activity (Klimkowicz-Pawlas *et al.*, 2019).

Lastly, using the soil quality index enables farmers to assess the current status of soil. This allows in turn to identify critical points for sustainable development, assess the possible impacts before any intervention, and monitor the impact of human interventions, thus helping to determine whether the use of soil is sustainable (De Laurentiis *et al.,* 2019). A proper understanding of the soil fertility conditions and is essential for food safety and sustainable development of agricultural systems. Reliable methods for the assessment of soil fertility are of great assistance for the management and monitoring of this resource. In general terms, assessed soils from the Sucre Department display high quality, indicating that soil fertility is well correlated with potential crop yields (Chabala *et al.,* 2020), as reflected in the variety of crops present in the municipalities. A better understanding of the interactions between crops and soil fertility will help to inform decisions aimed to increase crop productivity.

CONCLUSION

Soil quality is a major proxy for soil functional capacity within the ecological and land-use limits, while maintaining productivity and plant health. Soil degradation leads to a reduction in ecosystem functions and services of interest to humans and conservation of nature. According to the results, the macronutrients P and Ca displayed high values and S content was low. Phosphorus, an essential nutrient for plant development, interacts with other nutrients such as C and N. On the other side, when a high Ca level cannot be absorbed, it combines with other components to create non-soluble compounds that are difficult for plants to absorb. Cation ratios Mg/K, Ca/K and (Ca+Mg)/K indicated a deficiency of potassium. Correlation analyses suggest that Fe is interacting with Cu and that Ca is interacting with CEC. The PCA indicated that crop physiological processes depend on a balance between the parameters K, Ca, CEC, EC, Mg and of the cation ratios Mg/K, Ca/K, and (Ca/Mg)K. On the other hand, the SQI indicates high quality levels in soils assessed at 200 productivity units in selected municipalities of the Sucre Department of Colombia. Indicators S, P, Mn, Fe, Zn, Cu, K, and Na determined the current fertility status of studied soils. Therefore, it is recommended to monitor these soils, implementing fertilization plans according to the needs of each assessed soil. Physicochemical and cation ratio results will inform decision-making in order to define corrective strategies to increase soil fertility increase within the study area, as well as to develop decisions and actions at the national and local levels. A proper understanding of the conditions and dynamics of soil fertility is fundamental for food safety and the sustainable development of the agricultural system. In Latin America, Colombia is the third country with the highest resources, climate diversity, and annual precipitation rates, characteristics that favor its role in food production. Therefore, Colombia is considered by The United Nations Food and Agriculture Organization (FAO) as a country with great potential to be a pantry of the world. In this context, to ensure food security, regulatory measures should be implemented in agricultural activities and soil management. In this sense, the results of this study will serve as a baseline to propose monitoring and follow-up strategies on the agricultural practices in the region. Fertility was assessed using simple procedures and available information, which implies that this methodology can be replicated in other Colombian departments.

AUTHOR CONTRIBUTIONS

S. Rodelo-Torrente performed the literature review, analyzed, and interpreted the data, prepared the original draft. A.C. Torregroza-Espinosa performed

analyzed and interpreted the data, writing - original draft, writing – review and editing. D. Pinto Osorio helped in the contextualization and prepared the original draft. M.I. Moreno Pallares performed the literature review, experimental design, analyzed and interpreted the data, writing – original draft, writing – review, and editing. A. Corrales Paternina helped in the contextualization and prepared the original draft. A. Echeverría-González helped in the contextualization and prepared the original draft.

ACKNOWLEDGMENTS

The author acknowledges funding support from the Government of Sucre (Colombia) through royalty system [Project: "Application of engineering techniques that increase the resilience of agroecosystems to climate variability in the Department of Sucre" [BPIN2017000100029] and executed by the University of the Costa and the University of Sucre (Colombia).

CONFLICT OF INTEREST

The authors declare no potential conflict of interest regarding the publication of this work. In addition, ethical issues including plagiarism, informed consent, misconduct, data fabrication and, or falsification, double publication and, or submission, and redundancy have been completely witnessed by the authors.

OPEN ACCESS

PUBLISHER'S NOTE

ABBREVIATIONS

%	Percentage
>	Greater-than sign
<	Less-than sign
≥	Greater-than or equal to sign
±	Plus or minus sign
A.A.	Atomic absorption
Al	Aluminum
AP	Annual Precipitation
Av A	Average Altitude
Av T	Average Temperature
C	Clay
Ca	Calcium
CEC	Cation exchange capacity
$CaCO_3$	Calcium carbonate
CL	Clay loam
cm	Centimeter
Cu	Copper
DTPA	Diethyle netriamine pentaacetic acid
e.g.	For example
EC	Electrical conductivity
EPA	Environmental Protection Agency
Eq.	Equation
Fe	Iron
Fig.	Figure
g	Gram
h	Hectare
Im	Indicator mean
Imax	Indicator maximum value
Imin	Indicator minimum value
K	Potassium
KCL	Potassium Chloride

Km^2	Square kilometre
L	Loam
LS	Loamy sand
M	Unit of molar concentration.
masl	Meters Above Sea Level
Mg	Magnesium
mm	Millimetre
Mn	Manganese
meq/100 g	Cation exchange capacity as milli-equivalents per 100 grams
Mun	Municipiality
N	Nitrogen
Na	Sodium
NO_3-*N*	Nitrate Nitrogen
NOM	Norm
NTC	Colombian Technical Standard
Nv	Normalized value
OM	Organic Matter
p-value	Statistical significance
P	Phosphorus
PCA	Principal component analysis
pH	Potential of hydrogen
ppm	Parts per million
R^2	R-squared
S	Sulfur
SCL	Sandy clay loam
SD	Standard deviation
SEMARNAT	Ministry of Environment and Natural Resources
SFI	Soil fertility index
SL	Silt loam
SQI	Soil quality index
SR	Sub-region
Zn	Zinc

REFERENCES

Agronet., (2021). Red de información y comunicación del sector Agropecuario Colombiano. MinAgricultura.

Amsili, J.P.; van Es, H.M.; Schindelbeck, R.R., (2021). Cropping system and soil texture shape soil health outcomes and scoring functions. Soil Secur., 4: 1000012 **(11 pages).**

Bader, B.R.; Taban, S.K.; Fahmi, A.H.; Abood, M.A.; Hamdi, G.J., (2021). Potassium availability in soil amended with organic matter and phosphorous fertiliser under water stress during maize (Zea mays) growth. J. Saudi Soc. Agric. Sci., 20(6): 390-394 **(5 pages).**

Bonomelli, C.; Mogollon, R.; de Freitas, S.T.; Zoffoli, J.P.; Contreras, C., (2020). Nutritional relationships in bitter pit-affected fruit and the feasibility of vis-NIR models to determine calcium concentration in 'fuji' apples. Agronomy., 10: 1474 **(13 pages).**

Bünemann, E.K.; Bongiorno, G.; Bai, Z.; Creamer, R.E.; De Deyn, G.; de Goede, R.; Fleskens, L.; Geissen, V.; Kuyper, T.W.; Mäder, P.; Pulleman, M.; Sukkel, W.; van Groenigen, J.W.; Brussaard, L. (2018). Soil quality – A critical review. Soil Biol. Biochem., 120: 105-125 **(21 pages).**

Bustamante, N.; Danoucaras, N.; McIntyre, N.; Díaz-Martínez, J.; Restrepo-Baena, O.J., (2016). Review of improving the water management for the informal gold mining in Colombia. Revista Facultad de Ingeniería Universidad de Antioquia., 79: 174-184 **(11 pages).**

CCME, (2014). Canadian environmental quality guidelines. Canadian council of ministers of the environment.

Chabala, L.M.; Chimungu, J.G.; Lark, R.M.; Mtambanengwe, F.; Nalivata, P.C.; Phiri, E.; Sakala, G.M., (2020). Eliciting experts' tacit models for the interpretation of soil information, an example from the evaluation of potential benefits from conservation agriculture. Geoderma., 376: 114545 **(11 pages).**

Chang, H.; Wang, Q.; Li, Z.; Wu, J.; Xu, X.; Shi, Z., (2020). The effects of calcium combined with chitosan amendment on the bioavailability of exogenous pb in calcareous soil. J. Integr. Agric., 19(5): 1375-1386 **(12 pages).**

Coblinski, J.A.; Inda, A.V.; Demattê, J.A.M.; Dotto, A.C.; Gholizadeh, A.; Giasson, É., (2021). Identification of minerals in subtropical soils with different textural classes by VIS–NIR–SWIR reflectance spectroscopy. Catena (Giessen)., 203: 105334 **(10 pages).**

Cornell, R.M.; Schwertmann, U., (2006). The iron oxides: structure, properties, reactions, occurences and uses. 2nd Edition. Wiley.

De Laurentiis, V.; Secchi, M.; Bos, U.; Horn, R.; Laurent, A.; Sala, S., (2019). Soil quality index: Exploring options for a comprehensive assessment of land use impacts in LCA. J. Cleaner Prod., 215:63-74 **(12 pages).**

Delsouz Khaki, B.; Honarjoo, N.; Davatgar, N.; Jalalian, A.; Torabi Golsefidi, H., (2017). Assessment of two soil fertility indexes to evaluate paddy fields for rice cultivation. Sustainability., 9(8): 1299 **(13 pages).**

DNP., (2003). Organización de las Naciones Unidas para la Agricultura y la Alimentación (FAO). Programa de desarrollo sostenible de la región de La Mojana, Bogotá. Departamento Nacional de Planeación **(567 pages).**

FAO., (2021). Food and Agriculture Organization of the United Nations. Soil portal.

Huang, W.; Zong, M.; Fan, Z.; Feng, Y.; Li, S.; Duan, C.; Li, H., (2021). Determining the impacts of deforestation and corn cultivation on soil quality in tropical acidic red soils using a

soil quality index. Ecol. Indic., 125: 107580 **(10 pages).**
ICONTEC., (2004). NTC 3656, Gestión ambiental suelo, Toma de muestras de suelo para determinar contaminación. Instituto Colombiano de Normas Técnicas y Certificación. Bogotá, Colombia.
IDEAM, (2018). Atlas climatológico de Colombia. Instituto De Hidrología, Meteorología y Estudios Ambientales.
IGAC, (2016). Suelos y tierras de Colombia, subdirección de agrología. Instituto Geográfico Agustín Codazzi. Bogotá DC, Tomo 1 **(854 pages).**
IGAC, (2021). Colombia, un país con una diversidad de suelos ignorada y desperdiciada. Bogotá, Colombia. Instituto Geográfico Agustín Codazzi.
Karbassi, A.R.; Pazoki, M., (2015). Environmental qualitative assessment of rivers sediments. Global J. Environ. Sci. Manage., 1(2): 109-116 **(8 Pages)**.
Karbassi, A.R.; Heidari, M., (2015). An investigation on role of salinity, pH and DO on heavy metals elimination throughout estuarial mixture. Global J. Environ. Sci. Manage., 1(1): 41-46 **(6 pages)**.
Klimkowicz-Pawlas, A.; Ukalska-Jaruga, A.; Smreczak, B., (2019). Soil quality index for agricultural areas under different levels of anthropopressure. Int. Agrophys., 33: 455-462 **(8 pages).**
Kurgat, B.K.; Ngenoh, E.; Bett, H.K.; Stöber, S.; Mwonga, S.; Lotze-Campen, H.; Rosenstock, T.S., (2018). Drivers of sustainable intensification in kenyan rural and peri-urban vegetable production. Int. J. Agric. Sustainability., 16(4-5): 385-398 **(14 pages).**
Lal, R., (2015). Restoring soil quality to mitigate soil degradation. Sustainability., 7(5): 5875-5895 **(21 pages).**
León-Moreno, C.E.; Rojas-Molina, J.; Castilla-Campos, C.E., (2019). Physicochemical characteristics of cacao (Theobroma cacao L.) soils in Colombia: Are they adequate to improve productivity? Agronomía Colombiana., 37(1): 28-38 **(11 pages).**
León, S.L.A., (2001). Evaluación de la fertilidad del suelo. En: Silva F. (ed.). Fertilidad de suelos, diagnóstico y control. 2a edición. Sociedad Colombiana de la Ciencia del Suelo **(15 pages).**
Marrugo-Negrete, J.; Pinedo-Hernandez, J.; Díez, S., (2017). Assessment of heavy metal pollution, spatial distribution and origin in agricultural soils along the Sinú River Basin, Colombia. Environ. Res., 154: 380–388 **(9 pages).**
Martínez-Mera, E.A.; Torregroza-Espinosa, A.C.; Valencia-García, A.; Rojas Jerónimo, L., (2017). Relationship between soil physicochemical characteristics and nitrogen-fixing bacteria in agricultural soils of the Atlántico department, Colombia. Soil and Environment., 36: 174-181 **(8 pages).** https://doi.org/10.1016/j.heliyon.2019.e02217
Martínez-Mera, E.A.; Torregroza-Espinosa, A.C.; Crissien-Borrero, T.J.; Marrugo-Negrete, J.L.; González-Márquez, L.C., (2019). Evaluation of contaminants in agricultural soils in an Irrigation District in Colombia. Heliyon., 5(8): e02217 **(9 pages).**
Moraru, S.S.; Ene, A.; Badila, A., (2020). Physical and hydro-physical characteristics of soil in the context of climate change. A case study in danube river basin, SE Romania. Sustainability., 12(9174): 9174 **(26 pages).**
Mukherjee, A.; Lal, R., (2014). Comparison of soil quality index using three methods. PLoS One., 9(8): e105981 **(15 pages).**
Muñoz-Rojas, M., (2018). Soil quality indicators: critical tools in ecosystem restoration. Curr. Opin. Environ. Sci. Health., 5: 47-52 **(6 pages).**
Ndung'u, M.; Ngatia, L.W.; Onwonga, R.N.; Mucheru-Muna, M.W.; Fu, R.; Moriasi, D.N.; Ngetich, K.F., (2021). The influence of organic and inorganic nutrient inputs on soil organic carbon functional groups content and maize yields. Heliyon., 7(8): e07881 **(10 pages).**
Nguemezi, C.; Tematio, P.; Yemefack, M.; Tsozue, D.; Silatsa, T.B.F., (2020). Soil quality and soil fertility status in major soil groups at the Tombel area, South-West Cameroon. Heliyon., 6(2): e03432 **(10 pages).**
Novello, O.A.; Quintero, C.E., (2009). Contenidos de fósforo total en suelos distrito Villa Eloisa (Santa Fe). Inf. Agronómicas., 41: 11–15 **(5 pages).**
Obriot, F.; Stauffer, M.; Goubard, Y.; Cheviron, N.; Peres, G.; Eden, M.; Revallier, A.; Vieublé-Gonod, L.; Houot, S., (2016). Multi-criteria indices to evaluate the effects of repeated organic amendment applications on soil and crop quality. Agric. Ecosyst. Environ., 232: 165-178 **(14 pages).**
Paz-Ferreiro, J.; Fu, S., (2016). Biological indices for soil quality evaluation: Perspectives and limitations. Land Degrad. Dev., 27(1): 14-25 **(12 pages).**
R Core Team, (2020). R: A language and environment for statistical computing. R Foundation for Statistical Computing.
Ruan, L.; Zhang, J.; Xin, X., (2014). Effect of poor-quality irrigation water on potassium release from soils under long-term fertilization. Acta Agric. Scand. Sect. B., 64(1): 45-55 **(11 pages).**
Silva-Leal, J.A.; Pérez-Vidal, A.; Torres-Lozada, P., (2021). Effect of biosolids on the nitrogen and phosphorus contents of soil used for sugarcane cultivation. Heliyon., 7(3): e06360 **(8 pages).**
Torri, S.I.; Correa, R.S.; Renella, G., (2017). Biosolid application to agricultural land a contribution to global phosphorus recycle: a review. Pedosphere., 27(1): 1–16 **(16 pages).**
Vanlauwe, B.; AbdelGadir, A.H.; Adewopo, J.; Adjei-Nsiah, S.; Ampadu-Boakye, T.; Asare, R. et al., (2017). Looking back and moving forward: 50 years of soil and soil fertility management research in sub-Saharan Africa. Int. J. of Agric. Sustainability., 15(6): 613-631 **(19 pages).**
Van Leeuwen, J. P.; Creamer, R. E.; Cluzeau, D.; Debeljak, M.; Gatti, F.; Henriksen, C. B.; Kuzmanovski, V.; Menta, C.; Pérès, G.; Picaud, C.; Saby, N.P.A.; Trajanov, A.; Trinsoutrot-Gattin, I.; Visioli, G.; Rutgers, M., (2019). Modeling of soil functions for assessing soil quality: soil biodiversity and habitat provisioning. Front. Environ. Sci., 7: 113 **(13 pages).**
Villasanti, C.; Román, P.; Pantoja, A., (2013). El manejo del suelo en la producción de hortalizas con buenas prácticas agrícolas. In Food and Agriculture Organization of the United Nations **(31 pages).**
Yu, H.; Huang. X.; Ning, J.; Zhu, B.; Cheng, Y., (2014). Effect of cation exchange capacity of soil on stabilized soil strength. Soils Found., 54(6): 1236-1240 **(5 pages).**
Yu, H.; Liu, C.; Zhu, J.; Li, F.; Deng, D.; Wang, Q.; Liu, C., (2016). Cadmium availability in rice paddy fields from a mining area: The effects of soil properties highlighting iron fractions and pH value. Environ. Pollut., 209: 38-45 **(8 pages).**
Zhang, C.; Xue, S.; Liu, G.; Song, Z., (2011). A comparison of soil qualities of different revegetation types in the loess plateau, china. Plant Soil., 347(1/2): 163-178 **(16 pages).**

AUTHOR (S) BIOSKETCHES

Rodelo-Torrente, S., M.Sc. Student, Departamento de Civil y Ambiental. Universidad de la Costa, Barranquilla Atlántico, Colombia.
- Email: *srodelo2@cuc.edu.co*
- ORCID: 0000-0002-5820-6701
- Web of Science ResearcherID: NA
- Scopus Author ID: NA
- Academic Homepage: https://www.researchgate.net/profile/Sara-Rodelo-Torrente

Torregroza-Espinosa, A.C., Ph.D., Associate Professor, Departamento de Productividad e Innovación. Universidad de la Costa, Barranquilla Atlántico, Colombia.
- Email: *atorregr4@cuc.edu.co*
- ORCID: 0000-0001-8077-8880
- Web of Science ResearcherID: ABB-5481-2021
- Scopus Author ID: 57189332407
- Academic Homepage: https://www.researchgate.net/profile/Ana-Torregroza

Moreno Pallares, M., Ph.D. Candidate, Departamento de Biología. Universidad del Atlántico, Barranquilla Atlántico, Colombia.
- Email: *odonata12@gmail.com*
- ORCID: 0000-0002-4136-0104
- Web of Science ResearcherID: ABE-3273-2021
- Scopus Author ID: NA
- Academic Homepage: https://www.researchgate.net/profile/Maria-Moreno-110

Pinto Osorio, D., Ph.D., Professor, Departamento de Civil y Ambiental. Universidad de la Costa, Barranquilla Atlántico, Colombia.
- Email: *dpinto3@cuc.edu.co*
- ORCID: 0000-0002-1496-5722
- Web of Science ResearcherID: AAV-5458-2021
- Scopus Author ID: 57195677095
- Academic Homepage: https://www.researchgate.net/profile/Diana-Pinto-Osorio

Corrales Paternina, A., M.Sc., Professor, Departamento de Productividad e Innovación. Universidad de la Costa, Barranquilla Atlántico, Colombia.
- Email: *acorrales@cuc.edu.co*
- ORCID: 0000-0003-1046-467X
- Web of Science ResearcherID: NA
- Scopus Author ID: 57209807305
- Academic Homepage: https://www.researchgate.net/profile/Amaira-Corrales

Echeverría González, A., M.Sc., Professor, Departamento de Civil y Ambiental. Universidad de la Costa, Barranquilla Atlántico, Colombia.
- Email: *aecheverria@cuc.edu.co*
- ORCID: 0000-0002-0256-1130
- Web of Science ResearcherID: NA
- Scopus Author ID: 57218249185
- Academic Homepage: https://www.researchgate.net/profile/Ana-Echeverria-Gonzalez

HOW TO CITE THIS ARTICLE

Rodelo-Torrente, S.; Torregroza-Espinosa, A.C.; Moreno Pallares, M.; Pinto Osorio, D.; Corrales Paternina, A.; Echeverría-González, A., (2022). Soil fertility in agricultural production units of tropical areas. Global J. Environ. Sci. Manage., 8(3): 403-418.

DOI: 10.22034/gjesm.2022.03.08

url: https://www.gjesm.net/article_248238.html

Global J. Environ. Sci. Manage. 8(3): 419-436, Summer 2022, Serial #31

Global Journal of Environmental Science and Management
(GJESM)

Homepage: https://www.gjesm.net/

CASE STUDY

Optimization of solid waste collection system in a tourism destination

C. Le Dinh[1,2], T. Fujiwara[2], M. Asari[3], B. Nguyen Duy[2], S.T. Pham Phu[1,*]

[1] *The University of Danang – University of Technology and Education, 48 Cao Thang St, Hai Chau District, Danang City, Vietnam*

[2] *Graduate School of Environmental and Life Science, Okayama University, Japan*

[3] *Graduate School of Global Environmental Studies, Kyoto University, Yoshida-Honmachi, Sakyo-ku, Kyoto, Japan*

ARTICLE INFO

Article History:
Received 09 August 2021
Revised 26 October 2021
Accepted 03 December 2021

Keywords:
Geographic Information System
Hoi An
Optimization
Recovery recycling stations (RRSs)
Solid waste collection
Vehicle routing problem

ABSTRACT

BACKGROUND AND OBJECTIVES: Prior to the COVID-19 pandemic, Hoi An City was one of the most famous tourist destinations in the world. This led to a rapid increase in solid waste generation, leading to problems and challenges in solid waste collection and management. This problem is also being experienced by other developing countries of the world. Despite the existence of established waste management strategies, targets set for the collection of recyclable waste have not been met. This study introduces solutions to the problems and challenges faced by the waste management sector in Hoi An city and other developing countries. This study aimed to i) optimize the map of the recovery recycling stations in an urban community, ii) develop an effective solid waste collection system, and iii) provide management tools to enhance recycling activities, contributing to improving waste management in Hoi An city.
METHODS: The RRSs were integrated into a solid waste collection system in the urban communities of Hoi An City, were conducted through location-allocation analysis in a geographic information system environment. Routing problems of carts were solved in the combination of the rescheduling of existing solid waste collection activities in the study site. The economic evaluation by scenarios was also calculated for ten years to assess the feasibility of scenarios.
FINDINGS: Thirty-four locations were identified and optimized to accommodate the RRSs and new collection routes. The distances travelled and working time increased in proportion to the increase in waste separation effectiveness. Waste separation is vital to the effectiveness of the new solid waste collection system. The optimal solid waste practice model (in scenarios 2 and 4) revealed the positive results in improving the solid waste collection system, operating economy, and local adaptation.
CONCLUSION: This study redesigned the solid waste collection system to solve the current problems in the tourism destination of Hoi An city. This study contributed as a case study of integrating urban recovery recycling stations into optimizing a solid waste collection system in a tourism destination. Introducing strict waste separation was the pivotal first step in systematically upgrading the solid waste collection system in Hoi An City. This study's findings provide government officials and service providers with methods that can be applied to solve the problems faced by Hoi An city's existing solid waste collection and management system.

DOI: 10.22034/gjesm.2022.03.09

NUMBER OF REFERENCES	NUMBER OF FIGURES	NUMBER OF TABLES
37	10	2

*Corresponding Author:
Email: *ppstoan@gmail.com*
Phone: +849 8485 8827
ORCID: 0000-0002-5539-2852

Note: Discussion period for this manuscript open until October 1, 2022 on GJESM website at the "Show Article".

INTRODUCTION

The urgency for enhancements to the solid waste collection system (SWCS) has arisen due to the boom in the tourism industry. An increase in tourist numbers over recent years has brought about many environmental problems, specifically an increase in solid waste generation (Zambrano-Monserrate *et al.,* 2021). The upsurge in solid waste generation has increased the challenges faced in the solid waste management (SWM) of governments globally (Sharma, 2016). Hoi An City is categorized as a UNESCO World Heritage Site (Giang *et al.,* 2017). The upsurge in tourism-related activities has resulted in a dramatic increase in solid waste generation in Hoi An City (Song Toan *et al.*, 2018). This is the biggest challenge faced by SWM in Hoi An City. Solid waste collection (SWC) is one of the most critical components of an SWM system, accounting for between 50% and 90% cost of SWM (Das and Bhattacharyya, 2015). The SWCS in the tourism destination of Hoi An city (TDoHAC) has been facing many problems, namely illegal SWC that is not in line with current laws and procedures (Cuong *et al.*, 2021), improper gathering waste practices, and comingling separated solid waste (Song Toan *et al.*, 2019). The enhancement of the SWCS in TDoHAC was an urgency for tourism activities and sustainable development. Currently, the SWM national strategies in developing countries are focused on enhancing the recycling system towards a sound-material cycle society (Sharma Kapil and Jain, 2019). In Vietnam, solid waste is required to be separated into recyclable waste, food waste, and other waste by the new national environmental protection law (NASRV, 2020). Moreover, the adjustment of the national strategy for integrated management of solid waste also highlighted that SWM must consider the life cycle of solid waste from generation to final treatment (PMSRV, 2018). Despite the strategies towards the reversed logistic system for recyclable waste, the implementations in the developing countries have not achieved the expected results and faced many problems. The informal recycling system in developing countries may not be efficient in recovery and recycling (Zhu *et al.*, 2021). In Vietnam, about 10% of total domestic waste was recycled (The World Bank, 2018). A significant amount of recyclable waste was detected at the landfills (Song Toan *et al.*, 2021). The recycling activities are operated by the informal and private sectors, which are the scavengers, waste pickers, and junk shop collectors. Despite the vital role of the informal sector (Tong *et al.*, 2021), the operation of informal systems, particularly in developing countries, normally contributed to local pollutants (Bali Swain *et al.*, 2020). The informal recyclers usually adopted outdated technologies and improperly managed pollutants, leading to the environmental pollution of air, soil, and water (Yang *et al.*, 2018). The operation of informal sectors conflicts with the environmental goals of the government. So, the transition from informal to formal recycling system is inevitable. The integration of informal sectors into formal SWM system can enhance the management practices to ensure environmental protection in a systematic approach. This integration can also help local authorities in actualizing the strategies of SWM on waste separation and integrated SWM. The transition from the informal to the formal recycling system may lead to a restructuring of the municipal SWM system, whereby a redesign of the integrated collection system is inevitable. In this study, the Recycling Recovery Systems (RRSs) will be established to collect recyclable materials from resident areas. The integrated collection system is also studied and optimized. The changes were intentionally made to the entire system by integrating RRSs with the aim to formalize the reversed logistic system. Moreover, the optimization of collection routes falls typically under the umbrella of vehicle routing problem (VRP) and arc routing problem (ARP). ARP is used to SWC in case the solid waste is discharged along a street segment. ARP is considered as Capacitated ARP if there is a vehicle capacity constraint (Wøhlk, 2008). CARP is proven to be an NP-hardness (Nondeterministic Polynomial time-hardness) problem that requires many resources to solve (Liu *et al.*, 2021). The counterpart of ARP is VRP, which solves problems of SWC for truck fleets to travel between depots and collection points. This problem also falls into capacitated VRP if routing is constrained (Longo *et al.*, 2006). The optimization of collection routes of TDoHAC was conducted under the umbrella of VRP due to the existence of solving tool integrated into geographic information system (GIS) software. It is undeniable that SWM has spatial nature. Thus, taking advantage of new technologies,

namely GIS, should be prioritized. GIS is a popular tool in environment-related studies. There are many GIS applications used for optimization in SWM. TransCAD and ArcGIS have been the two most popular tools for optimization (Murray, 2021). ArcGIS Network Analyst (ANA) was applied for the optimization of SWCS. A study used ANA to analyze SWC and create optimal vehicle routes in three waste collection scenarios in Sfax, Tunisia. Thanks to ELECTRE III method, this study suggested an efficient and environmentally-friendly scenario for SWC (Amal *et al.*, 2020). ANA was also used to optimize the collection routes of dustbins in Vellore city, India. The method for choosing the transfer station was the median center following various design factors to minimize Euclidean distance. The optimized routes showed a reduction of 59.12% in traveled distances (Lella *et al.*, 2017). In Vietnam, a study conducted optimization of SWC with a focus on interrelationships between parameters in a dual-phase SWCS. A GIS-based dual-phase model was built, and total system cost was estimated in Hai Phong city, Vietnam. The model showed a 13.76% reduction in travel distance (Hoang Lan *et al.*, 2018). Another study proposed a model for optimizing municipal SWC in a static context and a dynamic context using GIS analysis, equation-based modeling, and agent-based modeling in Ha Giang city, Vietnam. The results showed a reduction in cost by 11.3% (Khanh *et al.*, 2017). Above-mentioning studies have strongly optimized the distances and time of collection routes without much concerning the waste separation program. This study designed and planned SWCS of TDoHAC based on the existing SWCS in considering its problems and challenges, especially solid waste separation program. The applications of ANA into optimizing SWC in Vietnam and Hoi An city were still limited. This would be the first effort to apply ANA to the optimization of SWCS in Hoi An city, Vietnam. Moreover, integrating the RRSs system into SWCS was considered a comprehensive solution for actualizing the SWM strategies and targets of collecting recyclable waste. This study integrated the collection of recyclable waste through urban RRSs into the official SWM system. This can be suggested as the first research to consider integrating informal recyclable waste collection into the official SWM system regarding optimization of SWCS in Vietnam and among developing countries. The aims of the current study was an effort to i) optimize the map of the recovery recycling stations (RRSs) in an urban community, ii) develop the solid waste collection system, and iii) provide management tools to enhance recycling activities and improve waste management in Hoi An city.

MATERIALS AND METHODS

Hoi An city is a famous tourist city in the central of Vietnam (Fig. 1). The downtown in the city's centre is the core tourism destination which attracts about 5,000 tourists per day. The tourist activities cause the high density of waste generation in the tourism area by 15 ton/km^2 (Song Toan *et al.*, 2019), which has brung many negative impacts on the environment and landscape of the world cultural heritage site.

The main component of solid waste in TDoHAC was kitchen waste, accounting for 46.8% of total waste generation. Tissue, garden waste, and plastic bags were also the significant components with 11.54%, 8.68%, and 7.84%, respectively. The other waste were glass (1.83%), incombustible waste (1.56%), combustible waste (1.13%), textile (2.88%), rubber (0.84%), leather (1.34%), as well as wood and bamboo (1.7%). Notably, the proportion of recyclable waste was 12.85%, including metal (1.16%), paper (3.79%), cardboard (3.9%), plastic (2.95%), and PET (1.05%) (Song Toan *et al.*, 2019). These types of waste were recyclable and valuable, which were usually sold to junk shops. Thus, the solid waste from TDoHAC illustrated a high potential for recycling. However, only a small amount of recyclable waste was collected by waste workers in TDoHAC, while the remaining large amount of recyclable waste was mainly collected by the informal sector (Song Toan *et al.*, 2019). This study made an effort to integrate the activities of the informal sector into formal SWM. Regarding SWCS, waste is collected daily by carts and trucks, two primary vehicles for SWC in TDoHAC. Carts are also used for collecting waste from street sweeping. There are two meeting points for carts, where carts gather to meet compaction trucks. The capacity of compaction trucks ranges from 6 to 9 m^3. There were four main sessions of SWC, Early morning, Morning, Afternoon, and Evening. The majority of the workload was conducted in the morning. The

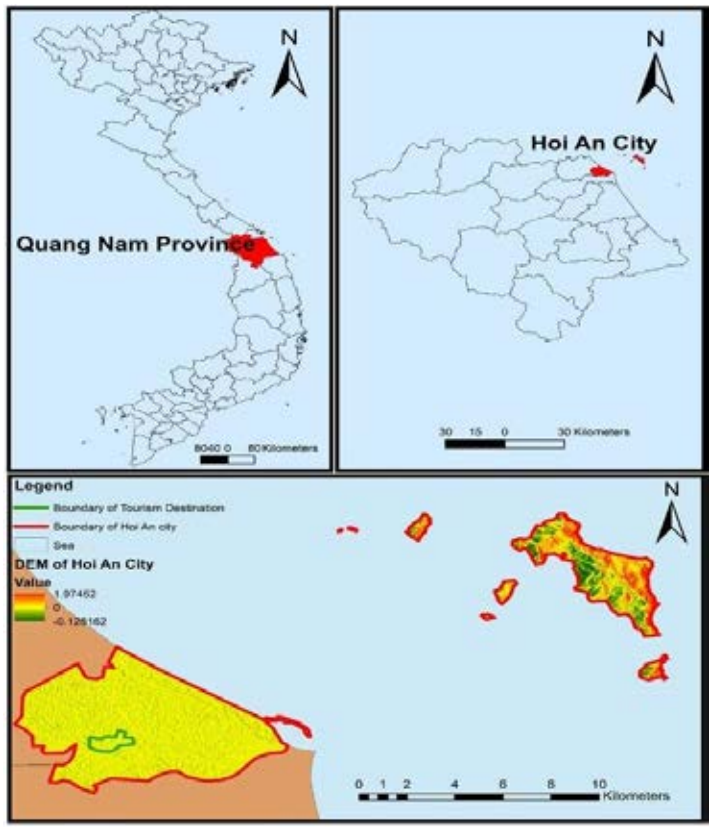

Fig. 1: Geographic location of the study area and topographic conditions of Hoi An city in Vietnam

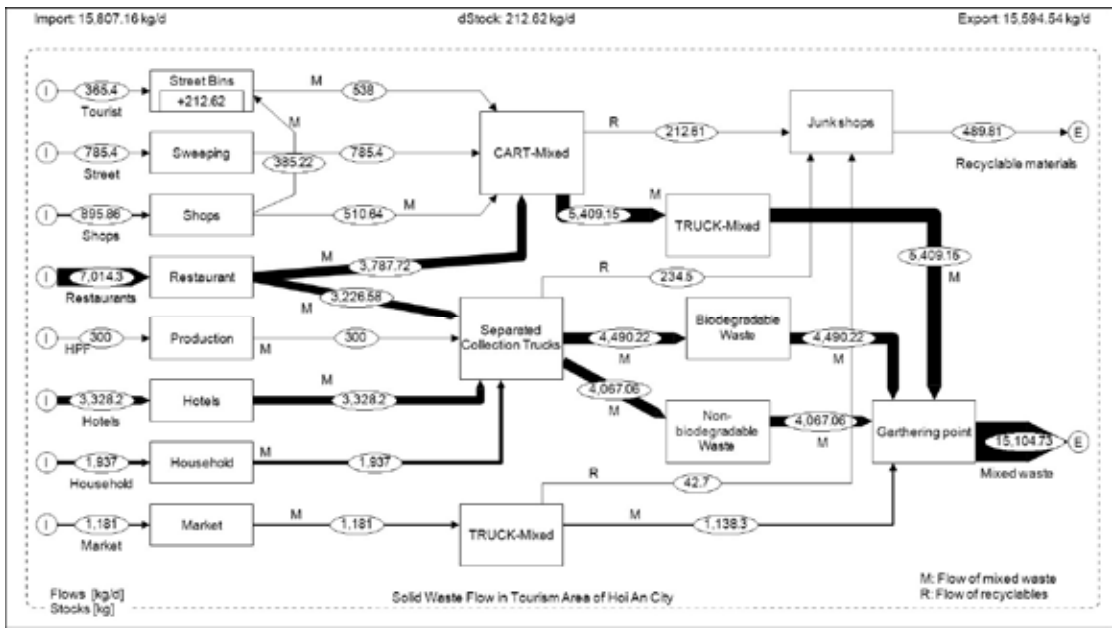

Fig. 2: The S0 (existing solid waste collection in TDoHAC) (Song Toan *et al.*, 2019)

amount of solid waste generated was 15,807.16 kg, and the amount of solid waste storage in TDoHAC was 212.62 kg (Fig. 2). Solid waste was mingled and discharged at a landfill or waste treatment facilities.

There were problems in the current SWCS. The separated waste was mixed before being transferred to waste treatment facilities due to no distinct routes for collecting separated solid waste. Solid waste was also illegally discharged into carts and trucks. The biodegradable waste, which harms tourism activities, was only collected every two days. The business sectors showed no enthusiasm for storing biodegradable waste, so that they illegally discharged biodegradable waste into carts or trucks on Tuesday, Thursday, and Saturday. Regulation on time of waste gathering (5:00 AM – 6:00 AM) was commonly violated because citizens gathered waste along the street right after the end of business activities, causing adverse effects on urban aesthetics and tourism activities (Cuong *et al.*, 2021). This led to an urge to optimize SWCS in TDoHAC.

The planned scenarios for solid waste collection

The planned scenarios (S) were found based on two concepts of minimization (S1 and S2) and optimization (S3 and S4). Four scenarios were constructed to address existing problems of SWCS in TDoHAC. The construction of these scenarios also considered new procedures about solid waste separation at source and the existing condition of waste treatment facilities of Hoi An city. Solid waste in Hoi An city is separated into recyclable waste and mixed waste (S1 and S2) as well as recyclable waste, combustible waste, and bio-degradable waste (S3 and S4). Despite concepts and scenarios, the municipal separation and collection of recyclable materials were compulsory due to Vietnamese strategies. This denoted the intense relationships between scenarios and national strategies on SWM.

Fig. 3 shows the waste flow of S1 and S2. The appearances of CART-Rec and RRSs were showed and no waste was stored. Solid waste was separated into recyclable waste and mixed waste. Moreover, the time for curbside collection of trucks were changed to start at approximately 0:15 AM. The amount of recyclable waste increased from 489.91 kg (S0) to 1028.58 kg (S1) and 1579.49 kg (S2). S1 and S2 addressed the problems of existing SWCS. No waste stored and daily collection of bio-degradable waste in TDoHAC can satisfy the demand of business sectors. Distinct routes for collecting recyclable waste meant that there would be no mixture of separated waste. The time frame for SWC was changed to meet the requirements of tourism activities.

Fig. 4 denotes the flow of solid waste for S3 and S4. No waste was kept in TDoHAC, being similar to S1 and S2. S3 and S4 were constructed for the increase in waste separation effectiveness. The SWCS in these two scenarios was more complex compared to other scenarios. There were appearances of CART-Com (carts for combustible waste collection), CART-2 Compartments (carts for sweeping in S3 and S4 in addition to CART-Rec. The trucks were distinctly used for collecting biodegradable waste (TRUCK-Bio), combustible waste (TRUCK-Com), and recyclable waste (TRUCK-Rec). Moreover, the time frames for curbside collection of trucks (biodegradable waste and combustible waste) were also changed, from 0:15 AM to 5:00 AM.

Process of optimization

This research was conducted in three main stages: preparing GIS data, Creating network datasets, and Using ANA to analyze the results (Fig. 5).

Stage 1: Preparing GIS data

This study is performed from December 14, 2019, until March 7, 2020, to collect the spatial data related to SWC in TDoHAC using 747A+ GPS Trip Recorders (Cuong *et al.*, 2021). Population information was collected by document review (Song Toan *et al.*, 2019). Slope and elevation data are not integrated into the model due to the plain research area (Fig. 1).

Stage 2: Creating network dataset

Firstly, the study manually chose the locations for candidate RRSs due to the below criteria.

- Existing locations of bins
- The governmental procedures must be satisfied
- The distances between locations are not larger than 250 meters (Zamorano *et al.*, 2009)
- RRSs must not impede citizens' commuting (Zamorano *et al.*, 2009)
- RRSs should be located in the passable roads (Zamorano *et al.*, 2009)

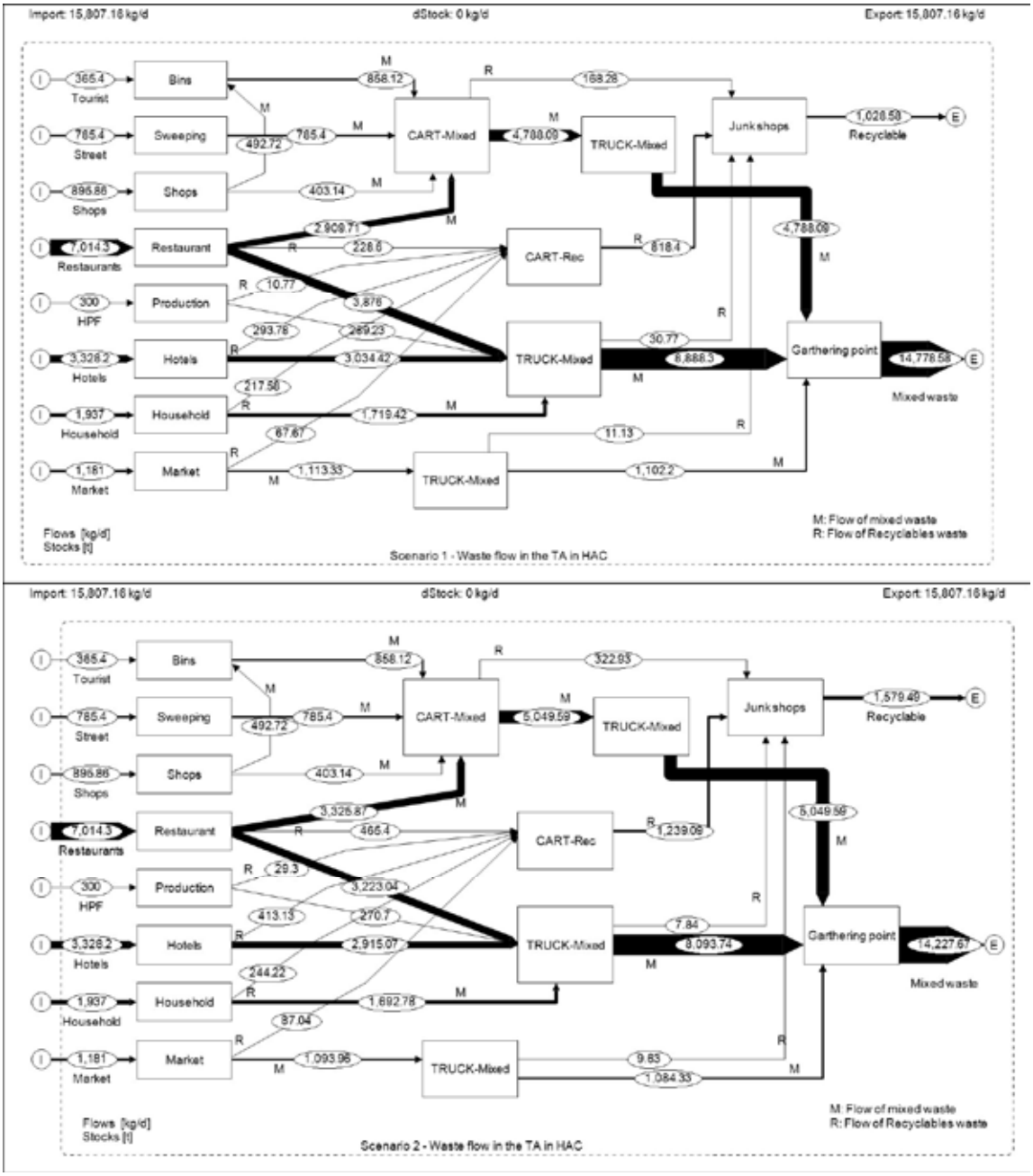

Fig. 3: Waste flow of S1 and S2

- RRSs must ensure the minimum distance from the demographic unit (DU) to the nearest bins (Pires *et al.*, 2018)
- The service area of RRSs must be maximized

At the end of this stage, the locations of the candidate RRSs were then used for location-allocation analysis in the following stages.

The second part is about routes for combustible waste collection by carts. Results of surveys denoted that the total amount of waste collected was similar among the existing four main routes of compaction

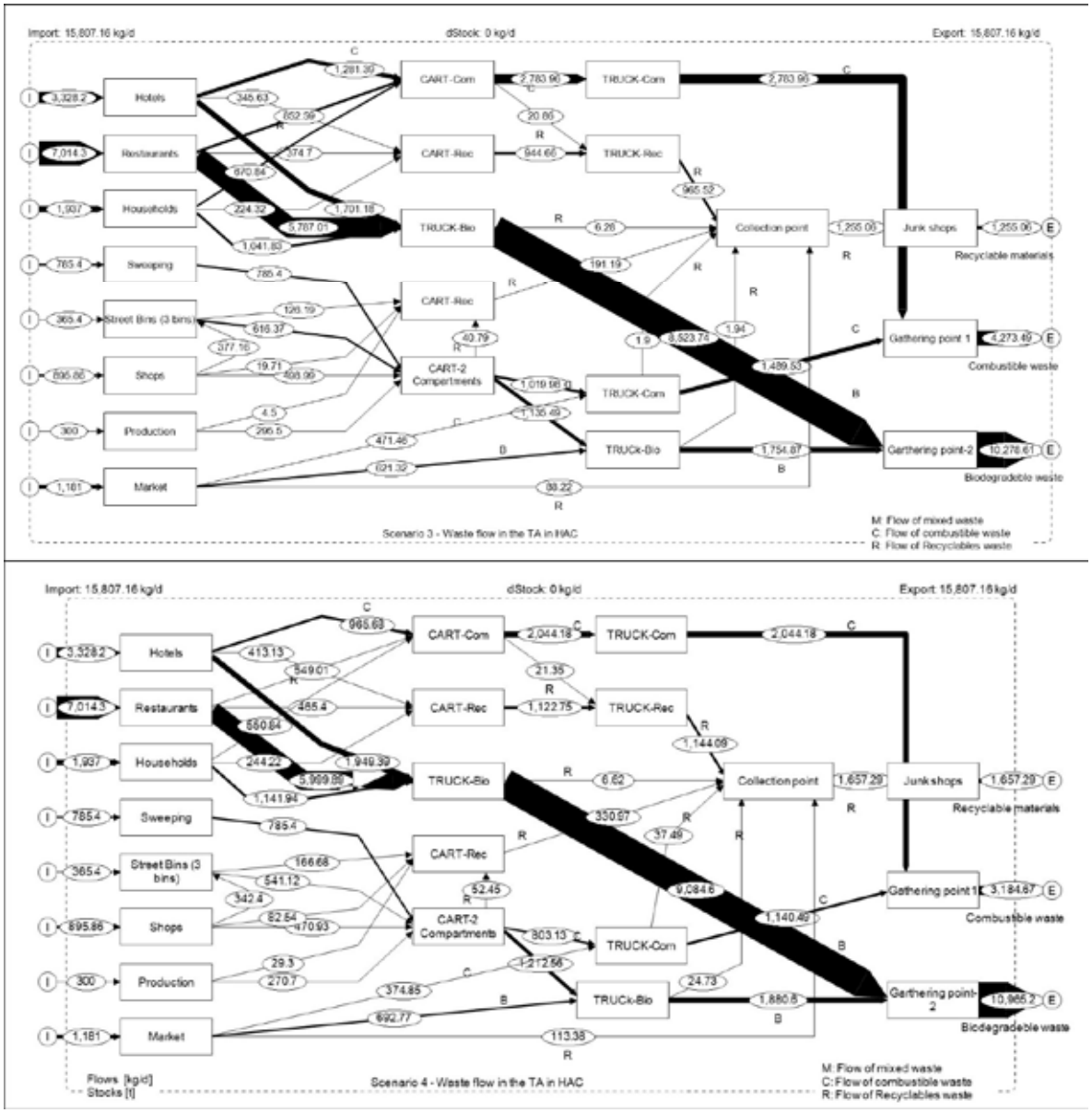

Fig. 4: Waste flow of S3 and S4

trucks. Thus new routes for combustible SWC by carts were built based on these routes. However, these routes were the curbside collection in densely populated areas. Thus optimization of the combustible SWC falls under the umbrella of ARP. The ARP was converted into VRP based on available conversion between ARP and VRP (Baldacci and Maniezzo, 2006). Line data was converted into point data, with the distance between points being five meters.

Stage 3: Using ANA to analyze the results

ANA solved VRP of compaction trucks and carts as well as optimized locations and numbers of RRSs. Handy carts started and ended at the parking areas. However, vehicles must be empty before coming

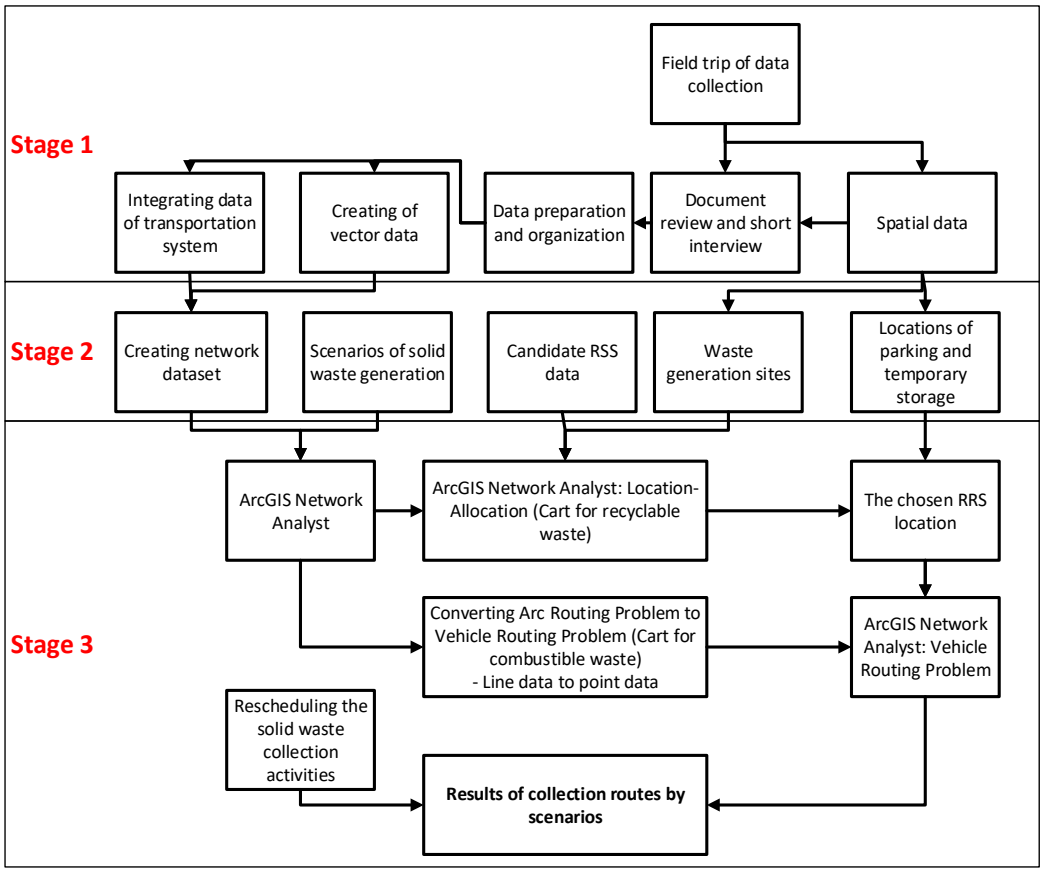

Fig. 5: The process of method applied

back to parking areas. This was not supported in ANA so that this problem was solved in two steps.

Step 1: The carts started at the parking area and collected waste from stations. Then, they moved to meeting points to discharge the waste. The average speed chosen was 3 km/h.

Step 2: The carts came back to the parking area from meeting points. The starting points were meeting points, while the endpoint was the parking area. The average speed chosen was 5 km/h (1.389 m/s) (Cavagna *et al.*, 1983).

Rescheduling existing SWCS was also conducted in this stage. The time frames of four compaction trucks (curbside collection) were changed to early morning. The routes of sweeping, compaction trucks (curbside collection) remained unchanged.

Economic assessment by scenarios

The cost-benefit analysis was calculated in ten years. The salary in the early morning was duplicated due to regulations on labour (GSRV, 2015). The average salary of drivers and workers was about 217 USD/month. 30.4 was the average number of days in a month. Moreover, the financial loss of SWM was about 17,007 USD/year (Song Toan *et al.*, 2019).

The economic benefits of applying new SWCS by scenarios were calculated using Eq. 1.

$$EB = B_{RW} + MRW - (IV + MR + OC_{Truck} + OC_{Cart}) \quad (1)$$

The money from selling recyclable waste was calculated using Eq. 2.

$$B_{RW} = A_{RW} . P_{RW} \quad (2)$$

Where;

B_{RW}: money from selling recyclable waste (USD).

A_{RW}: estimated amount of recyclable waste by scenarios
P_{RW}: the price of the recyclable waste

Prices were 634 USD/ton for metals, 95 USD/ton for plastics, and 90 USD/ton for paper (HAPWC, 2017). Metal, sellable plastics, and paper accounted for 1.16%, 4%, and 7.69% of waste generation in TDoHAC (Song Toan *et al.*, 2019). Thus the average price for recyclable waste was 141 USD. Fluctuation in the price of recyclable waste was assumed insignificant during the three years.

The money gained from reducing waste to landfill were calculated using Eq. 3.

$$MRW = RW + CW + BW \quad (3)$$

Where;
MRW: money gained from reducing waste to landfill
RW: money gained from reducing recyclable waste to landfill
CW: money gained from reducing combustible waste to landfill
BW: money gained from reducing biodegradable waste to landfill

The initial investments for RRS and CART-2 Compartments were calculated using Eq. 4.

$$IV = IV_{RRS} + IV_{Cart} \quad (4)$$

Where;
IV: Initial investment for RRS and CART-2 Compartments
IV_{RRS}: Initial investment for RRS (130 USD/RRS)
IV_{Cart}: Initial investment for CART-2 Compartments (130 USD/cart)

The costs for maintenance and repairing for RRS and CART-2 Compartments were calculated using Eq. 5.

$$MR = MR_{RRS} + MR_{Cart} \quad (5)$$

Where;
MR: Maintenance and repairing cost for RRS and CART-2 Compartments
MR_{RRS}: Maintenance and repairing cost for RRS
MR_{Cart}: Maintenance and repairing cost for CART-2 Compartments

The standard repair and maintenance rates of an RRS or a two-compartment cart were 15% per year (Hoang Lan *et al.*, 2018)

The operational costs for truck fleets were calculated using Eq. 6.

$$OC_{Truck} = Fuel + S_{Driver} + S_{W\_Truck} \quad (6)$$

Where;
OC_{Truck}: Operational costs for truck fleets
Fuel: Cost for additional distances that truck traveled (0.84 USD/km) (Hoang Lan *et al.*, 2018)
S_{Driver}: Salary for drivers
S_{W_Truck}: Salary for workers followed trucks

The operational costs for CART-Rec and CART-2 Compartments were calculated using Eq. 7.

$$OC_{Cart} = S_{W\_Rec} + S_{W\_2Com} \quad (7)$$

OC_{Cart}: Operational cost for CART-Rec and CART-2 Compartments
S_{W_Rec}: Salary for workers driving CART-Rec
S_{W_2Com}: Salary for workers driving CART-2 Compartments

RESULTS AND DISCUSSION

A total of 204 candidates were chosen for location-allocation analysis. Table 1 illustrates the results of the location-allocation analysis. The

Table 1: Results of location-allocation analysis for choosing RRS locations

Content of analysis	Maximum walking distance			
	100 m	150 m	180 m	200 m
Number of RRS	93	49	34	31
Number of Demographic Unit (DU)	8045	8045	8045	8045
Number of DU covered	7608	7980	8037	8037
Percentage of coverage (%)	94.57%	99.19%	99.90%	99.90%

numbers of RRS had inverse relationships with maximum walking distance and the number of DU covered. The number of RRSs decreased from 93 to 31 when the maximum walking distance increased from 100 meters to 200 meters as well as the number of DU covered increased from 7608 to 8037. TDoHAC is a crowded area with tourism activities so that the number of RRS must be minimized. Operational cost proportionally relates to the fluctuation in the number of dustbins or transfer stations (Höke and Yalcinkaya, 2020). The percentage of DU used designated dumping was reduced to 55.2% if the distance from DU to dumping sites was more than 200 m, and an increase of 1% in the distance led to a rise of 0.48% in improperly discharging waste (Wang *et al.*, 2018). The maximum distance of 180 m was chosen for the subsequent analysis of CART-Rec. This maximum distance was also 20 m larger than the optimal results of the city of Mashhad (Erfani *et al.*, 2017). The bins in the Mashhad were for mixed waste so that the maximum distance of 180 m would be over the requirement of the number of bins. However, in Hoi An city, RRSs were designed for recyclable material, in which the amount of waste would be far lesser. Moreover, the maximum distance of 180 m meat that the number of RRSs can be reduced compared to 150 m. Thus, a maximum distance of 180 m was chosen for TDoHAC due to existing local conditions.

The optimized collection routes by scenarios

Figs. 6, 7, 8, and 9 show that the SWCS was gradually more complex, from S1 to S4. The RRSs and collection routes of recyclable waste appeared in S1 (Fig. 6). The study integrated the system of RRSs and created collection routes for Cart-Rec in all four scenarios. This was an effort to make the collection of recyclable waste official in TDoHAC. Fig. 8 denoted the appearance of routes for combustible waste. The increase in the variety of vehicles for SWC was also denoted from S1 to S4 (Figs. 6, 7, 8, and 9).

The new collection routes can combat existing problems and challenges of the current SWCS in TDoHAC. Firstly, the solid was not stored in the TDoHAC. Solid waste was collected three times

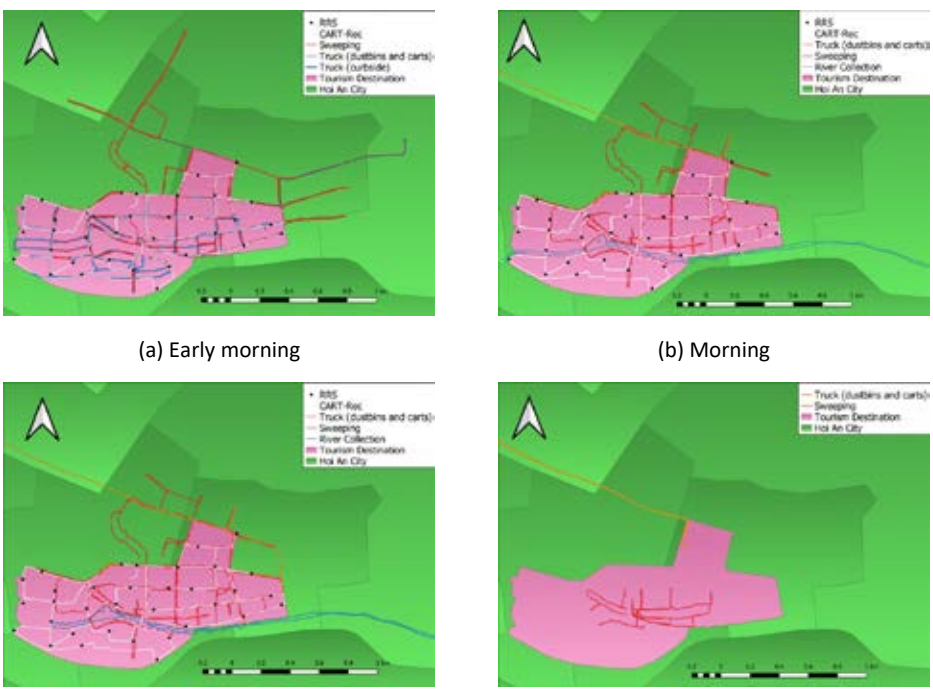

(a) Early morning (b) Morning

(c) Afternoon (d) Evening

Fig. 6: Collection route of S1

(a) Early morning

(b) Morning

(c) Afternoon

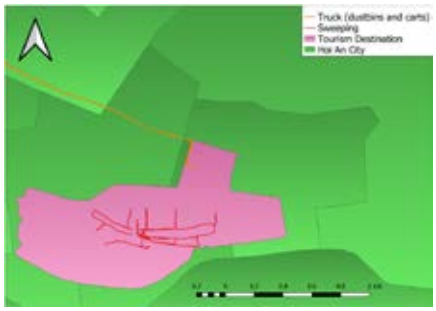

(d) Evening

Fig. 7: Collection route of S2

(a) Early morning

(b) Morning

(c) Afternoon

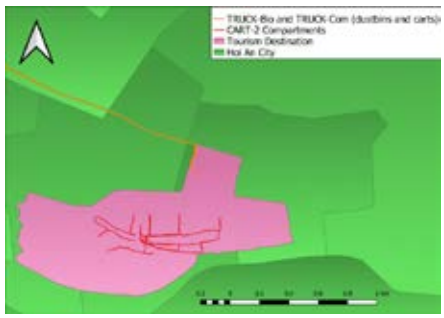

(d) Evening

Fig. 8: Collection route of S3

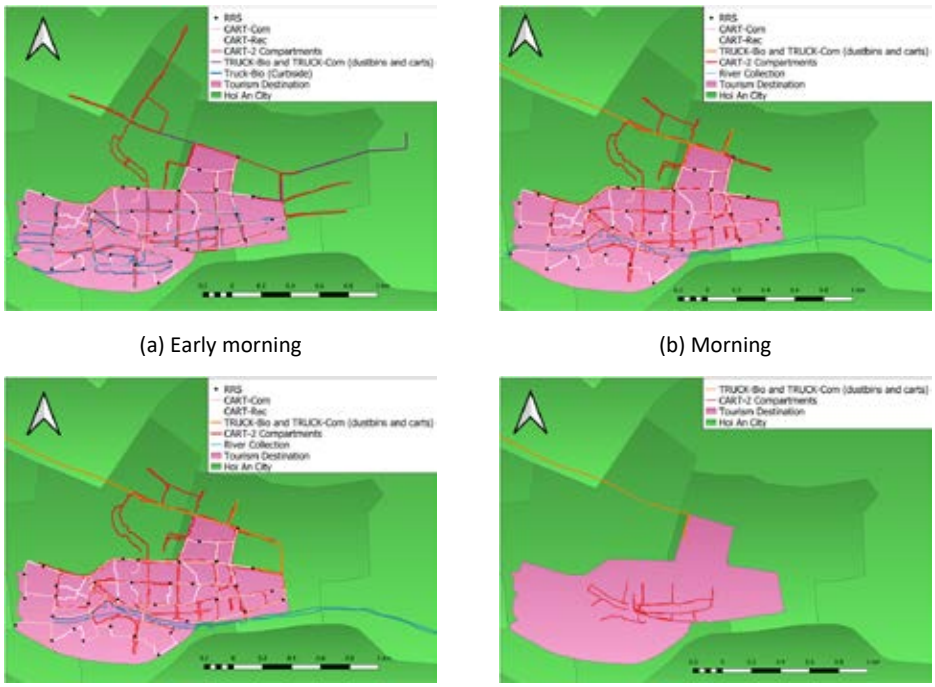

(a) Early morning (b) Morning

(c) Afternoon (d) Evening

Fig. 9: Collection route of S4

a day, meeting the demand of business sectors of no waste storage. This satisfied the demand from business sectors in the study site. The TDoHAC was in a high density of ancient buildings with small areas so that the solid waste storage in the study site was not welcomed. The new collection system solved the demand of business sectors. Secondly, the citizens' belief in solid waste separation program will be boosted. The current SWC practices of mixing waste after being separated led to the citizens' doubt on solid waste separation program. Regarding new collection system, there were different routes for the collection of separated waste in TDoHAC. The appearance of distinct routes would limit the commingling of separated waste. Thirdly, the new procedures for conducting solid waste separation were fulfilled. Solid waste was separated into two types in the minimization concept and three types in the optimization concept. This ultimately met the requirements of new Vietnamese regulations and strategies on SWM. Fourthly, the new SWCS can also minimize the risk of illegal collection due to rescheduling time frames and frequencies of SWC. The changes in the timeframes for the curbside collection by trucks to early morning also solved the existing improper waste gathering practices since the solid waste was soonly collected right after the end of business activities. Finally, the collection routes for urban RRSs system were created and optimized. The foundation of urban RRSs system was the first step for integrating the informal sector into the SWM. Thus, the optimized routes ensured the operation of these RRSs.

Table 2 illustrates information on SWCS by scenarios. Distance and time proportionally increased with the complexity of scenarios and the effectiveness of waste separation. Distance and time were largest in S4 that waste separation was most effectively conducted. Distance traveled by truck increased from 83.98 km (S0, S1, S2) to 89.7 km (S3, S4). In contrast, working time increased by three hours between S0, S1, S2, and S3, S4. Regarding carts, the total distance traveled increased from 160.82 km (S0) to 191.07 km (S1), 193.36 km (S2), 280.90 km (S3), and 290.98 km (S4) while working time increased from 172.89 hours (S0) to 174.99

Table 2: The information for the solid waste collection by scenarios

Content of analysis		S0		S1		S2		S3		S4	
		Truck	Cart	Truck	Cart	Truck	Cart	Truck	Cart	Truck	Cart
Distance (km/day)		83.98	160.82	83.98	191.07	83.98	193.36	89.77	280.90	89.77	290.98
Time (hour/day)		13.52	172.89	13.52	174.99	13.52	178.94	16.59	207.25	16.59	210.40
Labour (person/day)	Driver	4		4		4		5		5	
	Worker (Truck)	8		8		8		8		8	
	Worker (Cart)		52		63		65		81		83
Truck (trip/day)		8		8		8		11		11	
Traditional Cart (trip/day)			59		61		64		24		27
Two-compartment cart (trip/day)									52		52
Number of truck		5		5		5		5		5	
Number of traditional carts used			38		34		35		12		13
Number of two-compartment carts used									31		31

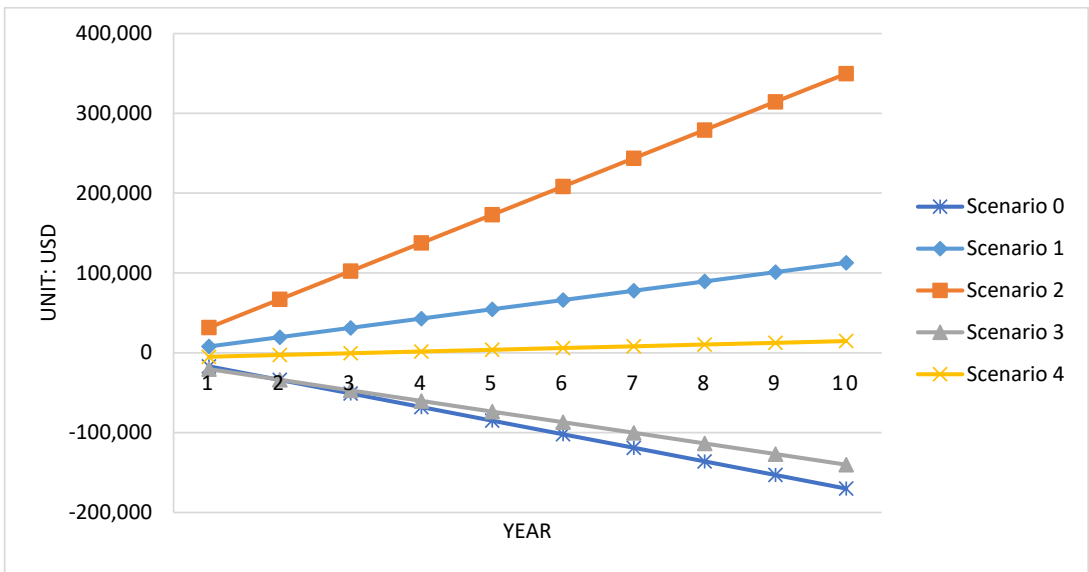

Fig. 10: Economic assessment by scenarios

hours (S1), 178.94 hours (S2), 207.25 hours (S3), and 210.40 hours (S4). The number of trips of carts increased approximately 30%, from 59 trips (S0) to 76 trips (S3) and 79 trips (S4). This increase was due to recyclable waste and combustible waste collection by traditional carts. The largest number of trips for carts in S3 and S4 belonged to the two-compartment carts, 52 trips a day. The combustible waste was also collected in sweeping (S3 and S4), leading to the change from traditional carts to two-compartment carts. The number of carts used fluctuated from 38 carts used in S0 to 34, 35 carts in S1 and S2 as well as 43 and 44 carts in S3 and S4. While traditional carts were popularly used in S1 (38 carts), S2 (34

carts), and S3 (35 carts), the two-compartment carts were dominantly used in S3 and S4, with 31 two-compartment carts in each scenario. The increase in complexity and numbers of new collection routes also led to a need for more workers and drivers and enhanced the management skills of the service provider's staff. In general, the implementation of new collection systems required more resources. The workload, working time, traveled distances, and the number of workers increased primarily in S2 and S4. The economic benefits of applying new collection systems would be the driving force for the service provider (Fig. 10). Moreover, the strategies and regulations on SWM were achieved. Thus, the tradeoffs for the changes would be acceptable.

Economic assessment by scenarios

Fig. 10 denotes the economic assessment by scenarios in TDoHAC. S2 marked the financial gain, while S0 (existing SWCS) indicated the highest financial loss in ten years. S0 showed the financial problems of the existing SWCS. Illegal SWC led to financial loss and detriments to the environment by increasing the amount of mixed waste discharged at the landfill. As a result, the enhancement of SWCS was an urgent need for TDoHAC. The effectiveness of waste separation illustrated a critical role in enhancing the SWCS. Regarding the minimization concept, the economic gain from conducting the new SWCS of S2 was approximately three times larger than S1. The recyclable waste in S2 was about 1.6 tons/day, while that of S1 was only about 1 ton/day. This was the explanation for the differences in financial gain between S1 and S2. In terms of optimization concept, the effectiveness of solid waste separation again showed a critical role. In S3, the financial gain was highly negative at -140,139 USD compared to S4 with 14,675 USD after ten years (higher effectiveness of solid waste separation at source). In S3 and S4, solid waste was separated into three types, namely recyclable waste, combustible waste, and biodegradable waste. A variety of waste types meant that the operational costs would increase due to the collection of combustible waste. However, the financial gain of S4 was positive despite the adverse financial gain in the initial three years. Additionally, the financial gain did not consider the benefits of selling compost produced from biodegradable waste due to its high economic value (Limon and Villarino, 2020). This showed that the optimization of SWCS was economically feasible; if any, the effectiveness of solid waste separation fulfilled the expectations of scenarios. These results were also similar to another study on the cost efficiency of selective collection. The cities conducting selective collection were more cost-efficient in spite of higher costs escalating (Campos-Alba *et al.*, 2021).

The cooperation of citizens and business sectors plays a vital role in the success of waste separation program and the implementation of a new collection system (Weekes *et al.*, 2021). The effectiveness and implementation of solid waste separation at source in Vietnam were the most serve problems (Lien *et al.*, 2021). Fortunately, citizens showed a positive attitude towards running the waste separation at source program if the separated waste could be collected daily (Song Toan *et al.*, 2019).

CONCLUSION

This study redesigned the SWCS due to the planned scenarios of SWM practice. The current problems of SWCS in TDoHAC were addressed. ANA was used to define new routes for CART-Rec, CART-Com, trucks and identify the optimal locations of 34 RRSs. The integration of new urban RRSs was analyzed and illustrated through the optimized process. The maximum distance of 180 m was chosen due to the constraints of social behaviours and requirements of tourism activities in TDoHAC. Thus 34 urban RRSs were identified and located in TDoHAC as the recovering facilities for recyclable waste. The establishment of RRSs was considered as the first effort to formalize activities of the informal sector in Hoi An city. ANA solved routing problems of carts and trucks in TDoHAC. The collecting distances and working time increased with effectiveness in waste separation. Total collecting distance by truck increased from 83.98 km (S0, S1, S2) to 89.7 km (S3, S4) while working time by truck increased by three hours between the group of S0, S1, S2 and the group of S3, S4. Regarding carts, total distance traveled increased from 160.82 km (S0), to 191.07 km (S1), 193.36 km (S2), 280.90 km (S3), and 290.98 km (S4) while working time increased from 172.89 hours (S0) to 174.99 hours (S1), 178.94 hours (S2), 207.25

hours (S3), and 210.40 hours (S4). The economic assessment results showed the positive results of applying the new collection system. S2 and S4 indicated the benefits of 349,652 USD and 14,675 USD after ten years. However, the effectiveness of solid waste separation was the precursor to the success of applying the novel collection systems. The failure in solid waste separation would also lead to unsuccess in improving the solid waste collection system. S3 showed a loss of 140,139 USD after ten years of application. Future studies should focus more on improving the effectiveness of solid waste separation at soure, which would be the challenge of many developing countries in the world. Governmental officials and service providers benefit from the findings on strategically managing SWCS to boost the effectiveness and efficiency of SWCS in Hoi An city. The two concepts of minimization (S1 and S2) and optimization (S3 and S4) and their tradeoffs were clearly illustrated to officers and managers in Hoi An city. Moreover, the concept of converting the informal sector into the formal sector would also be the solution for achieving the national strategies on SWM, especially the collection of recyclable waste towards the sound-material cycle society. This study contributed as a case study of the application of ANA and the integration of urban recovery recycling stations into the optimization of SWCS for a tourism destination. The novelty of this research was the integration of the informal sector into the SWM system to formalize the operation of recyclable collection in a systematic view. Despite the national strategies of developing countries towards a sound-material cycle society, the holistic practices have not been well mentioned and researched. This study was an effort to actualize the SWM strategies and national targets of collecting recyclable waste of developing countries towards a sound-material cycle society.

ACKNOWLEDGEMENT

This study was supported by Hoi An Public Work Company as well as financially supported by Graduate School of Environmental and Life Science, Okayama University and Graduate School of Global Environmental Studies, Kyoto University [Project GSGES20-10].

CONFLICT OF INTEREST

The authors declare no potential conflict of interest regarding the publication of this work. In addition, the ethical issues including plagiarism, informed consent, misconduct, data fabrication and, or falsification, double publication and, or submission, and redundancy have been completely witnessed by the authors.

OPEN ACCESS

PUBLISHER'S NOTE

ABBREVIATIONS

%	Percentage
3Rs	Reduce, reuse, and recycle
AM	After midnight
ANA	ArcGIS network analyst
ARP	Arc routing problem
CART-2 Compartments	Carts for sweeping in S3 and S4
CART-Com	Carts for collection combustible waste
CART-Rec	Carts for collecting recyclable carts
COVID-19	Coronavirus disease

DU	Demographic unit
Eq.	Equation
Fig	Figure
GIS	Geographic information system
GPS	Global positioning system
GSRV	Government of the Socialist Republic of Viet Nam
HAPWC	Hoi An Public Works Joint Stock Company
hour/day	Hour per day
kg	Kilogram
km	Kilometer
km/day	Kilometer per day
km/h	Kilometer per hour
km^2	Square kilometer
m	Meter
m/s	Meter per second
m^3	Cubic meter
NASRV	National Assembly of Socialist Republic of Viet Nam
NP-hardness	Nondeterministic Polynomial time-hardness
person/day	Person per day
PM	Past morning
PMSRV	Prime Minister of the Socialist Republic of Viet Nam
RRSs	Recyclable Recovering Stations
S	Scenario
SWC	Solid waste collection
SWCS	Solid waste collection system
SWM	Solid waste management
TDoHAC	The tourism destination of Hoi An city
trip/day	Trip per day
TRUCK-Bio	Trucks for collecting biodegradable waste
TRUCK-Com	Trucks for collecting combustible waste
TRUCK-Rec	Trucks for collecting recyclable waste
UNESCO	The United Nations Educational, Scientific and Cultural Organization
USA	The United States
USD	The United States dollar
USD/cart	United States dollar per cart
USD/km	United States dollar per kilometre
USD/month	United States dollar per month
USD/RRS	United States dollar per recyclable recovering station
USD/ton	United States dollar per ton
USD/year	United States dollar per year
VRP	Vehicle routing problem

REFERENCES

Amal, L.; Son, L.H.; Chabchoub, H.; Lahiani, H., (2020). Analysis of municipal solid waste collection using GIS and multi-criteria decision aid. Appl. Geomat., 12(2): 193-208 **(16 pages).**

Baldacci, R.; Maniezzo, V., (2006). Exact methods based on node-routing formulations for undirected arc-routing problems. Networks, 47(1): 52-60 **(9 pages).**

Bali Swain, R.; Kambhampati, U. S.; Karimu, A., (2020). Regulation, governance and the role of the informal sector in influencing environmental quality? Ecol Econ, 173: 106649 **(12 pages).**

Campos-Alba, C. M.; Garrido-Rodríguez, J. C.; Plata-Díaz, A. M.; Pérez-López, G., (2021). The selective collection of municipal solid waste and other factors determining cost efficiency. An analysis of service provision by spanish municipalities. Waste Manage., 134: 11-20 **(10 pages)**.

Cavagna, G.A.; Franzetti, P.; Fuchimoto, T., (1983). The mechanics of walking in children. J. Physiol., 343(1): 323-339 **(17 pages).**

Cuong, L.D.; Takeshi, F.; Misuzu, A.; Song Toan, P.P., (2021). Solid waste collection system in tourism destination – the status, problems, and challenges. Chem. Eng. Trans., 83: 43-48 **(6 pages).**

Das, S.; Bhattacharyya, B.K., (2015). Optimization of municipal solid waste collection and transportation routes. Waste Manage., 43: 9-18 **(10 pages).**

Erfani, S. M. H.; Danesh, S.; Karrabi, S. M.; Shad, R., (2017). A novel approach to find and optimize bin locations and collection routes using a geographic information system. Waste Management and Research, 35(7): 776-785 **(10 pages)**.

Giang, H.M.; Takeshi, F.; Song Toan, P.P., (2017). Municipal waste generation and composition in a tourist city - Hoi An, Vietnam. J. Jpn. Soc. Civ. Eng., 5(1): 123-132 **(10 pages).**

GSRV, (2015). Decree no. 05/2015/NĐ-CP on defining and providing guidance on the implementation of labor code **(25 pages).**

HAPWC, (2017). Daily reporting book. In: Hoi An Public Work Company.

Hoang Lan, V.; Kelvin Tsun Wai, N.; Damien, B., (2018). Parameter interrelationships in a dual-phase GIS-based municipal solid waste collection model. Waste Manage., 78: 258-270 **(13 pages).**

Höke, M. C.; Yalcinkaya, S., (2020). Municipal solid waste transfer station planning through vehicle routing problem-based scenario analysis. Waste Manage. Res., 39(1): 185-196 **(12 pages)**.

Khanh, N.-T.; Anh, N.-T.-N.; Doanh, N.-N.; Van, D.-T.-H., (2017). Optimization of municipal solid waste transportation by integrating GIS analysis, Equation-based, and Agent-based model. Waste Manage., 59: 14-22 **(9 pages).**

Lella, J.; Mandla, V.R.; Zhu, X., (2017). Solid waste collection/ transport optimization and vegetation land cover estimation using geographic information system (GIS): A case study of a proposed smart city. Sustainable Cities Soc., 35: 336-349 **(14 pages).**

Lien, T. T. K.; Allen, H. H.; Song Toan, P. P., (2021). Situation, Challenges, and Solutions of Policy Implementation on Municipal Waste Management in Vietnam toward Sustainability. Sustainability, 13(6): 3517-3533 **(16 pages)**.

Limon, M. R.; Villarino, C. B. J., (2020). Knowledge, attitudes and practices on household food waste: Bases for formulation of a recycling system. Glob. J. Environ. Sci. Manag., 6(3): 323-340 **(18 pages)**.

Liu, J.; Tang, K.; Yao, X., (2021). Robust Optimization in Uncertain Capacitated Arc Routing Problems: Progresses and Perspectives [Review Article]. IEEE Comput. Intell. Mag., 16(1): 63-82 **(20 pages)**.

Longo, H.; De Aragão, M.P.; Uchoa, E., (2006). Solving capacitated arc routing problems using a transformation to the CVRP. Comput. Oper. Res., 33(6): 1823-1837 **(15 pages).**

Murray, A.T., (2021). Contemporary optimization application through geographic information systems. Omega, 99: 1 - 15 **(15 pages).**

NASRV, (2020). Law No. 72/2020/QH14 dated November 17, 2020 on environmental protection. Hanoi, Viet Nam: National Assembly of Socialist Republic of Viet Nam.

Pires, A.; Martinho, G.; Rodrigues, S.; Gomes, M.I., (2018). Sustainable solid waste collection and management: Springer International Publishing.

PMSRV, (2018). Decision No. 491/QĐ-TTg dated May 7, 2018 on approval of adjustment of the national strategy for integrated management of solid waste to the year of 2025 and vision for 2050. Hanoi, Viet Nam: Prime Minister of the Socialist Republic of Viet Nam.

Sharma Kapil, D.; Jain, S., (2019). Overview of municipal solid waste generation, composition, and management in India. J. Environ. Eng., 145(3): 04018143 (04018141-04018118) **(18 pages).**

Sharma, R., (2016). Evaluating total carrying capacity of tourism using impact indicators. Global J. Environ. Sci. Manage., 2(2): 187-196 **(10 pages).**

Song Toan, P.P.; Minh Giang, H.; Takeshi, F., (2018). Analyzing SWM practices for the hotel industry. Global J. Environ. Sci. Manage., 4(1): 19-30 **(12 pages).**

Song Toan, P.P.; Takeshi, F.; Minh Giang, H.; Dinh, P.V., (2019). SWM practice in a tourism destination – The status and challenges: A case study in Hoi An City, Vietnam. Waste Manage. Res., 37(11): 1077-1088 **(12 pages).**

Song Toan, P.P.; Takeshi, F.; Naoya, A.; Cuong, L.D.; Giang, H.M.; Dinh, P.V., (2021). Analyzing the characterization of municipal solid waste in Da Nang City, Vietnam. Chem. Eng. Trans., 83: 241-246 **(6 pages).**

The World Bank, (2018). Solid and industrial hazardous waste management assessment—options and action area to implement the national strategy. 1818 H Street NW, Washington, DC 20433, USA: World Bank Publications, The World Bank Group.

Tong, Y.D.; Huynh, T.D.X.; Khong, T.D., (2021). Understanding the role of informal sector for sustainable development of municipal SWM system: A case study in Vietnam. Waste Manage., 124: 118-127 **(10 pages).**

Wang, F.; Cheng, Z.; Reisner, A.; Liu, Y., (2018). Compliance with household SWM in rural villages in developing countries. J. Cleaner Prod., 202: 293-298 **(6 pages).**

Weekes, J. G.; Musa Wasil, J. C.; Malave Llamas, K.; Morales Agrinzoni, C., (2021). Solid waste management system for small island developing states. Glob. J. Environ. Sci. Manag., 7(2): 259-272 **(14 pages)**.

Wøhlk, S., (2008). An approximation algorithm for the capacitated arc routing problem. Open Oper. Res. J.(2): 8-12 **(5 pages)**.

Yang, H.; Ma, M.; Thompson, J. R.; Flower, R. J., (2018). Waste management, informal recycling, environmental pollution and public health. J. Epidemiology and Community Health, 72(3): 1-7 **(8 pages)**.

Zambrano-Monserrate, M. A.; Ruano, M. A.; Ormeño-Candelario, V., (2021). Determinants of municipal solid waste: a global analysis by countries' income level. Environ. Sci. Pollut. Res., 28(44): 62421-62430 **(10 pages)**.

Zamorano, M.; Molero, E.; Grindlay, A.; Rodríguez, M.L.; Hurtado, A.; Calvo, F.J., (2009). A planning scenario for the application of geographical information systems in municipal waste collection: A case of Churriana de la Vega (Granada, Spain). Resour. Conserv. Recycl., 54(2): 123-133 **(11 pages).**

Zhu, Y.; Zhang, Y.; Luo, D.; Chong, Z.; Li, E.; Kong, X., (2021). A review of municipal solid waste in China: characteristics, compositions, influential factors and treatment technologies. Environ. Develop. Sustainability. 23(5): 6603-6622 **(20 pages).**

AUTHOR (S) BIOSKETCHES

Le Dinh, C., M.Sc., *Graduate School of Environmental and Life Science, Okayama University, Japan.*
- *Email: cuongldrs@gmail.com*
- *ORCID: 0000-0002-5229-6953*
- Web of Science ResearcherID: ABE-3283-2021
- Scopus Author ID: 57222026956
- Homepage: https://www.gels.okayama-u.ac.jp/en/intro/division/resource_e.html

Fujiwara, T., Ph.D., Professor, *Graduate School of Environmental and Life Science, Okayama University, Japan.*
- *Email: takeshi@cc.okayama-u.ac.jp*
- *ORCID: 0000-0000-0000-0000*
- Web of Science ResearcherID: B-1873-2011
- Scopus Author ID: 35407437200
- Academic or organizational link: https://researchmap.jp/read0013802/?lang=english

Asari, M., Ph.D., Associate Professor, Graduate School of Global Environmental Studies, Kyoto University, Japan.
- *Email: mezase530@gmail.com*
- *ORCID: 0000-0003-3233-0154*
- Web of Science ResearcherID: NA
- Scopus Author ID: NA
- Academic or organizational link: https://www.gels.okayama-u.ac.jp/en/intro/division/resource_e.html

Bao, N. D., Engineer, *Graduate School of Environmental and Life Science, Okayama University, Japan.*
- *Email: baoduy.2196@gmail.com*
- *ORCID: 0000-0002-8076-6975*
- Web of Science ResearcherID: NA
- Scopus Author ID: NA
- Homepage: https://www.gels.okayama-u.ac.jp/en/intro/division/resource_e.html

Song Toan, P.P., Ph.D., Assistant Professor, *The University of Danang – University of Technology and Education, 48 Cao Thang St, Hai Chau District, Danang City, Vietnam.*
- *Email: ppstoan@gmail.com*
- *ORCID: 0000-0002-5539-2852*
- Web of Science ResearcherID: E-9998-2019
- Scopus Author ID: 57201079513
- Homepage: http://scv.udn.vn/ppstoan/

HOW TO CITE THIS ARTICLE

Cuong, L.D.; Fujiwara, T.; Asari, M.; Bao, N.D; Song Toan, P.P., (2022). Optimization of solid waste collection system in a tourism destination. Global J. Environ. Sci. Manage., 8(3): 419-436.

DOI: 10.22034/gjesm.2022.03.09

url: https://www.gjesm.net/article_247731.html

Global J. Environ. Sci. Manage. 8(3): 437-448, Summer 2022, Serial #31

Global Journal of Environmental Science and Management
(GJESM)

Homepage: https://www.gjesm.net/

CASE STUDY

Immobilization of resin photocatalyst in removal of soluble effluent organic matter and potential for disinfection by-products

E.N. Hidayah[1*], R.B. Pachwarya[2], O.H. Cahyonugroho[1]

[1] *Department of Environmental Engineering, Universitas Pembangunan Nasional Veteran Jawa Timur, Indonesia*

[2] *Department of Chemistry, Motilal Nehru College, University of Delhi, Delhi, India*

ARTICLE INFO

Article History:
Received 09 September 2021
Revised 16 November 2021
Accepted 19 December 2021

Keywords:
Disinfection by-products
Dissolved organic matter
Immobilized photocatalyst
Resin

ABSTRACT

BACKGROUND AND OBJECTIVES: The existence of organic matter is one of the main issues for wastewater reclamation since chlorination is applied most frequently before use wastewater reclamation for many purposes. One of the eco-friendly and effective methods is using innovative material through resin immobilized heterogeneous photocatalyst, which is based on the principle of advanced oxidation processes. Resin immobilized photocatalyst has been using for pollutant reduction, however lack of studies focused on dissolved effluent organic matter and its impact on the formation carcinogenic as by-product of water or wastewater treatment. This study aims to characterize organic matter by resin immobilized photocatalyzed titanium dioxide and zinc oxide and to determine its effectiveness in removing organic matter and potential for disinfection by-products in treated wastewater compare with resin only.
METHODS: The bulk parameters, including total organic carbon, aromatic organic carbon as ultraviolet at 254 nm wavelength and specific ultraviolet absorbance value, and disinfection by-products formation potential, including trihalomethanes and haloacetic acids concentration was measured.
FINDINGS: The results present that all materials could remove organic carbon in the range 58.18% - 93.45%, aromatic organic carbon removal 48.77% - 76.51%, and specific ultraviolet absorbance value decreased into less than 2 L/mg-m after longer contact time. Disinfection by-products formation potential concentration removal decreased and indicated the consistency results with bulk parameters removal. Resin immobilized photocatalyzed zinc oxide performed a higher efficiency removal than resin immobilized photocatalyzed titanium dioxide and resin only.
CONCLUSION: This study exhibited the performance of resin immobilized photocatalyst with titanium dioxide and zinc oxide in removing dissolved organic matter and to control the formation of disinfection by-products. A combination between bulk parameters and disinfection by-products formation potential removal concluded that the aromatic structure, was mainly haloacetic acids precursors, while the non-aromatic organic fraction was probably trihalomethanes precursors.

DOI: 10.22034/gjesm.2022.03.10

NUMBER OF REFERENCES	NUMBER OF FIGURES	NUMBER OF TABLES
29	5	1

*Corresponding Author:
Email: *euisnh.tl@upnjatim.ac.id*
Phone: +62812 1787 0003
ORCID: 0000-0003-2055-3051

Note: Discussion period for this manuscript open until October 1, 2022 on GJESM website at the "Show Article".

INTRODUCTION

Wastewater reclamation has been an alternative way for conserving water resources for sustainable usage. It will continue to be the advantage of industries since it will reduce operational costs and decrease wastewater discharge quantity. Several methods have been designed for wastewater reclamation to remove organic matter using membrane filtration, adsorption onto activated carbon, chemical oxidation, removing suspended solids by filtration, removing nutrients by biological process, and removing pathogen disinfection processes (Englande *et al.,* 2015). However, the usage of cost-effective, eco-friendly, and sustainable agents such as electrons, microorganisms, sunlight, and enzyme has been applied to degrade pollutants in the most effective ways to completely resolve the requirements for the quality of effluent wastewater reclamation (Yadav *et al.,* 2019). The chlorination method, wastewater disinfection which is regarded as costly processes, is most frequently applied before use wastewater reclamation for many purposes. It is applied to protect humans against exposure to waterborne pathogenic microorganisms (Nieuwenhuijsen *et al.,* 2009). However, the reaction between the existence of organic matter in treated water/wastewater and chlorine or the other chemical disinfection can rise the formation of carcinogenic and disinfection by-products (DBPs) that are possibly detrimental to human and aquatic organisms (Liang and Singer, 2003; Bond *et al.,* 2012; Hidayah *et al.,* 2016). Even tertiary-treated wastewater can contain high total nitrogen (TN), and it lead to the other species of DBPs formation which caused by nitrogen, such as nitrosodimethylamine or NDMA (Najm and Trussell, 2001), and a high organic carbon concentration can conduct to the formation of numerous chlorinated DBPs species after exposure to chlorine (McBean *et al.,* 2010). Although chlorine toxicity can be anticipated by dechlorinating the effluent before its usage, it does not reduce DBPs concentration (Verdugo *et al.,* 2020). Therefore, it is necessary to consider the selected technology that could simultaneously reduce organic matter and remove pathogens during wastewater reclamation treatment. The alternatives of the greenness and efficiencies processes are an integration of nanotechnology with the conventional technique to enhance the quality of effluent wastewater treatment. Ion exchange using resin technology is one of the promising physical treatment process to remove pollutant (Cornellisen *et al.,* 2008). Resin is mainly used as ion exchange materials which are high molecular weight insoluble polyelectrolytes that can release counter ions to trap equally charged ions from surrounding liquid. Less information about harmful effect of resin has been reported, probably due to the usage of resin has been managed well. At the same time, it is unable to remove or break out the pollutants when solely utilized thoroughly. Using a new innovative material through resin immobilized heterogeneous photocatalyst with ultraviolet (UV) light or sunlight is based on the principle of advanced oxidation processes (AOPs) for wastewater treatment is an alternative material that could be applied in advanced technologies (Pachwarya and Meena, 2011; Bethi *et al.,* 2016). The developed photocatalyst Methylene Blue Immobilized Resin Dowex-11 (MBIRD11) has been studied as an alternative process to remove high pollutants. However, it has not yet been opportunely implemented because of the economic issues and problems related to separating photocatalyst particles from the suspension after treatment (Pachwarya and Meena, 2011). The oxide semiconductor photocatalysts, such as titanium dioxide (TiO_2), have performed to be the most widely implemented due to their strong oxidizing power, long-term photostability, and non-toxicity (Uyguner *et al.,* 2017). Recently, zinc oxide (ZnO) has been applied as an alternative photocatalyst to TiO_2 as it has the same bandgap energy and suitable highest quality of electrical, optical and mechanical properties but shows a higher efficiency of absorption across a significant compound of the solar spectra when compared to TiO_2 (Ong *et al.,* 2018). In this study, the removal of bulk parameters of organic matter from tofu wastewater used for reclaimed water was investigated on resin only and resin immobilized with two different photocatalysts, namely TiO_2 and ZnO. Bulk parameters includes organic matter parameters through quantitative analysis,and qualitatively analysis through high performance size exclusion chromatography, which is fractionated organic matter based on its molecular weight. Fluorescence spectroscopy could assess organic matter based on its fluorophores organic matter (Sillanpää *et al.,* 2015; Hidayah *et al.,*

2016). The results will be related to DBPs formation potential (DBPFP), including haloacetic acids (HAAs) and trihalomethanes (THMs). Roughly, this study exhibited characterization of organic matter and its impact on the possibility of the formation halogenated organic carbon through resin treatment. The aims of the current study is to characterize organic matter by resin immobilized photocatalyzed TiO_2 and ZnO and determine the effectiveness of resin immobilized photocatalyst TiO_2 and ZnO in removing organic matter and in reducing DBPFP of treated wastewater. This study has been carried out in Water Laboratory of University Pembangunan Nasional Veteran Jawa Timur Indonesia in 2021.

MATERIALS AND METHODS

This study used source water from the effluent of the settling tank after the activated sludge process in the tofu wastewater treatment plant in Surabaya, Indonesia, which was collected in July 2021. The first step was preparing resin-immobilized photocatalyst TiO_2 (RIP-TiO_2) and ZnO (RIP-ZnO) with ratio photocatalyst over Dowex-11 resin 1:10 in 1000 mL distilled water and shake well in the dark place for three days in order to complete immobilization. Further, filter both ZnO and TiO_2 immobilized resin from the solution, cleanse the resin with deionized water twice and utilize it as a photocatalyst (Pachwarya and Meena, 2009). The second step was experimenting with a simple photocatalytic reactor. Source water samples 1500 mL were put on the reactor mixer with three samples tested at a time, and 15 gram (g) of original Dowex-11 resin, 15 g of RIP-TiO_2, and 15 g of RIP-ZnO was added and mixing at 50 rpm. Treated samples were collected twice every 30 – 60 minutes for 15 hours and filtered through a 0.45 µm cellulose acetate filter (Toyo Roshi, Japan) before further analysis. All samples have to be filtered in order to remove particulate organic matter, since this study focus on dissolved organic matter. The raw sample and treated sample were quantified for bulk parameters, a quantitative parameters to measure dissolved organic matter, such as total organic carbon (TOC), ultraviolet absorbance for aromatic carbon as detected at 254 nm (UV_{254}), according to protocol Standard Methods (APHA, 2012), and specific UV absorbance (SUVA) value with regard to the UV_{254} concentration over TOC concentration (Edzwald and Tobiason, 2011). Measurement of aromatic organic matter has been well known at wavelength 254 nm, TOC quantified the dissolved organic carbon concentration, while SUVA value identified hydrophobicity and hydrophilicity organic matter (Sillanpää *et al.*, 2015). TOC was measured by using TOC Analyzer 5000A, Shimadzu. UV_{254} was quantified by using a UV/visible (UV/vis) spectrophotometer (Carry 100 Bio UV-Visible Spectrophotometer). Analysis of DBPs formation was initiated by adding natrium hydroxide (NaOH) or sulfuric acid (H_2SO_4) solution (Merck, Germany), then adding an amount of phosphate buffer solution (0.8 M, Merck, Germany), for keeping the pH value of samples at 7.0 ± 0.2. In order to ensure free residual chlorine existed 1 mg/L at 25 °C incubation period in the end of a seven days, then an adequate amount of 30 mg Cl_2/mL sodium hypochlorite solution (Merck, Germany) was spiked into the samples. the DPD ferrous method was applied to measure residual chlorine (APHA, 2012), then 0.04 M sodium thiosulfate solution (Merck, Germany) was added to dechlorinated samples. The purge and trap module (Model LCS-2000, Tekmar USA) and an electron capture detector (ECD) was installed with packed-column gas chromatographic (GC) method using a Model 3400 GC, Varian, USA was conducted to analyze trihalomethanes (THMs) concentration. In addition, haloacetic acids (HAAs) involved liquid-liquid extraction with methyl tertiary butyl ether (MTBE) and esterification with diazomethane before GC-ECD analysis. The percentage efficiency removal of TOC, UV254, THMs, and HAAs was calculated according to the initial concentration minus the effluent concentration and the result was divided by the initial concentration. Further, those percentage data were plotted into the graph, while the SUVA value was plotted on the graph directly without percentage removal because the value is used to indicate the hydrophobicity and hydrophilicity properties of dissolved organic matter.

RESULTS AND DISCUSSION

Bulk parameters of dissolved organic matter removal by resin immobilized photocatalyst

Characteristic effluent organic matter of the settling tank after activated sludge process in the tofu wastewater treatment plant has a high TOC concentration (17.24 mg/L), high UV_{254} concentration (0.5514/cm), and SUVA value 3.1984 L/mg/m. The

initial concentration of bulk parameters indicates that tofu wastewater has high dissolved organic matter and content of mixture aromatic humic substances-like, mixture hydrophobicity, and a mixture of molecular weight. This study measured the organic content in terms of BOD and COD, though it does not the main parameters in this study. BOD and COD concentration is 710 mg/L and 1550 mg/L, respectively. The waste from tofu processing usually has a high amount of organic substances, in term of BOD is about 600-1000 mg/L and COD is about 1500-3000 mg/L, or approximate TOC 15-30 mg/L (Hidayah *et al.*, 2016). Figs. 1 and 2 show the removal of TOC and UV_{254} of tofu wastewater after treatment by using resin, RIP-TiO_2, and RIP-ZnO. Those data were collected from dosage 15 gram of each treatment and the process was at indoor room and under room temperature. Firstly, the results show that resin, RIP-TiO_2, and RIP-ZnO could remove dissolved organic matter and aromatic organic matter, as compared at the same time sampling. All materials have performed their efficiency in removing organic matter in higher percentage removal than aromatic organic carbon. TOC has been removed with percentage value 58.18% - 93.45%, while UV_{254} has been occupied with percentage removal 48.77% - 76.51%. The percentage reduction was quite significant although the effluent quality standard for TOC and UV_{254} has not being provided in the national regulation. TOC indicates total dissolved organic carbon, which included aromatic and aliphatic compounds, hydrophobic and hydrophilic compounds, humic substances-like and non-humic substances-like. Meanwhile, UV_{254} indicates organic matter that contains aromatic rings or unsaturated double bonds in their molecular structures. Most organic matter has been composed of aromatic carbon double bonds (Sillanpää *et al.*, 2015; Hidayah *et al.*, 2016). It is reasonable that TOC has been removed in a higher percentage than UV_{254} because TOC represents whole dissolved organic carbon. Comparison between percentage removal of TOC and UV_{254} has pointed out the removal amount of aliphatic compound. It seems that an aliphatic compound has a lower removal than aromatic compound in the resin and resin immobilized. In some cases, low resin and resin immobilized photocatalyst removal might be due to competition with non-targeted ions (Finkbeiner *et al.*, 2018). Secondly, resin and resin immobilized photocatalyst showed better performance during a longer contact time. TOC removal up to 50% after longer contact time and depends on the material used, such as RIP-ZnO took about 2.5 hours, RIP-TiO_2 needed a longer time about 3.5 hours, and resin only spent about 9 hours. UV_{254} removal took about 6 hours, 8 hours, and more than 15 hours by using RIP-ZnO, RIP-TiO_2, and resin only, respectively. A longer contact time resulted in a better removal and found the optimal time of contact between resin immobilized photocatalyst and raw samples were more than 10 hours. In comparison, resin without photocatalyst seems to have a longer contact time than usual and lower efficiency. Photocatalyst technology was initiated by the generation of electron/hole pairs through excitation by photons. Further, it was able to conduct with oxygen and water to produce reactive oxidative species (ROS), highly reactive with many pollutants, including organic matter (Ye *et al.*, 2019).

Third, TOC removal seems a state that reached a stable condition after 10 hours of processing time. It means that resin and resin immobilized photocatalyst have almost its capacity in removing dissolved organic matter. Meanwhile, resin and resin immobilized photocatalyst indicates a higher capacity to remove UV_{254} than TOC because the graph line does not exhibit equilibrium conditions at a contact time of more than 10 hours. Previous studies suggested that an increase of organic matter reduction through resins was affected by the structure of resin, because the larger organic matter species is easier to entry due to open structures (Bolto *et al.*, 2002). In addition, the selectivity of the resins increased with an increase in the number of carbon atoms and in the number of aromatic rings in the organic anion around the exchange site (Graf *et al.*, 2014). Fourth, a comparison between resin and resin immobilized photocatalyst revealed that resin immobilized has a higher removal than resin only, and even RIP-ZnO performed a slightly higher removal of TOC and UV_{254} than RIP-TiO_2. The high photocatalytic efficiency of ZnO and TiO_2 has been well known because both photocatalytic exhibit an appropriate band gap of about 3.2 eV. However, the ZnO photocatalyst performed slightly higher than TiO_2 photocatalyst because of the better crystallinity of the ZnO, which leads to better photocatalytic degradation. ZnO has a hexagonal

crystalline structure, and it is favorable to the electron and hole transport in the resin material. On the other hand, TiO_2 has an amorphous structure, and it's less favorable for the charge carrier diffusion (Ishchenko *et al.,* 2016). Fig. 3 shows the SUVA value of source water over time during treatment using resin, RIP-TiO_2, and RIP-ZnO. The SUVA value of tofu wastewater decreased gradually to 2.182, 1.818, 1.566 L/mg/m under treatment processes by using resin, RIP-TiO_2, RIP-ZnO, respectively. It indicates

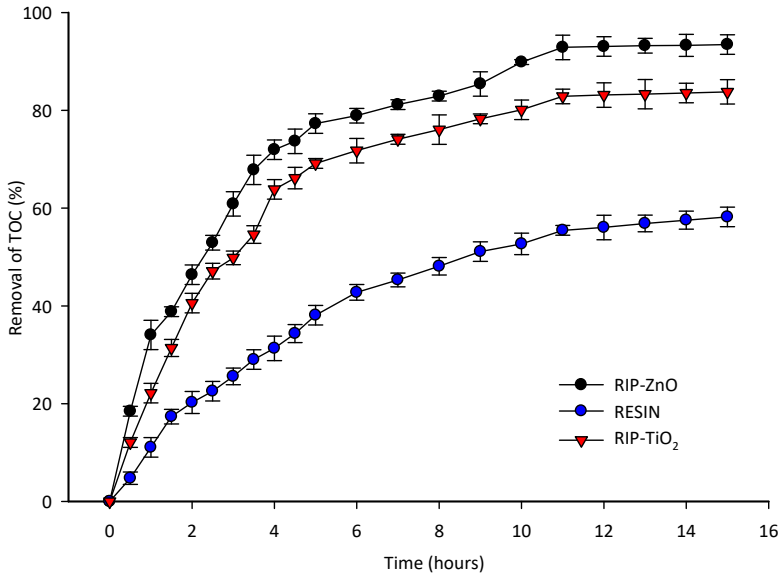

Fig. 1: Performance of resin, RIP-TiO_2, and RIP-ZnO in removing TOC and (b) UV_{254} in tofu wastewater.

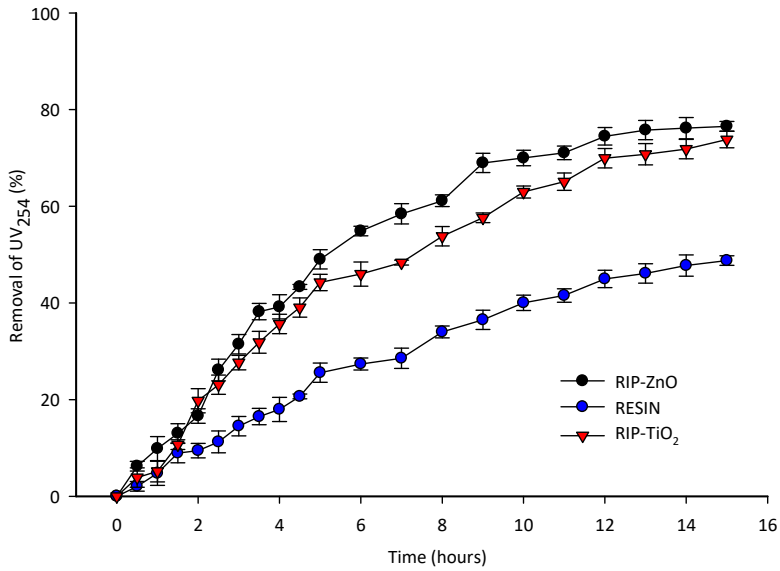

Fig. 2: Performance of resin, RIP-TiO_2, and RIP-ZnO in removing UV_{254} in tofu wastewater

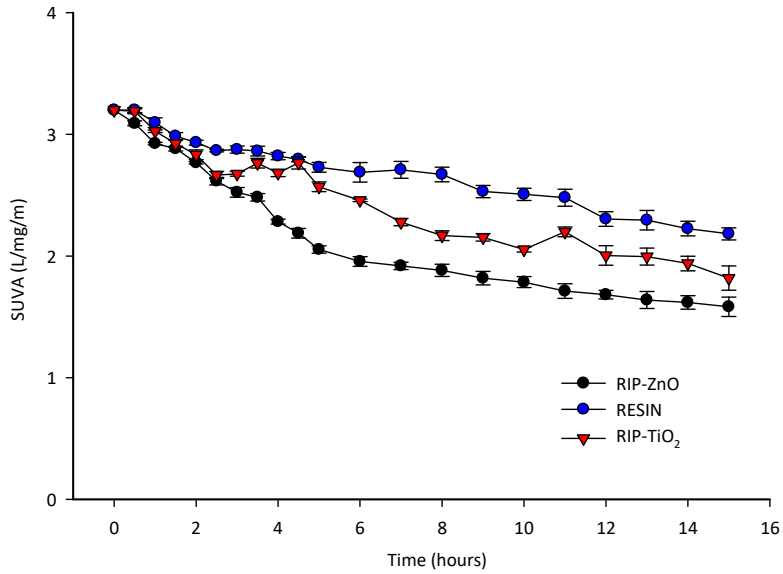

Fig. 3: The changing of SUVA value in tofu wastewater under various processes of resin, RIP-TiO_2, and RIP-ZnO

the changing of organic properties from a mixture of humic-like, mixture hydrophobicity, and mixture molecular weight into mostly low hydrophobicity, non-humic and low molecular weight. As Fig. 1 indicates the removal of total organic carbon in terms of aromatic and aliphatic compounds, and Fig. 2 shows the removal of unsaturated double bonds, it means that the amount of aliphatic compound or less aromatic compound existed in the treated samples. The result of SUVA value, which presents low aromatic, non-humic substances, and low molecular weight organics, has been supported by TOC and UV_{254} analysis, which means that there is a consistency among all parameters of organic matter. The SUVA value of treated samples, which is below the initial value, confirmed the preferential removal humic, a high molecular weight and hydrophobic of organic matter. In addition, the competition between various properties of organic matter components might occur in the systems at a different time process. Overall, the removal of organic matter through resin and resin immobilized photocatalyst suggested the mechanism of entropy sorption, releasing free water molecules because of the dehydration of hydrophobic moieties (Li and Sengupta, 2004). In addition, the increasing hydrophobic character could increase the reduction affinity because of their weak interactivity with water molecules. Resin could be applied to reduce a naturally harmful charged organic matter, and the addition of photocatalyst will improve the performance of resin in oxidizing the organic matter (Ye *et al.,* 2019).

Effect of Resin Immobilized Photocatalyst on the Formation Potential of DBPs

Figs. 4 and 5 show the removal concentration of trihalomethanes (THMs) and haloacetic acids (HAAs), respectively. The reduction of THMs compared to the raw water is in the percentage 51.30 – 75.23 %, while HAAs removal exhibits a higher removal than THMs, in the range 64.89 – 84.94 %. The percentage reduction was quite significant although the effluent quality standard for THMs and HAAs has not being provided in the national regulation. THMs and HAAs is a chlorinated by-product, which are carcinogenic. Dissolved organic matter is known as a precursor for the formation of those products, therefore removal THMs and HAAs could indicated the presence of dissolved organic matter in treated water. Resin and resin immobilized photocatalyst showed a better performance removal of DBPs during a longer contact time. Performance of resin and resin immobilized photocatalyst in removing DBPs indicates the consistency performance in removing bulk parameters of organic matter. Firstly,

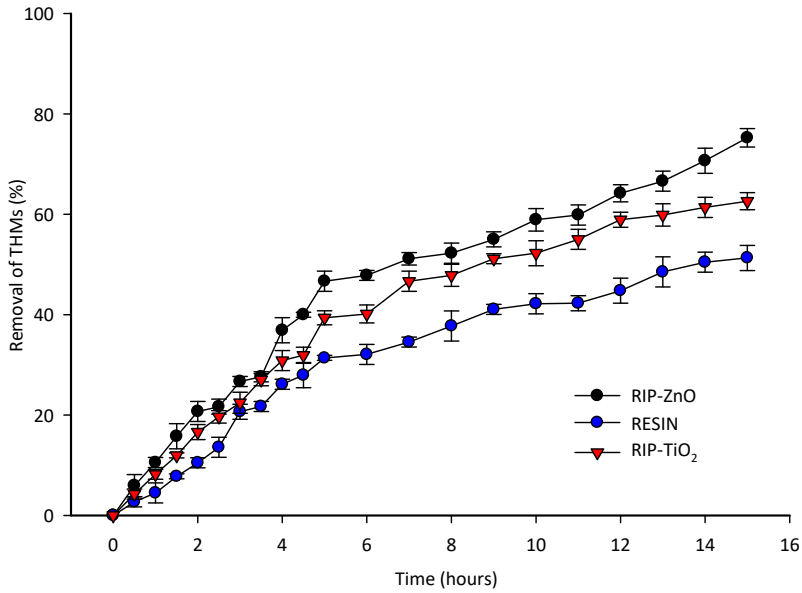

Fig. 4: The changing of THMs concentration in tofu wastewater under various processes of resin, RIP-TiO_2, and RIP-ZnO

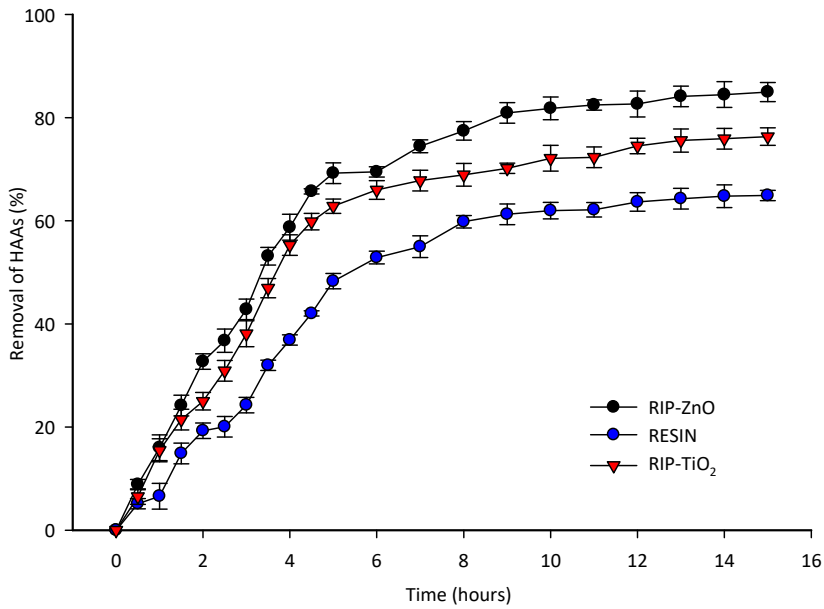

Fig. 5: The changing of HAAs concentration in tofu wastewater under various processes of resin, RIP-TiO_2, and RIP-ZnO

the removal of THMs has a similar percentage with UV_{254} removal. Resin and resin immobilized photocatalyst could gain a higher capacity to remove THMs more than 15 hours contact time, as Fig. 5 has not shown the equilibrium state of line removal THMs. Resin immobilized photocatalyst with ZnO has a higher removal of THMs than resin immobilized photocatalyst with TiO_2 and resin only. Secondly, the removal HAAs seems by TOC removal. HAAs removal performed an almost equilibrium state after 10 hours of contacting time. The resin and resin immobilized photocatalyst almost

Table 1: Resumed of comparison between this study and the previous study regarding the characteristic of dissolved organic matters through resin ion exchange

Component	This study	Previous studies
Aliphatic and aromatic compound	Aliphatic compound has a lower removal than aromatic compound in the resin and resin immobilized	Low resin and resin immobilized photocatalyst removal might be due to competition with non-targeted ions (Finkbeiner *et al.,* 2018)
Removal UV_{254} and TOC	Removal UV_{254} is higher than removal TOC	High molecular weight organic matter is easier to be removed than lower molecular weight (Graf *et al.,* 2014)
SUVA value	Decreasing SUVA value indicated less hydrophobic organic matter	Dehydration of hydrophobic moieties (Li and Sengupta, 2004)
DBPFP	Aromatic and hydrophobic compound were THMs precursors and total organic carbon was HAAs precursors	aromatic and hydrophobic fractions were HAAs precursors (Liang and Singer, 2003); hydrophobic fractions of organic matter were THMFP precursors (Lamsal *et al.,* 2012)
Resin immobilized photocatalyst and resin only	Resin immobilized photocatalyst ZnO is better than TiO_2 and resin only in tofu wastewater	Resin immobilized photocatalyst ZnO is better than TiO_2 in textile wastewater (Pachwarya and Meena, 2011)

obtained its capacity in removing HAAs. However, comparison among these resins represented that resin immobilized photocatalyst with ZnO is much better than resin material in this study. It has been well known that dissolved organic matter is a precursor for DBPs formation, as the higher DOC concentration is accompanied by a higher DBPFP (Liang and Singer, 2003; Bond *et al.,* 2012; Hidayah *et al.,* 2016). This research led to the conjecture that conjugated C=C double bonds and aromatic structure and, which UV_{254} represents, were mainly HAAs precursors, while the non-aromatic organic fraction was probably THMs precursors. Previous studies found that hydrophobicity and hydrophilicity properties of organic matter had influenced the DBPFP, such as hydrophobic fractions of organic matter were THMFP precursors (Lamsal *et al.,* 2012), hydrophilic organics had a higher HAAFP concentration (Wang *et al.,* 2013). However, different studies obtained different conclusions, that aromatic and hydrophobic fractions were HAAs precursors than THMs precursors (Liang and Singer, 2003) and THMFP was triggered due to hydrophilic fractions (Hwang *et al.,* 2000). According to the humic and non-humic compounds, it was concluded that the fraction of the humic substance was the precursors for HAAs, while the biopolymer fraction was the precursors for THMs (Hidayah *et al.,* 2016).

Table 1 resumed the comparison between this study and the previous study regarding the characteristic of dissolved organic matters under different treatment process, and its formation of DBPs concentration. Aromatic organic matter is mainly consist of high molecular weight and has hydrophobic properties. The molecular weight of organic matter influences the resin performance due to the size exclusion effect (Bazri and Mohseni, 2016). Low molecular weight diffuses more easily into the resin pores and is not restricted to exchange sites outside, whereas larger molecules are rejected due to size exclusion (Winter *et al.,* 2018). In addition, the resin has limited capacity, and larger molecules blocked the possibility of the resin surface at high TOC concentration (Levchuk *et al.,* 2018). Hydrophobicity considered, the hydrophobic compounds lack an affinity for water, insoluble in water, which results in reduction of the compound from the solution, or called by therefore entropy-assisted sorption (Li and Sengupta, 2004). The reduction of organic matter by using resin is driven primarily by charge. More highly charged molecules of organics are preferentially reduced because of the stronger affinity to the resin (Liu *et al.,* 2017). Overall, the removal of DBPFP is strongly related to the reduction of bulk parameters of organic matter, including TOC, UV_{254}, and SUVA value because bulk parameters represented the properties of organic matters. Therefore, controlling bulk parameters removal leads to the monitoring and removing DBPFP concentration. Further, it is necessary to identify the characteristic of organic matter in the source water to know the appropriate treatment

process in removing organic matter. This study shows that resin immobilized photocatalyst has a better performance than resin only, and the used resin should be regenerated for further usage until the resin has lower exchange capacity. An example of the treatment train for reclaimed water, which is applied resin technology, will be conventional treatment such as coagulation, flocculation, sedimentation, filtration, resin technology, disinfection and collected water. Therefore, the following treatment processes are needed to obtain the criteria standard for reclaimed water as regulated by the government, primarily related to the concentration of dissolved organic matter, THMs, and HAAs.

CONCLUSION

This study observed the usage of resin, RIP-TiO_2, and RIP-ZnO for treating tofu wastewater into reclaimed water with a focus on the bulk parameters, including TOC, UV_{254}, SUVA value, and DBPs concentration, including THMs and HAAs concentration. It was characterized that tofu wastewater has high dissolved organic matter and content of mixture aromatic humic substances-like, mixture hydrophobicity, and a mixture of molecular weight. After treatment, it was confirmed that all materials preferentially reduce bulk parameters and DBPs concentration under different percentage removal, about 48%-93% of bulk parameters concentration removal, and 51%-85% of DBPs concentration removal. RIP-ZnO performed a slightly higher removal of TOC, UV_{254}, THMs, and HAAs concentration than RIP-TiO_2, while resin exhibited the lowest capacity removal. TOC has been removed in a higher percentage than UV_{254} since TOC represents whole dissolved organic carbon. Comparison between percentage removal of TOC and UV_{254} has pointed out the removal amount of aliphatic compound. It seems that an aliphatic compound has a lower removal than aromatic compound in the resin and resin immobilized. Decreasing SUVA value indicated changing of organic properties from a mixture of humic-like, mixture hydrophobicity, and mixture molecular weight into mostly low hydrophobicity, non-humic, and low molecular weight. Performance of resin and resin immobilized photocatalyst in removing DBPs indicates the consistency performance in removing bulk parameters of organic matter. Removal of THMs has a similar percentage with UV_{254} removal, while the removal HAAs seems by TOC removal. Controlling bulk parameters removal, such as TOC, UV_{254}, and SUVA value, is one of the efforts to monitor and control the formation of DBPs. Identify the characteristic of organic matter in the raw water is one of the strategies to know the appropriate treatment process. Further treatment processes are needed to obtain the criteria standard for reclaimed water because the proposed process does not always directly reduce DBPs reactivity, but it facilitates a better removal of DBPs precursors.

AUTHOR CONTRIBUTIONS

E.N. Hidayah performed the experimental work, analyzed the data, and wrote the manuscript and reviewed the literatures. R.B. Pachwarya analyzed the data, interpreted the results, and reviewed the manuscripts. O.H. Cahyonugroho performed the experimental, presented the data, and wrote the manuscript.

ACKNOWLEDGEMENT

This study was financially supported Lembaga Penelitian dan Pengabdian kepada Masyarakat (LPPM), Universitas Pembangunan Nasional Veteran Jawa Timur through research scheme International Research Collaboration (KLN) with contract No: [SPP/89/UN.63.8/LT/IV/2021].

CONFLICT OF INTEREST

The authors declare no potential conflict of interest regarding the publication of this work. Also, ethical issues, including plagiarism, informed consent, misconduct, data fabrication and/or falsification, double publication and submission, as well as redundancy, have been entirely witnessed by the authors.

PUBLISHER'S NOTE

ABBREVIATIONS

AOPs	Advanced oxidation processes
BOD	Biological oxygen demand
COD	Chemical oxygen demand
cm	Centimeter
^{o}C	Degree celcius
DBPFP	Disinfection by-products formation potential
DBPs	Disinfection by-products
C=C	Double bond carbon
ECD	Electron capture detector
GC	Gas chromatographic
GC-ECD	Gas chromatographic- electron capture detector
HAAs	Haloacetic acids
L/mg/m	Liter milligram meter
MBIRD11	Methylene blue immobilized resin dowex-11
MTBE	Methyl tertiary butyl ether
µm	Micrometer
mg	Miligram
mg Cl_2/mL	Miligram Chlorine per mililiter
mg/L	Miligram per liter
M	Molar
NaOH	Natrium hydroxide
NDMA	Nitrosodimethylamine
DPD	N,N-diethyl-p-phenylene diamine
%	Percent
RIP	Resin immobilized photocatalyzed
RIP-TiO_2	Resin immobilized photocatalyzed-titanium dioxide
RIP-ZnO	Resin immobilized photocatalyzed - zinc oxide
rpm	Radian per minutes
ROS	Reactive oxidative species
SUVA	Specific ultraviolet absorbance
H_2SO_4	Sulfuric acid
TiO2	Titanium dioxide
THMs	Trihalomethanes
TN	Total nitrogen
TOC	Total organic carbon
UV	Ultraviolet
UV_{254}	Ultraviolet at 254 nm wavelength
UV/vis	Ultraviolet visible
ZnO	Zinc oxide

REFERENCES

APHA, (2012). Standard methods for the examination of water and wastewaters, 21th ed. American Public Health Association: Washington, DC.

Bazri, M.M.; Mohseni, M., (2016). Impact of natural organic matter properties on the kinetics of suspended ion exchange process. Water Res., 91: 147-155 **(9 pages)**.

Bethi, B.; Sonawane, S.H.; Bhanvase, B.A.; Gumfekar, S.P., (2016). Nanomaterials-based advanced oxidation processes for wastewater treatment: A review. Chem. Eng. Process. Process Intensif., 109:178-189 **(12 pages)**.

Bolto, B.; Dixon, D.; Eldridge, R.; King, S.; Linge, K., (2002). Removal of natural organic matter by ion exchange. Water Res., 36(20): 5057-5065 **(9 pages)**.

Bond, T.; Templeton, M.R.; Graham, N., (2012). Precursors of nitrogenous disinfection by-products in drinking water: a critical review and analysis. J. Hazard. Mater., 235-236: 1-16 **(16 pages)**.

Cornellisen, E.R.; Moreau, N.; Siegers, W.G.; Abrahamse, A.J.; Rietveld, L.C.; Grefte, A.; Dignum, M.; Amy, G.; Wessels, L.P., (2008). Selection of anionic exchange resins for removal of natural organic matter (NOM) fractions. Water Res., 42(1-2): 413-423 **(11 pages)**.

Englande, A.J.; Krenkel, P.; Shamas, J., (2015). Wastewater treatment and water reclamation. Reference Module in Earth Systems and Environmental Sciences 639-670 **(32**

pages).

Finkbeiner, P.; Redman, J.; Patriarca, V.; Moore, G.; Jefferson, B.; Jarvis, P., (2018). Understanding the potential for selective natural organic matter removal by ion exchange. Water Res., 146: 256-263 **(8 pages)**.

Graf, K.C.; Cornwell, D.A.; Boyer, T.H., (2014). Removal of dissolved organic carbon from surface water by anion exchange and adsorption: bench-scale testing to simulate a two-stage countercurrent process. Sep. Purif. Technol., 122: 523-532 **(10 pages)**.

Hidayah, E.N.; Chou, Y.C.; Yeh, H.H., (2016). Using HPSEC to identify NOM fraction removal and the correlation with disinfection by-product precursors. Water Sci & Technol. Water Supply 16(2): 305-313 **(9 pages)**.

Hwang, C.J.; Sclimenti, M.J.; Krasner, S.W., (2000). Disinfection by-product formation reactivities of natural organic matter fractions of a low-humic water. In: natural organic matter and disinfection by-products, characterization and control in drinking water; Barrett, S.E., Krasner, S.W. and Amy, G.L., Eds.; American Chemical Society: Washington, DC, 173-187 **(15 pages)**.

Ishchenko, A.; Cherezov, V.; Liu, W., (2016). Preparation and delivery of protein microcrystals in lipidic cubic phase for serial fem to second crystallography. J. Vis. Exp., 115: 54463 **(8 pages).**

Lamsal, R.; Montreuil, K.R.; Kent, F.C.; Walsh, M.E.; Gagnon, G.A., (2012). Characterization and removal of natural organic matter by an integrated membrane system. Desalination 303: 12-16 **(5 pages)**.

Levchuk, I.; Márquez, J.J.R.; Sillanpää, M., (2018). Removal of natural organic matter (NOM) from water by ion exchange–a review. Chemosphere 192: 90-104 **(15 pages)**.

Li, P.; SenGupta, A.K., (2004). Sorption of hydrophobic ionizable organic compounds (HIOCs) onto polymeric ion exchangers. React. Funct. Polym., 60: 27-39 **(13 pages)**.

Liang, L.; Singer, P.C., (2003). Factors influencing the formation and relative distribution of haloacetic acids and trihalomethanes in drinking water. Environ. Sci. Technol., 37(13): 2920-2928 **(9 pages)**.

Liu, Y.; Xu, F.; Liu, C., (2017). Coupled hydro-biogeochemical processes controlling Cr reductive immobilization in Columbia River hyporheic zone. Environ. Sci. Technol., 51(3): 1508-1517 **(10 pages)**.

McBean, E.; Zhu, Z.; Zeng, W., (2010). Modeling formation and control of disinfection byproducts in chlorinated drinking waters. Water Sci. Technol. Water Supply 10(5): 730-739 **(10 pages)**.

Najm, I.; Trussell, R.R., (2001). NDMA formation in water and wastewater. J. Am. Water Work Assn., 93(2): 92-99 **(8 pages)**.

Nieuwenhuijsen, M.J.; Martinez, D.; Grellier, J.; Bennet, J.; Best, N.; Iszatt, N.; Vrijheid, M.; Toledano, M.B., (2009). Chlorination disinfection by-products in drinking water and congenital anomalies: review and meta-analyses. Environ. Health Perspect. 117(10): 1486-1493 **(8 pages)**.

Ong, C.B.; Ng, L.Y.; Mohammad, A.W., (2018). A review of ZnO nanoparticles as solar photocatalysts: Synthesis, mechanisms and applications. Renewable Sustainable Energy Rev., 81: 536-551 **(16 pages)**.

Pachwarya, R.B.; Meena, R.C., (2011). Degradation of Azo dyes ponceau S, S-IV from the wastewater of textile industries in a new photocatalytic reactor with high efficiency using recently developed photocatalyst MBIRD-11. Energy Sources Part A., 33(18): 1651-1660 **(10 pages)**.

Sillanpää, M.; Matilainen, A.; Lahtinen, T., (2015). Characterization of NOM. In: natural organic matter in water: characterization and treatment method; Silaanpää, M., Eds.; Butterworth-Heinemann: Oxford, 17–53 **(37 pages)**.

Uyguner, C.S.; Birben, N.C.; Bekbolet, M., (2017). Elucidation of background organic matter matrix effect on photocatalytic treatment of contaminants using TiO2: a review. Catal. Today 284: 202-214 **(13 pages)**.

Verdugo, E.M.; Gifford, M.; Glover, C.; Cuthberson, A.A.; Trenholm, T.A.; Kimura, S.Y.; Liberatore, H.K.; Richardson, S.D.; Stanford, B.D.; Summers, R.S.; Dickenson, E.R.V., (2020). Controlling disinfection byproducts from treated wastewater using adsorption with granular activated carbon: Impact of pre-ozonation and pre-chlorination. Water Res. X., 9: 1-11 **(11 pages)**.

Wang, D.S.; Zhao, Y.M.; Yan, M.Q.; Chow, C.W.K., (2013). Removal of DBP precursors in micro-polluted source waters: A comparative study on the enhanced coagulation behaviour. Sep. Purif. Technol., 118: 271-278 **(8 pages)**.

Winter, J.; Wray, H.E.; Schultz, M.; Vortisch, R.; Barbeau, B.; Berube, P., (2018). The impact of loading approach and biological activity on NOM removal by ion exchange resins. Water Res., 134: 301-310 **(10 pages)**.

Yadav, A.; Bakshi, S.; Yadukrishnan, P.; Lingwan, M.; Dolde, U.; Wenkel, S.; Masakapalli, S.K.; Datta, S., (2019). The B-Box-containing microprotein miP1a/BBX31 regulates photomorphogenesis and UV-B protection. Plant Physiol., 179: 1876– 1892 **(17 pages)**.

Ye, Y.; Bruning, H.: Liu, W.; Rijnaard, H.; Ytenma, D., (2019) Effect of dissolved natural organic matter on the photocatalytic micropollutant removal performance of TiO_2 nanotube array. J. Photochem. Photobiol., A 371: 216-222 **(7 pages)**.

AUTHOR (S) BIOSKETCHES

Hidayah, E.N., Ph.D., Assistant professor, Department of Environmental Engineering, Universitas Pembangunan Nasional Veteran Jawa Timur, Indonesia.
- Email: *euisnh.tl@upnjatim.ac.id*
- ORCID: 0000-0003-2055-3051
- Web of Science ResearcherID: I-6347-2019
- Scopus Author ID: 57189696484
- Academic Homepage: http://teklingk.upnjatim.ac.id

Pachwarya, R.B., Ph.D., Associate Professor, Department of Chemistry, Motilal Nehru College, University of Delhi, Dehi, India.
- Email: *pachwarya@gmail.com*
- ORCID: 0000-0002-4326-6250
- Web of Science ResearcherID: NA
- Scopus Author ID: 35079170800
- Academic Homepage: http://www.mlncdu.ac.in/Chemistry.html

Cahyonugroho, O.H., Ph.D. Candidate, Associate Professor, Department of Environmental Engineering, Universitas Pembangunan Nasional Veteran Jawa Timur, Indonesia.
- Email: *okhecah@gmail.com*
- ORCID: 0000-0001-9721-5515
- Web of Science ResearcherID: NA
- Scopus Author ID: 57201197732
- Academic Homepage: http://teklingk.upnjatim.ac.id

HOW TO CITE THIS ARTICLE

Hidayah, E.N.; Pachwarya, R.B.; Cahyonugroho, O.H., (2022). Immobilization of resin photocatalyst in removal of soluble effluent organic matter and potential for disinfection by-products. Global J. Environ. Sci. Manage., 8(3): 437-448.

DOI: 10.22034/gjesm.2022.03.10

url: https://www.gjesm.net/article_248294.html

PUBLICATION ETHICS

The ethical policy of GJESM is based on the Committee on Publication Ethics (COPE) guidelines and complies with International Committee of GJESM Editorial Board codes of conduct. Readers, authors, reviewers and editors should follow these ethical policies once working with GJESM. The ethical policy of GJESM is liable to determine which of the typical research papers or articles submitted to the journal should be published in the concerned issue. For information on this matter in publishing and ethical guidelines please visit http://publicationethics.org

Duties and Responsibilities of Publishers

1. GJESM is committing to ensure that editorial decisions on manuscript submissions are the final.
2. GJESM is promising to ensure that the decision on manuscript submissions is only made based on professional judgment and will not be affected by any commercial interests.
3. GJESM is committing to maintain the integrity of academic and research records.
4. GJESM is monitoring the ethics by Editor-in-Chief, Associate Editors, Editorial Board Members, Reviewers, Authors, and Readers.
5. GJESM is always checking the plagiarism and fraudulent data issues involving in the submitted manuscript.
6. GJESM is always willing to publish corrections, clarifications and retractions involving its publications as and when needed.

Duties and Responsibilities of Editors

1. The Editors of the journal should have the full authority to reject/accept a manuscript.
2. The Editors of the journal should maintain the confidentiality of submitted manuscripts under review or until they are published.
3. The Editor-in-Chief should take a decision on submitted manuscripts, whether to be published or not with other editors and reviewers
4. The Editors of the journal should preserve the anonymity of reviewers.
5. The Editors of the journal should disclose and try to avoid any conflict of interest.
6. The Editors of the journal should maintain academic integrity and strive to meet the needs of readers and authors.
7. The Editors of the journal should be willing to investigate plagiarism and fraudulent data issues and willing to publish corrections, clarifications, retractions, and apologies when needed.
8. The Editors of the journal should have the limit themselves only to the intellectual content.
9. The Editors of the journal must not disclose any information about submitted manuscripts to anyone other than the corresponding author, reviewers, potential reviewers, other editorial advisers, and the publisher, as appropriate.
10. Unpublished materials disclosed in a submitted paper will not be used by the editor or the members of the editorial board for their own research purposes without the author's explicit written consent.

Duties and Responsibilities of Reviewers

1. The Reviewers of the journal should assist the Editors in taking the decision for publishing the submitted manuscripts.
2. The Reviewers should maintain the confidentiality of manuscripts, which they are invited to review.
3. The Reviewers should provide comments in time that will help editors to make decision on the submitted manuscript to be published or not.
4. The Reviewers are bound to treat the manuscript received for peer reviewing as confidential, and must not use the information obtained through peer review for personal advantage.
5. The Reviewers comments against each invited manuscript should be technical, professional and objective.
6. The Reviewers should not review the manuscripts in which they have found conflicts of interest with any of the authors, companies, or institutions.
7. The Reviewers should disclose and try to avoid any conflict of interest.

Duties and Responsibilities of Authors

1. Manuscripts must be submitted only in English and should be written according to sound grammar and proper terminology.
2. Manuscripts must be submitted with the understanding that they have not been published elsewhere (except in the form of an abstract or as part of a published lecture, review, or thesis) and are not currently under consideration by another journal published by or any other publisher.
3. The submitting (corresponding) author is responsible for ensuring that the manuscript article's publication has been approved by all the other coauthors.
4. In order to sustain the peer review system, authors have an obligation to participate in peer review process to evaluate manuscripts from others.
5. It is also the authors' responsibility to ensure that the manuscripts emanating from a particular institution are submitted with the approval of the necessary institution.
6. It is a condition for submission of a manuscript that the authors permit editing of the paper for readability.
7. Authors are requested to clearly identify who provided financial support for the conduct of research and/or preparation of the manuscript and briefly describe the role of the funder/sponsor in any part of the work.
8. A copy right release and conflict of interest disclosure form must be signed by the corresponding author in case of multiple authorships, prior to the acceptation of the

manuscript, by all authors, for publication to be legally responsible towards the Journal ethics and privacy policy.

9. Under open access license, authors retain ownership of the copyright for their content, but allow anyone to download, reuse, reprint, modify, distribute, and/ or copy the content as long as the original authors and source are cited properly.
10. All authors have agreed to allow the corresponding author to serve as the primary correspondent with the editorial office, to review the edited manuscript and proof.
11. When author(s) discovers a significant error or inaccuracy in his/her own published work, it is the author's obligation to promptly notify the journal editor or publisher to retract or correct the manuscript.
12. All authors must know that that the submitted manuscripts under review or published with GJESM are subject to screening using Plagiarism Prevention Software. Plagiarism is a serious violation of publication ethics.

Violation of Publication Ethics

1. **Plagiarism:** Plagiarism is intentionally using someone else's ideas or other original material as if they are one's own. Copying even one sentence from someone else's manuscript, or even one of your own that has previously been published, without proper citation is considered by GJESM Journals as plagiarism. All manuscripts under review or published with GJESM are subject to screening using plagiarism prevention software. Thus, plagiarism is a serious violation of publication ethics. The development of CrossCheck is a service that helps editors to verify the originality of papers. CrossCheck is powered by the Ithenticate software from iParadigms, known in the academic community as providers of Turnitin. For a searchable list of all journals in the CrossCheck database, please visit: www.ithenticate.com/search
2. **Data Fabrication and Falsification:** Data fabrication and falsification means the researcher did not really carry out the study, but made up data or results and had recorded or reported the fabricated information. Data falsification means the researcher did the experiment, but manipulated, changed, or omitted data or results from the research findings.
3. **Simultaneous Submission:** Simultaneous submission occurs when a manuscript (or substantial sections from a manuscript) is submitted to a journal when it is already under consideration by another journal.
4. **Duplicate Publication:** Duplicate publication occurs when two or more papers, without full cross referencing, share essentially the same hypotheses, data, discussion points, and conclusions.
5. **Redundant Publications:** Redundant publications involve the inappropriate division of study outcomes into several articles, most often consequent to the desire to plump academic vitae.
6. **Improper Author Contribution or Attribution:** All listed authors must have made a significant scientific contribution to the research in the manuscript and approved all its claims. Don't forget to list everyone who made a significant scientific contribution, including students and laboratory technicians.
7. **Citation Manipulation:** Citation Manipulation is including excessive citations, in the submitted manuscript, that do not contribute to the scholarly content of the article and have been included solely for the purpose of increasing citations to a given author's work, or to articles published in a particular journal. This leads to misrepresenting the importance of the specific work and journal in which it appears and is thus a form of scientific misconduct.

Handling Cases of Misconduct

Once GJESM confirms a violation against GJESM's publication ethics, GJESM addresses ethical concerns diligently following an issue-specific standard practice as summarized below.

1. The first action of the journal Editor is to inform the Editorial Office of GJESM by supplying copies of the relevant material and a draft letter to the corresponding author asking for an explanation in a nonjudgmental manner.
2. If the author's explanation is unacceptable and it seems that serious unethical conduct has taken place, the matter is referred to the Publication Committee via Editorial Office. After deliberation, the Committee will decide whether the case is sufficiently serious to warrant a ban on future submissions.
3. If the infraction is less severe, the Editor, upon the advice of the Publication Committee, sends the author a letter of reprimand and reminds the author of GJESM publication policies; if the manuscript has been published, the Editor may request the author to publish an apology in the journal to correct the record.
4. Notification will be sent to corresponding author and any work by the author responsible for the violation or any work these persons coauthored that is under review by GJESM journal will be rejected immediately.
5. The authors are prohibited from serving on GJESM editorial board and serving as a reviewer for GJESM Journal. GJESM reserves the right to take more actions.
6. In extreme cases, notifications will be sent to the affiliations of the authors and the authors are prohibited from submitting their work to GJESM for 5 years.
7. In serious cases of fraud that result in retraction of the article, a retraction notice will be published in the journal and will be linked to the article in the online version. The online version will also be marked "retracted" with the retraction date.

GUIDE FOR AUTHORS

"Global Journal of Environmental Science and Management" (GJESM) is a double blind peer reviewed electronic and print quarterly publication concerned with all aspects of environmental science and management. GJESM publishes original research papers, review papers, case reports and short communications, letters to editor and authors' response about letters to editor across the broad field of environment. These include but are not limited to environmental science, environmental management, environmental engineering, environmental planning and design, urban and regional landscape design and industrial ecology. Environmentalist disciplines are invited to contribute their knowledge and experience. The publication appears at regular intervals time quarterly. The Journal database is fully open access and full text of published articles are available for everyone who can get access to the Journal website free of cost. The authors never pay any charges for submission, article processing and publication.

Guide for Authors: More details on guide for authors refer: http://gjesm.net/journal/authors.note

GENERAL

1. Authors should submit their contributions electronically through the GJESM website submission system to the Editorial Office.

2. Manuscripts must be submitted only in English and should be written according to sound grammar and proper terminology. Manuscripts should be typed in Times New Roman of 11 pt. font and in MS-Word format in one column with 2.5 cm margin at each side. Manuscript submission must be applied once in order to obtain only one submission ID number. More than one submission for a single manuscript can lose the chance of the manuscript consideration. Manuscript must be accompanied by a covering letter including title and author(s) name.

3. There are no strict formatting requirements but all manuscripts must contain the essential elements needed to convey your manuscript, for example Abstract, Keywords, Introduction, Materials and Methods, Results, Conclusions, Artwork and Tables with Captions. Please ensure the figures and the tables included in the single file are placed next to the relevant text in the manuscript, rather than at the bottom or the top of the file. There are no strict requirements on reference formatting at submission. References can be in any style or format as long as the style is consistent.

BEFORE YOU BEGIN

1. Peer-Review Process: In order to sustain the peer review system, authors have an obligation to participate in peer review process to evaluate manuscripts from others. When appropriate, authors are obliged to provide retractions and/or corrections of errors to the editors and the Publisher. All papers submitted to GJESM journal will be peer reviewed for at least one round. GJESM journal adopts a double-blinded review policy: authors are blind to reviewers, but reviewers are not blind to authors. After receiving reviewers' comments, the editorial team member makes a decision. Because reviewers sometimes do not agree with each other, the final decision sent to the author may not exactly reflect recommendations by any of the reviewers. The decision after each round of peer review may include (a) Accept without any further changes, (b) Accept with minor revision, (c) Major changes are necessary for resubmission and (d) Decline without encouraging resubmission.

2. Post-Publication Evaluation: In addition to rapid Peer Review Process, the GJESM Journal has Post-Publication Evaluation by the scientific community. Post-Publication Evaluation is concentrated to ensure that the quality of published research, review and case report meets certain standards and the conclusions that are presented are justified. The post-publication evaluation includes online comments and citations on published papers. Authors may respond to the comments of the scientific community and may revise their manuscript. The Post-Publication Evaluation is described in such a way; it is allowing authors to publish quickly about Environmental science, management, engineering and technology concepts.

3. Publication Ethics: The ethical policy of GJESM is based on the Committee on Publication Ethics (COPE) guidelines and complies with International Committee of GJESM Editorial Board codes of conduct. Readers, authors, reviewers and editors should follow these ethical policies once working with GJESM. The ethical policy of GJESM is liable to determine which of the typical research papers or articles submitted to the journal should be published in the concerned issue. The ethical policy insisted the Editor-in-Chief, may confer with other editors or reviewers in making the decision. Visit at: http://publicationethics.org

4. Conflict of Interest: Authors are requested to evident whether impending conflicts do or do not exist. A copyright transfer agreement is signed by the corresponding author, upon the acceptance of the manuscript, on behalf of all authors, for publication to be legally responsible towards the journal ethics and privacy policy. Authors will be notified as soon as possible of decisions concerning the suitability of their manuscripts for publication in the journal. The submitted materials may be considered for inclusion but cannot be returned and Editors of the journal reserve the right to accept or reject any article in any stage, if necessary. Conflict of Interest Disclosure form can be found at: www.gjesm.org/conflict_of_interest_discloure_form.docx

5. Submission Declaration and Verification: While submitting a manuscript to GJESM, all contributing author(s) must verify that the manuscript represents authentic and valid work and that neither this manuscript nor one with significantly similar content under their authorship has been published or is being considered for publication elsewhere including electronically in the same form, in English or in other language, without the written consent the copy right holder.

6. Authorship: All contributing authors should qualify for authorship and corresponding author should sign the authorship form while submitting the manuscript. It can be found at:
(http://www.gjesm.net/data/gjesm/news/authorship_form.docx).

7. Changes to Authorship: After the manuscript is submitted or accepted for publication, the corresponding author is required to send a request to add or remove an author or to rearrange the author names of the submitted/accepted manuscript by sending the change of authorship form to editorial office. No authorship change is allowed after publication of manuscript. More details may be found at:
(http://www.gjesm.net/data/gjesm/news/change_of_authorship_form.docx)

8. Retained Author Rights: As an author, author or authors' employer or institution retains certain rights. For more information on author rights, found at:
www.gjesm.org/retained_authors_right.docx.

9. Copy Right: Journals should make clear the type of copyright under which authors' work will be published. For open access articles the publisher uses an exclusive licensing agreement in which authors retain copyright in their manuscript. More details may be found at: (www.gjesm.org/copyright_form.docx)

10. User license Agreement: GJESM provides access to archived material through GJESM archives. Manuscripts are the parts of an open archive are made freely available from GJESM website after certain period, which begins from the final publication date of the manuscript. All articles published open access will be immediately and permanently free for everyone to read and download. Permitted reuse is defined by Creative Commons user license called ***Creative Commons Attribution***. Visit at: **(**Creative Commons Attribution 4.0 International (CC BY 4.0)**)**

11. Plagiarism Prevention and Violation of Publication Ethics: All manuscripts under review or published with GJESM are subject to screening using Plagiarism Prevention Software. Plagiarism is a serious violation of publication ethics. Other violations include duplicate publication, data fabrication and falsification, and improper credit of author contribution. Thus, the Plagiarism or Fraudulent or knowingly inaccurate statements constitute unethical behavior are unacceptable and submitting the same manuscript to more than one journal concurrently constitutes unethical publishing behavior and is unacceptable. The development of CrossCheck is a service that helps editors to verify the originality of papers. CrossCheck is powered by the Ithenticate software from iParadigms, known in the academic community as providers of Turnitin. For more details visit at: www.ithenticate.com/search

12. Handling Cases of Misconduct: Once GJESM confirms a violation against GJESM's publication ethics, the following actions will be taken.

a. The work is rejected / retracted immediately. Notification will be sent to corresponding authors. In extreme cases, notifications will be sent to the affiliations of the authors.
b. The authors are prohibited from submitting their work to GJESM for 5 years.
c. Any work by the authors responsible for the violation or any work these persons coauthored that is under review by any GJESM journal will be rejected immediately.
d. The authors are prohibited from serving on GJESM editorial board. GJESM reserves the right to take more actions.

MANUSCRIPT PREPARATION

1. Title Page: The title page should include: the name(s) of the author(s), a concise and informative title, the affiliation(s) and address (es) of the author(s), and e-mail address, telephone and fax numbers of the corresponding author.

2. Manuscript Title: Title of up to 17 words should not contain the name of locations, countries or cities of the research as well as abbreviations. The title should be oriented to Environmental issues while not being obscure or meaningless.

3. Abstract: An abstract of 150 to 250 words that sketches the purpose of the study; basic procedures; main findings its novelty; discussions and the principal conclusions, should not contain any undefined abbreviations or references.

4. Keywords: Provide 5 to 7 keywords which can be used for indexing purposes. Keywords should not repeat the words of the manuscript title or contain abbreviations and shall be written in alphabetical order as separated by semicolon.

5. Introduction: The Introduction should state the purpose of the investigation and identify clearly the gap of knowledge that will be filled in the Literature review study. Date and location of the research carried out throughout the study must be mentioned at the end of this section.

6. Materials and methods: The Materials and Methods section should provide enough information to permit repetition of the experimental work. It should include clear descriptions and explanations of sampling procedures, experimental design, and essential sample characteristics and descriptive statistics, hypothesis tested, exact references to literature describing the tests used in the manuscript, number of data involved in statistical tests, etc.

7. Results and Discussion: The Results section should describe the outcome of the study. Data should be presented as concisely as possible - if appropriate in the form of tables or figures, although very large tables should be avoided. The Discussion should be an interpretation of the results and their significance with reference to work by other authors. Please note that the policy of the Journal with respect to units and symbols is that of SI symbols.

8. Tables: Do not submit tables and graphs as photograph. Place explanatory matters in footnotes, not in the heading. Do not use internal horizontal and vertical rules. Tables should be called out in the text and should have a clear and rational structure and consecutive numerical order. All tables should be numbered 1, 2, 3, etc. Give enough information in subtitles so that each table is understandable without reference to the text. Footnotes to tables should be indicated by superscript lower-case letters (or asterisks for significance values and other statistical data) and included beneath the table body.

9. Figures: Figures/ illustrations should be in high quality art work, within 200-300 dpi and separately provided in Excel format. Ensure that figures are clear, labeled, and of a size that can be reproduced legibly in the journal. Each figure should have a concise caption describing accurately what the figure depicts. Figure captions begin with the term Fig. Figures should be with the captions placed below in limited numbers. No punctuation is to be placed at the end of the caption.

10. Conclusion: This section should highlight the major, firm discoveries, and state what the added value of the main finding is, without literature references.

11. Acknowledgements: Acknowledgments of people, grants, funds, etc. should be placed in a separate section before the reference list. The names of funding organizations should be written in full. Financial support affiliation of the study, if exists, must be mentioned in this section. Thereby, the Grant number of financial support must be included.

12. References: All the references should be cited throughout the manuscript text as well as in the Reference section organized in accordance with Harvard system. Groups of references should be listed first alphabetically, then chronologically. The number of references extracted from each journal should not exceed 3 to 5 citations, which is the average acceptable amount. The number of references should not be less than 30 for original paper, less than 100 for review paper. It is substantially recommended to the authors to refer to more recent references rather than old and out of date ones. Volume, issue and pages of the whole references must be specified according to the GJESM format.

Citing and listing of Web references: As a minimum, the full URL should be given. Any further information, if known (Author names, dates, reference to a source publication, etc.), should also be given.

Text: All citations in the text should refer to: 1. Single author: the author's name (without initials, unless there is ambiguity) and the year of publication; 2. Two authors: both authors' names and the year of publication; and 3. Three or more authors: first author's name followed by "et al." and the year of publication. Citations may be made directly (or parenthetically). Groups of references should be listed first alphabetically, then chronologically. Examples: "as demonstrated (Allan, 1996a, 1996b, 1999; Allan and Jones, 1995). Kramer *et al.,* (2000) have recently shown …".

List: References should be arranged first alphabetically and then further sorted chronologically if necessary. More than one reference from the same Author(s) in the same year must be identified by the letters "a", "b", "c", etc., placed after the year of publication.

Journal article: Nouri J.; Lorestani B.; Yousefi N.; Khorasani N.; Hassani A. H.; Seif, F.; Cheraghi M., (2011). Phytoremediation potential of native plants grown in the vicinity of Ahangaran lead-zinc mine. Environ. Earth Sci., 62(3): 639-644.

Book: Davis, M. L., (2005). Introduction to Environmental Engineering, 3rd. Ed. McGraw Hill Inc.

Book chapter: Mettam, G. R.; Adams, L. B., (1999). How to prepare an electronic version of your article, in: Jones, B. S., Smith, R. Z. (Eds.), Introduction to the electronic age. E-Publishing Inc., New York.

Conference paper: Brown, J., (2005). Evaluating surveys of transparent governance. In UNDESA, 6th. Global forum on reinventing government: towards participatory and transparent governance. Seoul, Republic of Korea 24-27 May. United Nations: New York.

Dissertation: Trent, J. W., (1975). Experimental acute renal failure. Ph.D. Dissertation, University of California. USA.

Online document: Cartwright, J., (2007). Big stars have weather too. IOP Publishing Physics Web.
http://physicsworld.com/cws/article/news/2007/jun/26/big-stars-have-weather-too

AFTER ACCEPTANCE

1. Online Proof Correction: Corresponding authors will receive an e-mail with a link to our online proofing system, allowing annotation and correction of proofs online. Use this proof only for checking the typesetting, editing, completeness and correctness of the text, tables and figures. Significant changes to the article as accepted for publication will only be considered at this stage with permission from the Editor-in-Chief. It is important to ensure that all corrections are sent back to us in one communication. Please check carefully before replying, as inclusion of any subsequent corrections cannot be guaranteed. Proofreading is solely the corresponding author responsibility.

2. Offprints: The offprints can be downloading from the GJESM website once the final corrected manuscripts are disseminated.

AUTHORS INQUIRIES

Authors can track their submitted article through GJESM website on author's login section at: http://gjesm.net/contacts?_action=login

Global Journal of Environmental Science and Management (GJESM)

Copyright Transfer Agreement

1. Parties of the agreement

Author (s):

Manuscript Title:

Manuscript ID:

(Herewith referred to as the "materials"),

Journal Title: Global Journal of Environmental Science and Management (GJESM)

2. Subject of the agreement

A) Copyright
1- The Author and each co-authors shall transfer and sell to the Publisher for the length of the copyright starting from the moment the present agreement comes into force the exclusive rights to the materials, including the rights to translate, reproduce, transfer, distribute or otherwise use the materials or parts (fragments) contained therein, for publication in scientific, academic, technical or professional journals or other periodicals and in derivative works thereof, worldwide, in English, in print or in electronic editions of such journals, periodicals and derivative works in all media or formats now existing or that may exist in future, as well as the right to license (or give permission to) third parties to use the materials for publication in such journals, periodicals and derivative works worldwide. The transfer under this agreement includes the right to adapt the presentation of the materials for use in conjunction with computer systems and programs, reproduction or publication in machine-readable format and incorporation into retrieval systems.
2- Reproduction, placement, transfer or any other distribution or use of the materials, or any parts of the materials contained therein, in any way permitted under this Agreement, shall be accompanied by reference to the Journal and mentioning of the Publisher, namely: the title of the article, the name of the Author (Co-authors), the name of the Journal, volume/number, copyright of the publisher.

B) Reserved Rights
The Author (Co-authors) or the employer of the Author (Co-authors) of the materials shall retain all proprietary rights (with the exception of the rights transferred to the Publisher under the present Agreement).

C) Author Guarantee
The Author (Co-authors) guarantees that the materials are an original work, submitted only to GJESM, and have not been published previously.
In case the materials were written jointly with co-authors, the Author guarantees that he/she has informed them of the terms of this Agreement and obtained their signatures or written permission to singe on their behalf.
The Author guarantees as well that:
The materials do not contain libelous statements.
The materials do not infringe on other persons' rights (including without limitation copyrights, patent rights and the trademark right).
The materials do not contain facts or instructions that can cause damage or injury to third parties and their publication does not cause the disclosure of any secret or confidential information

Author (Corresponding Author):

Correspondence Address:

Phone:

Fax:

Email:

Corresponding Author Name: Signature Date

On Behalf of the Publisher:

Iran Solid Waste Association,
Faculty of Environment, University of Tehran,
Postal Code: 1417854511, Tehran,
Iran

Telefax: (+9821) 2610 5110

Email: *editor@gjesm.net*
Gjesm.publication@gmail.com

Website: www.gjesm.net

Accepted for publication ☑ Signature Date

PLEASE NOTE: The accepted manuscript cannot be processed for publication until the publisher has received this signed form. The form MUST be signed by the Corresponding Author and then scanned and sent through the system or email. If the manuscript is not published in the Journal, this release will not take effect.

The sole responsibility for the whole content (s) of the article remains only with the corresponding author. However, Editor would reserve the right to adjust the style to certain standards of uniformity before publication.

CONFLICT OF INTEREST DISCLOSURE FORM

Conflict of Interest is defined as a set of conditions in which professional judgment concerning a primary interest, such as the validity of research, may be influenced by a secondary interest, such as financial gain. A Conflict of Interest Disclosure is an agreement or notification from the authors that they have not been paid for the work, or if they have, stating the source of their payment. The purpose of Conflict of Interest Disclosure form is to provide readers of authors' manuscript with information about authors' interests that could influence how the authors receive the work. The corresponding author (on behalf of all co-authors) should submit a conflict of interest disclosure form and is responsible for the accuracy and completeness of the submitted manuscript. Conflict of Interest Disclosure form can be signed by the corresponding author on behalf of all co-authors and stating that the submitted manuscript is the authors' original work, has not received prior publication and is not under consideration for publication elsewhere, permission has been received to use any material in the manuscript much as tables, figures etc. or no permissions have necessary to publish the authors' work.

1. Name of the corresponding author

2. Affiliation including e-mail and phone number

3. Manuscript Title

4. Do the authors or authors' institution at any time receive payment or services from a third party (government, commercial, private foundation, etc.) for any aspect of the submitted manuscript (including but not limited to grants, data monitoring board, study design, manuscript preparation, statistical analysis, etc.)?

   Are there any relevant conflicts of interest? Yes / No

5. Do the authors have any patents, whether planned, pending or issued, broadly relevant to the work?

   Are there any relevant conflicts of interest? Yes / No

6. Are there other relationships or activities that readers could perceive to have influenced, or that give the appearance of potentially influencing, what the authors' information in the submitted manuscript?

   Are there any relevant conflicts of interest? Yes / No

7. Are there any aspect of the work covered in this manuscript that has involved either experimental animals or human patients has been conducted with the ethical approval of all relevant bodies or not.

   Are there any relevant conflicts of interest? Yes / No

Corresponding Author Signature | Print Name | Date

AUTHORSHIP FORM

By completing and signing the following statements, the corresponding author acknowledges and accepts the responsibility on behalf of all contributing authors, if any, concerning Authorship Responsibility.

Manuscript title:

Corresponding author:

Affiliation:

Email:

Phone No:

By signing and filling this form, the corresponding author certifies that each author has met all criteria below (A, B, C, and D) and indicates each author general and specific contributions by listing his or her name next to the relevant section.

A. I certify that

- The manuscript is authentic and valid and that neither this manuscript nor one with considerably similar content under my authorship has been published or is being considered for publication elsewhere, except as described in an attachment, nor copies of closely related manuscripts are provided.
- I will provide the data or will contribute fully in providing and obtaining the data on which the manuscript is based for examination by the editors or their assignees, if requested.
- Every author has agreed to allow the corresponding author to serve as the primary correspondent with the editorial office, to review the edited manuscript and proof.

B. Each author has given final approval of the submitted manuscript.

C. Each author has participated sufficiently in the work to take public responsibility for the whole content.

D. Each author qualifies for authorship by listing his or her name on the appropriate line of the categories of contributions listed below. List appropriate author next to each section – each author must be listed in at least 1 field. More than 1 author can be listed in each field.

- conception and design
- acquisition of data
- analysis and interpretation of data
- drafting of the manuscript
- critical revision of the manuscript for important intellectual content
- statistical analysis
- obtaining funding
- administrative, technical, or material support
- supervision
- no additional contributions
- other (specify)

Corresponding Author Signature **Print Name** **Date**

CHANGE OF AUTHORSHIP FORM

Manuscript Title:

Corresponding Author:

Please check all that apply.

☐ New author(s) have been added.

☐ There is a change in the order of authorship.

☐ An author wishes to remove his/her name. An author's name may only be removed at his/her own request in writing.

ORIGINAL AUTHORSHIP

List ALL AUTHORS in the same order as the original (first) submission.

Print Name	Print Name
Name (1)	Name (6)
Name (2)	Name (7)
Name (3)	Name (8)
Name (4)	Name (9)
Name (5)	Name (10)

NEW AUTHORSHIP

List the ALL AUTHORS in same order as the new version.

Print Name	Print Name
Name (1)	Name (6)
Name (2)	Name (7)
Name (3)	Name (8)
Name (4)	Name (9)
Name (5)	Name (10)

I attest that:

1. The manuscript is not currently under consideration, in press, or published elsewhere, and the research reported will not be submitted for publication elsewhere until a final decision has been made as to its acceptability by the journal (posting of submitted material on a web site may be considered prior publication-note this in your cover letter).
2. The manuscript is truthfully original work without fabrication, fraud, or plagiarism.
3. I have made an important scientific contribution to the study and am thoroughly familiar with the primary data.
4. I have read the complete manuscript and take responsibility for the content and completeness of the manuscript and understand that I share responsibility if the paper, or part of the paper, is found to be faulty or fraudulent.

Corresponding Author Signature Name Date

SUBSCRIPTION FORM

Subscription form

Global Journal of Environmental Science and Management

Please enter my annual subscription to the Global Journal of Environmental Science and Management (GJESM), including 4 quarterly issues for the Year ..... Vol. ..... Nos.....

	Domestic (Rials)	International (USD)
▪ Institutional	3,000,000	150
▪ Individual	2,000,000	100
▪ Student	1,000,000	80
▪ Single Copy	500,000	50

Name: **Tel.:** **Email:**

Mailing Address:

Payment method: Check or money order must be made in order of:
Account #. 0101834143005, Account name: J. Nouri
Bank Melli Iran, IAU Branch, Code 1017, Tehran, Iran

□ Bank receipt enclosed

** Please allow 3 to 5 weeks for delivery*

Please send this filled in order form along with the Bank receipt payment to:

Global Journal of Environmental Science
and Management
No. 2, Kouhestan Deadend, Janpour Street,
Darabad, Tehran 1956934461 Iran

Global

Journal of Environmental Science and Management

CONTENTS

Volume 8, Number 3, Summer 2022

(Serial # 31)